Contribution des données d'imagerie à une approche par traits fonctionnels de l'écologie des copépodes arctiques et subarctiques

Laure Vilgrain

Contribution des données d'imagerie à une approche par traits fonctionnels de l'écologie des copépodes arctiques et subarctiques

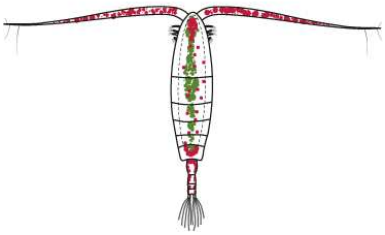

Thèse en cotutelle

-

Doctorat interuniversitaire en océanographie (Université Laval)

-

Doctorat Instrumentation, télédétection, observation et techniques spatiales pour l'océan, l'atmosphère et le climat (Sorbonne Université - ED129)

Laure Vilgrain

Jury composé de :

Pr. Jean-Benoit Charassin	Président
Pr. Beatrix Beisner	Rapportrice
Dr. David Nérini	Rapporteur
Dr. Mathieu Ardyna	Examinateur
Pr. Frédéric Maps	Directeur (Université Laval)
Dr. Sakina-Dorothée Ayata	Directrice (Sorbonne Université)

Résumé

Les copépodes dominent la biomasse du mésozooplancton des régions arctiques et subarctiques, où lumière, glace et production primaire varient fortement selon les saisons. En transformant le carbone fixé par les microalgues en réserves lipidiques pour survivre l'hiver, les *Calanus* spp. constituent une source d'énergie cruciale pour les poissons, oiseaux et mammifères marins. Historiquement, les copépodes sont étudiés par un comptage taxonomique après un échantillonnage par filets. Cette thèse propose un autre paradigme en combinant l'utilisation d'outils d'imagerie plus récents et une approche dite « par traits fonctionnels ». Les traits fonctionnels sont des propriétés mesurables à l'échelle individuelle et influençant le succès écologique des organismes (*i.e.* taille, régime trophique, migration verticale). Ils sont partagés par plusieurs espèces et peuvent être reliés à des fonctionnalités des écosystèmes comme l'export de carbone ou l'énergie disponible pour les réseaux trophiques par exemple. Comme une majorité des traits possèdent une signature morphologique, nous les avons définis sur deux types d'images individuelles du plancton, complémentaires et couramment utilisées : des images *in situ* de l'Underwater Vision Profiler (UVP) et des images en couleur prises lors d'observations au stéréomicroscope. L'objectif de cette thèse est de comprendre comment les traits fonctionnels des copépodes, identifiés sur des images, peuvent être reliés aux dynamiques environnementales et au fonctionnement des écosystèmes arctiques et subarctiques. Dans le Chapitre 1, nous analysons des images *in situ* prises par l'UVP au moment de la fonte printanière de la banquise dans l'arctique canadien. Des variables morphologiques sont utilisées pour projeter les images dans un espace statistique, et les axes synthétisent les variations morphologiques en trois traits continus : la taille, l'opacité (qui nous renseigne sur les structures pigmentées), et la complexité du contour (indiquant probablement un taux d'activité par la visibilité des appendices). Cette analyse exploratoire a révélé des traits nouveaux, dont les variations étaient fortement corrélées à la fonte de la banquise et à l'efflorescence des algues. Plusieurs arguments indiquent que les maxima d'opacité des individus peuvent être attribués à la présence d'astaxanthine, un pigment caroténoïde rouge. Dans le Chapitre 2, une revue de la littérature a mis en évidence les conditions écologiques propices à la coloration des copépodes pour divers écosystèmes aquatiques à l'échelle globale. Nous démontrons que la pigmentation rouge peut participer au succès des individus (croissance, survie, reproduction) grâce aux propriétés antioxydantes de l'astaxanthine. Comme la pigmentation semble ajustable à de courtes échelles temporelles et avantageuse dans diverses conditions environnementales (lumière intense, basses températures et couvert de glace, ou grandes profondeurs), nous pensons qu'elle peut être considéré comme un de "couteau-suisse" de protection métabolique. Dans le Chapitre 3, une méthode de déconvolution de la couleur de l'astaxanthine a été utilisée pour produire un indice de rougeur sur des images de copépodes arctiques observés au stéréomicroscope. L'indice a été validé par comparaison avec une quantification chimique des pigments, et peut être utilisé pour des images prises dans diverses conditions grâce à une étape préalable de calibration des canaux de couleur. Cette thèse montre qu'il est possible d'extraire un maximum d'information à partir d'une image de plancton pour dégager des tendances écologiques sur de grands jeux de données, tout en gardant accès à la variabilité interindividuelle. Utiliser les traits définis ici (taille, pression de broutage, taux d'antioxydants), en combinaison avec d'autres outils, pourrait participer à la compréhension du fonctionnement des réseaux trophiques.

Abstract

Copepods dominate the mesozooplankton biomass of arctic and sub-arctic regions, where light, ice and primary production are highly variable according to the season. By converting carbon fixed by microalgae into lipid reserves for winter survival, *Calanus* spp. are a crucial source of energy for fish, birds and marine mammals. Historically, copepods have been studied by taxonomic counting after net sampling. This thesis proposes an alternative paradigm by combining the use of more recent imaging tools and functional trait-based approach. Functional traits are properties that are measurable at the individual scale and influence the ecological success of organisms (*i.e.* size, trophic regime, vertical migration). They are shared by several species and can be related to ecosystem functionalities such as carbon export or energy available for food webs for example. As a majority of them have a morphological signature, we defined them on two types of individual plankton images, complementary and commonly used: in situ images from the Underwater Vision Profiler (UVP) and color images taken during stereomicroscope observations. The objective of this thesis is to understand how functional traits of copepods, identified in images, can be related to environmental dynamics and functioning of arctic and sub-arctic ecosystems. In Chapter 1, we analyze in situ images taken by the UVP at the time of spring melt in the Canadian arctic. Morphological variables are used to project the images into a statistical space, and the axes synthesize morphological variation into three continuous features: size, opacity (which tells us about pigmented structures), and complexity of contour (likely indicating feeding activity through appendage visibility). This exploratory analysis revealed novel traits, having variations strongly correlated with sea ice melt and algal blooms phenology. Several arguments indicate that opacity maxima in individuals can be attributed to the presence of astaxanthin, a red carotenoid pigment. In Chapter 2, a review of the literature highlighted the ecological conditions conducive to copepod coloration for various aquatic ecosystems on a global scale. We demonstrate that red pigmentation can participate in the success of individuals (growth, survival, reproduction) through the antioxidant properties of astaxanthin. Since pigmentation appears to be adjustable on short time scales and advantageous under various environmental conditions (intense light, low temperatures and ice cover, or great depths), we believe it can be considered as a "swiss army knife" of metabolic protection. In Chapter 3, an astaxanthin color deconvolution method was used to produce a redness index on stereomicroscope images of arctic copepods. The index was validated by comparison with a chemical quantification of the pigments, and can be used for images taken under various conditions thanks to a prior calibration step of the color channels. This thesis shows that it is possible to extract a maximum amount of information from a plankton image to identify ecological trends on large datasets, while keeping access to inter-individual variability. Using the traits defined here (size, grazing pressure, antioxidant levels), in combination with other tools, could participate in understanding the functioning of food webs.

Table des matières

Liste des figures

Liste des tableaux

Liste des abréviations, sigles, acronymes

Å: Ångström

ABP: Astaxanthin Biosynthesis Pathway

$\overline{AC}$: average astaxanthin content for the copepods of one sample (total astaxanthin content of the sample divided by the number of copepods in the sample)

AMSR2: Advanced Microwave Scanning Radiometer 2

ANOVA: Analysis of Variance

RGB_{med}: median of R, G, B color channels in an image

B_a: blue channel value computed from the astaxanthin absorbance spectrum

B_{med}: median value of the blue channel in one image

B_{pix}: value of the blue channel in a pixel of the original image

B^*_{pix}: value of the blue channel in one pixel of the gray world calibrated image

B_w: blue value of the white color (=1)

C matrix: matrix of Corrected Optical Density values

^{14}C: Carbon 14

CTD: Conductivity-Temperature-Depth sensors

CCGS: Canadian Coast Guard Ship

°C: Degree Celsius

CHE: Cholinesterase

Chl *a*: Chlorophylle *a*

CV: Copepodite stage five

DM: Dry mass

D matrix: Deconvolution matrix

DNA: Deoxyribonucleic Acid

DOC: Dissolved organic carbon

DVM: Diel vertical migration

G_a: Green channel value computed from the astaxanthin absorbance spectrum

G_{med}: median value of the green channel in one image

GST: Glutathione S-transferase

G_{pix}: value of the green channel in one pixel of an original image

G^*_{pix}: value of the green channel in one pixel of a gray world calibrated image

G_w: green value of the white color (=1)

h: hour

HSB: Hue-Saturation-Brightness

Hz: Hertz

HPLC: High Performance Liquid Chromatography

Hsp: Heat shock protein

IO PAN: Institute of Oceanology Polish Academy of Sciences

IFCB: Imaging FlowCytobot

IPCC: Intergovernmental Panel on Climate Change

ISIIS: In-situ Ichthyoplankton Imaging System

Kg: kilogram

kHz: kiloHerz

L: liter

L*a*b color space: name of the color space

LOKI: Lightframe On-sight Key species Investigation

$LOO^{\bullet}$: Lipid radicals

M: million

m: meters

MAAs: Mycosporine-like amino acids

min: minutes

mg: milligrams

mm: millimeters

mmol: millimoles

ml: milliliters

n: total number of images

NADP: Nicotinamide adenine dinucleotide phosphate

NADPH: Reduced form of NADP

N, E, S, W: North, East, South, West

nm: nanometers

n_{pix}: total number of pixels

n_{sample}: total number of copepods by sample

OD: Optical Density

OD matrix: Optical Density matrix

$OH^{\bullet}$: Hydroxyl radicals

OWD: Open Water days

PCA: Principal component analysis

PC: Principal components

R: R programming language

R_a: Red channel value computed from the astaxanthin absorbance spectrum

RGB: Red, Green, Blue color channels

$\overline{RI}$: average redness index for 10 copepods of one sample

RI_{cop} : redness index computed for one image (one copepod)

R_{med}: median value of the red channel in one image

RNA: Ribonucleic acid

ROS: Reactive Oxygen Species

R/V: Research Vessel

R_{pix}: value of the red channel in one pixel of an original image

R^*_{pix}: value of the red channel in one pixel of a gray world calibrated image

R_w: R value of the white color (=1)

MBARI-ISUS: Monterey Bay Aquarium Research Institute - In Situ Ultraviolet Spectrophotometer

SCM: Sub-surface chlorophylle maximum

SCF fluorometer: Seapoint Chlorophyll Fluorometer

Seabird SBE 43: Dissolved Oxygen Sensor

SI: Système international

SPC: Scripps Pier Cam

SPH: Shared Pathway Hypothesis

spp.: species

UV: ultraviolet radiation

UVP: Underwater Vision Profiler

UVP 5: Underwater Vision Profiler 5th version

UVP 5 HD: Underwater Vision Profiler 5th version High Definition

UVP 6: Underwater Vision Profiler 6th version

λ: wavelength

µg: microgram

µg.mgDM^{-1}: microgram per milligram of dry mass

µm: micrometer

When asked "why study plankton?" we might invoke carbon flux, climate change, etc. If the answer seems inadequate to explain a devotion to plankton, do not hesitate to say that the organisms of the plankton are gorgeous, "art forms of the drifting world". It is not difficult to provide evidence.

John R Dolan, Beauty of the plankton: from the first issue of Haeckel's Art Forms of Nature, Journal of Plankton Research, 2023

Remerciements

J’avais été prévenue : une thèse, c’est un parcours initiatique. Je remercie infiniment mes deux directeurs de thèse de m’avoir aussi bien accompagnée dans ces challenges scientifiques et personnels. Frédéric et Sakina ont formé un duo bienveillant, solide et complémentaire. J’ai pu m’appuyer sur eux à toutes les étapes administratives (avec les joies de la cotutelle et de ses avenants) et scientifiques, de l’analyse des données à la relecture des articles. Merci Fred de m’avoir offert la possibilité de travailler dans le cadre si épanouissant de l’Université Laval et d’être toujours resté enthousiaste et à l’écoute même dans les moments difficiles. Sakina, une étude récente a montré que c’est un encadrement par une femme en milieu de carrière, peu expérimentée et bénéficiant d'une subvention nationale qui permet d’avoir un doctorat le plus productif (Corsini et al. 2022). C’est fou, les auteurs doivent te connaitre. Je te remercie infiniment pour ta constance, ta rigueur et ta gentillesse qui m’inspirent et me donnent de la force. Il faut absolument qu’au moins la moitié des professeurs et des chercheurs soient des femmes, surtout si elles sont comme toi. Merci aussi à Jean-Olivier de m’avoir fait confiance pour le stage de master et de m’avoir fait découvrir le plaisir de travailler sur des images de plancton (avec R, évidemment), et d’avoir été là en cas de problèmes depuis.

Je remercie les deux membres de mon comité de suivi, Sünnje Basedow et Emilia Trudnowska, qui m’ont encouragée et validée au long de ces années. Merci à Emilia, et aussi à Barbara Niehoff, de m’avoir invitée dans leurs groupes de recherche en Pologne et en Allemagne pour connaitre les copépodes arctiques de plus près, et ce, même en périodes de confinement et des déconfinements.

Je remercie Marc Picheral, Amanda Elineau et Camille Catalano pour les formations et conseils qu’ils m’ont fourni pour l’utilisation de l’Underwater Vision Profiler, et pour l’aide qu’ils m’ont donné à distance lors des missions. Sur le terrain, c’était une immense chance pour moi de travailler avec Claudie Marec (dans l’Arctique canadien) et Jason Stockwell (sur le Lac Champlain) qui m’ont accompagnée et fait confiance avec le déploiement de l’UVP et les manipulations associées. Je remercie énormément Marie-Hélène Forget et Marcel Babin de m’avoir permis de participer à la mission DarkEdge et notamment pour leur aide à bord lors des problèmes liés à la pandémie. Merci à l’équipage de la Coast Guard et d’Amundsen Science de m’avoir fait découvrir les eaux arctiques et son zooplancton dans des conditions extraordinaires. Pour l’analyse automatique d’images en couleur, je suis très reconnaissante à Jean-François Lalonde pour ses pistes de réflexions, Martin Schröder pour son implication spontanée si précieuse, ainsi qu’à Saeideh Sadeghpour Gildeh pour son aide complémentaire. Merci aux deux équipes scientifiques avec qui j’ai passé le plus de temps, pour la bonne ambiance dans les labos et le soutien scientifique. Tout d’abord, à l’équipe COMPLEx à Villefranche, et particulièrement à Thelma, Salomé, Ophélie, Camille, Louis, les

volleyeurs et à tous les étudiants de master pour les beaux moments au bord de l'eau, dans les montagnes et à la trinquette. Ensuite, à toute l'équipe NEOLab à Québec : Inge, Sarah, Sara, Andéol, Fanny, Lucie, Hediyeh, Olivier, Leila, Cyril, en particulier pour l'aide dans la préparation des présentations orales. Un merci tout spécial à Maxime pour les histoires de moutons et les soirées documentaires.

Au-delà de tout, je connais la chance que de vivre au sein d'un réseau dense, diversifié et résilient de proches, de famille et d'amis, que je vais regrouper sous le terme très scientifique de potos-système.

Merci à ma Maya d'amour, qui est là chaque jour (sans exagération) aussi bien pour les meilleures nouvelles et que dans les plus grands doutes. Merci de m'avoir toujours accueillie chez toi avant que je saute dans un train Gare de Lyon, et de t'occuper de mon poney pour qu'on puisse galoper dans les chemins du perche quand je rentre. Tu détiens haut la main la première place de la mémoire de Whatsapp (550Mo à deux jours de tes 30 ans) et ça me parait la moindre des choses avec un océan qui nous sépare.

Mon Simon : je ne sais pas si tu es meilleur pour faire la route du Rhum sur Mario Kart ou pour réussir une quiche au bleu, mais ça tombe bien, je n'ai pas besoin de choisir et on peut faire les deux en même temps. Tu es le plus génial des secouristes de gens en burn-out ou en rupture : merci infiniment de ton écoute inégalable et tes blagues qualitatives.

Merci à toi Lolo pour le chemin qu'on a fait ensemble et ton soutien aux moments où je croyais le moins en moi. On a prouvé qu'en s'accrochant, c'est possible de progresser à l'infini personnellement et professionnellement.

Merci à ma maman qui a réussi, je crois, à me transmettre sa force de caractère et sa persévérance. Merci de m'avoir permis de grandir heureuse près de l'océan et de ses habitants, que je pouvais aller voir en rentrant de l'école avec les pieds dans le platin. Merci d'avoir été là physiquement, moralement et financièrement pour me soutenir depuis toujours dans mes études (et bravo d'avoir appris si vite à utiliser le mot *copépode*). Merci à toute ma famille bizarre, qui prouve que recomposée ne veut pas du tout dire moins bien. Mes grands frères et sœurs Julien, Pauline et Arthur vous êtes les meilleures sources d'inspiration avec vos passions allant des courants atmosphériques à la gouvernance des villes de Jordanie en passant par la compagnie des trains du midi. Même si on est sur trois fuseaux horaires, vous êtes toujours proches de moi. Merci en particulier à ma grande sœur de m'avoir aidée à évoluer depuis que je suis née, le chemin est vraiment plus facile quand quelqu'un ouvre la voie. Un immense merci à ma Véro, qui veille sur moi depuis mes 7 ans et m'encourage avec tout son cœur et son énergie dans ce que j'entreprends. Merci Papa

de m'avoir donné la passion de vivre dans la nature, d'aller chercher des châtaignes, de protéger les araignées et de vivre sans clôtures. Enfin, merci à mes deux merveilles de petits frères et sœurs de m'apprendre le ping-pong avec 10 ans de décalage, entre une promenade dans les champs et une partie de cartes.

Merci à mon marin d'amour de m'avoir soutenu dans ces périodes de houle et de doutes. Merci pour tous tes petits mots, tes idées farfelues et les surprises qui font que la vie plus douce et joyeuse. Merci aussi de me faire découvrir ton monde peuplé de glace et de fromage en grains, j'ai bien de la chance de t'avoir trouvé aussi loin de chez moi. Un jour, je saurai patiner et gérer mon stress : tiens bon !

Merci à mes colocs Alexia, Adèle et Oli d'avoir vécu les dernières années de ma thèse chaque jour avec moi. Alexia tout d'abord : comment j'aurai fait pour aimer autant le Québec sans toi ? Merci pour toute ta joie de vivre et de ton énergie politique et sociale. Merci aussi de m'avoir m'a permis de rencontrer les gens incroyables de la Sutherband : Raphaël, Maude SG, Sammy, Léa, Maude PL, Alexis, Adrien, Aurélie, et tous les autres. J'ai pas du tout aimé quand tu es partie vivre ailleurs, tu le sais ! Mais heureusement j'ai pu rencontrer Adèle, mon petit rayon de niaiserie : en vérité, à Miami, le tout est plus grand que la somme des parties, tu fais partie de mes raisons d'aimer la vie ! Et tout ça, partagé avec la présence chaleureuse d'Oli, et parfois d'Eli. Un grand merci à mes colocs du dessus, PO, Margaux et Laura. Bien sûr, une mention spéciale à mon Popo, que je ne vois pas souvent mais qui est toujours là pour une bière, des crêpes avec une écoute en or. J'ai le cœur gros de partir loin de vous.

Vous prendrez la formule en trio ? Merci à mon âme-frère Andéol de partager avec moi la couleur des sentiments, celle des chœurs de l'armée russe, et celle de tout ce qui est quétaine au marché de noël : le rouge. ROUGE ? Les copépodes ! Merci à Arthuro d'être là avec une grande assiduité : pour les bières du Fou-bar et mes crises de sanglots, surtout que ces deux activités arrivent souvent dans la vie quand même !! C'était aussi génial de découvrir le Québec et les Unlocks avec les copains de la Takuteam : un grand merci à Simon et Marie pour leurs petites attentions débordantes d'amour, à Fanny et Lena pour leurs talents d'imitatrices hors pair, à Lucie Bou pour son rire, à Adèle pour son énergie aventureuse, à Lucie Tou pour sa détermination sans limites, à Manu pour sa douceur, à Foucaut pour les entrainements sportifs et son humour noir, et à Guillaume et Bérénice pour leur soutien même à 20m de la ligne d'arrivée.

Merci aussi à tous les gens que j'ai rencontré sur l'Amundsen pour les moments merveilleux, et surtout à Emma et Hugo, avec qui le temps c'est un peu arrêté, en mer et sur terre en 2021. Je remercie aussi chaleureusement ma Gaëllounette, pour les bons moments en mer, le soutien et l'aide précieuse dans la relecture de ce manuscrit.

Enfin, merci à mes tous mes Copains d'abord qui sont quelque part de l'autre côté de l'Atlantique, *ceux avec qui je m'ambiance, qui connaissent mes darons et mes faiblesses.* Un énorme merci à Manon et Sacha, qui m'ont accompagné depuis toujours et dans tout ce que j'ai été. Merci à la Big Idea, qui, par leurs chansons géniales, me permettent d'avoir l'impression d'être à côté d'eux avec mes écouteurs dans les rues de Québec. Manon, Sacha, Victor, Sinclair, Juliette, Pierre, Matéo, Anna, Louis, Lucille, Arnaud, Anna, Etienne, Mathieu et tous les autres avec qui la vie est à la bonne franquette : vous m'inspirez et vous me manquez les copains. Mais j'ai juste à penser à vous pour que la fête commence !

Avant-propos

Cette thèse présente le travail de mon projet de doctorat, effectué en cotutelle entre Sorbonne Université (France) et l'Université Laval (Québec, Canada). J'ai débuté mon doctorat au Laboratoire d'Océanographie de Villefranche-sur-Mer (LOV, UMR 7093 de Sorbonne Université), en continuation de mon stage de seconde année de master qui a été encadré par Sakina-Dorothée Ayata et Jean-Olivier Irisson, en collaboration avec Frédéric Maps (Université Laval). Depuis le début de mon projet en septembre 2019, j'ai donc évolué au contact et avec le grand soutien scientifique des membres de l'équipe COMPLEx (COMPutational PLankton Ecology) du Laboratoire de Villefranche-sur-Mer. En septembre 2021, ma co-directrice Sakina-Dorothée Ayata a rejoint le Laboratoire d'Océanographie et du Climat : Expérimentations et Approches Numériques (LOCEAN, UMR 7159 de Sorbonne Université, Paris), où ma soutenance va se dérouler. Jusqu'à août 2021, au rythme des confinements et des déconfinements, j'ai travaillé depuis Villefranche-sur-Mer et j'ai séjourné en Allemagne (Alfred Wegner Institute, Bremerhaven) et en Pologne (The Institute of Oceanology of the Polish Academy of Sciences) pour des collaborations scientifiques. De septembre 2021 jusqu'à la fin de mon doctorat en 2023, j'ai travaillé à l'Université Laval dans le laboratoire de mon co-directeur Frédéric Maps.

Ce document suit le format de l'Université Laval pour une thèse avec insertion d'articles. Il contient une introduction générale, trois chapitres écrits en anglais au format d'articles scientifiques, et une conclusion explicitant la cohérence de l'ensemble du projet de doctorat et son insertion dans l'état actuel de la recherche en océanographie. Le premier article est publié et le texte du Chapitre 1 est similaire à la version publiée, à l'exception de la numérotation des figures et tableaux qui a été adaptée pour l'ensemble du manuscrit de thèse. Le second article a été publié quelques jours avant la soutenance, et le texte du chapitre 2 correspond à la dernière version du manuscrit avant les proofs, il y aura de très légers changements (fautes de frappe, formulations) par rapport à la version publiée. Le dernier chapitre est une ébauche d'article, relue par la majorité des co-auteurs et qui sera soumis prochainement. Mes contributions et celles de mes co-auteurs sont détaillées ici :

Chapitre 1 : Trait-based approach using in situ copepod images reveals contrasting ecological patterns across an Arctic ice melt zone

Vilgrain, L., Maps F., Picheral M., Babin M., Aubry C., Irisson J-O, and Ayata S-D. 2021. Trait-based approach using in situ copepod images reveals contrasting ecological patterns across an Arctic ice melt zone. Limnology and Oceanography, 66: 1155-1167. https://doi.org/10.1002/lno.11672

- Soumis : 1er mai 2020 ; Accepté : 14 novembre 2020 ; Publié : 15 janvier 2021

- Marcel Babin a conçu le projet GreenEdge. Marc Picheral a développé l'Underwater Vision Profiler et a collecté et trié les images de zooplancton. Cyril Aubry a collecté le zooplancton par filets puis à trier et compter les différentes espèces. Jean-Olivier Irisson, Sakina-Dorothée Ayata et Frédéric Maps ont conçu les idées de recherche. J'ai réalisé toutes les analyses statistiques avec le support régulier de Jean-Olivier Irisson, et l'aide complémentaire de Sakina-Dorothée Ayata et de Frédéric Maps. J'ai pensé et écrit la version initiale du manuscrit et tous les auteurs ont contribué à l'amélioration des différentes versions et ont approuvé la version finale.
- Article récompensé par le Prix d'excellence de la publication étudiante 2021 décerné par Québec-Océan. Il a également été nominé par la Fondation de la mer et l'Institut de l'Océan de SU en 2021.

Chapitre 2 : Copepods' true colors: astaxanthin pigmentation as an indicator of fitness

Vilgrain L., Maps F., Basedow S., Trudnowska E., Madoui A., Niehoff B., Ayata S-D. 2023. Copepods' true colors: astaxanthin pigmentation as an indicator of fitness. Ecosphere, 14(6): e4489. https://doi.org/10.1002/ecs2.4489

- Première soumission : 25 mai 2022 ; Seconde soumission après corrections : 1er décembre 2022 ; Accepté : 12 décembre 2022 ; Publié : 8 juin 2023.
- Frédéric Maps, Sakina-Dorothée Ayata et Sünnje Basedow ont fourni le financement au projet permettant cette publication. J'ai conçu les idées et la structure de la revue de littérature, rassemblé les données provenant des différents articles, effectué les analyses statistiques et les graphiques et écrit la version initiale du manuscrit. Emilia Trudnowska et Barbara Niehoff m'ont invitée dans leurs instituts de recherche et m'ont appuyé dans l'analyse et les discussions concernant la pigmentation des copépodes. Amin Madoui a contribué à l'analyse de la littérature concernant les aspects génétiques et moléculaires. Tous les auteurs ont contribué significativement à l'amélioration du manuscrit et ont accepté la version finale.

Chapitre 3 : Automatic quantification of red astaxanthin pigmentation on stereo-microscope images of Arctic copepods (*Calanus* spp.)

Vilgrain L., Schröder S-M., Trudnowska E., Irisson J-O., Basedow S., Maps F. & Ayata S-D. *In prep*. Automatic quantification of red astaxanthin pigmentation on stereo-microscope images of Arctic copepods (*Calanus* spp.).

- Soumission envisagée d'ici décembre 2023

- Frédéric Maps, Sakina-Dorothée Ayata et Sünnje Basedow ont fourni le financement du projet permettant cette publication. Emilia Trudnowska a collecté le plancton et fourni l'ensemble des images et des échantillons pour l'analyse chimique des pigments. Simon-Martin Schröder et Jean-Olivier Irisson m'ont aidé à produire certaines les codes pour l'analyse d'images que j'ai assemblé et adapté à l'ensemble du jeu de données d'images. J'ai produit les figures et écrit la première version du manuscrit.

Introduction

L'importance écologique des copépodes arctiques et subarctiques

Un être vivant est dit planctonique lorsque ses déplacements se font passivement au gré des courants dans les milieux aquatiques (Sardet et al. 2015). Le plancton subit donc les variations des propriétés physiques et chimiques des masses d'eau dans lesquelles il vit. Dans les régions arctiques et subarctiques, la saisonnalité est particulièrement marquée : la durée du jour passe de huit heures à seize heures aux latitudes situées entre 50° et 66°N, et des périodes d'obscurité prolongée et de jours continus alternent au nord du cercle arctique, situé légèrement au-delà de 66°N (Berge et al. 2015) (Figure 1). Le couvert de glace de mer se forme puis disparaît cycliquement d'octobre à avril, atteignant les côtes du Canada et du sud du Groenland comme limite maximum d'extension actuelle (Meredith et al. 2019 - IPCC 2019). Les assemblages d'algues planctoniques et sympagiques peuplant ces milieux sont composés de classes d'eucaryotes tels que des diatomées, des prymnésiophycées, des prasinophycées ainsi que d'autres organismes photoautotrophes de plus petite taille. La composition de ces groupes est influencée par les conditions du milieu telles que la disponibilité en nutriments (nitrates et acide silicique), la lumière et la température environnante (Ardyna & Arrigo 2020). En association à de fortes concentrations de silice, le pic de l'efflorescence pélagique est dominé par des diatomées centriques à croissance rapide (par ex. *Chaetoceros* spp. et *Thalassiosira* spp.) et d'autres espèces pennées (*Fragilariopsis* spp) (Lovejoy et al. 2002, Lafond et al. 2019). L'apogée et la durée de l'efflorescence varie d'avril à août selon la latitude (Figure 1) et est sujette aux changements climatiques (Wassman & Reigstad 2011, Ardyna & Arrigo 2020). C'est cette rapide et forte production primaire, souvent dominée par les diatomées, qui conditionne le développement du mésozooplancton sur lequel j'ai travaillé dans le cadre de cette thèse (Daase et al. 2021).

Le mésozooplancton regroupe un ensemble d'organismes hétérotrophes mesurant de 0.2 à 20 mm, dont la mobilité importante mais néanmoins insuffisante pour s'affranchir des courants marins horizontaux. Les communautés polaires du mésozooplancton sont composées de crustacés, de chaetognathes, de cténophores, de cnidaires, d'appendiculaires, de mollusques ainsi que de grands protistes (Hopcroft et al. 2005, Forest et al. 2012, Daase et al. 2021) (Figure 2). Dans ces régions, et comme dans la majorité des écosystèmes productifs, les copépodes dominent d'un point de vue numérique, aussi bien en densité (nombre d'individus) qu'en biomasse (Irigoien et al. 2002, Turner 2004). Les espèces les plus communes sont les grands *Calanus hyperboreus* (dont les stades adultes mesurent jusqu'à 6 mm), *Calanus glacialis*, *Calanus finmarchicus* et *Metridia longa* qui sont de taille moyenne (adultes entre 1 et 3 mm), et les plus petits *Pseudocalanus* spp., *Microcalanus pygmaeus et Oithona similis* (adultes < 1 mm) (Beaugrand 2002, Darnis et al. 2008, Forest et al. 2012). Les

populations de *Calanus* peuvent atteindre entre 80 à 90% de la biomasse du mésozooplancton, et leur biomasse est fortement corrélée à celle du mésozooplancton total dans l'Atlantique Nord et l'Arctique (Aarflot et al. 2018, Carstensen et al. 2019) (Figure 3). En raison de leur biomasse importante et de leurs rôles écologiques déterminants (détaillés par la suite), cette thèse porte principalement sur les trois espèces de copépodes du genre *Calanus*. Gardons néanmoins à l'esprit que les espèces de protistes hétérotrophes et mixotrophes ainsi que les petits copépodes omnivores et carnivores, souvent actifs tout au long de l'année, sont une autre composante importante des communautés zooplanctoniques en termes de biomasse et pour le cycle des nutriments (Riisgaard et al. 2014, Stoecker & Lavrentyev 2018, Barth-Jensen et al. 2022).

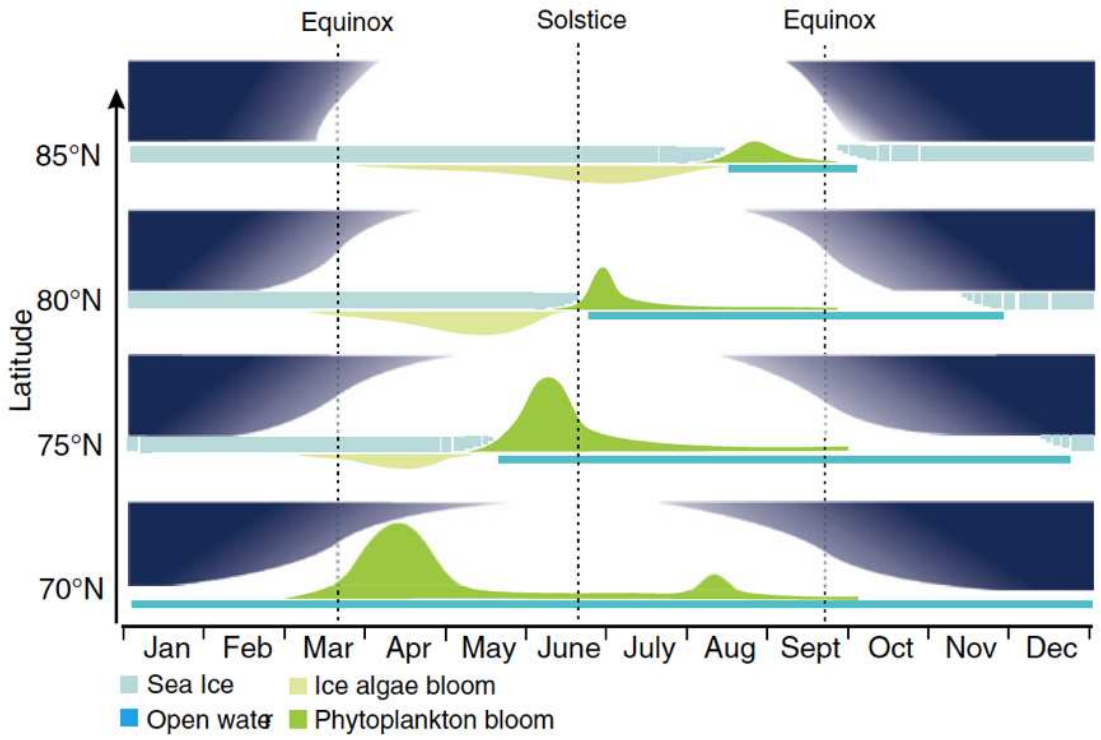

Figure 1. Compréhension conceptuelle de la période d'efflorescence des algues de glace et du phytoplancton dans l'Arctique, du sud au nord. Figure issue de Daase et al. (2021), modifiée d'après Zenkevitch (1963) et Leu et al. (2011).

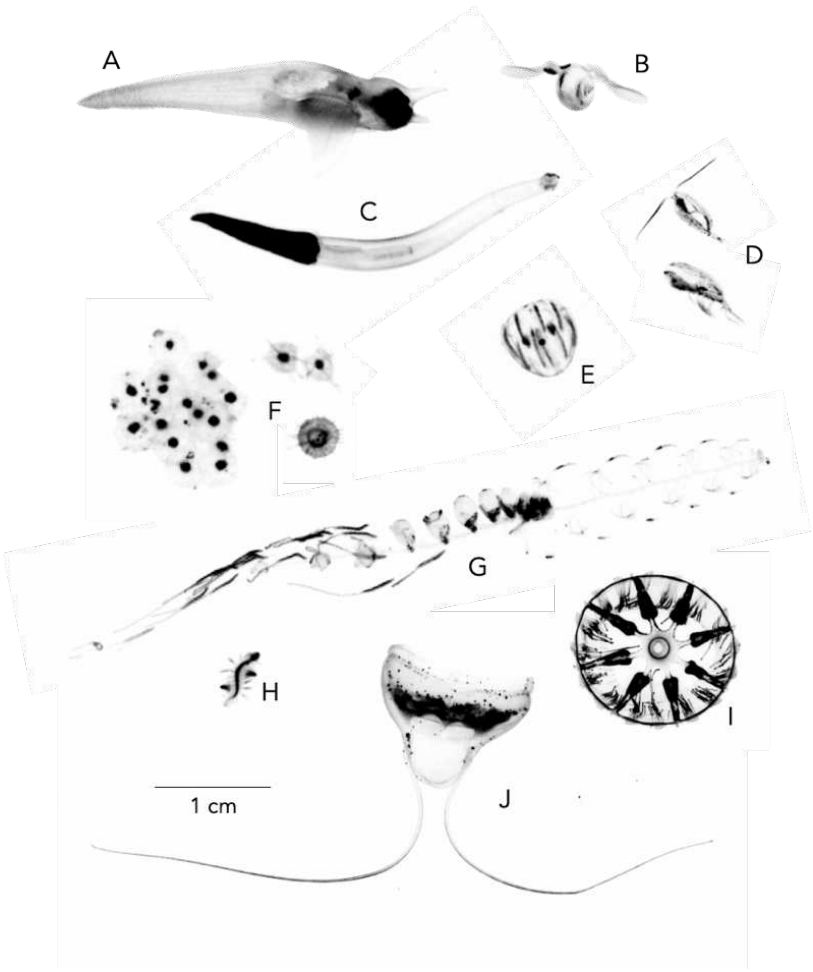

Figure 2. L'écosystème zooplanctonique arctique imagé par l'Underwater Vision Profiler 5HD pendant la mission GreenEdge en 2016. Mollusque ptéropode *Clione limacina* (A), Mollusque ptéropode *Limanica helicina* (B), Chaetognathe (C), Copepodes *Calanus hyperboreus* (D), Cténophore (E), Rhizaires (F), Siphonophore (G), Anélide (H), Hydrozoaire *Botrynema ellinorae* (I), Hydrozoaire *Solmundella bitentaculata* (J).

Les espèces de *Calanus* et les grandes diatomées du début de l'efflorescence printanière ont des relations écologiques très fortes. A l'échelle globale, les indices supportant l'hypothèse d'un lien évolutif entre ces deux grands groupes sont : l'apparition évolutive tardive de certaines espèces de Calanidae à des périodes géologiques probablement proches de celles de l'explosion de la spéciation des diatomées (début du tertiaire) (Bradford-Grieve 2002, Behrenfeld et al. 2021), et le régime très majoritairement herbivore des *Calanus* en comparaison à d'autres genres plus anciens (Bradford-Grieve 2002, Falk-Petersen et al. 2009). De nombreuses raisons environnementales ont influencé indépendamment l'évolution de ces organismes (Kooistra et al. 2007, Berge et al. 2012) mais certaines

caractéristiques ont motivé des chercheurs à tester l'hypothèse d'une "course évolutive aux armements". Il y a par exemple l'épaisseur de la frustule des diatomées en lien avec la forme des pièces buccales des copépodes (Michels & Gorb 2015, Pančić et al. 2019, Petrucciani et al. 2022), ou la production de toxines contre le broutage par les diatomées en lien avec la résistance de certains copépodes (Irigoien et al. 2002, Lauritano et al. 2012, Miesner et al. 2016). Les interaction copépodes-diatomées sont vivement débattues (Vincent & Bowler 2022) mais semblent très importantes dans les régions (sub)arctiques où on observe une synchronisation entre la sortie de diapause des *Calanus* et le pic d'abondance des diatomées. Chez ces copépodes, l'accumulation de réserves se situe au sein de sacs lipidiques (visibles sur la Figure 3) et l'importance du transfert trophique avec les diatomées a été démontrée par des analyses des lipides (Scott et al. 2002, Falk-Petersen et al. 2009, Saiz et al. 2013). Les individus doivent accumuler des réserves lipidiques au-delà d'un certain seuil qui leur permettra de survivre à l'hiver, en profondeur, dans un état métabolique réduit (*diapause*, Falk-Petersen et al. 2009, Schmid et al. 2018). Les adultes remontent en surface au printemps suivant pour leur reproduction (Daase et al. 2021).

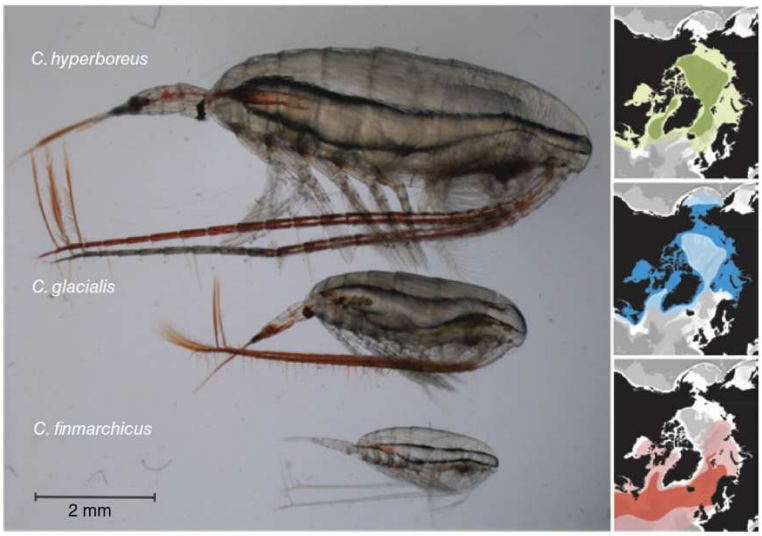

Figure 3. Adultes femelles des trois espèces congénères de *Calanus* et leur zone de répartition : le cœur de leur zone de distribution apparaît en teinte foncée sur les cartes de droite. Figure issue de Daase et al. (2021).

La grande capacité des copépodes du genre *Calanus* à stocker les lipides et leur cycle de vie avec une période de diapause en profondeur sont des composantes clés des écosystèmes nordiques de l'hémisphère nord (Record et al. 2018). Premièrement, leurs populations constituent une source très riche de nourriture pour les stades larvaires et juvéniles des poissons, dont la morue arctique *Boreogadus saida* qui domine largement la biomasse des poissons pélagiques en Arctique (Bouchard

& Fortier 2020, Pedro et al. 2023). Ils sont aussi consommés par certaines espèces d'oiseaux (Karnovsky et al. 2003) et de mammifères marins (Mayo & Marx 1990, Berge et al. 2012, Record et al. 2019, Fortune et al. 2020). Deuxièmement, ce sont des acteurs de la pompe à carbone biologique, en particulier par la production de pelotes fécales qui, par effet ballaste et sédimentation, transportent rapidement vers les profondeurs le carbone fixé à la surface (Turner 2015, Steinberg & Landry 2017). Unique chez les espèces polaires, le déplacement hivernal vers les eaux profondes, froides et isolées de la surface où ils vont respirer leurs réserves lipidiques pendant les longs mois de diapause, accélère très efficacement l'export de carbone ("*lipid pump*", Jónasdóttir et al. 2015, Tarling et al. 2022). Par ces propriétés, ils fournissent des services écosystémiques : (1) de support, comme composante de la biodiversité et de la résilience des écosystèmes, (2) d'approvisionnement, comme ressources alimentaires des poissons de pêcheries d'intérêt et (3) de régulation, par leur rôle dans la séquestration du carbone (Figure 4, Costanza et al. 1997, Méral 2012, Townsend et al. 2018).

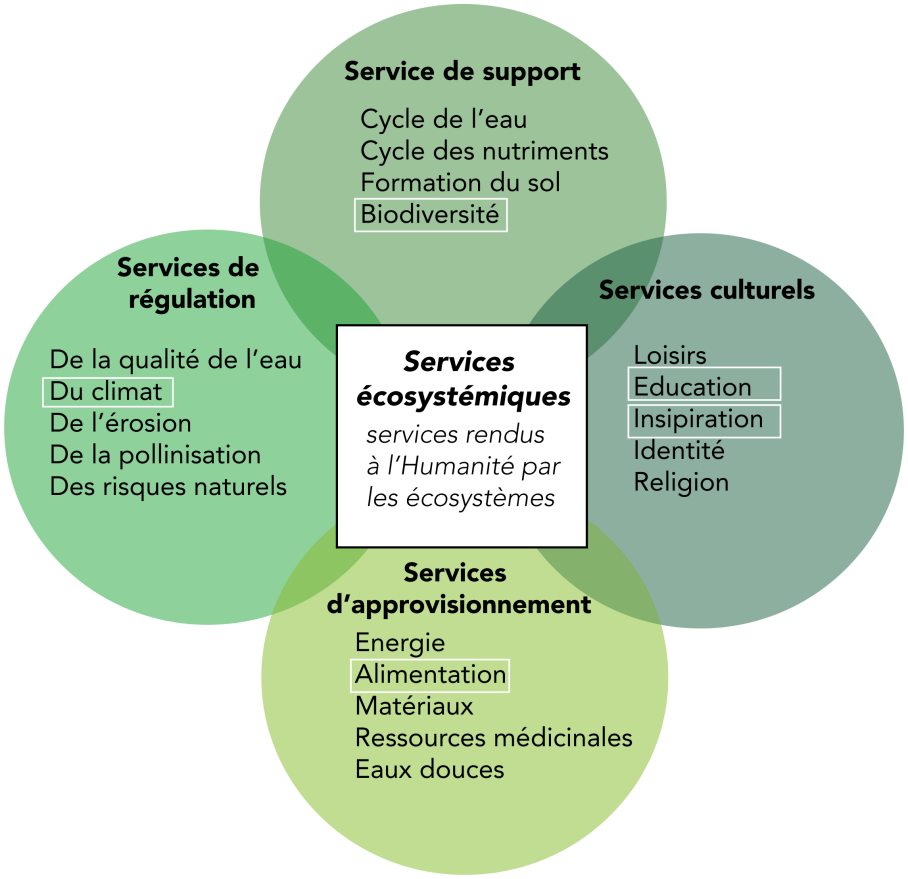

Figure 4. Les quatre types de services écosystémiques. Les services apportés par le zooplancton sont entourés en blanc. Figure modifiée d'après Vacht et al. (2018) avec des informations de Méral (2012).

Toutes les raisons invoquées jusqu'ici justifient la pertinence de l'étude de l'écologie des copépodes arctiques et subarctiques. Néanmoins, la première raison pour laquelle de nombreux chercheurs étudient ces organismes réside souvent ailleurs. Dans un article récent, John Dolan présente des planches de dessins spectaculaires faites par Ernst Haeckels en 1900, et nous rappelle que "pour expliquer une dévotion au plancton, il ne faut pas hésiter à dire que ces organismes sont magnifiques" (Dolan 2023), comme illustré pour les copépodes sur la Figure 5. La fascination et l'inspiration qu'apportent l'observation du plancton et celle de la biodiversité en général, suffit probablement à expliquer l'impulsion des scientifiques à étudier les mécanismes du vivant. Cette source d'émerveillement représente également un service écosystémique, dit culturel (Figure 4), qui peut lui aussi être menacé par l'impact des activités anthropiques.

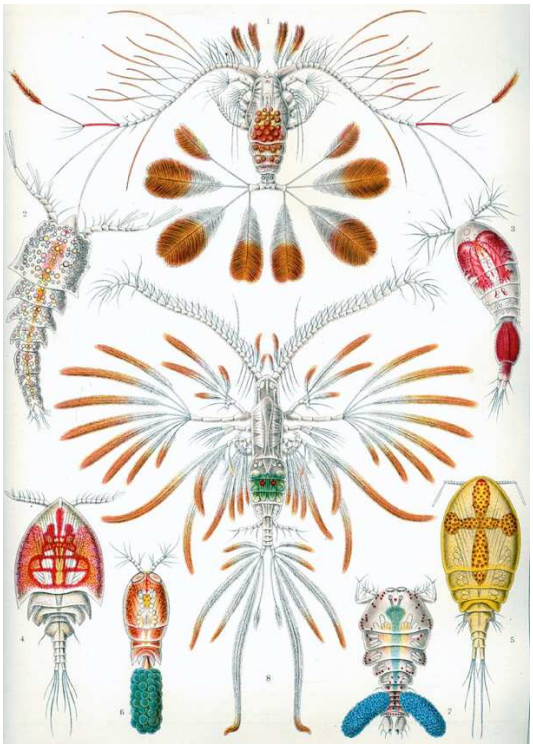

Figure 5. Dessins de copépodes réalisés par Ernst Haeckel, dans *Kunstformen der Natur* en 1904 (planche 56: Copepoda).

Puisque le mode de vie des *Calanus* dépend des variations saisonnières et des dynamiques de la banquise, leur succès écologique est questionné par la communauté scientifique dans un contexte de changement climatique. Les principales préoccupations concernent le déplacement vers le nord des espèces (Beaugrand 2002), la perte de la synchronisation entre l'efflorescence de production primaire et la sortie de diapause (*match/mismatch*, Søreide et al. 2010, Pierson et al. 2013) et une

diminution de la taille et du métabolisme lipidique des individus, entraînant une perte d'énergie dans les réseaux trophiques (Møller et al. 2012, Kortsch et al. 2015). Les études récentes ont effectivement montré un déplacement vers le nord des communautés de *Calanus* (Freer et al. 2022) associé à des changements dans la durée de leur diapause (Wilson et al. 2016, Flores et al. 2023, *in prep*.). Néanmoins, de nombreuses études ont insisté sur la grande plasticité écologique des trois espèces (Renaud et al. 2018, Trudnowska et al. 2020). Sur la période 1993 à 2016, leurs abondances maximales sont corrélées aux faibles concentrations en glace où ils trouvent des conditions de nourriture optimales (Ershova et al. 2021) dans une niche de température encore viable (survie et reproduction jusqu'à 5°C, Hildebrandt et al. 2014).

L'approche par traits fonctionnels : un autre angle de vue sur les écosystèmes

L'utilisation d'approches dites "basées sur les traits fonctionnels" est apparue en écologie végétale dans les années 1970 (Grime 1974) et a commencé à être couramment utilisée en écologie aquatique à partir des années 2000 (Usseglio-Polatera et al. 2000, Litchman et al. 2013, Kiørboe et al. 2018, Martini et al. 2021). Son but est de simplifier la complexité d'un écosystème en se concentrant sur quelques caractéristiques dépassant la classification par espèce, mais influençant les stratégies écologiques des organismes (Litchman et al. 2013). Ces caractéristiques sont nommées des traits fonctionnels, dont la définition est restée assez vague jusqu'au cadre théorique apporté par Violle et al. (2007). Un trait fonctionnel est une propriété (morphologique, physiologique, phénologique) mesurable à l'échelle individuelle et influençant la *fitness* d'un organisme (Violle et al. 2007). La *fitness* correspond au succès écologique d'un individu, et possède trois composantes : la croissance, la survie et la reproduction. Elle se calcule théoriquement par le nombre de descendants, qui sera élevé lorsqu'un individu a grandi, survécu et a pu se reproduire efficacement. C'est bien l'ensemble des traits fonctionnels d'un individu, et non son appartenance à une espèce donnée, qui va définir sa capacité à transférer ses gènes à la génération suivante (c.-à-d. sa *fitness*). Les intérêts théoriques de cette approche sont (1) de se placer à l'échelle individuelle, puisque les interactions écologiques se déroulent entre des individus et non pas entre groupes taxonomiques ; (2) de décrire les êtres vivants avec des propriétés quantitatives plutôt que de les placer dans des catégories taxonomiques (Mcgill et al. 2006) ; (3) de pouvoir mieux comprendre les compromis écologiques (*trade-offs*) établis à partir des traits potentiels d'un individu. Ce concept de compromis écologique est central en écologie évolutive : un individu va disposer d'un jeu de traits fonctionnels, et son

phénotype final ne peut pas être optimal pour toutes les tâches. Ainsi, des compromis sont sélectionnés à l'échelle évolutive, et il a été démontré que les meilleurs phénotypes sont des moyennes pondérées de phénotypes spécialisés pour une seule tâche, grâce au concept mathématique du front de Pareto (Shoval et al. 2012). Comprendre les variations interindividuelles des traits fonctionnels et les compromis écologiques associés offre des opportunités pour disséquer le fonctionnement des écosystèmes aquatiques et leur sensibilité aux changements globaux (Figure 6, Martini et al. 2021).

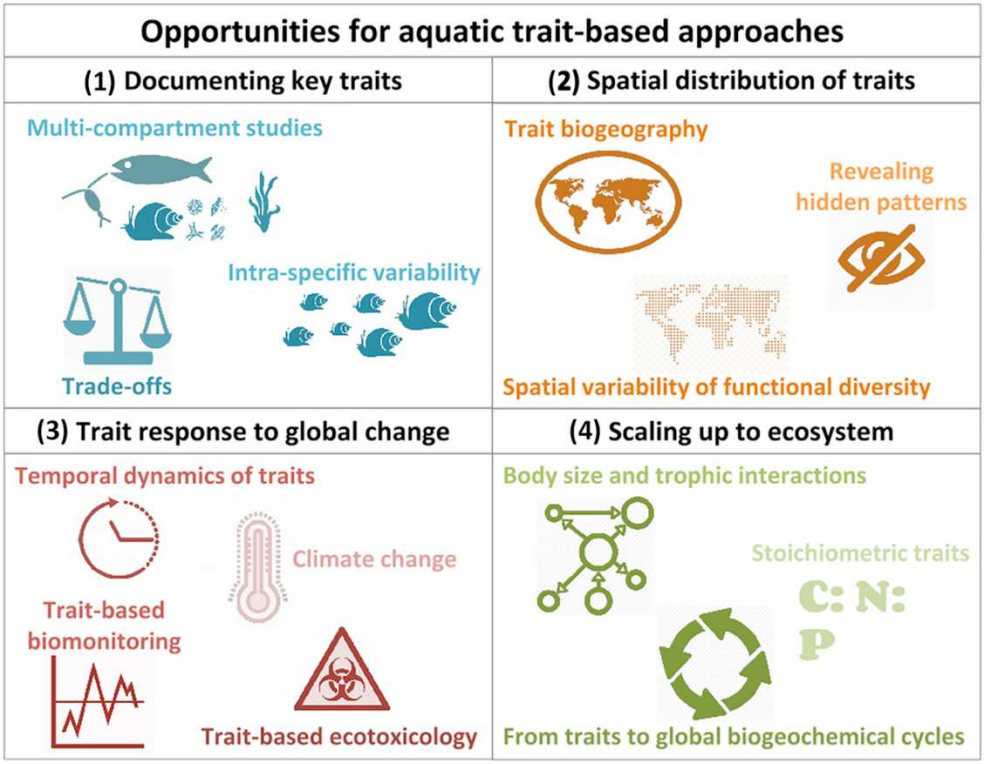

Figure 6. Principales opportunités apportées par les approches par traits fonctionnels en écologie aquatique, issue de Martini et al. (2021).

Chez le zooplancton et les copépodes en particulier, les traits fonctionnels les plus étudiés sont la taille (Fig. 7, rouge), les modes trophiques (Fig. 7, vert), le taux de production de pelotes fécales (Fig. 7, violet) et la capacité de migration verticale (Fig. 7, bleu). En appliquant une approche par traits pour les copépodes, il a été démontré, par exemple, que le type de stratégie d'alimentation (à l'affût = "*ambush feeding*" ou par création d'un courant = "*feeding-current feeding*") influence le risque de prédation vécu par un individu à cause des perturbations hydrodynamiques générées dans l'eau environnante (Kiørboe et al. 2018). Avec une étude de la distribution en taille des copépodes de l'Atlantique Nord, l'altération de l'export de carbone sur les 55 dernières années a également été mis en évidence (Brun et al. 2019). Une analyse exhaustive récente fait émerger 4 grandes régions

océaniques distinguant les copépodes selon leur taille, leur pourcentage de myélinisation, leur capacité à porter leurs œufs et leurs modes et stratégies d'alimentation (Benedetti et al. 2022). Selon cette même étude, les régions arctiques et subarctiques sont dominées par des copépodes de grande taille, majoritairement herbivores ou omnivores, ne portant pas leurs œufs dans des sacs ovigères, et se nourrissant par la création d'un courant d'eau pour l'interception des particules alimentaires (« *feeding-current feeders* »).

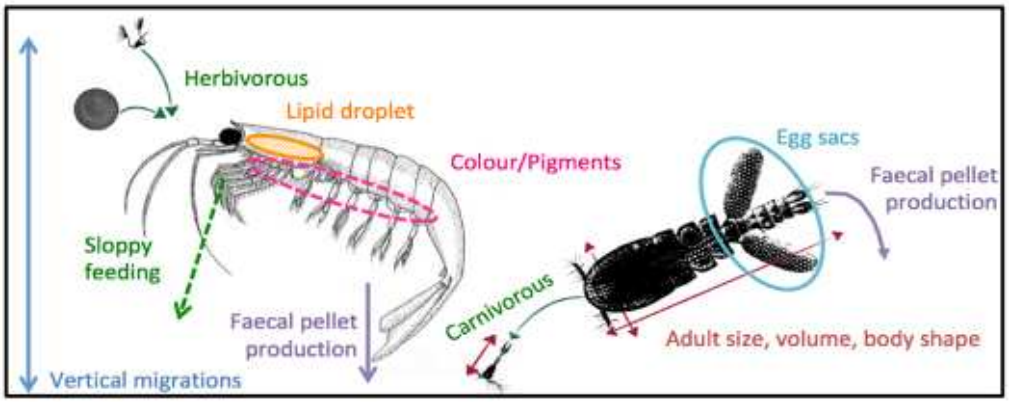

Figure 7. Illustration des traits du mesozooplancton, pour le krill (à gauche) et pour les copépodes (à droite). Figure de Sakina-Dorothée Ayata.

En résumé, les copépodes des hautes latitudes de l'hémisphère nord présentent une faible diversité taxonomique (Rombouts et al. 2009) avec la dominance de trois espèces du genre *Calanus* (Aarflot et al. 2018) qui possèdent des traits d'histoire de vie (diapause, reproduction) et des modes d'alimentation (herbivores, filtreurs) comparables (Benedetti et al. 2022). Les principales différences entre ces espèces concernent des caractéristiques morphologiques comme leur taille ou leur contenu lipidique essentiellement confiné à un organe de stockage très visible, le sac lipidique (Schmid et al. 2018; Renaud et al. 2018, Fig. 6 jaune). Dans cette thèse, nous allons nous intéresser à certains traits morphologiques et une intention particulière sera portée à la pigmentation (Fig. 7, rose) qui est largement ignorée dans les études écologiques passées sur le zooplancton arctique.

Des filets à l'imagerie : évolution des méthodes d'étude du plancton

Classiquement, le plancton est étudié après avoir été pêché par un filet à plancton dont la taille de la maille, la forme de l'ouverture, la vitesse et le mode de déploiement (verticalement, de façon oblique ou en surface) varient selon le type de plancton ciblé. Après avoir été pêché, un

échantillon de plancton est généralement fixé (avec du formaldéhyde ou de l'alcool). Au laboratoire, il est sous-échantillonné (avec une boîte de Motoda par exemple), puis observé au microscope ou à la loupe binoculaire dans le but de trier et de compter les espèces (Sameoto et al. 2000). Ces méthodes ont permis la découverte de la biodiversité planctonique et l'étude de leur écologie depuis plus d'un siècle (Dolan 2021). Néanmoins, cet outil de collecte présente des limitations inhérentes : 1) il abime ou détruit les organismes les plus fragiles, pourtant nombreux au sein du plancton ; 2) il intègre la biomasse des organismes sur un grand volume mais l'information de distribution verticale ou horizontale précise des organismes est perdue ; et 3) le temps de tri et d'analyse du plancton limite les dimensions spatiales et temporelles des études écologiques.

En réponse à ces biais et avec le développement technologique de l'imagerie, des systèmes d'imagerie du plancton sont apparus depuis une vingtaine d'années. Souvent, ils permettent à la fois de compter les particules et de produire des images du plancton vivant (Lombard et al. 2019, Orenstein et al. 2022, Giering et al. 2022). Il existe un grand nombre de systèmes d'imagerie qui varient selon les gammes de tailles étudiées et selon l'utilisation, qu'elle soit *in situ* (déployé dans l'eau) ou en laboratoire (après collecte de l'échantillon par d'autres moyens) (Figure 8).

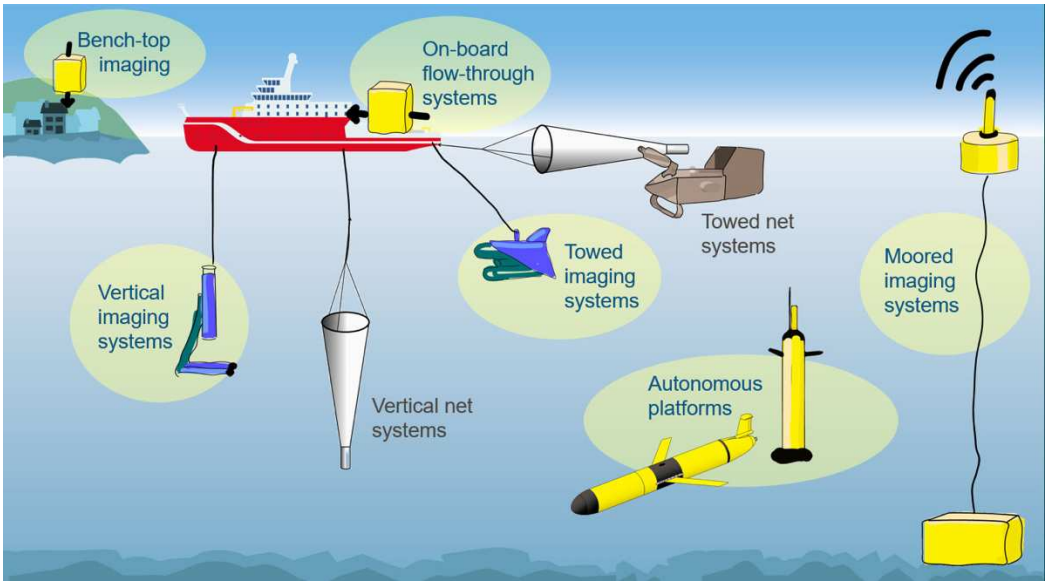

Figure 8. Les différents outils d'étude du plancton avec les instruments d'imagerie mis en évidence par les zones jaunes. Les systèmes d'imagerie installés sur des plates-formes autonomes et amarrées permettent une couverture globale en réduisant la dépendance vis-à-vis des navires. Figure issue de Giering et al. (2022).

Pour l'étude du microphytoplanton collecté dans des bouteilles, le FlowCAM ou l'IFCB peuvent être utilisés (Sosik & Olson 2007, Jakobsen & Carstensen 2011, Figure 9 a-h). Pour l'étude du micro- et méso-zooplankton après collecte par filet, le Zooscan (Gorsky et al. 2010) ou plus

récemment le Planktoscope (Pollina et al. 2022) sont disponibles (Figure 9h, r, i v). L'acquisition d'images i*n situ* est possible par l'ISIIS ou le Zooglider, qui sont des systèmes tractés scannant la colonne d'eau (Cowen & Guigand 2008, Ohman et al. 2019) (Figure 9q, z, δ, w, ɣ). Enfin, l'Underwater Vision Profiler (UVP) peut être déployé le long de profils verticaux sur une rosette en association avec les données environnementales des capteurs classiques, et sa version la plus récente peut être déployée sur des mouillages fixes, ou sur des flotteurs ARGO et des gliders (Picheral et al. 2010, 2022) (Figure 9j, k, l, m, x, α, β). Les avantages principaux de la plupart de ces imageurs sont leur capacité à être quantitatifs (le volume d'eau imagé est connu donc les concentrations des organismes peuvent être estimées) et la haute fréquence de l'acquisition d'images permettant d'obtenir des résolutions spatiales et temporelles fines (Greer et al. 2023). Les imageurs *in situ* sont aussi capables de photographier des organismes très fragiles comme les rhizaires ou les organismes gélatineux avec leurs extensions et tentacules (Figure 9α et ɣ) (Biard et al. 2016, Ohman 2019).

L'acquisition d'images à grande fréquence produit d'énormes volumes d'images (des dizaines de milliers par échantillonnage) définies comme des "marine big data" (Guidi et al. 2020, Irisson et al. 2022). L'analyse de ces grands jeux de données nécessite donc une automatisation. La plateforme web Ecotaxa développée au Laboratoire d'Océanographie de Villefranche-sur-Mer permet de stocker, visualiser et classifier des millions d'images. Les images peuvent être partagées facilement, en association avec une licence d'utilisation (https://ecotaxa.obs-vlfr.fr/, Picheral et al. 2017, Irisson et al. 2022). Même si tous les types d'image présentés sur la Figure 9 ci-dessus n'y sont pas encore transférables, le nombre exponentiel d'images stockées sur Ecotaxa illustre l'explosion de l'utilisation de l'imagerie au cours des 20 dernières années (Figure 10). Une classification automatique supervisée basée sur des forêts aléatoires (*random forest*) permet de classer automatiquement les taxons du mésozooplancton, accélérant le traitement de ces images. Le processus de classification est itératif, et à mesure que le jeu d'apprentissage grandit, la prédiction est de plus en plus performante. Cela reste un processus long, et d'autres initiatives de classification par clustering non-supervisé offrent une alternative efficace (comme Morphocluster, Schröder et al. 2020).

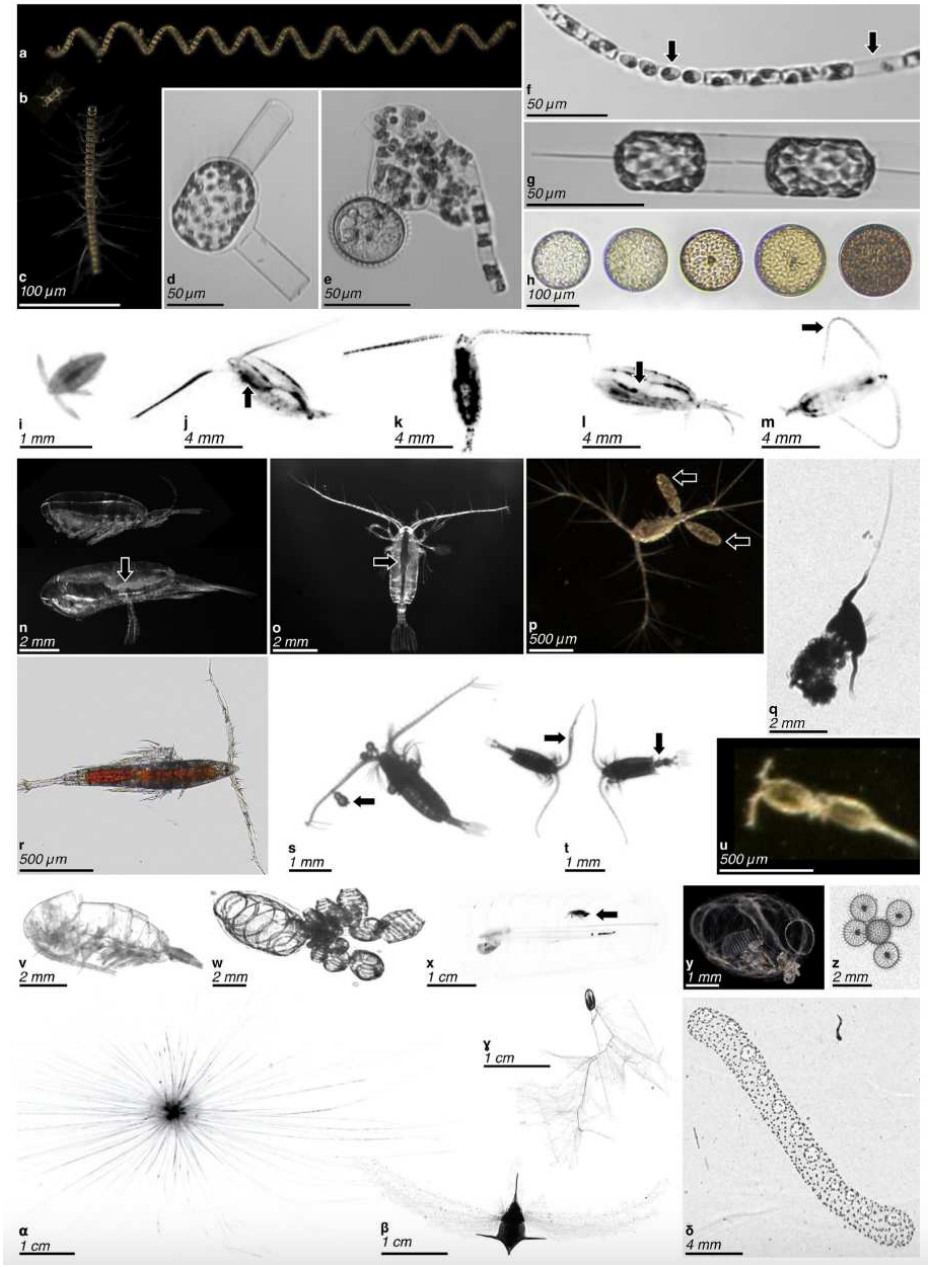

Figure 9. Exemples d'images de plancton de divers instruments, figure issue de Orenstein et al. (2022). Différents organismes : diatomées (a-h), copépodes (i-v), autres taxons (w-δ). Différents instruments : Scripps Pier Cam [SPC] (a, b, c, p, u, y); Imaging FlowCytobot [IFCB] (d, e, f, g); Planktoscope (h, r); ZooScan (i, v); Underwater Vision Profiler 5 [UVP5] (j, k, l, m, x, α, β); Lightframe On-sight Key species Investigation [LOKI] (n, o); ZooGlider; (q, z, δ); ZooCAM (s, t, v), ISIIS (w, ɣ). Cette légende est simplifiée, les détails se trouvent dans l'article original.

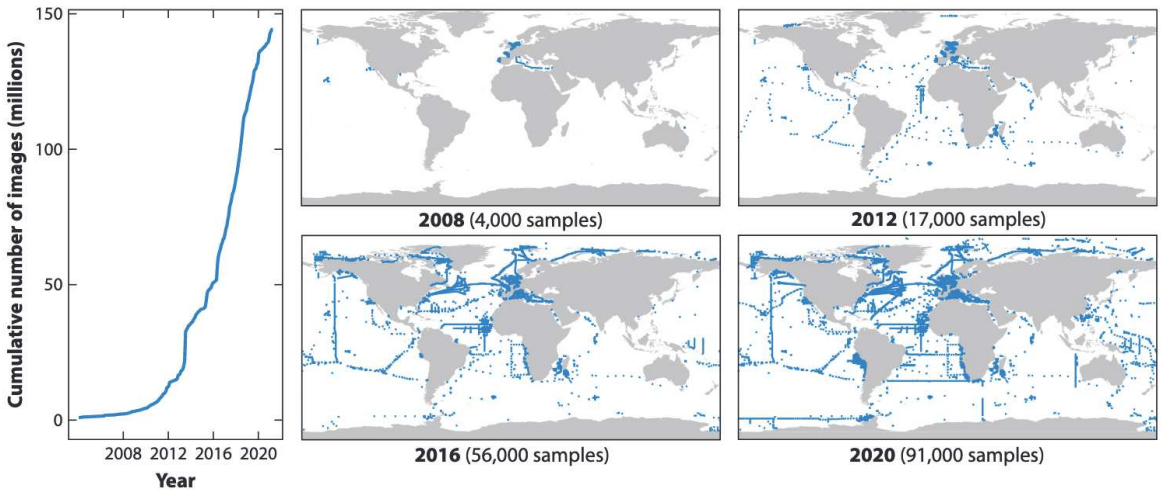

Figure 10. Accumulation au cours du temps de l'ensemble des images de plancton stockées sur la plateforme EcoTaxa (panneau de gauche), et position des zones d'échantillonnage associées (panneaux de droite). Les jeux de données ont été collectés par différents instruments (UVP, IFCB, FlowCam, ZooScan, ISIIS, etc. Abréviations détaillées dans la légende la figure 9) et transférées sur la plateforme par des utilisateurs de plus de 350 organisations. Figure issue de Irisson et al. (2022).

En écologie, les données d'imagerie associées aux techniques de classification automatique ont permis notamment de cartographier les grands groupes planctoniques à l'échelle globale (Lombard et al. 2019) et de mettre en évidence l'importance de groupes planctoniques fragiles sous-estimés (Biard et al. 2016). Avec ces progrès, les filets à plancton vont-ils être remplacés par des systèmes d'imagerie quantitative *in situ* ? Une étude récente a montré que les chercheurs étaient en accord pour dire que les imageurs du plancton sont des outils précieux qui apportent des avantages par rapport aux prélèvements par filet (Giering et al. 2022). Par contre, la confiance dans la capacité de l'apprentissage machine à classer taxonomiquement le plancton est assez faible, et diminue avec un niveau croissant d'expertise en taxonomie (Figure 11, Giering et al. 2022). Seul l'avis des experts les plus qualifiés en apprentissage machine est associé à un score de confiance plus élevé. Ces résultats s'expliquent probablement par la résolution limitante des images (certains détails taxonomiques ne sont pas visibles), et selon les auteurs, par la nécessité d'avoir des données contextuelles sur la présence d'un organisme pour mieux évaluer sa taxonomie. Une première conclusion est que les deux méthodologies semblent apporter des informations complémentaires sur les communautés planctoniques et pourraient être utilisées stratégiquement en combinaison. Une seconde conclusion est la nécessité d'un travail conjoint entre taxonomistes et informaticiens.

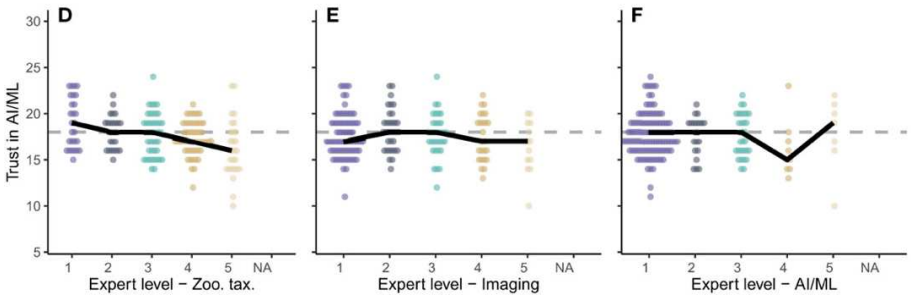

Figure 11. Confiance dans l'intelligence artificielle/apprentissage machine pour la classification du zooplancton en fonction de l'expertise. Niveau d'expertise (1-Novice, 5-Expert) : en taxonomie du zooplancton, en imagerie du zooplancton et en intelligence artificielle/apprentissage machine. Les points indiquent les scores individuels de chaque participant à l'enquête, des lignes noires pleines relient les médianes pour chaque niveau d'expertise. Portion d'une figure issue de Giering et al. (2022).

La capacité des algorithmes à classer automatiquement les images de plancton d'instruments quantitatifs reste donc limitante. Néanmoins, une image d'un organisme zooplanctonique n'est pas seulement l'image d'une espèce donnée. Chacune de ces images contient des informations morphologiques qui peuvent être utilisées afin de caractériser des traits fonctionnels morphologiques intéressants pour comprendre le fonctionnement des écosystèmes (Figure 5). Les techniques d'apprentissage machine et de vision par ordinateur sont idéales pour détecter, segmenter et quantifier des parties d'intérêt sur un individu (Figure 12, Orenstein et al. 2022). Certains traits sont directement mesurables sur les images (par ex. : taille, extensions cellulaires ou appendices, bioluminescence, réserves lipidiques, etc.) et d'autres peuvent être inférés par interprétation de la présence de certaines structures ou en complément de métadonnées environnementales (par ex. : biovolume, taux métabolique, stratégies de reproduction et de dormance, etc.) (Orenstein et al. 2022).

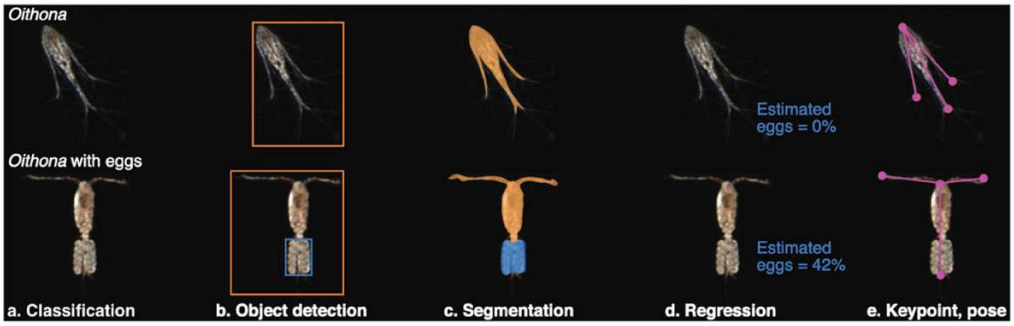

Figure 12. Exemples de différentes techniques pour l'extraction de traits sur des images de zooplancton. Une photo de copépode portant des œufs (Scripps Plankton Camera) est utilisée pour illustrer la classification sémantique (a), la détection d'un objet (b), la segmentation ou la régression pour identifier les sacs d'œufs (c, d), et l'estimation de la pose pour estimer l'orientation et l'extension des appendices d'un individu (e). Figure issue de Orenstein et al. (2022).

La problématique de cette thèse s'inscrit dans ce cadre, et propose de chercher des traits fonctionnels morphologiques d'intérêt sur des images de copépodes arctiques et subarctiques afin de répondre aux questions suivantes :

1. Comment varient les traits morphologiques des copépodes (particulièrement les *Calanus* spp.) selon les conditions environnementales des régions arctiques et subarctiques (saisonnalité, dynamiques de glace, etc.) ?
2. Que nous disent les variations de ces traits sur le fonctionnement des réseaux trophiques de ces régions ?
3. Une question méthodologique précède nécessairement ces deux problématiques écologiques : comment identifier automatiquement et objectivement des traits fonctionnels sur des images de copépodes, en particulier à partir de celles issues de loupes binoculaires encore couramment utilisées en écologie planctonique ?

Données d'imagerie et objectifs des trois chapitres de thèse

Deux types d'images de copépodes provenant de régions arctiques seront utilisées pour répondre à la problématique de recherche : des images *in situ* prises par l'Underwater Vision Profiler (Picheral et al. 2010) et des photographies à haute résolution prises par observation à la loupe binoculaire après collecte par filet (Trudnowska et al. 2022). Ces deux types d'images présentent des caractéristiques contrastées en termes de fréquence d'acquisition, de résolution et de couleur (Table 1) et apportent donc des informations complémentaires sur les traits morphologiques détectables et le contexte écologique.

D'une part, les copépodes *Calanus* observés à la loupe binoculaire sont pris en photo depuis des dizaines d'années dans les régions arctiques et subarctiques. En haute résolution et en couleur, ces images permettent une identification taxonomique à l'espèce des individus. Elles rendent aussi possible la mesure de la taille et de la surface des sacs lipidiques grâce à des logiciels d'annotation manuelle comme ImageJ (Maps et al. 2010, Vogedes et al. 2010, Trudnowska et al. 2020). Dans le cadre du projet CARDINAL qui finance ce projet de doctorat, une liste non-exhaustive d'images a été identifiée : ~1 500 images de copépodes des eaux norvégiennes, >10 000 provenant de l'archipel du Svalbard, >7 000 venant du Golfe du St-Laurent (Basedow et al. 2019, Trudnowska et al. 2020, Blais 2021). Les analyses numériques et automatiques de ces images offrent donc des perspectives d'études écologiques pour le futur, mais sont également un moyen de revisiter le passé en analysant des collections historiques d'images.

Table 1. Comparaison technique des images prises par l'Underwater Vision Profiler (UVP) et par un appareil photographique reflex d'une observation au stéréo-microscope. Les avantages et désavantages des méthodes sont surlignés en vert et en rouge, respectivement.

Images de l'Underwater Vision Profiler (UVP)	**Images d'observation à la loupe binoculaire après échantillonnage au filet**
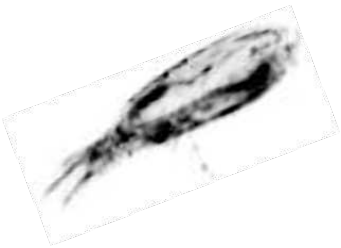	
Acquisition automatique à haute fréquence 1 image/5 cm (20Hz)	Acquisition non automatique photographies manuelles
In situ profondeur précise, organismes vivant	*Ex situ* profondeur exacte indisponible, organisme non vivant
Fréquence d'acquisition haute dizaines de milliers d'images	Fréquence d'acquisition intermédiaire quelques centaines d'images
Intercalibration toutes les images sont comparables	Intercalibration la luminosité et la résolution peuvent varier
Résolution 1 pixel = 86µm (Kiko et al. 2022)	Résolution 1 pixel ~ 2µm (Trudnowska et al. 2020)
Couleur noir et blanc	Couleur 3 canaux Rouge, Vert, Bleu (RGB)

D'autre part, l'Underwater Vision Profiler (UVP) est un système d'imagerie quantitative développé au Laboratoire d'Océanographie de Villefranche-sur-Mer et dont les deux dernières versions sont très utilisées à travers le monde (UVP5 : Picheral et al. 2010, UVP6 : Picheral et al. 2022). L'instrument peut acquérir plus d'un millier d'images du mésozooplancton (0.7mm à quelques centimètres) le long de profils verticaux allant jusqu'à 6 000 m de profondeur. Comme l'UVP peut

être déployé sur une rosette-CTD, il est possible d'obtenir des images inter-calibrées des organismes vivants au sein de leur milieu naturel, et en association avec les données physico-chimiques environnantes. Des UVP sont régulièrement déployés en arctique par des équipes canadiennes, polonaises, allemandes et norvégiennes et cet instrument est particulièrement adéquat pour l'étude de la morphologie des *Calanus* de grande taille qui sont bien définis sur les images.

Dans le cadre du Chapitre 1, environ 28 000 images de copépodes prises par l'Underwater Vision Profiler dans les 100 premiers mètres des eaux arctiques canadiennes pendant la campagne GreenEdge au printemps-été 2016 sont utilisées. Les images ont été récupérées à plus de 150 stations réparties autour de la lisière de glace, et permettent d'aborder 3 questions de recherche : 1) Quels traits peut-on quantifier objectivement sur des images individuelles de copépodes prises *in situ* ? 2) Peut-on détecter l'influence des dynamiques spatio-temporelles de la glace de mer et de la distribution des masses sur la distribution de ces traits ? 3) Quelles sont les implications écologiques de telles variations ? Ce chapitre nous permettra de définir trois traits d'intérêt expliquant le maximum de variations morphologiques sur les images UVP, puis de les cartographier à l'échelle d'une baie arctique et de son couvert de glace. Nous verrons que les variations d'opacité (et donc de structures colorées) sont très visibles sur les images UVP et ont soulevé des questionnements sur les raisons de ces variations. En comparant les images aux observations de copépodes *Calanus* à la loupe binoculaire (Table 1), il est possible de noter que les variations d'opacités sont souvent reliées aux variations de leur pigmentation rouge, répartie dans leurs antennes, à la base de leurs péréiopodes, à l'extrémité postérieure de leur sac lipidique et dans leur segment génital. La pigmentation est généralement peu étudiée chez le zooplancton, mais a commencé à être décrite dans les milieux d'eau douce (Hairston 1976, 1979, Hansson 2004, Schneider et al. 2016) et elle est attribuée à des pigments caroténoïdes (Matsuno 2001). Au sujet des copépodes *Calanus* des régions (sub)arctiques pourtant très pigmentés, les travaux sont très rares et concernent surtout l'utilisation de la pigmentation comme un moyen de distinguer les deux espèces *C. finmarchicus* et *C. glacialis*, qui se partagent souvent les mêmes niches écologiques (Nielsen et al. 2014, Choquet et al. 2018, Lindeque et al. 2022). D'un point de vue écologique, deux études ont essayé de faire un lien entre la pigmentation et le stress lumineux en marge de glace à l'ouest du Groenland (Hylander et al. 2015), et entre la pigmentation et les caractéristiques des masses d'eaux atlantiques et arctiques dans le détroit de Fram (Trudnowska et al. 2020). Ces initiatives sont intéressantes mais offrent des réponses encore très partielles sur les raisons des variations de la pigmentation chez ces organismes.

Pour toutes ces raisons, le Chapitre 2 utilise une approche basée sur les traits fonctionnels pour mieux comprendre les enjeux écologiques liés à la pigmentation des copépodes à l'échelle globale, qui permettra ensuite de retourner au cas d'étude des copépodes arctiques et subarctiques.

Une revue de littérature a été réalisée, rassemblant des données de milieux d'eaux douces et d'écosystèmes marins des latitudes tropicales et tempérées. Les questions de recherches associées sont : 1) Est-ce que la pigmentation caroténoïde est un trait fonctionnel commun chez les copépodes ? Quels sont les forçages biotiques et abiotiques qui l'influencent ? 3) Quels avantages écologiques peuvent apporter les pigments rouges et bleus sur le succès écologique des individus ? Nous essayerons de démontrer que la couleur est un trait déterminant pour le succès écologique de nombreuses espèces de copépodes, et qu'elle peut impacter le fonctionnement des réseaux trophiques pélagiques.

Le Chapitre 3 a pour objectif de produire un indice permettant d'estimer la pigmentation caroténoïde à partir d'images de copépodes *Calanus* photographiés sous la loupe binoculaire. Une méthode automatique est développée pour segmenter et quantifier la couleur induite par les pigments caroténoïdes sur 699 images de copépodes collectés entre le Groenland et l'archipel du Svalbard. Les copépodes présentent des quantités de pigmentation variable et les images sont associées à des quantifications chimiques par chromatographie liquide à haute performance (HPLC, (Stoń-Egiert & Kosakowska 2005). Nous pourrons donc répondre à cette question de recherche : est-ce qu'il est possible de produire un indice de pigmentation à partir d'images, qui soit cohérent avec les quantifications chimiques classiques des pigments ? L'objectif final de la méthode est d'avoir un indice efficace et rapide pour mesurer ce trait fonctionnel sur un ensemble d'images historiques et futures. Un tel indice sera utile pour poursuivre les pistes de recherche soulevées par le Chapitre 2 sur les enjeux écologiques de la pigmentation carotenoïde chez les copépodes, de l'échelle moléculaire à celle de l'écosystème.

1. Trait-based approach using *in situ* copepod images reveals contrasting ecological patterns across an Arctic ice melt zone

1.1. Résumé

Les techniques d'imagerie sont de plus en plus utilisées dans les études en écologie, et produisent des quantités croissantes de données. La quantification de traits fonctionnels à partir d'images d'individus peut fournir des informations originales sur les processus écosystémiques. Comme les autres traits fonctionnels, les traits morphologiques sont des caractéristiques individuelles influençant le succès écologique d'un organisme. Nous avons mesuré ces caractéristiques sur des images *in situ*, pour étudier une communauté de zooplancton arctique au moment de la fonte printanière de la banquise. Des descripteurs morphologiques (*e.g.,* l'aire, les niveaux de gris, la complexité de l'objet) ont été déterminés automatiquement sur ~28 000 images individuelles de copépodes provenant d'une caméra sous-marine haute résolution déployée à plus de 150 sites d'échantillonnage à travers la lisière de glace. Un espace morphologique défini statistiquement a permis de synthétiser les informations morphologiques en trois traits interprétables et continus (taille, opacité et visibilité des appendices). Cette nouvelle approche offre des avantages théoriques et méthodologiques car elle donne accès à la variabilité inter et intra-spécifique, tout en analysant automatiquement un grand nombre d'images individuelles. La distribution spatiale des traits morphologiques a révélé que les grands copépodes étaient présents sous le couvert de glace, tandis que les eaux libres accueillent des individus plus petits. Dans ces eaux libres de glace, les copépodes semblent également se nourrir plus activement, comme le suggère la plus grande visibilité de leurs appendices. La distribution de ces traits s'explique probablement par un contrôle *bottom-up* : les concentrations élevées de phytoplancton dans les eaux libres et lumineuses encouragent les individus à se nourrir activement et stimulent le développement des jeunes stades de copépodes de petite taille. De plus, les copépodes situés à la lisière de la glace étaient plus opaques, vraisemblablement en raison de leur contenu digestif ou d'une forte pigmentation rouge. L'utilisation d'une analyse de traits morphologiques a permis de révéler des signaux écologiques qui auraient été inaccessibles autrement, comme des variations de couleur et de posture, chez des copépodes vivant en lisière de glace dans un écosystème arctique.

1.2. Abstract

Imaging techniques are increasingly used in ecology studies, producing vast quantities of data. Inferring functional traits from individual images can provide original insights on ecosystem processes. Morphological traits are, as other functional traits, individual characteristics influencing an organism's fitness. We measured them from in situ image data to study an Arctic zooplankton community during sea ice break-up. Morphological descriptors (e.g., area, lightness, complexity) were automatically measured on ~ 28,000 individual copepod images from a high-resolution underwater camera deployed at more than 150 sampling sites across the ice-edge. A statistically-defined morphological space allowed synthesizing morphological information into interpretable and continuous traits (size, opacity, and appendages visibility). This novel approach provides theoretical and methodological advantages because it gives access to both inter- and intra-specific variability by automatically analyzing a large dataset of individual images. The spatial distribution of morphological traits revealed that large copepods are associated with ice-covered waters, while open waters host smaller individuals. In those ice-free waters, copepods also seem to feed more actively, as suggested by the increased visibility of their appendages. These traits distributions are likely explained by bottom-up control: high phytoplankton concentrations in the well-lit open waters encourages individuals to actively feed and stimulates the development of small copepod stages. Furthermore, copepods located at the ice edge were opaquer, presumably because of full guts or an increase in red pigmentation. Our morphological trait-based approach revealed ecological patterns that would have been inaccessible otherwise, including color and posture variations of copepods associated with ice-edge environments in Arctic ecosystems.

1.3. Introduction

Functional traits are any features—morphological, physiological, etc—measurable at the individual-level and affecting the fitness of the organism (Violle et al. 2007). They can be classified according to the ecological function that they influence, such as feeding, growth, reproduction, and survival (Litchman et al. 2013). Trait-based approaches appeared in plant ecology in the 70s (Grime 1974) and started being used by aquatic ecologists in the early 2000s (Willby et al. 2000; Usseglio-Polatera et al. 2000; Benedetti et al. 2016; Martini et al. 2021). Trait-based analyses are relevant in community ecology because an individual's set of traits given environment determines its success (Violle et al. 2007). Ecological interactions (predation, mutualism, etc.) happen between individuals, not between taxonomic groups. Therefore, using trait composition can simplify the analysis of

ecosystem complexity by focusing on a few characteristics transcending taxonomic distinctions and impacting ecological strategies (Litchman et al. 2013). By studying the composition and distribution of individual traits in an ecosystem, its structure and dominant processes can emerge from individual properties (Kiørboe et al. 2018). In zooplankton communities, for example, body length can influence secondary productivity and feeding mode can modify nutrients and energy transfers (Hébert et al. 2017).

Brun et al. (2019) demonstrated that over the past 55 years, climate change has altered zooplankton-fueled carbon export by changing the distribution of large-bodied individuals. Their study quantitatively linked shifts in individual properties (body size) and ecosystem functioning (carbon cycling). It shows how modulation in trait composition due to anthropogenic or natural perturbations could impact the ability of ecosystems to provide goods and services to human societies (Mouillot et al. 2013). More generally, trait-based approaches represent a way to focus on continuous, quantitative descriptors of fitness components (size spectrum, feeding intensity, etc.) rather than a set of discrete species; these metrics can more easily highlight subtle gradients and rates of change. As recommended by McGill et al. (2006), with functional trait measurements ecology can move from research questions centered around "How many species and why?" to ones focused on "How much variation in traits and why?"

Our study aims to answer the latter question for the copepod community during ice break up in an Arctic environment using a statistical description of body shapes ("morphometrics", Caillon et al. 2018). Sea ice melt is the primary driver of the spring phytoplankton bloom (Perrette et al. 2011). This intense pulse of primary production is partly captured by zooplankton that convert it into energy-rich lipid stores, fueling the whole trophic network all year long (Berge et al. 2012). In Arctic environments, zooplankton communities are dominated by only a few copepod species. Many of them share ecological characteristics, like feeding mode and ontogenetic migration, while presenting a continuum of morphological traits, such as size or lipid content, which are key drivers of ecosystem functioning (Schmid et al. 2018; Renaud et al. 2018). As a hub of matter and energy, these copepods hold a key trophic position in arctic ecosystems and have a crucial role in the oceanic carbon pump because of their vertical migrations (Falk-Petersen et al. 2009; Turner 2015). By studying copepods with trait-based approaches, we aim to reveal new aspects of ecological processes occurring during the phytoplankton ice-edge spring bloom.

To achieve this objective, we sought to quantify individual traits of copepods. A powerful way to capture such traits is by analyzing *in situ* images (Picheral et al. 2010; Schmid et al. 2016). Modern devices can image thousands of individuals in their immediate environment while simultaneously measuring physical and biological variables like temperature or fluorescence.

Morphological traits that bear on ecological functions can be directly measured from each individual, yielding quantitative information on anatomical aspects (size, shape or transparency), and allowing to infer physiological or behavioral status (*e.g.*, presence of lipid stores, prey encounter rate through the volume occupied by tentacles of cnidarian; Schmid et al. 2018; Ohman et al. 2019). Indeed, morphological approaches have been shown to be an objective and practical way of explaining patterns of functional variability, in phytoplankton and fishes (Kruk et al. 2010; Caillon et al. 2018). We hypothesize that traits of copepods will vary between the eastern and western sides of Baffin Bay as a function of water mass properties and seasonality in the surface layer. To assess the environmental influence on copepod trait distribution, we will answer the following questions: (1) Which traits can be objectively quantified on individual copepods from *in situ* images? (2) Can we detect the influence of the spatio-temporal dynamics of ice melt and water mass properties on trait distribution? (3) What are the ecological implications of such variations?

1.4. Material and methods

1. 4. 1 GreenEdge expedition in Baffin Bay

We collected image data in Baffin Bay, a marginal Arctic sea located between Greenland and Canada, that is characterized by typical pan-Arctic environmental gradients (Tang et al. 2004). Water masses in the east and west of the bay have different origins and properties, creating strong gradients and influencing sea-ice formation and melt (Fig. 1.1). The Bay is particularly sensitive to climate change, with significant warming of Atlantic waters and freshening of Arctic waters measured between 1916 and 2003 (Zweng and Münchow 2006). The GreenEdge campaign took place aboard the CCGS Amundsen in June and July 2016. The cruise's main objective was to study the fate of organic matter newly produced during the transition period of ice break-up in spring/summer. The 163 sampling stations considered in this study were distributed along seven longitudinal transects crossing the ice edge (Fig. 1.1). Baffin Bay is covered by sea ice most of the year, except in August and September. In 2016, sea ice started to melt around the 10th of June in the sampling area and progressively disappeared, from east to west, at a rate of about 3.5 km d^{-1} (Randelhoff et al. 2019). As soon as snow on sea ice melts, and melt ponds form, the penetration of light allows for the start of primary production underneath it (Fortier et al. 2002; Arrigo et al. 2014; Oziel et al. 2019). Phytoplankton blooms generally develop a few days before (under sea ice) or after (in open waters) breakup (Randelhoff et al. 2019; Oziel et al. 2019). The sea ice gradually melted from east to west, illustrated by the strong east/west ice gradient along the three southern transects. However, by the time the ship navigated along transects, the three northern ones became almost ice-free (Fig. 1.1).

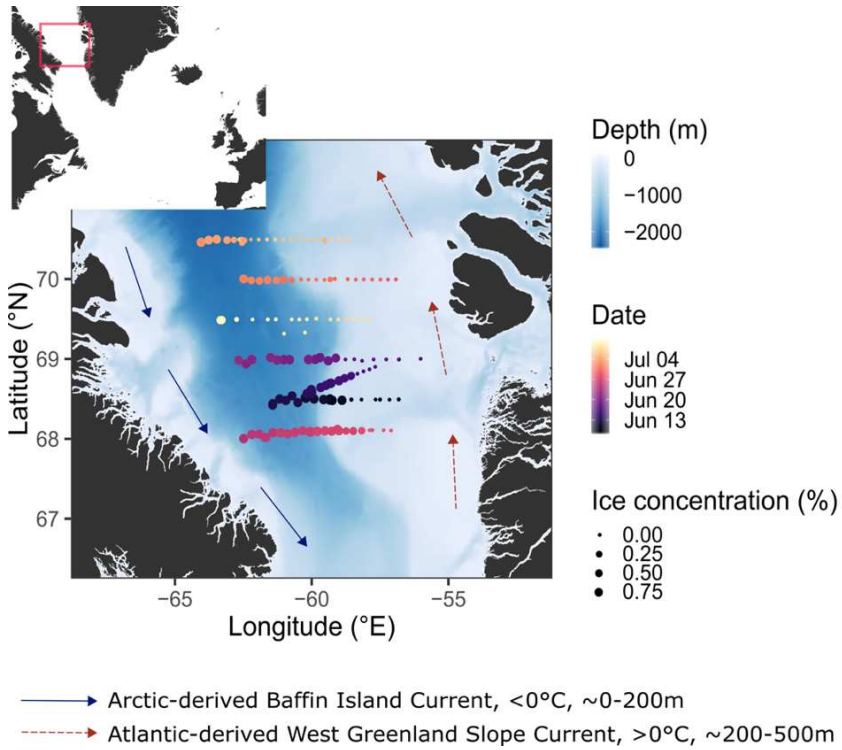

Figure 1.1. Sampling map of the GreenEdge cruise across the ice edge in Baffin Bay. Baffin Bay is a marginal Arctic Sea where the southward-flowing Baffin current carries cold, low salinity waters (blue arrows). The northward-flowing West Greenland Slope Current carries warmer and saltier water originating in the Atlantic (red arrows). Each point on the map is a station colored according to the sampling date (between the 9th of June and the 10th of July) and of size proportional to the concentration of sea ice at the time of sampling.

1. 4. 2 Sampling

In situ high-resolution imaging system: UVP5

The 5th version of the Underwater Vision Profiler (UVP5) was developed to image marine snow and zooplankton *in situ* and quantify their vertical distribution (Picheral et al. 2010). In the present study, it was mounted on the CTD-rosette so each image is associated with the environmental variables at coincident sampling locations. The UVP5 was set to acquire images at a frequency of 20 Hz which yields a typical sampling rate of 22.1 ± 9 images/m (~1 image every 5 cm). Each 22×18×0.35 cm image sampled a 1.02 liter volume of seawater, with a resolution of 0.088 mm pixel^{-1}. The on-board computer automatically segmented and saved objects with an Equivalent Spherical Diameter (ESD) > 850 µm. Morphological descriptors (size, gray level distribution, etc.) were calculated for each object/individual in postprocessing with the ZooProcess software (Gorsky et al. 2010). Images, their metadata, and morphological descriptors were stored in the EcoTaxa web

application (https://ecotaxa.obs-vlfr.fr/; Picheral et al. 2017). Morphological descriptors were used to train a random forest algorithm (Breiman 2001) that suggested a taxonomic classification for each object, which was then validated or corrected by a human annotator (the same user sorted 85% of the data but 9 others contributed). 1.2 M images were classified into 36 final categories (Table A.1). Of these 1.2 M images, detritus, "badfocus" and fibers accounted for 96% of the data and are not considered here. The remain data is comprised of living organisms (45,883 images), of which 83% were copepods. We kept only copepod images taken in the surface layer described hereafter, where they accounted for more than 90% of organisms.

Environmental data

An instrument package containing a Conductivity-Temperature-Depth profiler (CTD, Seabird SBE-911), a Seapoint SCF fluorimeter, an oxygen optode (Seabird, SBE 43) and a nitrate sensor (Satlantic, MBARI-ISUS) was deployed at each station to measure temperature (°C), potential temperature (°C), salinity (PSU), potential density ($kg.m^{-3}$), dissolved oxygen concentration ($ml.L^{-1}$), nitrate concentration ($mmol.m^{-3}$), and chlorophyll a (Chl a) concentration ($mg.m^{-3}$, estimated by fluorescence) (Lévesque et al., 2015; Bruyant et al. 2022). Profile deepest points range between 117 and 2130 m, with a median depth of 360 m. All profiles were averaged at 1 m bin intervals to reduce noise. Spurious outliers were detected as anomalies to a moving median and removed. Missing values were inferred through an iterative Principal Component Analysis (Josse and Husson 2012). Several variables describing the structure of the water column were derived from each profile: pycnocline depth (depth of the maximum of the standard deviation of the potential density, calculated on a centered and weighted moving window of 41 m along the profile), stratification index (difference between the average value of the surface density at 2–5 m and at 40–50 m). At each station, 8–10 Niskin bottles collected water for phytoplanktonic pigment analysis. Sample depths were typically every 5 m between 0 and 30 m, and every 10 m between 30 and 100 m, though there was some minor variation between profiles. Pigments were extracted immediately after sampling, preserved, and quantified via High Performance Liquid Chromatography (HPLC) according to Ras et al. (2008). The depth of the sub-surface Chl *a* maximum (SCM) was then estimated from the HPLC data. Finally, we used ice concentration estimates derived from the AMSR2 satellite sensor data on a 3.125 km grid for each station location between 2016/03/01 and 2016/07/14 (Beitsch et al. 2014; Kaleschke and Tian-Kunze 2016).

We focused our study on the upper water column because (1) ice melt will mostly influence surface waters, (2) algal bloom occur in surface waters, (3) copepods are mostly located close to the surface to feed in the spring/summer period (Williams and Poulet 1986; Helaouët and Beaugrand

2007). To define a surface layer with homogenous planktonic communities despite variable environmental conditions, we first used the temperature profiles (that showed the sharper variations, see Fig. A.1) to vertically segmented the water column into six layers: warm surface layer, transition layer, cold intermediate layer, deep thermocline layer, deep cooling layer and deep stable layer (Fig. A.1 for more details). Then, a PCA was performed on all planktonic densities obtained from UVP images in each layer to characterize the organismal distribution in the water column. Copepods were dominant close to the surface and were mainly associated with the three upper layers: warm, transition and cold intermediate layers (Fig. A.1). Consequently, these layers were merged to define an ecologically coherent surface layer whose bottom is the depth of the cold intermediate layer; the deepest point where the temperature is 0.3°C warmer than the minimum of the profile. This surface layer has a mean depth of 101.7 m (min = 52 m, max = 227 m) and is systematically deeper in the Arctic-influenced and ice-covered part of the Bay. Finally, this layer always contains the sub-surface Chl *a* maximum.

1. 4. 3 Numerical analysis

Environmental gradients

To describe the physical and biogeochemical conditions in the surface layer, we carried out a PCA (Legendre and Legendre 2012) on: (1) temperature, salinity, oxygen, nitrate and Chl *a* concentration averaged in the surface layer, (2) the variables derived to describe the structure of the water column (stratification index, pycnocline depth, sub-surface Chl *a* maximum (SCM) depth), (3) ice concentration (at the time of sampling and averaged over the cruise period), and (4) Open Water Days (OWD). OWD is the number of days a location has been free of ice (positive values) or, conversely how many days until the location thaws (negative values) (Randelhoff et al. 2019). After the PCA, the 163 stations were clustered by hierarchical classification carried out on the coordinates on the first three principal components, using a Euclidean distance and a synoptic Ward linkage (Murtagh and Legendre 2014). A threshold was set based on the aspect of the tree, hence defining groups of stations within which the aforementioned variables were homogeneous.

Construction of a multivariate morphological space from zooplankton images

To summarize the morphological characteristics of each object captured by the UVP, a morphological space was defined by performing a PCA on a selection of morphological descriptors (Table A.2). The number of metrics for each trait were limited to 3–5 descriptors by removing correlated descriptors to avoid over-representing any particular aspect. All ~ 28,000 copepods images located in the surface layer were used to construct this multivariate space. The descriptors were

normalized by the Box-Cox transformation (Asar et al. 2017) to satisfy the conditions for PCA application. Axes were considered significant only if their associated eigenvalue was greater than the average of all the eigenvalues (Kaiser-Guttman criterion; Cattell 1966). The position of each plankton image in the space is thus a function of its morphology. To ease interpretation of the axes, example images were mapped to their position in the morphological space as follows: for each pair of principal components (i.e., PC1 vs PC2 or PC3 vs PC4) a grid was defined and eight images were randomly chosen and superposed at each node of the grid. The coordinates of this reduced morphological space (taking into account only the significant axes) are then used as synthetic, highly informative morphological traits for further analysis.

Traits and environmental gradients

To interpret variations of morphological traits along environmental gradients, objects coordinates on significant PC axes were averaged by station in the surface layer. Variations of traits in space were statistically interpolated by kriging. As each station belongs to one environmental cluster, it was also possible to compare values of traits between environmental clusters using a box plot representation, ANOVA and post-hoc statistical tests.

Numerical tools

All statistical analyses were conducted in the programming environment R 3.5.3 (R Core Team 2019). The package *castr* was used to clean vertical environmental profiles (https://github.com/jiho/castr), car for Box-Cox transformation (Weisberg and Fox 2018), *FactoMineR* (Lê et al. 2008) and vegan (Oksanen et al. 2007) for multivariate analysis, *tidyverse* (Wickham et al. 2019) for data manipulations and graphics, *morphr* (https://github.com/jiho/morphr) for images representation in the morphological space and finally *gstats* (Pebesma 2004) and *fields* (Nychka et al. 2017) for statistical interpolations. All data (including images) and codes are available online in Supporting Information of the article (doi: 10.1002/lno.11672).

1.5. Results

1. 5. 1 Environmental gradients and seasonality

The first PCA on environmental variables revealed that PC1 is mostly structured by mean ice concentration, mean temperature and Open Water Days (Fig. 1.2). It separates cold, ice-covered waters to the west and warmer open waters to the east. PC2 has large, opposing contributions from pycnocline depth and stratification index, highlighting stations that are strongly stratified by the recent ice melt. Together, the principal components yielded three distinct clusters of stations. Stations from the western, ice-covered, cluster are strongly influenced by the Baffin Current; nitrate concentration is high (> 8 mmol m−3) and Chl *a* concentration is low. Stations from the eastern side, in open waters, are influenced by the relatively saltier and warmer Atlantic Current. At these stations, phytoplankton are abundant (high mean Chl *a* concentrations), the depth of the sub-surface Chl *a* maximum (SCM) increases from west to east (25–60 m), and nitrate concentration is relatively low indicating that the bloom is ending. The third cluster includes stations where ice has recently melted and are geographically spread along a central zone in the bay, larger on northern transects because of the timing of sampling (cf. Fig. 1.1). They are characterized by intermediate values of temperature, Chl *a*, and nitrate concentrations and a shallow Chl *a* maximum: the bloom is just starting, close to the surface.

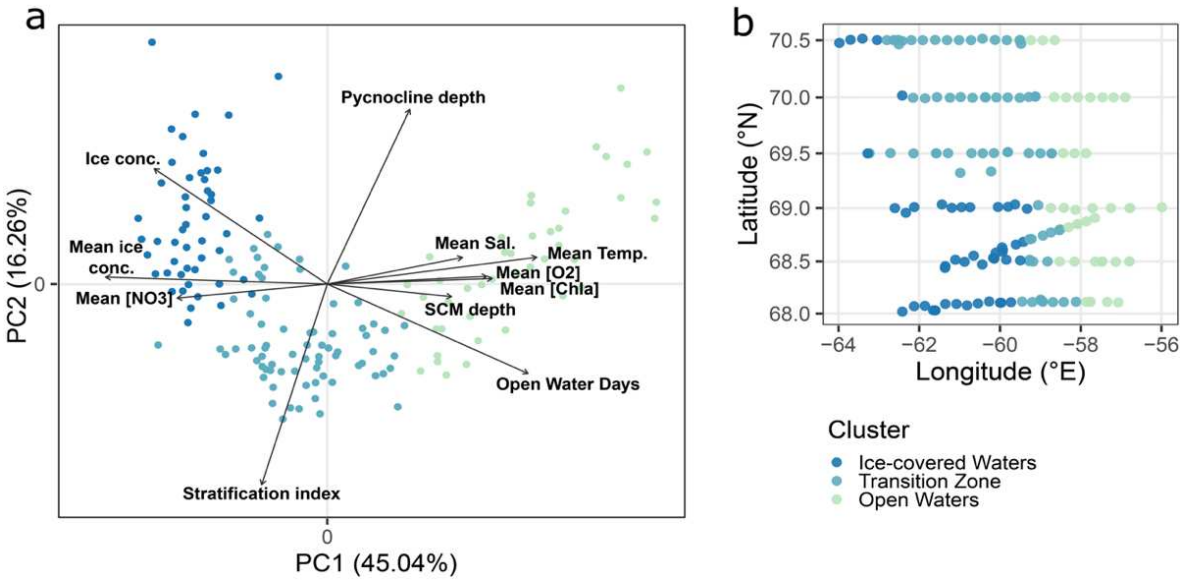

Figure 1.2. Principal component analysis performed on environmental variables and clustering of stations. Coordinates of stations on the first three PCA axes were used for clustering (Euclidian distance, Ward method). Color indicates cluster membership in both PCA space (a) and Baffin Bay (b).

1. 5. 2 Multivariate morphological space from zooplankton images

There were four significant axes describing the morphological space (Fig. 1.3). We assigned names to these four Principal Components to aid interpretation. We summarize the biological meaning of the various descriptors combined into one PC and define synthetic morphological traits. PC4, for example, broadly describes "complexity of shape/visibility of append- ages" (Fig. 1.3b): bilateral symmetry is enhanced by visible antennae; circularity is higher when the prosome shape is not altered by visible appendages; gray levels variations are more important if there is contrast between the body and append- ages; and so on. Image descriptors related to the organisms' size (e.g. major axis length, perimeter, area) contribute to PC1 and explain 36.4% of the variance (Fig. 1.3a). PC2 explains 25.9% of variance and is influenced by the opacity - how dark they appear in UVP images - of organisms. PC3 (16.9% of variance) quantifies the elongation of the organisms (Fig. 1.3b). Finally, PC4 (9.7% of variance) was interpreted as the visibility of appendages, as explained above. In our dataset, variations of elongation (PC3) can be explained by copepods' orientation variability on images. A copepod imaged laterally or dorsally will appear longer (PC3 > 0) than a one seen from the front or the back (PC3 < 0). Although PC3 describes variations that are important within the dataset, we can make the reasonable assumption that orientation of individuals is either random or slightly, but consistently, biased by the nominal flow generated by the UVP while sampling the water column. We will thus ignore PC3 for further analyses as there is no reason to link orientation relative to the camera with a specific ecological interpretation.

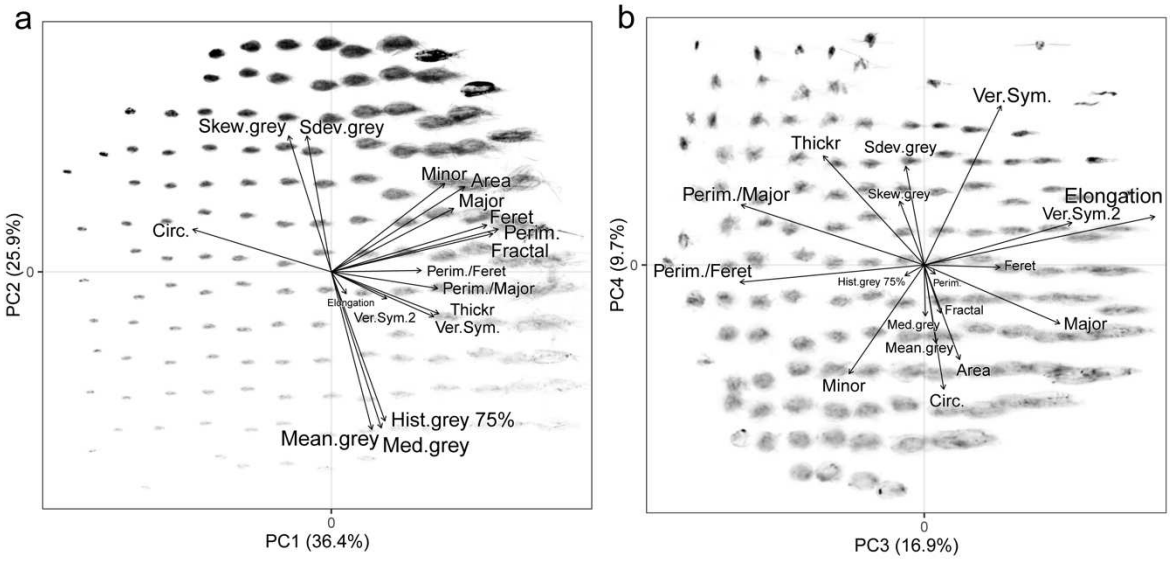

Figure 1.3. Morphological space of copepods' UVP images. The four significant axes of a PCA performed on morphological descriptors are represented: PC1 and PC2 in (a), PC3 and PC4 in (b). For each factorial plane, morphotypes are represented according to their coordinates in the morphological space: A grid was defined and

eight images close to the factorial plane considered were randomly selected, aligned and superimposed at each node of the grid for visualization. Definitions of morphological descriptors are presented in Table A.2; code used to project images in the morphological space is available (*morphr* package, https://github.com/jiho/morphr).

1. 5. 3 Distribution of morphological traits in Baffin Bay

The spatially interpolated PC values between each station revealed the spatial distribution of the size, opacity, and appendage visibility traits of copepods in Baffin Bay (Fig. 1.4). Since hundreds of images are available at each station, the computation of the mean value of each PC trait is statistically robust and allows us to illustrate the spatial distribution of dominant morphologies in the Bay. Copepods are typically larger (PC1) in western stations influenced by colder, fresher and ice-covered Arctic waters than in eastern stations where ice has already melted. Copepods present in the center of the Bay are generally opaquer in the UVP images as compared to copepods sampled at peripheral stations (PC2). Finally, it appears that more individuals have a complex perimeter with visible appendages in the east relative to western stations (PC4). In particular, large western copepods often have antennas folded along their body, whereas the smaller individuals in the east are imaged with extended antennae and pereiopods deployed.

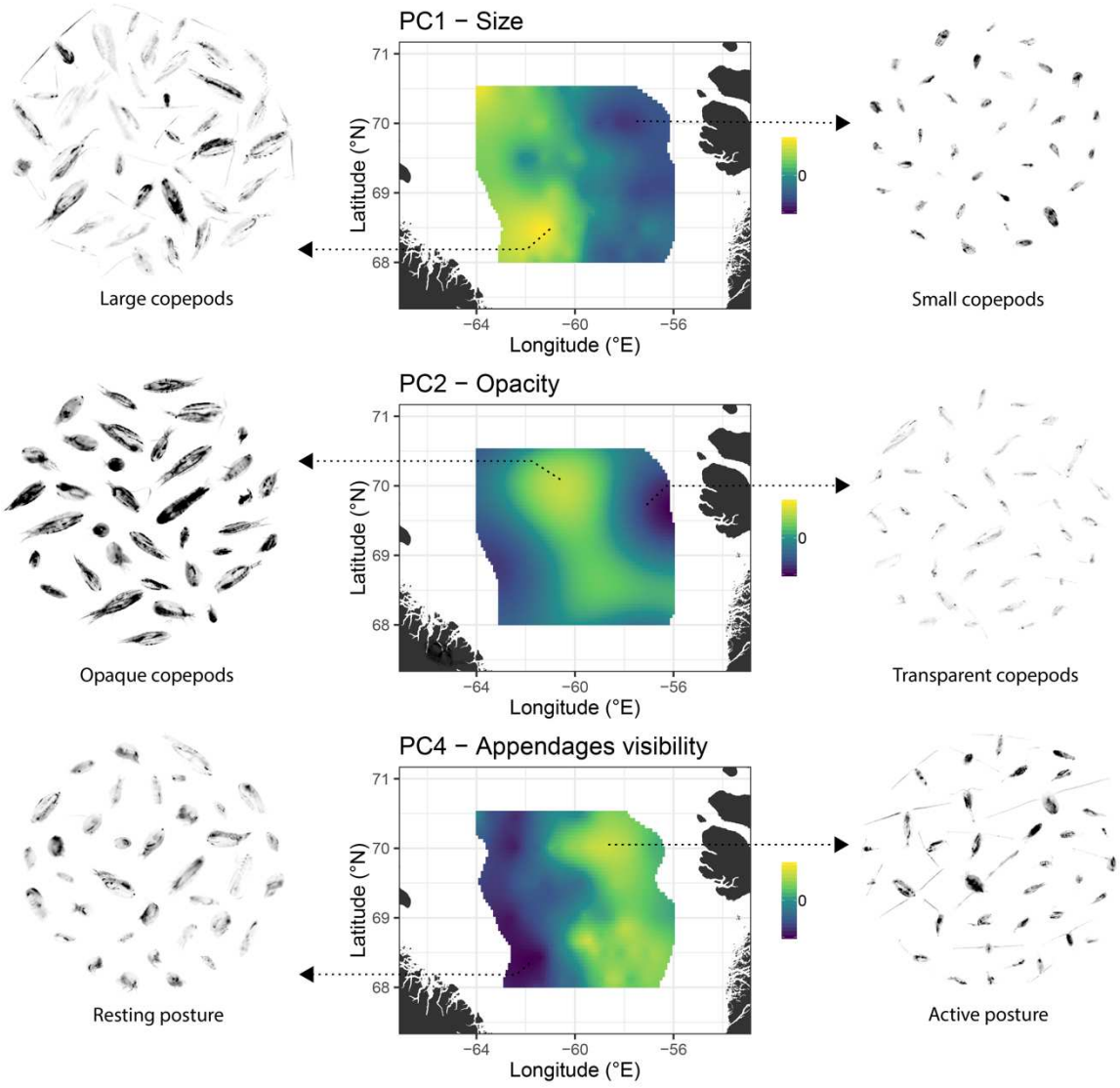

Figure 1.4. Morphological traits distribution in Baffin Bay. Kriging of each station's average coordinates on PC1, PC2, and PC4 of copepods images from the surface layer. PC1 reflects individual size, PC2 opacity, and PC4 perimeter complexity (visibility of appendages). To illustrate "extreme" morphologies that drive the average PC value of a station, 36 images were randomly selected within the 10% highest or lowest along each PC and displayed on the sides.

1. 5. 4 Traits and environmental characteristics

The spatial patterns in copepod morphological traits are confirmed by one-way ANOVA and post-hoc tests on the average trait values according to the environmental clustering (Fig. 1.5). Size (PC1) and appendage visibility (PC4) differ significantly between the three clusters with a gradient from western to eastern clusters (Fig. 1.5a,c). Water temperature and ice concentration were the most

important factors influencing the environmental clustering and could impact the size distribution. Appendage visibility (PC4) is significantly higher at the transition zone and in open waters where phytoplankton are present. Finally, the opacity of copepods (PC2, Fig. 1.5b) is significantly higher in the transition zone characterized by recent ice melt and a shallow bloom.

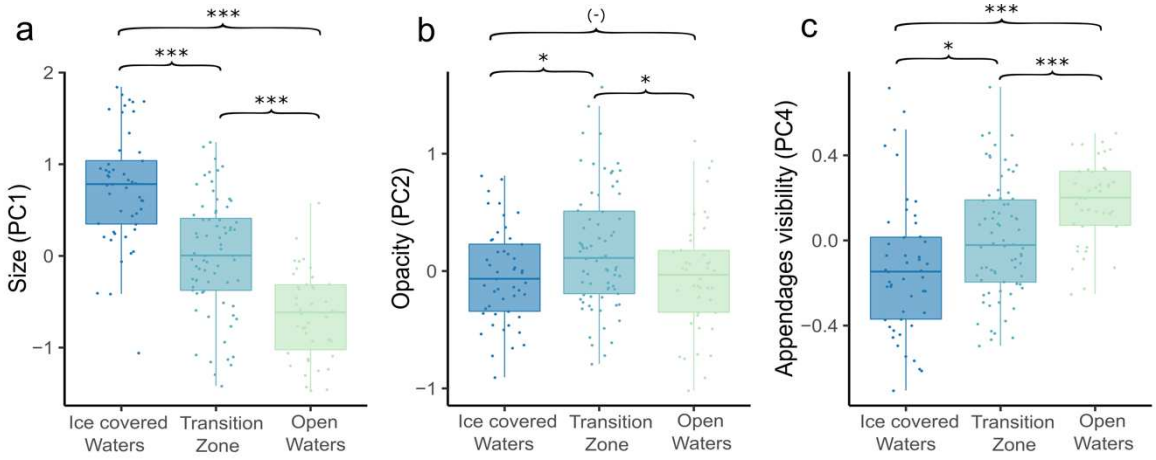

Figure 1.5. Trait values according to environmental clusters. Box plots represent average trait values (a = size, b = opacity, c = appendages visibility) for each environmental cluster defined in Fig. 1.2. Each point represents the average value of the PC at a station. ANOVA identified significant differences between all PCs (PC1: $p < 0.001$; PC2: $p = 0.015$; PC4: $p < 0.001$) and the significance of post-hoc statistical tests is indicated symbolically on the figure (-: $p > 0.05$, *: $p < 0.05$, **: $p < 0.01$, ***: $p < 0.001$).

1.6. Discussion

1. 6. 1 Benefits of morphological trait-based approach from individual *in situ* images

We combined individual-based imagery and multivariate statistical analysis to implement a morphological trait-based approach to zooplankton ecology. The combination of these techniques allowed us to analyze many more profiles (N = 163) than would be possible with conventional net or pump sampling. The acquisition of large datasets - typically thousands of images per cast – enabled statistically robust descriptions of trends of morphological traits. This novel description of the ecosystem allowed us to infer community structure and functioning from individual properties. Moreover, this approach offers a continuous representation of traits, which has benefits in comparison to discrete traits especially for further numerical analyses (McGill et al. 2006).

In our study, the four significant PC axes of our morpho- logical space explained 90% of the variance of the numerical descriptors of individual images and showed clear signals along environmental gradients. The ever-increasing production of images for plankton ecology paves the way for morphological trait-based studies that should provide original insights on ecosystem functioning. Many imaging devices already use morphological features to perform taxonomical classification of individuals (IFCB, Sosik and Olson 2007; FlowCam, Sieracki et al. 1998; LOKI, Schmid et al. 2016; ZooScan, Gorsky et al. 2010; Zooglider, Ellen et al. 2019). Freshwater and marine plankton morphology measured with such image processing methods could be easily analyzed using our approach.

The actual outcome of such analyses is highly dependent on the pixel resolution of the imaging system. In this study, we analyzed images of large Arctic zooplankton with a recent version of the Underwater Vision Profiler (Picheral et al. 2010). The instrument produces detailed high-resolution images of plankton at that size scale which makes the necessary morphological feature extraction possible. Systematic analyses should be performed using other devices and in other biogeographic regions to quantify the resolution bias of this morphological approach.

1. 6. 2 Size distribution as indicator of community structure

Our study aimed to elucidate patterns of morphological traits of copepods as a function of sea-ice dynamics (ice melt, ice-edge bloom, etc.). Results showed a strong west/east size gradient of the copepod community in Baffin Bay. Mean sizes are higher in Arctic-influenced and ice-covered waters than in ice- free and Atlantic-influenced waters. The consistent shift in size distribution is related to a change in the dominance of certain size classes; a complementary analysis of the spatial distribution of size (from PC1) showed elevated abundances of small individuals at eastern stations (Appendix A.2).

Therefore, our results allow us to propose two main hypotheses: size distribution may be linked to (1) the composition of communities advected by the currents, with small *Calanus finmarchicus* (~ 2–3 mm) dominating Atlantic waters, *C. hyperboreus* (up to 8 mm) being more abundant in Arctic waters (Beaugrand 2002); (2) the development of smaller copepodite life stages in ice-free and Chl *a* rich waters of the eastern Baffin Bay.

The UVP recorded images of copepods ranging from ca. 0.7–7 mm along the major axis, sizes typical of the dominant large Arctic species. However, the image resolution is not sufficient to distinguish copepod species and development stages precisely. Based on the taxonomic analysis of complementary vertical net sampling (Fig. A.3), the most likely species encountered in this size range are *Calanus hyperboreus*, *C. glacialis*, *C. finmarchicus*, *Metridia longa* and adult stages of

Pseudocalanus spp. (Sameoto 1984; Forest et al. 2012). *Oithona similis* and *Microcalanus* sp., typical Arctic zooplankton species, are too small to be captured in UVP images.

Net sampling revealed that adult abundances, possibly reflecting the composition of advected communities, are not very different from west to east. Only *C. glacialis* and *C. finmarchicus* adults were counted in slightly higher numbers in the eastern, Atlantic-influenced part of the Bay. *C. hyperboreus*, *M. longa*, and *Pseudocalanus* adults are homogeneously spread out among stations (Fig. A.3). The most striking element is that nauplii and young copepod stages from all *Calanus* species (Fig. A.3 b,c,f) are much more abundant in eastern Baffin Bay, which supports our second hypothesis. The strong size gradient is mostly caused by high recruitment of young copepod stages in response to sea ice melt and subsequent primary production pulse (Fig. 1.5). Indeed, *C. glacialis* and *C. finmarchicus* are mainly income breeders whose spawning is stimulated by Chl *a* concentration (Conover and Huntley 1991; Niehoff et al. 1999; Søreide et al. 2010). *C. hyperboreus* copepodites are also much more abundant in the east, but they are in late stages of development (no C1, some C2 and many C3 stages) because this capital breeder species spawns earlier in the season (Hirche and Niehoff 1996).

1. 6. 3 Variation of opacity: A reactive response to ice melt?

The transition zone between the ice-covered and open waters in the east (Fig. 1.2) was dominated by copepods that were opaquer (Fig. 1.4). We can expect that particles in the digestive tract are a major source of opacity. This is consistent with the observation that stations with the highest integrated Chl *a* concentration were also the areas of highest copepod opacity, particularly along the ice edge (Lafond et al., 2019). On the contrary, stations with low phytoplankton abundances and high phaeopigment concentrations (post-bloom conditions, Lafond et al. 2019) show weaker opacities.

A copepod's gut content is sometimes clearly distinguishable in UVP images (see Fig. 1.6 - 1a). It is not, however, the only colored structure visible on images. Red light illumination is used by several in situ imaging devices, including the UVP, because these wavelengths are known to reduce phototactic behavior of zooplankton (Cohen and Forward 2002). Raw UVP images of red objects will appear bright over a dark background. The pixel values in the images we worked with were inverted for practical reasons (Picheral et al. 2010) so that reddish areas appear dark. In UVP images from this study, localized darker regions are visible within the anterior ventral zone, the basis of pereiopods, antennas and at the posterior extremity of the lipid sac (Fig. 1.6 - 1b). Calanoid copepods usually concentrate astaxanthin, an antioxidant carotenoid pigment that they metabolize from precursors found in phytoplanktonic prey (Lotocka 2004). These pigments are good quenchers of oxygen-free radicals and can prevent lipid peroxidation (Hairston 1976; Miki 1991; Lotocka 2004; Weaver et al.

2018). Even if the role of pigmentation is rather well-known, there is still a lack of information on how it varies according to environmental conditions. Relatively high quantity and good quality of phytoplankton are necessary for copepods to successfully transform phytoplanktonic precursors into antioxidant pigments (Andersson et al. 2003). This metabolism could reduce the potential oxidative stress caused by solar radiation in near-surface blooms when the ice cover breaks up, and help maximize copepod survival, which requires large lipid reserves for their maturation (Hylander et al. 2015).

A third possible explanation of the observed opacity variation is related to reproduction phenology since reproductive structures, such as gonads and eggs, are also very pigmented (Fig. 1.6 - 1c). *C. finmarchicus* and *C. glacialis* depend mainly on the spring bloom to produce eggs, so their reproductive structures are likely to be mature and visible in females (Niehoff et al. 1999). Nevertheless, clearly identifying these structures in images captured in the surface layer was quite rare (about 10% of a random subsample of 150 images), while the occurrence of noticeable gut content and red pigments was much more common.

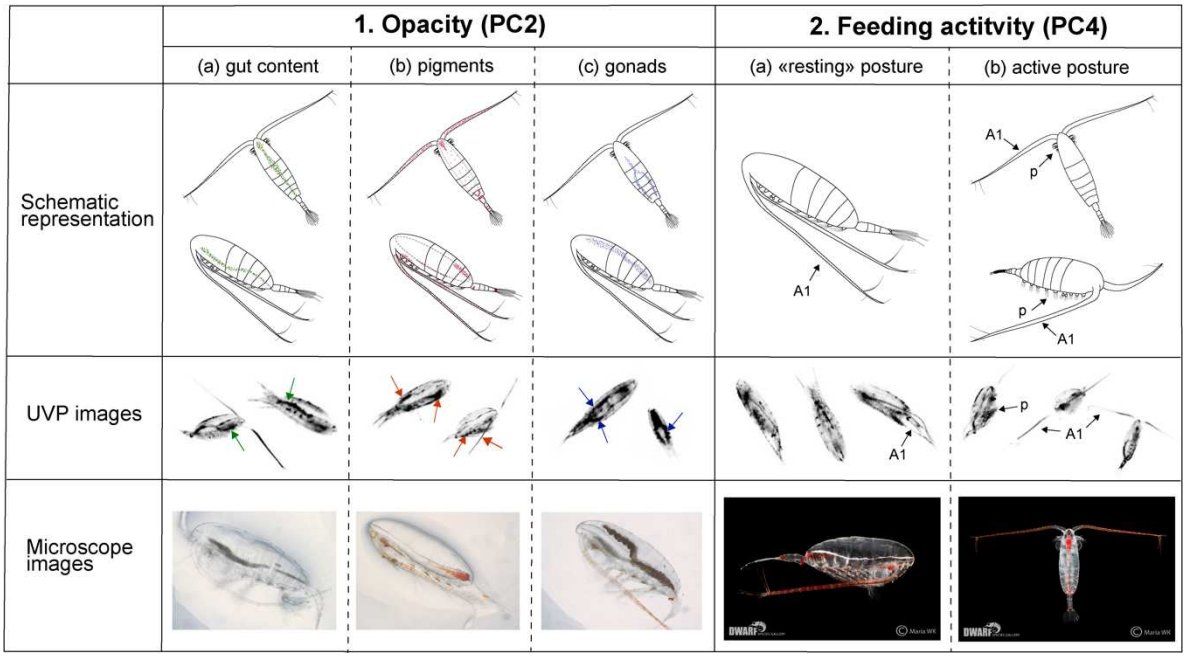

Figure 1.6. Illustration of opacity and feeding activity variations visible on copepods (*C. hyperboreus*) schemes, UVP images and stereo-microscope images. Opacity characterized by PC2 score can be linked to gut content (1a), red pigments (1b), or gonads (1c), and often a combination of the three. PC4 scores capture appendage extension and are potentially indicators of copepod feeding activity: Individuals in a resting posture have antennae (A1) along their body (2a), active filter-feeding copepods extend their antennae (A1) and sometimes pereiopods (p) deployed (2b). Stereo-microscope images illustrating opacity variations were taken by Geneviève Perrin (Institut Maurice-Lamontagne, Fisheries and Oceans Canada, Mont-Joli, Canada); those

illustrating feeding activity were taken by Maria Włodarska-Kowalczuk (Institute of Oceanology, Polish Academy of Sciences, Poland, http://www.iopan.gda.pl/pro jects/Dwarf/species_gallery/crustacea.html).

1. 6. 4 Unexpected indices of *in situ* feeding activity

The PC4 in our analysis revealed distinct patterns of appendage visibility in our images that we did not expect to resolve so clearly. Images with low score values on this axis often show copepods that have their antennae folded alongside their body. Lenz and Roncalli (2019) have interpreted this posture as a sign of diapause. More generally, the pose can be interpreted as the morphological signature of a rather inactive behavior, as also demonstrated from Zooglider images (Ohman 2019). Likewise, images with high PC4 values were typically of copepods that had appendages extended out of their body. In the Arctic, most copepods are "feeding-current feeders" (Marshall 1973; Barton et al. 2013): they create a current with their pereiopods to entrain particles and phytoplankton cells (Kiørboe 2011), while their antennae are spread out. We therefore hypothesize that the mean score value of PC4 for a sub-part of the community (here, copepods of the surface layer) is an indicator of the feeding activity of the community (Fig. 1.6 - 2a,b).

It follows that maximal feeding intensity occurs in the east- ern part of the Bay, where phytoplankton concentrations are the highest. Small and "active" copepods could be copepodites development stages hatched in spring, whose filtration activity is highest to ensure their development and successful overwintering. The stations with high Chl *a* concentration (81.5 +/− 29 $mg.m^{-2}$) and many pelagic diatoms (185,00 to 624,000 cells L^{-1}) were ice-free stations situated on the eastern part of transects 69°N and 70°N, close to the ice edge (Lafond et al. 2019). These stations also present a high PC4 mean value, which was expected since Arctic copepods and diatoms have a well-known prey–predator relationship (Scott et al. 2002).

1.7. Conclusions

Our morphological trait-based analysis of UVP images highlights the strong response of the surface copepod community to ice melt and phytoplankton dynamics. We mostly find non-feeding and large (adult) copepods in ice-covered waters, while ice break-up and increase of Chl *a* concentrations are associated with: (1) a large increase of small *Calanus* sp. stages abundances; (2) the pigmentation of copepods at the ice edge due to full gut content and astaxanthin accumulation; and (3) elevated feeding activity in open waters, as inferred from copepod posture.

1.8. References

Andersson, M., L. Van Nieuwerburgh, and P. Snoeijs. 2003. Pigment transfer from phytoplankton to zooplankton with emphasis on astaxanthin production in the Baltic Sea food web. Marine Ecology Progress Series 254:213–224.

Arrigo, K. R., D. K. Perovich, R. S. Pickart, Z. W. Brown, G. L. van Dijken, K. E. Lowry, M. M. Mills, M. A. Palmer, W. M. Balch, N. R. Bates, C. R. Benitez-Nelson, E. Brownlee, K. E. Frey, S. R. Laney, J. Mathis, A. Matsuoka, B. Greg Mitchell, G. W. K. Moore, R. A. Reynolds, H. M. Sosik, and J. H. Swift. 2014. Phytoplankton blooms beneath the sea ice in the Chukchi sea. Deep Sea Research Part II: Topical Studies in Oceanography 105:1–16.

Asar, Ö., O. Ilk, and O. Dag. 2017. Estimating Box-Cox power transformation parameter via goodness-of-fit tests. Communications in Statistics - Simulation and Computation 46:91–105.

Barton, A. D., A. J. Pershing, E. Litchman, N. R. Record, K. F. Edwards, Z. V. Finkel, T. Kiørboe, and B. A. Ward. 2013. The biogeography of marine plankton traits. Ecology Letters 16:522–534.

Beaugrand, G. 2002. Reorganization of North Atlantic Marine Copepod Biodiversity and Climate. Science 296:1692–1694.

Beitsch, A., L. Kaleschke, and S. Kern. 2014. Investigating High-Resolution AMSR2 Sea Ice Concentrations during the February 2013 Fracture Event in the Beaufort Sea. Remote Sensing 6:3841–3856.

Benedetti, F., S. Gasparini, and S.-D. Ayata. 2016. Identifying copepod functional groups from species functional traits. Journal of Plankton Research 38:159–166.

Berge, J., T. M. Gabrielsen, M. Moline, and P. E. Renaud. 2012. Evolution of the Arctic *Calanus* complex: an Arctic marine avocado? Journal of Plankton Research 34:191–195.

Breiman, L. 2001. Random Forests. Machine Learning 45:5–32.

Brun, P., K. Stamieszkin, A. W. Visser, P. Licandro, M. R. Payne, and T. Kiørboe. 2019. Climate change has altered zooplankton-fuelled carbon export in the North Atlantic. Nature Ecology & Evolution 3:416–423.

Caillon, F., V. Bonhomme, C. Möllmann, and R. Frelat. 2018. A morphometric dive into fish diversity. Ecosphere 9.

Cattell, R. B. 1966. The Scree Test For The Number Of Factors. Multivariate Behavioral Research 1:245–276.

Cohen, J. H., and R. B. Forward. 2002. Spectral Sensitivity of Vertically Migrating Marine Copepods. The Biological Bulletin 203:307–314.

Conover, R. J., and M. Huntley. 1991. Copepods in ice-covered seas—Distribution, adaptations to seasonally limited food, metabolism, growth patterns and life cycle strategies in polar seas. Journal of Marine Systems 2:1–41.

Ellen, J. S., C. A. Graff, and M. D. Ohman. 2019. Improving plankton image classification using context metadata. Limnology and Oceanography: Methods.

Falk-Petersen, S., P. Mayzaud, G. Kattner, and J. R. Sargent. 2009. Lipids and life strategy of Arctic *Calanus*. Marine Biology Research 5:18–39.

Forest, A., L. Stemmann, M. Picheral, L. Burdorf, D. Robert, L. Fortier, and M. Babin. 2012. Size distribution of particles and zooplankton across the shelf-basin system in southeast Beaufort Sea: combined results from an Underwater Vision Profiler and vertical net tows. Biogeosciences 9:1301–1320.

Fortier, M., L. Fortier, C. Michel, and L. Legendre. 2002. Climatic and biological forcing of the vertical flux of biogenic particles under seasonal Arctic sea ice. Marine Ecology Progress Series 225:1–16.

Gorsky, G., M. D. Ohman, M. Picheral, S. Gasparini, L. Stemmann, J.-B. Romagnan, A. Cawood, S. Pesant, C. Garcia-Comas, and F. Prejger. 2010. Digital zooplankton image analysis using the ZooScan integrated system. Journal of Plankton Research 32:285–303.

Grime, J. P. 1974. Vegetation classification by reference to strategies. Nature 250:26–31.

Hairston, N. C. 1976. Photoprotection by carotenoid pigments in the copepod *Diaptomus nevadensis*. Proceedings of the National Academy of Sciences 73:971–974.

Hébert, M.-P., B. E. Beisner, and R. Maranger. 2017. Linking zooplankton communities to ecosystem functioning: toward an effect-trait framework. Journal of Plankton Research 39:3–12.

Helaouët, P., and G. Beaugrand. 2007. Macroecology of *Calanus finmarchicus* and *C. helgolandicus* in the North Atlantic Ocean and adjacent seas. Marine Ecology Progress Series 345:147–165.

Hirche, H.-J., and B. Niehoff. 1996. Reproduction of the Arctic copepod *Calanus hyperboreus* in the Greenland Sea - field and laboratory observations. Polar Biology 16:209–219.

Hylander, S., T. Kiørboe, P. Snoeijs, R. Sommaruga, and T. G. Nielsen. 2015. Concentrations of sunscreens and antioxidant pigments in Arctic *Calanus* spp. in relation to ice cover, ultraviolet radiation, and the phytoplankton spring bloom: MAAs and astaxanthin in copepods. Limnology and Oceanography 60:2197–2206.

Josse, J., and F. Husson. 2012. Handling missing values in exploratory multivariate data analysis methods. Journal de la Société Française de Statistique 153:79–99.

Kaleschke, L., and X. Tian-Kunze. 2016. AMSR2 ASI 3.125 km Sea Ice Concentration Data, V0.1", Institute of Oceanography, University of Hamburg, Germany, digital media (ftp-projects.zmaw.de/seaice/), [BEGIN 01/03/2016 - END 14/07/2016].

Kiørboe, T. 2011. How zooplankton feed: mechanisms, traits and trade-offs. Biological Reviews 86:311–339.

Kiørboe, T., A. Visser, and K. H. Andersen. 2018. A trait-based approach to ocean ecology. ICES Journal of Marine Science 75:1849–1863.

Kruk, C., V. L. M. Huszar, E. T. H. M. Peeters, S. Bonilla, L. Costa, M. LüRling, C. S. Reynolds, and M. Scheffer. 2010. A morphological classification capturing functional variation in phytoplankton. Freshwater Biology 55:614–627.

Lafond, A., K. Leblanc, B. Quéguiner, B. Moriceau, A. Leynaert, V. Cornet, J. Legras, J. Ras, M. Parenteau, N. Garcia, M. Babin, and J.-E. Tremblay. 2019. Late spring bloom development of pelagic diatoms in Baffin Bay. Elem Sci Anth 7:44.

Lê, S., J. Josse, and F. Husson. 2008. FactoMineR: An *R* Package for Multivariate Analysis. Journal of Statistical Software 25.

Legendre, P., and L. Legendre. 2012. Chapter 9 - Ordination in reduced space. Pages 425–520 Developments in Environmental Modelling. Elsevier.

Lenz, P. H., and V. Roncalli. 2019. Diapause within the Context of Life-History Strategies in Calanid Copepods (Calanoida: Crustacea). The Biological Bulletin 237:170–179.

Lévesque, K., S. Morisset, T. Linkowski, and J. Zier. 2015. CCGS Amundsen Navigation (NAV) data recorded during the annual science expeditions in the Canadian Arctic. Canadian Cryospheric Information Network.

Litchman, E., M. D. Ohman, and T. Kiørboe. 2013. Trait-based approaches to zooplankton communities. Journal of Plankton Research 35:473–484.

Lotocka, M. 2004. Changes in carotenoid composition in different developmental stages of copepods: *Pseudocalanus acuspes* Giesbrecht and *Acartia* spp. Journal of Plankton Research 26:159–166.

Marshall, S. M. 1973. Respiration and Feeding in Copepods. Pages 57–120 Advances in Marine Biology. Elsevier.

Mcgill, B., B. Enquist, E. Weiher, and M. Westoby. 2006. Rebuilding community ecology from functional traits. Trends in Ecology & Evolution 21:178–185.

Miki, W. 1991. Biological functions and activities of animal carotenoids. Pure and Applied Chemistry 63:141–146.

Mouillot, D., N. A. J. Graham, S. Villéger, N. W. H. Mason, and D. R. Bellwood. 2013. A functional approach reveals community responses to disturbances. Trends in Ecology & Evolution 28:167–177.

Murtagh, F., and P. Legendre. 2014. Ward's Hierarchical Agglomerative Clustering Method: Which Algorithms Implement Ward's Criterion? Journal of Classification 31:274–295.

Niehoff, B., U. Klenke, H. Hirche, X. Irigoien, R. Head, and R. Harris. 1999. A high frequency time series at Weathership M, Norwegian Sea, during the 1997 spring bloom: the reproductive biology of *Calanus finmarchicus*. Marine Ecology Progress Series 176:81–92.

Nychka, D., R. Furrer, J. Paige, and S. Sain. 2017. fields: Tools for Spatial Data, R package version 9.8-3, https://github.com/NCAR/Fields.

Ohman, M. D. 2019. A sea of tentacles: optically discernible traits resolved from planktonic organisms in situ. ICES Journal of Marine Science 76:1959–1972.

Ohman, M. D., R. E. Davis, J. T. Sherman, K. R. Grindley, B. M. Whitmore, C. F. Nickels, and J. S. Ellen. 2019. Zooglider: An autonomous vehicle for optical and acoustic sensing of zooplankton. Limnology and Oceanography: Methods 17:69–86.

Oksanen, J., F. G. Blanchet, R. Kindt, P. Legendre, P. Minchin, R. O'Hara, G. Simpson, P. Solymos, M. Stevens, and H. Wagner. 2007. The vegan package. Community ecology package 10:631–637.

Oziel, L., P. Massicotte, A. Randelhoff, J. Ferland, A. Vladoiu, L. Lacour, V. Galindo, S. Lambert-Girard, D. Dumont, Y. Cuypers, P. Bouruet-Aubertot, C.-J. Mundy, J. Ehn, G. Bécu, C. Marec, M.-H. Forget, N. Garcia, P. Coupel, P. Raimbault, M.-N. Houssais, and M. Babin. 2019. Environmental factors influencing the seasonal dynamics of spring algal blooms in and beneath sea ice in western Baffin Bay. Elem Sci Anth 7:34.

Pebesma, E. J. 2004. Multivariable geostatistics in S: the gstat package. Computers & Geosciences 30:683–691.

Perrette, M., A. Yool, G. D. Quartly, and E. E. Popova. 2011. Near-ubiquity of ice-edge blooms in the Arctic. Biogeosciences 8:515–524.

Picheral, M., S. Colin, and J.-O. Irisson. 2017. EcoTaxa, a tool for the taxonomic classification of images. http://ecotaxa.obs-vlfr.fr.

Picheral, M., L. Guidi, L. Stemmann, D. M. Karl, G. Iddaoud, and G. Gorsky. 2010. The Underwater Vision Profiler 5: An advanced instrument for high spatial resolution studies of particle size spectra and zooplankton: Underwater vision profiler. Limnology and Oceanography: Methods 8:462–473.

Randelhoff, A., L. Oziel, P. Massicotte, G. Bécu, M. Galí, L. Lacour, D. Dumont, A. Vladoiu, C. Marec, F. Bruyant, M.-N. Houssais, J.-É. Tremblay, G. Deslongchamps, and M. Babin. 2019. The evolution of light and vertical mixing across a phytoplankton ice-edge bloom. Elem Sci Anth 7:20.

Ras, J., H. Claustre, and J. Uitz. 2008. Spatial variability of phytoplankton pigment distributions in the Subtropical South Pacific Ocean: comparison between in situ and predicted data. Biogeosciences 5:353–369.

Renaud, P. E., M. Daase, N. S. Banas, T. M. Gabrielsen, J. E. Søreide, Ø. Varpe, F. Cottier, S. Falk-Petersen, C. Halsband, D. Vogedes, K. Heggland, and J. Berge. 2018. Pelagic food-webs in a changing Arctic: a trait-based perspective suggests a mode of resilience. ICES Journal of Marine Science 75:1871–1881.

Sameoto, D. D. 1984. Vertical distribution of zooplankton biomass and species in northeastern Baffin Bay related to temperature and salinity. Polar Biology 2:213–224.

Schmid, M. S., C. Aubry, J. Grigor, and L. Fortier. 2016. The LOKI underwater imaging system and an automatic identification model for the detection of zooplankton taxa in the Arctic Ocean. Methods in Oceanography 15–16:129–160.

Schmid, M. S., F. Maps, and L. Fortier. 2018. Lipid load triggers migration to diapause in Arctic *Calanus* copepods—insights from underwater imaging. Journal of Plankton Research 40:311–325.

Scott, C., S. Kwasniewski, S. Falk-Petersen, and J. Sargent. 2002. Species differences, origins and functions of fatty alcohols and fatty acids in the wax esters and phospholipids of *Calanus hyperboreus*, *C. glacialis* and *C. finmarchicus* from Arctic waters. Marine Ecology Progress Series 235:127–134.

Sieracki, C., M. Sieracki, and C. Yentsch. 1998. An imaging-in-flow system for automated analysis of marine microplankton. Marine Ecology Progress Series 168:285–296.

Søreide, J. E., E. Leu, J. Berge, M. Graeve, and S. Falk-Petersen. 2010. Timing of blooms, algal food quality and *Calanus glacialis* reproduction and growth in a changing Arctic. Global Change Biology 16:3154–3163.

Sosik, H. M., and R. J. Olson. 2007. Automated taxonomic classification of phytoplankton sampled with imaging-in-flow cytometry. Limnology and Oceanography-Methods 5:204–216.

Tang, C. C. L., C. K. Ross, T. Yao, B. Petrie, B. M. DeTracey, and E. Dunlap. 2004. The circulation, water masses and sea-ice of Baffin Bay. Progress in Oceanography 63:183–228.

Turner, J. T. 2015. Zooplankton fecal pellets, marine snow, phytodetritus and the ocean's biological pump. Progress in Oceanography 130:205–248.

Usseglio-Polatera, P., M. Bournaud, P. Richoux, and H. Tachet. 2000. Biological and ecological traits of benthic freshwater macroinvertebrates: relationships and definition of groups with similar traits. Freshwater Biology 43:175–205.

Violle, C., M.-L. Navas, D. Vile, E. Kazakou, C. Fortunel, I. Hummel, and E. Garnier. 2007. Let the concept of trait be functional! Oikos 116:882–892.

Weaver, R. J., P. Wang, G. E. Hill, and P. A. Cobine. 2018. An *in vivo* test of the biologically relevant roles of carotenoids as antioxidants in animals. The Journal of Experimental Biology 221:jeb183665.

Weisberg, S., and J. Fox. 2018. An R Companion to Applied Regression. Third Edition. Sage publications.

Wickham, H., M. Averick, J. Bryan, W. Chang, L. McGowan, R. François, G. Grolemund, A. Hayes, L. Henry, J. Hester, M. Kuhn, T. Pedersen, E. Miller, S. Bache, K. Müller, J. Ooms, D. Robinson, D. Seidel, V. Spinu, K. Takahashi, D. Vaughan, C. Wilke, K. Woo, and H. Yutani. 2019. Welcome to the Tidyverse. Journal of Open Source Software 4:1686.

Willby, N. J., V. J. Abernethy, and B. O. L. Demars. 2000. Attribute-based classification of European hydrophytes and its relationship to habitat utilization. Freshwater Biology 43:43–74.

Williams, R., and S. A. Poulet. 1986. Relationship between the zooplankton, phytoplankton, particulate matter and dissolved free amino acids in the Celtic Sea: I. Unstratified water conditions. Marine Biology 90:279–284.

Zweng, M. M., and A. Münchow. 2006. Warming and freshening of Baffin Bay, 1916–2003. Journal of Geophysical Research 111:C07016.

2. Copepods' true colors: astaxanthin pigmentation as an indicator of fitness

2.1. Résumé

La pigmentation est un trait souvent négligé dans les études écologiques sur le zooplancton, dont les organismes sont le plus souvent incolores pour se fondre au milieu aquatique translucide. Cependant, l'un des taxons zooplanctoniques dominants dans les écosystèmes aquatiques - les copépodes - présentent souvent une coloration rouge-orange, ou même bleue vive, induite par l'accumulation de pigments caroténoïdes dans certaines parties du corps. Bien qu'il existe de nombreux traits fonctionnels décrivant la performance des copépodes (par exemple la taille, les modes d'alimentation ou de reproduction), il est surprenant que le rôle de la coloration n'ait pas encore été étudié de manière cohérente. En passant en revue 95 études, nous démontrons que la pigmentation induite par les caroténoïdes (principalement par les molécules d'astaxanthine) est un trait fonctionnel répandu chez les copépodes vivant en eau douce et en milieu marin. Nous essayons de comprendre les variations de leur pigmentation selon les gradients environnementaux, en examinant leurs relations avec la qualité et la quantité de nourriture, la température, le stress induit par les rayonnements ultraviolets, la pression de prédation, le métabolisme des lipides et les stratégies de reproduction. Nous montrons également que les tendances de pigmentation à grande échelle sont difficiles à expliquer en raison de la plasticité fondamentale de ce trait à de courtes échelles de temps (*i.e.* heures, jours). Les informations les plus récentes sur la bioconversion des caroténoïdes sont rassemblées (identification des gènes et des enzymes, influence du microbiote). À partir de cette revue de la littérature, nous émettons l'hypothèse que la pigmentation caroténoïde joue un rôle de "couteau suisse" pour le succès écologique (la *fitness*) des copépodes, utile dans diverses conditions écosystémiques grâce au fort pouvoir antioxydant de l'astaxanthine et à la régulation fine de son métabolisme. Avec des capacités antioxydantes plus importantes (survie), un métabolisme plus élevé (croissance) et des descendants nombreux et en meilleure condition (reproduction), les morphotypes rouges semblent mieux réussir que leurs congénères non colorés. Nous discutons également des stratégies de camouflage potentielles permises par la pigmentation rouge et bleue. Enfin, nous formulons de nouvelles directions de recherche sur ce sujet, de l'échelle moléculaire à celle des écosystèmes. Quantifier la pigmentation en utilisant une approche « par traits fonctionnels » pourrait être utile (1) pour obtenir un indicateur du succès écologique des copépodes et (2) pour mieux estimer le transfert d'antioxydants vers les niveaux trophiques supérieurs, incluant les humains.

2.2. Abstract

Pigmentation is often overlooked in zooplankton, since these organisms are mostly colorless as an adaptation to the translucid water medium. However, one of the dominant zooplankton taxa in aquatic ecosystems - copepods - often show a bright red-orange or blue coloration owing to the accumulation of carotenoid pigments in some parts of their bodies. Even though there are many functional traits describing copepod performance (e.g. size, feeding and reproductive modes), it is surprising that the role of such a simple and visible trait as coloration has not been studied in a coherent manner yet. Here, by reviewing 95 studies, we demonstrate that carotenoid-based pigmentation (mainly caused by astaxanthin molecules) is a widespread functional trait in freshwater and marine copepods. We propose a way to disentangle the complex and thus intriguing patterns of pigment expression along latitudinal and altitudinal gradients, addressing its relationship to diet quality and quantity, temperature, ultraviolet radiation stress, predation pressure, lipid metabolism, and reproduction. We also show that large scale variations in pigmentation are difficult to tackle because of the fundamental plasticity of this trait at short time scales (i.e. hours, days), and the most recent information about carotenoid bioconversion are addressed (genes and enzyme identification, influence of microbiota). From this literature review, we hypothesize that pigments play a "swiss-army knife" role for copepod fitness, useful in various ecosystem conditions, owing to the strong antioxidant power and the finely-tuned metabolism of astaxanthin. With larger antioxidant capacities (survival), higher metabolism (growth) and more offspring in better condition (reproduction), red morphs appear more successful than their uncolored siblings. Also, the potential camouflage strategies enabled by red and blue pigmentation are discussed. We finally formulate new directions and future research fields from molecular to ecosystem scales. Routine quantifications of copepod pigmentation through trait-based approaches could be useful (1) to obtain an accurate copepod fitness indicator and (2) to better estimate the transfer of antioxidant to higher trophic levels in ecosystems, including humans.

2.3. Introduction

Color is a morphological property that can be assessed at the individual level and that impacts survival, growth and reproduction of organisms; as such it corresponds to the definition of a functional trait (Violle et al. 2007). Carotenoid-based colors are caused by the presence of conjugated double-bond molecules able to absorb light at wavelengths of 400-500 nm in the visible region of the spectrum (de Carvalho and Caramujo 2017). These pigments are ubiquitous in animals and are known to influence individual fitness thanks to two distinct properties (Weaver et al. 2018b). First, they are

responsible for behavioral responses because strong pigmentation influences prey/predator interactions (e.g. red prey can be more targeted or camouflaged; Hansson 2004, Johnsen 2014) and sexual selection by conveying a true indicator of individual health condition (honest signal of fitness, Seehausen 1997, Negro et al. 1998, Torres and Velando 2005, McGraw 2005). Second, carotenoid pigments are electron acceptors with higher affinities than other cellular components, providing protection against oxidative damage on lipids, proteins and DNA. Numerous studies demonstrate that the accumulation of carotenoids improves animal health: it reduces disease occurrence in fish (Pickova et al. 1998, Pettersson and Lignell 1999, Nakano and Wiegertjes 2020) and can regulate immune functions and cancer proliferation in mammals (Chew and Park 2004), including humans (Donoso et al. 2021). The study of carotenoid-based color in animals is thus at the interface of physiology, ecology and behavioral studies and is well amenable to a functional trait-based approach (Martini et al. 2021).

Copepods are small planktonic crustaceans inhabiting oceans, rivers, lakes and ponds, and are probably the most abundant metazoans on our planet (Humes 1994). They represent a crucial link between micro-planktonic prey and higher consumers in aquatic food webs (Cavallo and Peck 2020). Moreover, they contribute to the biological carbon pump in the ocean by the production of sinking fecal pellets and by their vertical migrations (Turner 2015, Jónasdóttir et al. 2015). Their ecological importance is driven by several key functional traits, including their size distribution, feeding modes and dormancy strategies (Kiørboe et al. 2015, Benedetti et al. 2016, Brun et al. 2016, Benedetti et al. 2022). Color, in contrast, is a trait often overlooked in zooplankton organisms (including copepods), probably because it is assumed that transparency is the main strategy to hide in the water medium (Johnsen 2001). From a practical point of view, this general lack of interest might be caused by the typical preservation of plankton samples in fixatives (e.g. ethanol, formaldehyde) that lead to the leaking or oxidation of pigments, making color information unreliable. Nevertheless, red pigmentation in copepods was described in two species, *Diaptomus bacillifer* and *Acanthodiaptomus denticornis* as early as the nineteenth century in lakes of the French Alps (Blanchard 1890). Similar observations were later made in northern American and Swedish lakes (Brehm 1938, Hairston 1976, 1979, Byron 1982, Hansson 2004). From early on, red color was attributed to carotenoids. As in most crustaceans, astaxanthin and canthaxanthin are the principal carotenoid types found in copepods (Fisher et al. 1964, Czeczuga and Czerpak 1966, Matsuno 2001, de Carvalho and Caramujo 2017). Pigmented copepods are found in both marine and freshwater environments, particularly in polar and subpolar regions (Hylander et al. 2015), but also in sub-tropical systems (Lee et al. 2019). The red copepods from the North Atlantic (*Calanus* spp.) are valued in marine fisheries and aquaculture where they are sometimes nicknamed “red feed” (Pedersen et al. 2014). Their carotenoid-rich oil is now

sold for human health as an antioxidant, anticholesterolemic, and anti-inflammatory diet supplement (Gasmi et al. 2020). In equatorial regions, redness is much scarcer, but a complex of carotenoids and proteins can lead to a blue coloration which is very common in neustonic copepods (Herring 1965, Rahlff et al. 2018).

It is surprisingly complex to disentangle the physiological and ecological causes of copepod pigmentation. The main historical hypotheses tested in the literature (Table 2.1) was (1) the photoprotective role of astaxanthin against solar radiation (Hairston 1976), (2) the potential for heat absorption conferred by pigments that could lead to higher metabolic rates in individuals (metabolic stimulation hypothesis, Byron 1982), and (3) the use of astaxanthin esters as food reserves in association to lipid storage (Ringelberg and Hallegraeff 1976). The well-documented photoprotection hypothesis (Table 2.1, H_1) has been shown to be related to the buffering of reactive oxygen species (ROS) that are produced by the activity of high energy solar radiation. Regarding the metabolic stimulation hypothesis (Table 2.1, H_2), it was argued that heat absorption by pigments in such small animals would lead to an insignificant temperature gain (Hairston 1981). A higher metabolism in red individuals could be achieved not by heat increase, but rather by a better ROS buffering owing, again, to the protective action of carotenoids (Hairston 1976, Gorokhova et al. 2013). Finally, the food reserve hypothesis (Table 2.1, H_3) still lacks experimental confirmation, while actually raising another question: is there any reason why lipid storage is associated with red pigments? Thus, a more recent hypothesis concerns the specific protection of lipids (Table 2.1, H_4) against ROS induced by all types of oxidative stressors, not only by light (Schneider et al. 2016).

In this review, we present the current knowledge about the occurrence of carotenoid-based pigmentation in copepods, the biochemical processes leading to carotenoid accumulation, and its diverse physiological, biological and ecological consequences. In light of the powerful capacity of the carotenoid molecules to intercept reactive oxygen species (ROS), we demonstrate that all hypotheses could be further discussed and debated (Table 2.1). We also comment on color changes in relation to vertical migration and predation pressure. We will not discuss black pigmentation, sometimes described in the copepods *Candacia* sp. (Wilson 1950, Purcell 1983, Culverhouse 2006), because this color is almost undocumented and has not been associated to carotenoid pigments. Color variations related to the structure of the exoskeleton rather than to pigment molecules, i.e. iridescent Sapphirinid copepods (Kimura et al. 2020), are also not included in this review. We addressed three research questions: (1) To what extent is carotenoid-based color a common functional trait in copepods? (2) Which abiotic and biotic drivers influence carotenoid accumulation in freshwater and marine copepods? (3) What ecological advantages could red and blue pigments bring for individual fitness? To do so, we have retrieved information from 95 studies that contained the words “copepod”

associated with "carotenoid*", "astaxanthin" or "redness" anywhere in the text body. Carotenoid concentration ranges were identified according to ecosystem (freshwater vs marine), location (latitude, longitude, altitude), taxonomy and a few other contextual variables (Data1 and Data2). Another dataset was constructed to classify forcing variables (e.g. temperature, ultraviolet radiation or diet composition) according to their impact on carotenoid concentrations (e.g. positive, neutral, negative; Data3). Data obtained from literature search was finally organized to list the effects of red pigmentation on fitness-related variables in copepods, such as their survival rates, swimming speed, RNA:DNA metabolic index and 21 other indices assessing survival, growth or reproduction (Data4). Datasets and codes are available at DOI: https://doi.org/10.5281/zenodo.7671742, and easily visualized in a html file associated with the Rmarkdown code (Vilgrain 2023, RMarkdown: Allaire et al. 2021, R Core Team 2021; R version 4. 0. 3). In the Metadata1 to 4, we provided further details on how quantitative and qualitative information was chosen from the literature and reported within the datasets.

There are many possible reasons for copepods to exhibit red-orange or blue pigmentation (Table 2.1), and this property strongly varies in time and space. Our goal is to review and summarize the scattered knowledge about carotenoid accumulation in copepods. From this synthesis effort, we aim to unravel the copepod color puzzle and try to formulate new directions and future research fields broaden by this important trait. Ubiquitous and accurate quantification of pigmentation in copepods could then lead to new insights in pelagic ecosystems functioning and to a better monitoring of aquatic ecosystem health.

Table 2.1. Summary of historical and new hypotheses that have emerged to explain carotenoids accumulation in copepods.

Hypothesis	**Description**	**Confidence**[†]	**References**
H_1 - Photoprotective role hypothesis	Carotenoid pigments protect the whole individual against reactive oxygen species (ROS) produced by short light radiation	+++	Hairston 1976
	Under light stress, a trade-off can occur if visual predators are present	++	Hansson 2004 Hylander 2009a
H_2 - Metabolic stimulation hypothesis	Carotenoid pigments confer a potential for heat absorption leading to	(-)	Byron 1982

	higher metabolic rates for redder individuals		
H_3 - Food reserve hypothesis	Association of carotenoids with lipid reserves, both would be consumed as food in the future	(?)	Ringelberg & Hallegraef 1976
H_4 - Lipid protection and metabolism hypothesis	Carotenoids are synthetized and stocked with lipids as a protection against ROS mostly produced by oxygenated active metabolism, and by other external stressors	++	Foss et al.,1987 Schneider et al. 2016 Grosbois & Rautio 2018
H_5 - Egg and nauplii protection hypothesis	Accumulation of carotenoids in eggs, often transferred from lipid reserves, as a protection against ROS produced by various sources (examples: by active metabolism during rapid growth or induced in buoyant eggs by light radiation in surface waters)	+++	Lotocka et al. 2004 Schneider et al. 2016
	Astaxanthin forms (free, esters, caroteno-proteins) may thus change according to ontogeny	++	Lotocka et al. 2004
H_6 - Adaptive camouflage hypothesis	Red carotenoid coloration protects copepods by making them cryptic in deeper and darker waters, especially under the green-blue searchlights of predators	+	Johnsen 2005 Vestheim & Kaartvedt 2006
	Coupling with proteins induce color changes (blue color) in relation with depth or daily cycles as a camouflage strategy	(?)	This article
H_7 - Mating criteria hypothesis	Accumulation of red carotenoids in females to be assessed by males (*honest signal)* during mating	(-)	Powers et al. 2019

H_8 - Antioxidant "swiss army knife" hypothesis	Astaxanthin provides protection against all reactive oxygen species, especially from endogenous sources, and can improve growth, reproduction and survival at various moment of copepods' life cycle	+++	Lotocka et al. 2004 Gorokhova et al. Schneider al. 2016 This article
	Astaxanthin bioconversion and thus color and its intensity, are very plastic and finely regulated (enzyme activities, gene transcription) according to the internal and external conditions (visibility condition, living depth, reproductive status, lipid storage, etc)	+++	Johnsen 2005 Vestheim & Kaartvedt 2006 Hykander 2009a Gorokhova et al. 2013 This article

[†]Confidence levels have been estimated from this literature review: (-): hypothesis theoretically or experimentally refuted, (?): hypothesis still to be tested, +: hypothesis with low level of confidence, ++: hypothesis with medium level of confidence, +++: hypothesis with high level of confidence.

2.4. Carotenoid red and blue pigmentation in copepods

2. 4. 1 A shared and conserved functional trait

From 95 articles containing the keywords "*copepods*" and "*carotenoid**", "*astaxanthin*" or "*redness*", it appears that carotenoid-based color is a very common functional trait in copepods, as it was observed in at least 154 distinct locations in the world (Fig. 2.1). About 170 freshwater and marine copepod species from 65 genera are known to accumulate these pigments, and among these, the marine *Calanus* spp. and the freshwater *Diaptomus* spp. are the most studied (>30 reported observations each, see Data1). Of the 95 studies, 74% have quantified carotenoids, however, using various methods and units (Data1). Note that copepods have to be frozen (e.g. for chemical analyses) or taken in photos soon after sampling (within a few hours) to study their pigmentation. For all the following quantitative analyses, we used carotenoid concentrations measured by High Performance Liquid Chromatography (HPLC) and expressed in µg per mg of dry mass (usually written dry weight, but noted dry mass here to follow the conventions of the SI system). It was the most common method and unit in the literature (202 over 286 measurements for which latitude, longitude, altitude, species,

life stages and astaxanthin concentrations were provided). Because analytical machines are not capable of resolving very small concentrations of molecules, a measurement is here a HPLC quantification of pigments performed on a sample that contains multiple individuals (*e.g.* more than 10), then normalized by the mass of the sample. Whenever possible, we have converted some carotenoid quantifications expressed in other units, insofar they were extracted by chemical methods for monospecific samples of late copepodites or adults (details in Table B.1). Finally, 211 values in $\mu g.mgDM^{-1}$ were used for quantitative analyses in this article. Globally, carotenoid concentrations range from 0.00014 $\mu g.mgDM^{-1}$ to 17.2 $\mu g.mgDM^{-1}$ with an average of 1.22 $\mu g.mgDM^{-1}$. Data also allowed us to confirm previous findings (*e.g.* Hylander et al. 2014) that freshwater species concentrate more pigments than marine species, with a median of 2.243 $\mu g.mgDM^{-1}$ (n=66) vs. 0.137 $\mu g.mgDM^{-1}$ (n=145), respectively (Fig. 2.1 and Fig. B.1 for details by copepod genus). To statistically compare carotenoid concentrations between marine and freshwater ecosystems, we performed a Wilcoxon rank sum test because data on marine carotenoid concentrations was still not normally distributed after logarithmic transformation. This test was highly significant ($p<0.001$) and highlighted the strong difference in carotenoids accumulation by copepods between the two aquatic ecosystems.

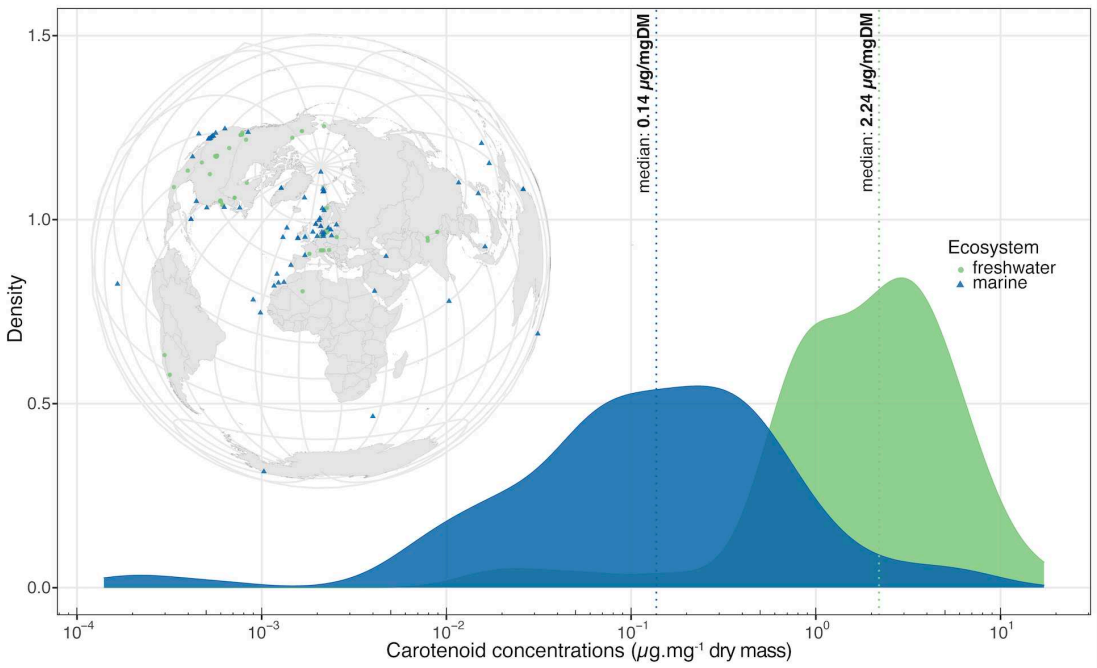

Figure 2.1. Carotenoid concentrations in freshwater and marine copepods across the world. Observations of pigmented copepod samples are available at 154 locations globally (inset map) from 95 studies published since 1949. Freshwater is in green and marine in blue. We used 211 pigments measurements ($\mu g.mg^{-1}$ dry mass) to plot density distributions of carotenoid concentrations with a log-transformed x-axis. The median copepod carotenoid content is higher in freshwater than in marine ecosystems (*Wilcoxon rank sum test*, $p<0.001$).

2. 4. 2 Localization, molecular forms and metabolism of carotenoid pigments

Carotenoids induce an orange to red - and sometimes even blue - coloration in copepods of many different species. These species inhabit environments characterized by various abiotic and biotic pressures, which is an indication that the utilization of carotenoids presents diverse and potentially positive roles in copepod biology. Disparities in carotenoid localization and forms result in different visual signatures, even for the same pigment quantity (Herring 1972) (Fig. 2.2). Indeed, coloration can be uniformly spread throughout the copepod's body, or clustered in some specific structures such as lipid droplets and lipid sacs, eggs, antennules or genital somites (Fig. 2.2). Although a few authors mentioned the presence of chromatophores (Herring 1972, Bandaranayake and Gentien 1982, Vestheim and Kaartvedt 2006; asterisk-shaped red patches on Fig. 2.2I), it is not clear whether copepod species have actually developed cells or organs dedicated to pigment production, similar to what has been demonstrated in the liver for birds (Mundy et al. 2016).

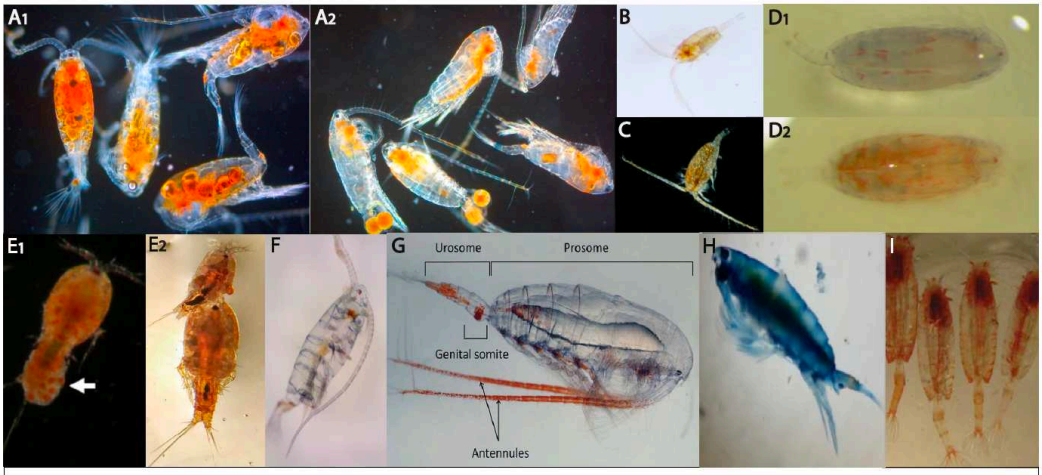

A : *Leptodiaptomus minutus*, **Canadian lake in winter (A1) and summer (A2),** Grobois & Rautio, 2018
B : *Diaptomus castor*, **fishless pond in Sweden,** Brüsin et al., 2016
C : *Eudiaptomus gracilis*, **lake in Sweden,** Hylander et al., 2012
D : *Undinela vulgaris*, **equatorial Atlantic at day (D1), and night (D2),** Kiko R., 2020 (personal observation)
E : *Tigriopus californicus*, **female with eggs (E1), mating adults (E2), US west coast,** Tsuboko-Ishii & Burton, 2018 & Powers et al., 2019
F : Unknown species, **blue hole in the Bahamas,** Lee et al., 2019
G : *Calanus sp*, **Arctic seas**, Choquet et al., 2018
H : *Pontella fera*, **equatorial Atlantic ocean,** Rahlff et al., 2018
I : *Pareuchaeta norvegica*, **Norvegian coast,** Kaartvedt & Vestheim, 2006

Figure 2.2. Examples of pigmented copepods from freshwater (A-C) and marine (D-I) ecosystems from the literature. Images were all taken from published articles, indicated on the figure. Carotenoids can be accumulated throughout the body in yellow-red (B, C, D2, E2, I) or blue (D1, H) hues. Also, they can be localized in specific structures such as lipid droplets and sacs (A1, G), eggs (A2, E1), antennules (G, H) or genital somite (G). Rights for images: Licenses obtained from Wiley for A1, A2, C, E2, I; License CC-BY-4.0 for B, F, G, H; License CC BY-NC-ND-3.0 for E1; Images D1 and D2 shared with the permission of Rainer Kiko.

Intensity or localization of pigmentation can also help identifying species: the recognition of red rather than red-orange pigmented individuals from the genus *Neocalanus* in live collections led to the discovery of a new *Neocalanus* species from the subarctic Pacific Ocean (Miller 1988), and the redness of antennas and genital somites can be used to distinguish two *Calanus* congeners (*C. finmarchicus* and *C. glacialis*; Nielsen et al. 2014, Choquet et al. 2018, Lindeque et al. 2022).

Two types of carotenoids are found in copepods: astaxanthin and canthaxanthin. Thirty-two studies provide a detailed description of carotenoid pigments' molecular forms for various species and developmental stages (170 measurements). In 96% of these measurements, astaxanthin was the dominant carotenoid (mentioned as "dominant" in the text or as indicated by a contribution of more than 50%). In only 6 cases, astaxanthin was in minority (<50%), while a mix of other phytoplanktonic carotenoid molecules (β-carotene, chlorophylls *a* and *b*, echinenone, β-doradexanthin) from the diet contributed the most (Bandaranayake and Gentien 1982, Lotocka 2004, Moeller et al. 2005, Rhodes 2007, Rautio et al. 2009). Canthaxanthin was found in only 21 samples of copepods, and always at low levels (traces, less than 5%). Astaxanthin is thus the dominant pigment in copepod species, as it is in non-copepod aquatic crustaceans (Matsuno 2001). It has to be synthesized from dietary phytoplankton carotenoids (Moeller et al. 2005, Babin et al. 2010, Caramujo et al. 2012) and its bioconversion involves a series of ketolase and hydroxylase enzymes that oxidize ß-carotene, lutein or zeaxanthin into astaxanthin (Weaver et al. 2018a). Parsimoniously, the most oxidized precursors from the diet will be favored. Three metabolic pathways coexist but most species, such as *Paraeuchaeta russelli* (Bandaranayake and Gentien 1982), *Cyclops kolensis* (Czeczuga et al. 2000), *Acartia bifilosa* and *Pseudocalanus acupes* (Lotocka 2004), rely on echinenone and canthaxanthin as intermediates. It has recently been suggested that carotenoid bioconversion is linked to mitochondrial activity: the Shared Pathway Hypothesis (SPH) (Powers and Hill 2021, Powers et al. 2022). It proposes that ketolations and hydroxylations of algal carotenoids (oxido-reduction reactions) are involving electrons donors located in inner mitochondrial membranes (probably NADP and NADPH, see Powers & Hill, 2021 for detailed explanations). The SPH offers new perspectives on the link between astaxanthin production and copepod fitness, which will be further discussed in the third part of this review. However, while respective genes and associated membrane enzymes were identified in turtles and birds (Mundy et al. 2016, Twyman et al. 2016), only candidates for possible genes have been proposed for crustaceans like copepods (Mojib et al. 2014). Latest advancements on the molecular bases of astaxanthin synthesis are discussed in the fourth part.

In the animals, astaxanthin can either be found in a free form, esterified with fatty acids (mono- or diesters) or associated with a protein (Matsuno 2001, Schneider et al. 2016). The proportion of each form can vary between species, but also at the individual level over time. Free astaxanthin can be incorporated into cell membranes where it preserves membrane structure by reducing phospholipid peroxidation (McNulty et al. 2007, see next paragraph). For the majority of copepod samples (61%) from a detailed dataset of astaxanthin forms (Data2), free astaxanthin is the dominant form. The remaining 39% preferentially accumulate astaxanthin esters. All samples with more than 70% of astaxanthin being esterified belong to copepod species known to accumulate large lipid storage *Calanus finmarchicus, C. pacificus, C. helgolandicus, Arctodiaptomus walterianus, Leptodiaptomus minutus*; Data2). In a one-year study, the amount of unesterified astaxanthin was relatively constant in adults of *Leptodiaptomus minutus* (Schneider et al. 2016), but the proportion of specific esters can vary substantially in them. Starvation of *Calanus pacificus* population first led to an increase of free astaxanthin from esters degradation, followed by an overall decrease in total astaxanthin content (Juhl et al. 1996). These observations led the authors to suggest a strong link between carotenoid pigmentation and lipid metabolism (Foss et al. 1987, Juhl et al. 1996, Lotocka 2004, Sommer et al. 2006, Schneider et al. 2016). Lotocka et al. (2004) formulated the hypothesis that astaxanthin forms vary with ontogeny, *i.e.* that free forms are dominant in nauplii and young copepodites and esterified forms in adult stages. However, the limited quantification of carotenoids according to development stage precludes statistical testing (Data2) (Hairston 1979, Lotocka 2004, Holeton et al. 2009, Cui et al. 2021). We suggest that ontogenic accumulation of astaxanthin esters may be especially important for species in which adults depend on lipid reserves for survival and reproduction, and for which the proportion of free astaxanthin and esters varies according to the individual state (reproductive stage, starvation, etc.) (Juhl et al. 1996, Schneider et al. 2016).

Occasionally, the formation of a caroteno-protein complex with astaxanthin or canthaxanthin induces a blue coloration (Cheesman et al. 1967, Mojib et al., 2014). This phenomenon was observed, but rarely quantified, in the freshwater copepod *Eudiaptomus amblyodon* (Czeczuga 1975) and in many marine pontellid and calanoid copepods. A uniform blue coloration (Fig 2.2H) is particularly common in neustonic copepods from equatorial waters and was described for the following species: *Labidocera glauca* (Smith 1941), *Labidocera nerrii*, *Labidocera woolastoni*, *Labidocera acutifrons*, *Pontellopsis regalis*, *Pontellopsis villosa*, *Anomalocera patersoni* (Herring 1972), *Pontella. fera* (Herring 1965, Rahlff et al. 2018), *Pontella valida* (Venkataramana et al. 2017), *Pontella sinica* (Ory et al. 2017), *Undinula vulgaris*, *Centropages furcatus* (Bandaranayake and Gentien 1982), *Ivellopsis denticauda (Rahlff et al. 2018), Acartia fossae (*Mojib et al., 2014*), Acartia eurythreaea (*Nakajima et al. 2013*), Farranula gibbula (*Medellín-Mora et al. 2021*), Saphirinna* sp. (Ory et al. 2017), and

*Corycaeus sp. (*Mojib et al., 2014, Ory et al. 2017). Recently, observations of *Undinula vulgaris* transitioning from a blue to a red coloration between day and night were made in Atlantic waters (Fig. 2.2D$_1$ and 2.2D$_2$ provided by R. Kiko; Kiko et al. 2020) and raises many questions about the metabolic control of carotenoid complexation with proteins. Furthermore, planktonic ecologists often observe bright red adults with blue eggs in *Paraeuchaeta* spp. and *Euchaeta* spp. for example (Lee et al. 1974, Bandaranayake and Gentien 1982, Vestheim et al. 2005). This intriguing phenomenon shows that astaxanthin can be found in different forms between the copepod body and the eggs, which also implies a link between astaxanthin and ontogenic development.

2. 4. 3 Physiological action modes of astaxanthin

The strong antioxidant power of astaxanthin is a unique property that could explain its ubiquity in copepods. To understand the molecular functions underlying this property, we provide a succinct description of its reactions with Reactive Oxygen Species (ROS) at the molecular level (Fig. 2.3). ROS are oxidant molecules, mainly produced by endogenous metabolism such as mitochondrial respiration, or sometimes induced by external stressors such as ultraviolet radiation (Krumova and Cosa 2016, details on Fig. 2.3A). In animals, the development of a complex antioxidant system was selected through evolution to avoid critical ROS damage on proteins, lipids and DNA (Fig 2.3B) which is the main cause of cell aging (Finkel and Holbrook 2000). However, oxidative stress can still occur when enzymatic and non-enzymatic antioxidant defenses are not efficient enough to neutralize all ROS (Monaghan et al. 2009). The astaxanthin molecule is an important part of this defense system since its long-conjugated carbon chain has a particularly strong antioxidant power (Miki 1991).

The antioxidant capacity of astaxanthin has two components represented on Fig. 2.3C: a strong quenching effect against singlet oxygen and a scavenging effect against free radicals (Miki 1991, Naguib 2000). In singlet oxygen quenching, the energy of an excited oxygen molecule (^{1}O2) is transferred to the carotenoid by direct contact, and the excessive energy is relaxed thanks to the vibration of the carbon chain. The astaxanthin activity for neutralizing singlet oxygen is approximately 10 times stronger than those of other carotenoids (Miki 1991). Astaxanthin is also very efficient to scavenge free radicals *i.e*. molecules with unpaired electrons (Terao 1989, Naguib 2000). In particular, it can trap lipid radicals (LOO$^\bullet$) produced in large quantities when hydroxyl radicals (OH$^\bullet$) degrade lipids through a chain reaction (*lipid peroxidation*, Girotti 1985). The product of the reaction between the radical (OH$^\bullet$ or LOO$^\bullet$) and astaxanthin is stable and stops the chain reaction of lipid degradation (Terao 1989). While the existence of these two mechanisms could explain the prevalence of astaxanthin in copepods, the precise environmental conditions favorable for astaxanthin

accumulation are still unclear. In the next part, we discuss the various biotic and abiotic forcings fostering copepod pigmentation.

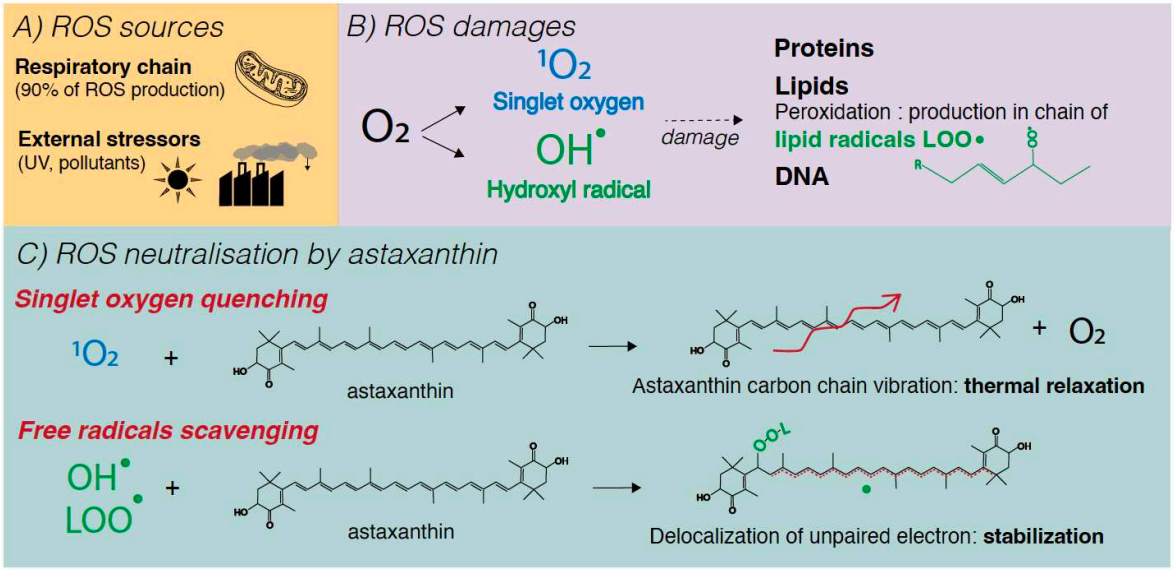

Figure 2.3. Reactive Oxygen Species (ROS): sources, damages and neutralization by astaxanthin. A) ROS are produced by active oxic metabolism and/or external stressors. B) Free radicals (atoms or compounds with one or more unpaired electrons, noted with the point symbol•, in green) and non-radical oxidants (atoms or compounds in an excited electronic state at high energy level, in blue) can induce damages on proteins, lipids and DNA. Note that lipid peroxidation by hydroxyl radicals (OH•) can lead to the chain production of lipid radicals (LOO•), also dangerous for cell components. C) Thanks to its long double-bonded carbon chain, astaxanthin can buffer singlet oxygen by quenching, or buffer free radicals by electron scavenging. This scheme is a synthesis of the information found in Balaban et al. (2005), Krumova and Cosa (2016), Girotti (1985) for sections A and B, and in Terao (1989), Miki (1991), Naguib (2000) for section C.

2.5. Effects of abiotic and biotic forcings on astaxanthin concentrations in copepods

2. 5. 1 Environmental controls on pigmentation

Among the most studied environmental variables that correlate with carotenoid pigmentation in copepods are lake elevation, latitude, temperature and solar radiation (Fig. 2.4., Siefken and Armitage 1968, Hairston 1979, Byron 1982, Hansson 2000). It has been recognized for a long time that copepods from high altitude lakes are the reddest (Fig. 2.4M). Indeed, we found the two highest concentrations of astaxanthin in copepods from lakes at 4,890 m (17.2 µg.mgDM^{-1}, Sommaruga

2010) and 3,613 m high (8.5 µg.mgDM^{-1}, Persaud et al. 2007). Including all freshwater measurements, we found a significant correlation between astaxanthin concentrations and lake elevation ($n = 65$; $p < 0.01$, Fig. B.2), but with a high variability ($R^2 = 0.12$). In marine ecosystems, three studies showed that latitude is positively correlated with carotenoid content at a regional scale: arctic and subarctic species are more pigmented than tropical and temperate species (Fig 2.4I) (Hansson 2000, Hansson et al. 2007, Hylander et al. 2009). However, when using the complete dataset assembled here, there is no significant correlation between latitude and carotenoid content at a global scale (Fig. B.3). This highlights how difficult it is to reveal a large-scale trend for a physiological trait that can be finely regulated at relatively short temporal, and thus small spatial, scales (paragraph 2. 7. 1). Moreover, studies were performed in different seasons and for various species, depths and ecosystems. Therefore, it is likely that this dataset may still not be exhaustive and representative enough to reach a statistical signal stronger than the effect of all these sources of variability.

Furthermore, we cannot regard the effects of altitude or latitude as independent factors of pigmentation, but we rather emphasize their relation with direct drivers such as temperature, solar radiation and ice-cover. Solar radiation, especially short wavelengths (ultraviolet), enhances astaxanthin accumulation in most cases (Fig. 2.4F, G). It can explain why copepods living in high altitude ecosystems are especially red, in particular if lakes or ponds are shallow and do not provide refuge at greater depths (see negative correlation between carotenoid content and lake depth, Fig. 2.4P). Similarly, the highest carotenoid concentrations in marine copepods, on par with their freshwater counterparts (Fig. B.1), were observed for *Tigriopus sp.* living in shallow supralittoral tidal pools subjected to strong solar radiation (Davenport et al. 2004, Weaver et al. 2018b). This confirms the expected antioxidant role of astaxanthin against UV-induced ROS. However, two observations contradict this hypothesis: *(i)* most marine copepods living under high solar radiation at low latitudes do not accumulate red pigments at all, or only very little (Fig. 2F) (Lee et al. 2019); *(ii)* some populations found in arctic lakes covered by ice in winter are bright red, even though light penetration is severely limited (Fig. 2.2A) (Grosbois and Rautio 2018). Therefore, the protection against light and UV radiation cannot be the *only* explanation for redness variability, especially because UV is strongly attenuated in aquatic ecosystems (Tedetti and Sempéré 2006).

Temperature is a key variable as it is almost always negatively correlated with carotenoid content *in vivo* (Fig. 2.4L), and arctic freshwater and marine copepods are known to show intense red colors (Siefken and Armitage 1968, Byron 1982, Garcia et al. 2008, Snoeijs and Häubner 2014, Schneider et al. 2016). This observation, in addition to *in vitro* experiments on astaxanthin molecules (Pedersen et al. 2014) suggests that astaxanthin is likely to be more stable at cold temperatures than at warm temperatures. As a consequence, the lack of red pigmentation in tropical environments with

strong solar radiation may be caused not by a lack of usefulness of astaxanthin molecules, but rather by molecular instability. Nevertheless, if redness is much scarcer in inter-tropical waters, blue color induced by astaxanthin complexation with protein is common for copepods living in the first centimeters under the surface (Rahlff et al. 2018). This stability of the various forms of astaxanthin (including caroteno-proteins) according to temperature would be interesting to investigate further, along latitudinal gradients in marine ecosystems.

As a conclusion, solar radiation and temperature are both key variables explaining pigmentation variations at a global scale, but are not sufficient to solve the color puzzle alone. In the next paragraphs, we discuss the effects of internal metabolism (diet, lipid synthesis) and external interactions (predation, camouflage) that also play an important role in copepod individuals' pigmentation.

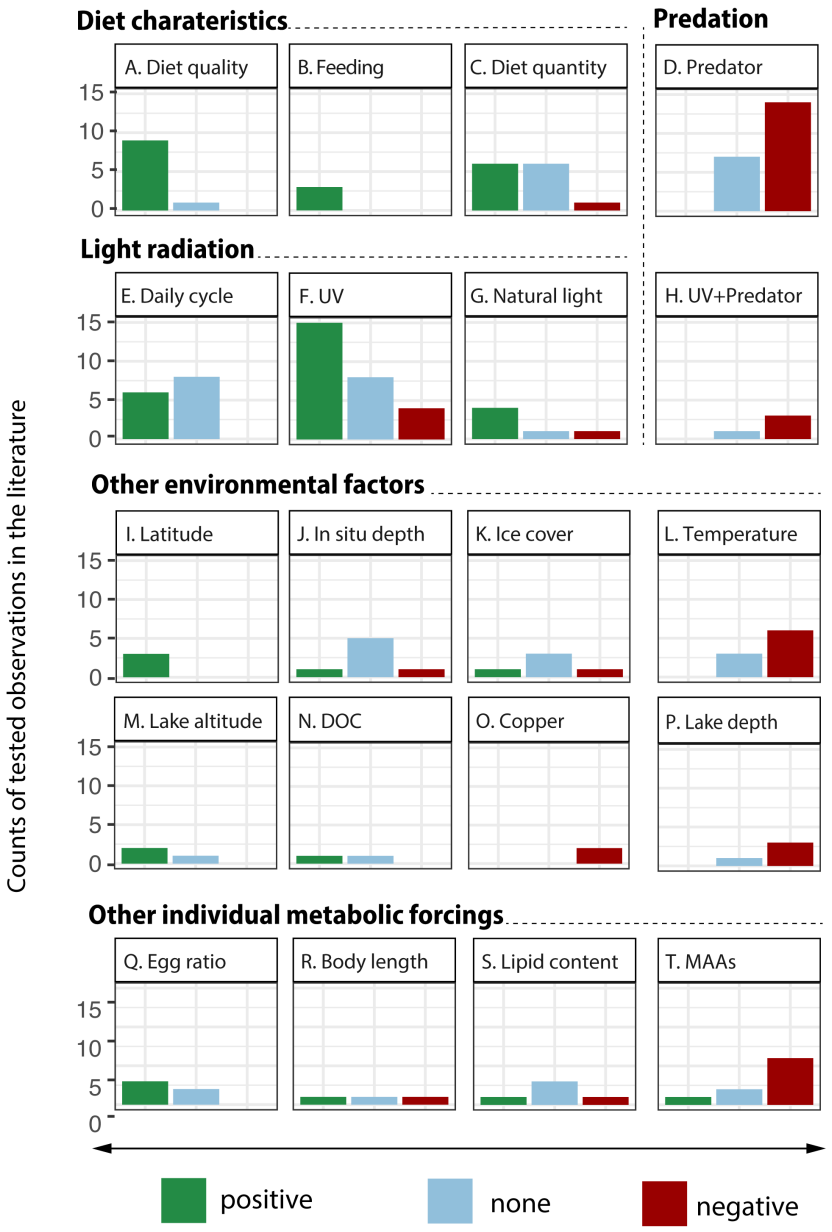

Figure 2.4. Counts of correlations between copepod carotenoid pigmentation and main environmental, biological or ecological forcings tested in the literature. All correlations between the carotenoid content of a copepod sample and a forcing variable (grouped in the categories: diet, predation pressure, light radiation stress, and other environmental or metabolic forcings) were retrieved from the literature (Data3). If statistically significant, the correlation was reported as "positive" (green) or "negative" (red). If not significant, the correlation was reported as "none" (blue). Only forcing variables with at least 2 tested correlations reported were considered (*in situ* or *experimental*). UV: Ultra-violet Radiation; MAAs: mycosporine-like amino acids (see Table 2.2).

2. 5. 2 Biological and metabolic drivers of pigmentation

Copepods rely on phytoplankton precursors to synthesize astaxanthin (Weaver et al. 2018a). As a consequence, variations in their phytoplanktonic diet and feeding activity have a significant impact on astaxanthin production (Fig. 2.4A, B, C). A minimum of algal carotenoids is a *sine qua non* condition for copepods to build astaxanthin stocks: the harpacticoid *Tigriopus* spp. loses its red color with a yeast diet lacking carotenoids (Davenport et al. 2004, Weaver et al. 2018a, Powers et al. 2019). An example of calanoid copepods from the Baltic sea shows that astaxanthin production in mesocosms was highest when the population was fed on a diverse phytoplankton community dominated by chlorophytes, dinoflagellates and diatoms with thin silica frustules in comparison with a diet composed of a low diversity of heavily silicified diatoms (Andersson et al. 2003). Diet quality (composition, diversity) is thus an undeniable driver of astaxanthin production (Fig. 2.4A, Andersson et al. 2003, Van Nieuwerburgh et al. 2005, Rhodes 2007).

Because algal communities strongly vary in terms of abundance and composition over time, it can be expected to see equivalent variations of astaxanthin accumulation in copepods. Indeed, for 33 of 37 time series, astaxanthin content showed seasonal patterns with maxima in winter (45%) or in spring (40%) (Data1 and code, "seasonal pic" column). However, the correlation with food quantity is not always obvious (Fig. 2.4C) and pigmentation can vary a lot among copepods living under the same food conditions (Hansson 2004). Holeton et al. (2009) showed that the astaxanthin production first increases linearly with increasing food concentration, but drops for algal concentrations (*Tetraselmis suecica*) higher than 150 $\mu gC.L^{-1}$ because of inefficient assimilation at too large food quantity, which implies that there is an optimal food concentration for astaxanthin production.

Redness and phytoplanktonic dynamics can also be fully decoupled, resulting in astaxanthin maxima in the cold, less productive season (Hairston 1979, Davenport et al. 2004). In the total darkness or in some turbid waters, some copepods are still bright red (Schneider et al. 2012, 2016, Trudnwoska et al. 2022). As discussed above, pigments have long been known to be associated with lipids in "fat cells" (Siefken and Armitage 1968, Ringelberg and Hallegraeff 1976) or in lipid droplets (Veen 2005, Grosbois and Rautio 2018). In this context, the most likely function of astaxanthin is to scavenge lipid peroxyl radicals (Table 2.1, H_4), inhibiting chain reactions of lipid degradation because of oxidative stress (Fig. 2.3C). Astaxanthin, which has a similar molecular length as fatty acids, can be incorporated into cell membrane bilayers where it preserves structure and intercepts radicals through the entire membrane (Woodall et al. 1997, McNulty et al. 2007). When esterified with fatty acids, astaxanthin could help diapausing and/or capital breeding species to protect their long-term energy deposits to survive rough and variable environments (Foss et al. 1987, Juhl et al. 1996,

Sommer et al. 2006, Schneider et al. 2016). More studies are, however, still needed to clarify the link between lipids and astaxanthin accumulation, because reported results are not consistent (Fig. 2.4S). The unique and very detailed study on the boreal copepod *Leptodiaptomus minutus* from Lake Simoncouche, Canada, showed a strong seasonal correlation between astaxanthin and lipid content, with maximum accumulation of astaxanthin in late fall at the peak of lipid anabolism (Schneider et al. 2016).

Consistently among all the experiments, the periods of net loss in astaxanthin coincided with peaks of egg production in spring and summer leading to minimum astaxanthin contents. There was a clear transfer of pigments from lipid stores to eggs, leading to new questions and hypotheses (Fig. 2.2A) (Grosbois and Rautio 2018). Observations of red pigments in eggs and spermatophores were first made in 1979 (Hairston 1979, Holeton et al. 2009, Schneider et al. 2017). A general positive correlation appears between carotenoid content and egg ratio (Fig. 2.4Q). In particular, eggs of *Tigriopus sp.* transit from dark gray to red as embryos develop (Weaver et al. 2018a), and astaxanthin of *Euchaeta japonica* blue eggs is apparently metabolized by early nauplii stages, who progressively become colorless with development (Lee et al. 1974). Astaxanthin accumulation in eggs and nauplii suggests an important role in early copepod development (Table 2.1, H_5). For example, it could protect buoyant eggs that stay in surface layers and are then exposed to higher UV radiation without the possibility of vertical migrations to avoid them (Hairston 1979, Browman et al. 2000). As suggested by Lotocka (2004), a broad-based role of astaxanthin in juveniles is conceivably to fight against ROS produced by yolk catabolism and rapid growth (Table 2.1, H_5), since most ROS are produced by normal metabolism and not by external stressors (Fig. 2.3A). However, further studies are needed to link astaxanthin content to hatching success and nauplii survival (new research perspectives are summarized in Table 2.3).

2. 5. 3 Impacts of intra- and inter-species interactions on pigmentation

The role of astaxanthin pigments cannot be reduced to antioxidative protection, especially considering that the main function of color in nature is to trigger behavioral responses and interactions (as for birds, flowers and fish). The accumulation of red pigments makes copepods more conspicuous in well-lit waters, increasing the risk of capture by visual predators (Hairston 1981). Some studies showed that copepods accumulate more pigments when they inhabit fishless freshwater environments (Luecke and O'Brien 1981, Byron 1982, Hansson 2000). The comparison of mean carotenoid concentrations between lakes with and without predation pressure by fish (with predators: 2.06 $\mu g.mgDM^{-1}$, n=34; without predators: 3.35 $\mu g.mgDM^{-1}$, n = 22) was significant using the data collected for this review (*Wilcoxon rank sum test*, p-value = 0.03597, Fig. B.4). This result suggests

again the influence of predation pressure on carotenoid pigmentation. It has, however, to be noted that such habitats are often shallow ponds that freeze up or evaporate seasonally and where copepods are subjected to strong radiation which also promotes coloration (Fig. B.4, points colored according to altitude). Other studies showed that copepods are able to adjust the level of pigmentation according to fish threat in lakes (Fig. 2.4D) (Hansson 2004, Schneider et al. 2016, Lee et al. 2019). *In vitro*, pigmentation is reduced a few days or weeks after perceiving chemical cues of predators (Hansson 2004, Veen 2005, Hylander et al. 2012, Brüsin et al. 2016). These observations indicate that astaxanthin synthesis and degradation are fine regulated at the cellular level according to predation pressure (see section 2.7).

Another zooplankton strategy to avoid visual predation is diel vertical migration (DVM). By spending time at depth, copepods diminish their probability to be targeted by visual predators in brighter surface waters. Furthermore, because light wavelengths from 600 to 750 nm are absorbed in the upper few meters by water molecules, red color is the optimal coloration for zooplankton crypticity at depth (Johnsen 2002, 2005). When deep visual predators use green-blue "bioluminescent searchlights", red animals appear black and are completely hidden. Also, we can observe a color gradient from blue and transparent animals in surface layers to red in the deep waters (Johnsen 2014). Accumulating red pigments, and thus being able to avoid predators at greater depths, could represent a selective advantage for vertically migrating copepods (i.e. *Paraeuchaeta noervegica*, Vestheim et al. 2005) or for copepods spending a large part of their life at great depths (i.e. diapausing *Calanus* spp., Kvile et al. 2019, Daase et al. 2021). According to Hays et al. (1994), large copepods are performing more extensive diel vertical migrations (DVM) than smaller taxa, but pigmentation is correlated with DVM only for the small (<1mm) copepod taxa. As size and color are the main factors influencing visibility, authors argued that only small species can afford to accumulate pigmentation without increasing their chance to be captured when residing in surface layers. However, the largest copepod species in the oceans (*Calanus hyperboreus*) is strongly pigmented and migrates vertically. In general, most published data of copepod redness associated to position in the water column do not provide evidence for depth-dependent pigmentation (Fig. 2.4J).

The intensity of the color or the color itself might also change according to visibility conditions. Vestheim & Kaartvedt (2006) showed that copepods were redder by night than by day, presumably avoiding visual predation in brighter waters. Blue color, on the other hand, is mostly constant for neustonic copepods (Fig. 2.2H) and represents an antioxidant defense against ultraviolet radiation (Herring 1972, Nakajima et al. 2013, Venkataramana et al. 2017), in addition to a camouflage from fish and birds in surface waters. Indeed, their blue reflectance perfectly matches water color (Rahlff et al. 2018), which might be advantageous for some blue copepods performing

reverse vertical migrations (Chae & Nishida 1995, Tester et al. 2004). Recent observations of copepods transitioning from blue during the day to red at night (Fig. 2.2D1 and D2, R. Kiko personnal observation) offer new research questions: could color change according to day cycle and/or depth to provide a defense against visual predation? With the exception of blue neustonic population or red population living in shallow tidal pools or ponds (Sommaruga et al. 2010, Cui et al. 2021, Davenport et al. 2004) (Fig. 2.5), it could be argued that the use of astaxanthin as UV-protectant may be limited in deep lakes and offshore ocean because UV are absorbed in the few first meters (Tedetti and Sempéré 2006) and large refuge depths are available. In those contexts, color might be evolutionary selected for camouflage against predators and/or for its general antioxidant properties, rather than UV protection (Lotocka et al. 2004, Schneider et al. 2016). One counter example is the surface swarms of *Calanus* copepods showing a red color presumably used as a UV-protectant (Basedow et al. 2019). This is supported by the fact that the same species are transparent when they inhabit really turbid glacial waters (Trudnowska et al. 2022). However, the only trial of correlation between astaxanthin content and light radiation was not successful (Hylander et al. 2015). Carotenoids could help copepods against UV when they reside in surface layers, but only as one of the several functions that the astaxanthin “swiss army knife” allows (Fig. 2.5).

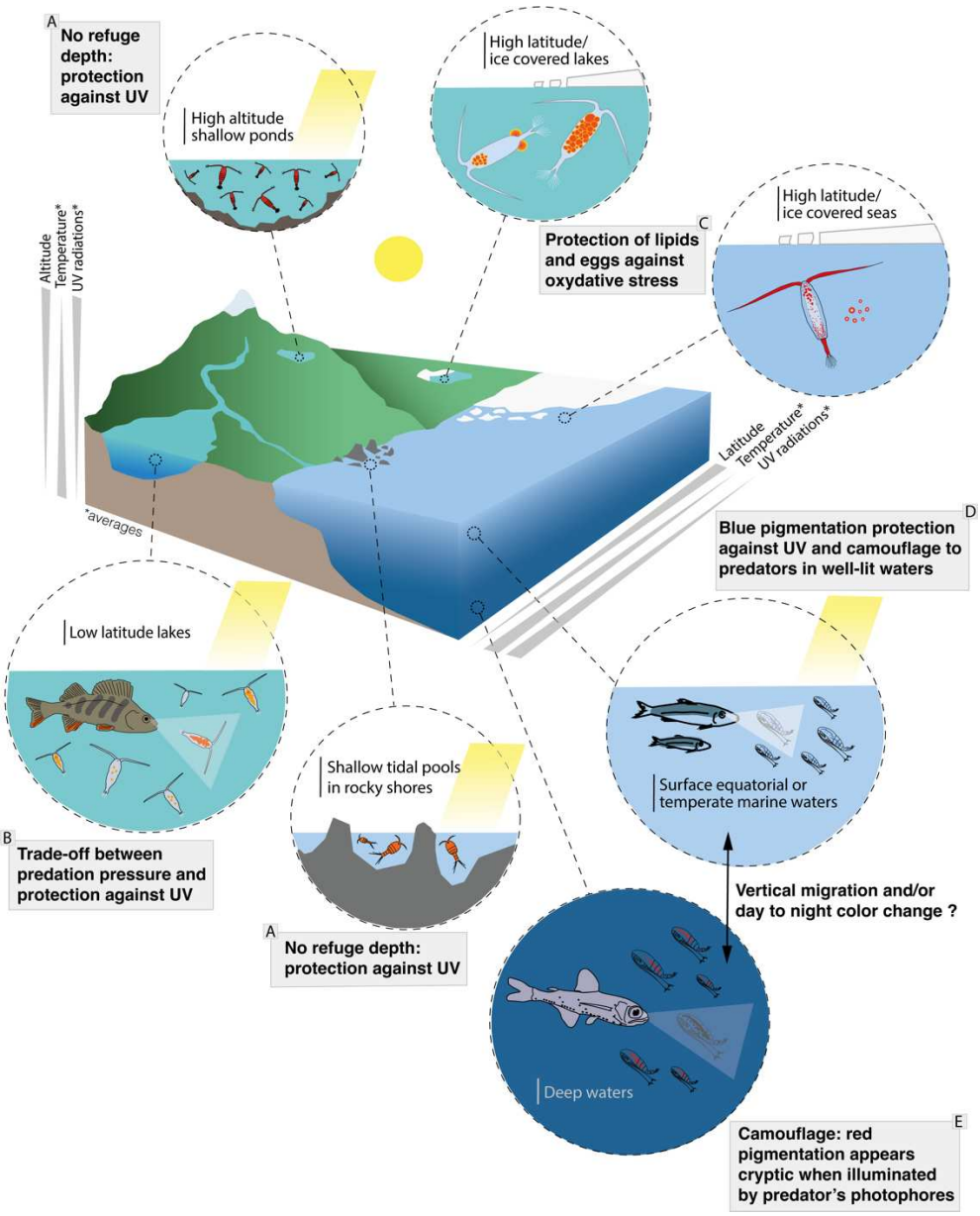

Figure 2.5. Carotenoid-based pigmentation as a swiss army knife for copepod fitness in aquatic ecosystems. This figure summarizes the multiple roles that astaxanthin pigmentation can have for copepods in aquatic ecosystems at a global scale. For various latitudes, altitudes, temperature and ultraviolet radiation (UV) conditions, red or blue pigments can improve copepods' fitness. Due to its antioxidant properties, it can buffer oxidative stress induced by ultraviolet radiation (A, B, D), or by internal metabolic byproducts or pollutants such as metallic ions. In particular, astaxanthin can protect lipids reserves and eggs (C), which benefits diapausing and capital-breeding species. Finally, color variations can impact ecological interactions, increasing or decreasing prey visibility to visual predators in well-lit (B, D) or dark waters (E). Carotenoid-based pigmentation is a widespread and plastic functional trait in copepods, providing indirect benefits for aquatic trophic networks by the transfer of antioxidants, up to humans.

As a general conclusion, astaxanthin synthesis is performed preferentially in cold environments, with an optimal diet quality and quantity and limited predation pressure. Then, its accumulation depends on light stress, mycosporine-like amino acids (MAAs) synthesis possibility (Table 2.2), lipid metabolism and egg production in females. The potential advantages conferred by pigmentation in terms of fitness are discussed hereafter.

Table 2.2. Carotenoids and mycosporine-like amino acids (MAAs).

A striking example linking environmental, physiological and ecological drivers influencing antioxidant defenses

Mycosporine-like amino acids (MAAs) are other photoprotective substances absorbing UV radiations. Their synthesis also depends on phytoplanktonic food availability (biological control), but with precursors different from carotenoid ones (Moeller et al. 2005). MAA accumulation is also triggered by light stress (environmental control), however, those molecules absorb at wavelengths between 310 nm and 360 nm (UV) and are not visible to predators in natural light. Consequently, MAAs do not enhance the risk of visual predation and are likely beneficial for individual fitness (ecological control). Studies that quantified both MAA and carotenoid contents often found a strong negative correlation between the abundances of these two compounds (Fig. 4T), meaning that one type of photoprotective molecule will be favored by individual metabolisms (Moeller et al. 2005; Persaud et al. 2007; Hylander et al. 2009). Hylander, Grenvald, et Kiørboe (2014) suggested that the generally smaller amount of carotenoid contents in marine ecosystems is due to a greater visual predation pressure, and a resulting preferential accumulation of MAAs. Yet, the difference of predation between freshwater and marine ecosystems has still to be proven. Nonetheless, it is likely that in very transparent tropical waters, MAAs presence would be especially valuable for fitness. In arctic ecosystems, MAAs synthesis was shown to be triggered by spring ice melting and consequent light stress for *Calanus* spp., whereas carotenoids are present, in lower but stable concentrations (Hylander et al. 2015). Could carotenoids and MAAs have complementary roles in these copepod polar species?

2.6. How does redness impact copepod fitness (reproduction, growth, survival)

After exploring the mechanisms triggering carotenoids production and the metabolic pathways involved, we estimated the effects of carotenoid content on individual fitness metrics such as percentage of survival, number of eggs produced or metabolic activity indices (Data4). We focused this analysis on redness because fitness variables were only tested on red copepods in the literature, even if blue pigmentation appears to be a clear advantage for neustonic animals (Rahlff et al. 2018). We found that red pigmentation is mostly beneficial for the copepods (Fig. 2.6). Out of 50 statistically

tested effects on one fitness variable, red pigmentation was favorable in 31 cases (62%), neutral in 11 cases (22%) and unfavorable in 8 cases (16%). The unfavorable effects are all linked to visual predation selectivity (Fig. 2.6). When red copepods were incubated with predators, which was always done in experimental settings and under white light (*i.e*, no tests with attenuated light typical of deep waters), they were preferentially preyed upon, and their probability to survive was lower than that of their transparent counterparts (Hairston 1976, 1979, Luecke and O'Brien 1981, Byron 1982, Gorokhova et al. 2013). However, redness was beneficial when measuring other survival metrics. The most repeated experiment was the survival (or mortality) test for transparent and red morphs that were exposed to visible and UV radiation (Hairston 1976, Ringelberg and Hallegraeff 1976, Luecke and O'Brien 1981, Byron 1982, Tartarotti 1999, Davenport et al. 2004, Caramujo et al. 2012), or that were exposed to copper or other pro-oxidant agents (Caramujo et al. 2012, Weaver et al. 2018a). In 71% of these experiments, redness was an advantage, presumably due to astaxanthin antioxidant activity. Molecular indicators such as hsp70 gene regulation and aconitase activity showed that carotenoid rich morphs presented less oxidative stress levels than transparent ones (Weaver et al. 2018a, Tartarotti et al. 2018). Coherently, red copepods expressed a better antioxidant capacity, inferred by Glutathione S-transferase (GST) activity, oxygen radical antioxidant capacity, and trolox equivalents (see Fig. 2.6; Hylander et al. 2012, Gorokhova et al. 2013, Tartarotti et al. 2018). Complementary results on survival also showed positive effects (Fig. 2.6): for example, red copepods suffered less from parasite infestations (Veen 2005).

As the redness trait provides advantages (*e.g.* antioxidant protection) at some costs (*e.g.* increased visibility to predators), trade-offs must exist at the individual level. When copepods were exposed to predator cues, their pigmentation decreased independently from ambient UV levels, suggesting that predation is treated as a more severe or immediate threat than energy-rich radiation (Hylander et al. 2009). To compensate for lacking UV protection, however, these copepods counteracted UV-induced oxidative stress by doubling the activity of the GST enzyme. The level of pigmentation can thus be considered as a plastic defense trait, which can be induced when needed (Hansson 2004, Hylander et al. 2012).

Color is also found to play a role in reproduction, which is a major measure of fitness (quantified by the number of descendants). The amount of eggs produced by females of the reddish marine *Eurytemora affinis* was significantly higher than their non-pigmented counterparts for the same food intake (Gorokhova et al. 2013) (Fig. 2.6). When the freshwater species *Diaptomus* and *Leptodiaptomus* cannot produce carotenoids (neither MAAs, see Table 2.2), they produce less offspring, which supports the hypothesis that, in absence of photoprotective agents, oxidative stress reduces reproductive success (Hylander et al. 2009) (Fig. 2.6). In one experiment, astaxanthin

concentration was also negatively correlated with ontogenetic development time: strong pigmentation allowed for a faster development of copepodites (Powers and Hill 2021). Molecular experiments are still required to fully elucidate the role of pigmentation in reproductive success (Table 2.3).

Even if sexual selection is mostly done through a developed chemosensory system or via mechanical cues in copepods (Ohtsuka and Huys 2001), another hypothesis is the role of coloration as a signal of individual quality when choosing a mate (*honest signal*; Powers et al. 2019, Powers and Hill 2021). This would imply that copepods are able to assess the color of their potential partners. Most recent studies showed that two types of eyes are present in copepods (Porter et al. 2017): a simple naupliar eye shared by the majority of species, and a more complex eye apparatus with a lens specific to Pontellid and Saphiirinid copepods (Land 1988, Manor et al. 2009, Takahashi et al. 2015). The structure and functioning of copepods' eyes remain poorly understood, but a recent genomic approach found opsins genes in diverse taxonomical groups, probably associated to photoreceptors functioning like rods to distinguish light variations (Porter et al. 2017). This is coherent considering copepods' ecological behavior of vertical migration according to light (Cohen and Forward 2002). In experimental studies, copepods are especially sensitive to blue and green light (Martin et al. 2005, Båtnes et al. 2015), but some surface Pontellids species have a broader wavelength sensitivity, including one pic at 600nm (Cohen and Forward 2002). Furthermore, polarization of light can be detected by copepods such as *Pontella karachiensis* or *Calanus finmarchicus* and is likely to be used to choose swimming direction or to perceive other individuals (Manor et al. 2009, Lerner and Browman 2016). According to these various studies, it is almost certain that copepods are able to detect variations in light intensity and perhaps light polarization (Takahashi et al. 2015). However, as most copepod photoreceptors are sensitive to only one type of short wavelength, it seems unlikely that they are able to distinguish colors of their congeners for sexual selection, especially for astaxanthin-red color. Consistently, experiments have failed to demonstrate selection of mates according to red pigmentation (Fig. 2.6, Powers et al. 2019). Nevertheless, for astaxanthin-blue copepods possessing complex eyes with broader wavelengths sensitivity and living in bright environments, further experiments are needed to understand if mate selection is influenced by light intensity, polarization and/or color variations.

Finally, it appears that individual growth (or metabolic capacity) is influenced by pigmentation (Fig. 2.6). The first studies documenting the link between carotenoids and copepod fitness showed that respiration rate was higher in pigmented populations of *Diaptomus* spp. than in unpigmented ones (Byron 1981). One explanation could be that the absorption of light by pigments leads to an increase of body temperature which in turn stimulates metabolism (metabolic stimulation hypothesis, Table 2.1 H_2; Byron 1981). This hypothesis was, however, criticized theoretically because

of the small size of a copepod and the high thermal conductivity of water (Hairston 1981), but not tested experimentally. Follow up studies assayed metabolic activity from the RNA:DNA ratio and concluded that the higher metabolism observed in pigmented copepods (at constant grazing rate) was likely to reflect the higher antioxidant defenses that enabled individuals to increase metabolic rates without the associated oxidative costs (Garcia et al. 2008, Gorokhova et al. 2013). Recently, the Shared Pathway Hypothesis (SPH) offers new perspectives on the link between astaxanthin concentrations and metabolic activity (Powers and Hill 2021, Powers et al. 2022). As discussed in paragraph 2.4.2, the SPH postulates that carotenoids bioconversion is linked to mitochondrial activity in the redox environment of the inner mitochondrial membrane. Powers and his colleagues (Powers and Hill, 2021, Powers et al. 2022) started to investigate the positive correlation between carotenoid concentrations and the functioning of the electron transport system in the mitochondria (ATP synthesis from Complex I and II, Fig. 2.6). If mitochondrial activity does enhance carotenoids ketolation, coloration could be considered as a true (*honest*) signal of individual fitness not because of an "ornamental resource allocation" linked to reproduction (as proposed for birds), but because color would be an honest indicator of the individual's "energetic capacity" (Powers and Hill 2021). This hypothesis seems relevant for copepods, which probably do not use color for sexual selection (Powers et al. 2019). The SPH could, thus, explain why the coloration decreased strongly when copepods were exposed to copper *in vitro* (Fig. 2.4O, Weaver et al. 2016) since copper disturbs the redox environment of the mitochondria. Impact on carotenoid's metabolism because of mitochondrial disturbance was again demonstrated recently (Powers et al. 2022). The decrease in coloration could also simply reflect pigments' degradation when used as antioxidants (Davenport et al. 2004, Caramujo et al. 2012). These various mechanisms are not mutually exclusive and all lead to the same general conclusion: redness is a good fitness indicator because it reflects a general antioxidant capacity (survival) and/or a good metabolic capacity (growth), beneficial for adults, eggs and offspring (reproduction).

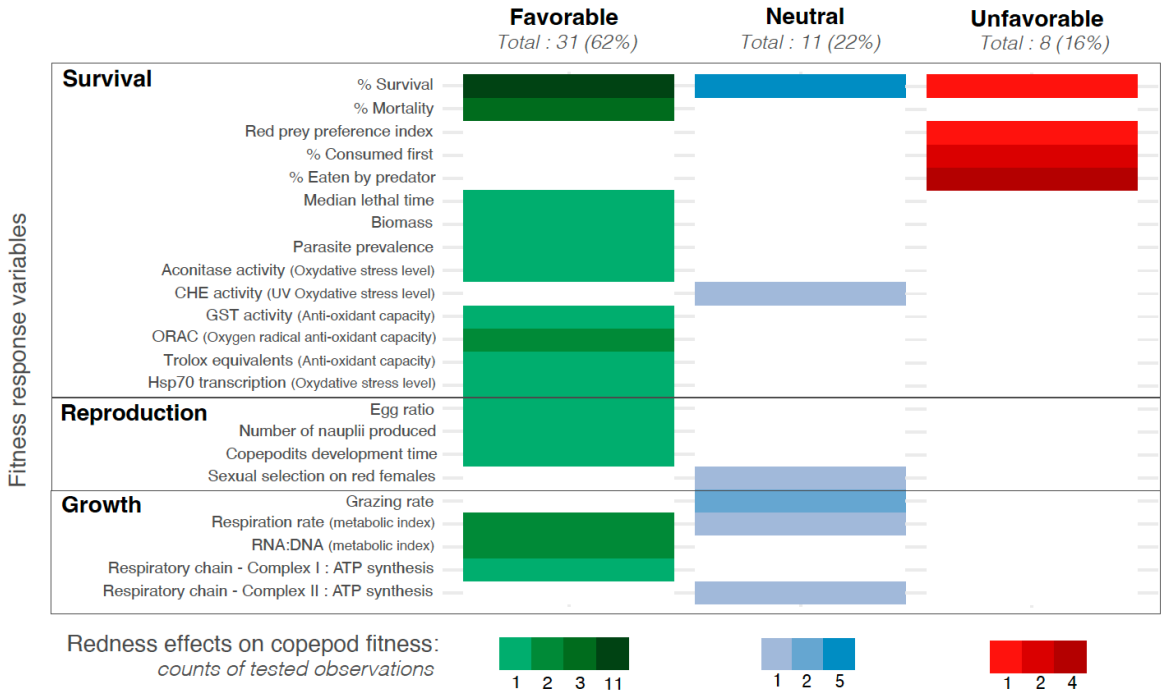

Figure 2.6. Carotenoid pigmentation effects on reproduction, growth and survival of copepods. From the literature, we compiled every correlation that was performed to link carotenoid pigmentation and a fitness response variable. Thus, each count on the figure quantifies how accumulation of red pigments impacts fitness in colored copepods, compared to copepod lacking carotenoids: positive correlation = favorable (green), negative correlation = unfavorable (red), no correlation = neutral (blue). Fifty correlations were used to create this figure, according to statistics strength or to method's quality as discussed by papers' authors (see "comments" column in Data4 for more details). CHE: cholinesterase; GST: Glutathione S-transferase; Hsp: Heat shock protein.

2.7. Perspectives and implications to monitor aquatic ecosystems in a context of anthropogenic pressures

2. 7. 1 The need for a mechanistic comprehension of a very plastic trait

We have demonstrated that copepod pigmentation fluctuates at large seasonal and regional scales and that these variations are driven by abiotic and biotic factors (summarized in Fig. 2.5). But copepod' color is also a very plastic trait that varies at small temporal and spatial scales (Vestheim & Kaartvedt 2006, Vestheim et al. 2005, Trudnowska et al. 2020). It changes rapidly according to light cycles with a maximum pigment accumulation occurring at night when feeding activity is high, and decreasing with sunrise (Kleppel et al. 1985) or just after (Ringelberg and Hallegraeff 1976,

Andersson et al. 2003). In the laboratory, color can disappear in few hours after net sampling (E. Trudnowska, personal observation), and reappear when exposed to light radiation after short time periods (*i.e.* minutes, hours or days) (Hansson 2000, Moeller et al. 2005, Garcia et al. 2008). In addition, a loss of color can be triggered within hours or days due to exposure to fish kairomones (Hansson 2004, Hylander et al. 2012). To understand such rapid variation, correlative approaches are informative (Fig. 2.4) but not sufficient. According to Gorohkova et al. (2013), "*pigmentation could be an example of a genetic system that leads to multiple fitness peaks under multiple selection pressures*": a mechanistic understanding of the carotenoid metabolism using transcriptomics and proteomics approaches is still needed to dissect this genetic system (Table 2.3).

Current industrial applications of astaxanthin in human dietary supplement (Guerin et al. 2003, Ye et al. 2018) pushed genetic engineering to decipher and optimize its biosynthesis (Zhang et al. 2020). The enzymes involved in the astaxanthin biosynthesis pathway are well characterized in prokaryotes, protists, fungi and plants. In animals, the investigation on the genetic basis of the carotenoid's bioconversion provided new arguments supporting the Shared-Pathway Hypothesis (SPH, Powers and Hill 2021). The first animal enzyme producing keto-carotenoids was identified by combining genetics and transcriptomics as a cytochrome p450 mono-oxygenase belonging to the family 2J19 (CYP2J19) found in the bird *Quelea quelea* (Lopes et al. 2016). Then, a CYP384A1 was identified in the red spider mite (Chelicerata) using a genetic approach (Wybouw et al. 2019). These two studies showed an elegant example of convergence evolution of cytochrome p450 to produce astaxanthin. More recently, homologs of CYP2J19 or CYP384A1 genes have been searched in orange-red decapods such as *Halocaridina rubra* (Weaver et al. 2020), *Neocaridina denticulata sinensis* (Huang et al. 2022), and *Exopalaemon carinicauda* (Jin et al. 2021), as well as in the copepod *Acartia fossae* (Mojib et al. 2014). They did not succeed in pointing to such homologs, but suggested other putative cytochrome p450 candidates. In the benthic copepod *Tigriopus californicus*, a sex-specific variation of astaxanthin content was found in hybrid versus parental lines and highlighted the link with the mitochondria and the presence of astaxanthin biosynthesis enzymes in copepods (Powers and Hill 2021). Future works based on molecular cloning of ABP enzyme-coding genes or mutant analysis will definitely help to characterize the genetic and molecular basis of astaxanthin bioconversion in copepods and other crustaceans, because until now, DNA analyses have not shown any differences in genomes of pigmented copepods in comparison to unpigmented ones (Gorokhova et al. 2013). This absence of differences suggests that astaxanthin biosynthesis enzymes are maybe not present in copepods, but would come from the food (Lemoine and Schoefs 2010). In microalgae, it was indeed demonstrated that astaxanthin production is enhanced by grazing-induced stress (Albini et al. 2019): in response to predation, astaxanthin biosynthesis enzymes could be expressed in

phytoplankton and used for astaxanthin production in copepods. Notifying that the gut is often the reddest part of the copepod, a last hypothesis could be that gut microbiota bacteria are performing the astaxanthin synthesis. Astaxanthin biosynthesis pathway enzymes have already been identified in several marine bacteria such as *Brevundimonas sp*. (Asker 2017, Chae et al. 2021), and this bacterium is also a major component of the gut microbial community in certain copepods (Chae et al. 2021). Thus, molecular studies of copepod gut microbiota could help to identify the role of bacteria in astaxanthin accumulation. The SPH, the food or the gut origin hypotheses of astaxanthin biosynthesis pathways are not mutually exclusive, and fine-tuned processes may occur to control the astaxanthin bioconversion. To guide future research, Table 2.3 summarizes potential perspectives about copepods' astaxanthin pigmentation research, including the need of interdisciplinary studies between molecular biologists and aquatic ecologists.

2. 7. 2 Astaxanthin content in the context of anthropogenic pressures

Living in the Anthropocene (Zalasiewicz et al. 2021), aquatic organisms are subjected to multiple threats caused by human activities, often pushing them beyond their physiological tolerance limits and their ecological niches. We have shown that esterified forms of astaxanthin are preferentially accumulated with lipids in cold, and sometimes ice-covered waters; and we discussed the hypothesis that astaxanthin and its esters may not be as stable in warm as in cold environments. If this hypothesis is verified, an increase in global temperature with climate change could reduce astaxanthin content and consequently the individual fitness of copepods, particularly in polar keystone species such as the *Calanus* or *Leptodiaptomus* congeners (Schneider et al. 2016, Trudnowska et al. 2020). Accumulation and protection of lipid stores for an extended time, *i.e.* during winter, is crucial for polar ecosystem food webs (Browman et al. 2000, Falk-Petersen et al. 2009, Turner 2015, Record et al. 2018). Lower astaxanthin content in copepods could then have a negative impact on the entire aquatic food web of these polar environments. The link between carotenoid accumulation, lipid protection, and temperature needs to be better understood in a context of climate change (Table 2.3).

Lipid degradation by oxidative stress can also be caused by human industrial pollution and the amount of oxidant pollutants, including metallic ions, released by anthropic activities is astonishing (Amoatey and Baawain 2019). As a first example, oil pollution induces lipid peroxidation in *Calanus finmarchicus* and a higher activity of their antioxidant enzymes is needed to compensate for such oxidative stress (Soloperto et al. 2022). Astaxanthin accumulation (known to occur in this species) would be a useful additional help against such human pollutants. Copper, as a second example, is released by mining, industrial and domestic emissions and is associated with chemical

fertilizers and pesticides (Flemming and Trevors 1989). This pollution could contribute to the degradation of astaxanthin molecules or to the inhibition of astaxanthin production by modification of the mitochondrial redox state (Caramujo et al. 2012). On the other hand, some *Tigriopus* species, often bright red, have shown to be very tolerant to copper pollution in contrast to other organisms in coastal areas (Medina et al. 2008), showing the increased resilience enabled by astaxanthin pigments.

Last but not least, astaxanthin is accumulated when the phytoplanktonic diet is diverse (Andersson et al. 2003, Van Nieuwerburgh et al. 2005, Rhodes 2007) and available in optimal - meaning not too abundant – quantities (Holeton et al. 2009). Excessive nutrient inputs leading to eutrophication of aquatic environments, with typical intense single-species phytoplanktonic blooms, could then be detrimental for astaxanthin copepod production.

2. 7. 3 Redness as a fitness index for copepod communities and aquatic food webs

Even if the ultimate mechanisms responsible for carotenoid accumulation in copepods are not yet completely understood, our current state of knowledge allows us to consider astaxanthin pigmentation as a "swiss army knife" for individual fitness in copepods (Table 2.1. H_8 and Fig. 2.5). As a concrete example, *Calanus finmarchicus* and *C. glacialis* seem more pigmented when they inhabit their preferred water masses (*i.e.* Atlantic and Arctic, respectively), showing that color could be a fitness indicator when individuals are apparently in the best conditions to bioconvert carotenoids ("*in their comfort zone*": Trudnowska et al., 2020). The trait-based approach to aquatic ecology (Martini et al. 2021) has motivated recent studies to quantify copepod functional traits such as size, feeding mode, lipid content or egg production in order to gain better insights into pelagic ecosystems functioning (Beaugrand 2002, Kinnard et al. 2011, Benedetti et al. 2016, Horne et al. 2016, Schneider et al. 2017, Schmid et al. 2018, de Melo Júnior et al. 2021, Orenstein et al. 2022). Because carotenoid-based pigmentation significantly impacts copepod fitness, indicating a "good health" state, redness could be added to the list of key zooplankton traits routinely monitored.

For a sample of a few individuals, quantification of astaxanthin pigmentation can be done by classic HPLC measurements; while quantification at the individual level can be done from zooplankton images using specific computer vision algorithms (Snoeijs and Häubner 2014, Brüsin et al. 2016). Using automatic underwater cameras, pigmentation could also be inferred, at least by gray levels variations in black and white images (Vilgrain et al. 2021). At the community level, satellite imaging has been used to identify red patches in surface layers of arctic and subarctic marine ecosystems (Basedow et al. 2019). Using those technics, monitoring programs could derive such redness indices to obtain information on zooplankton quantity and quality, and hence on favorable

foraging areas for predators such as whales, fish and birds (Berge et al. 2012, Basedow et al. 2019, Fortune et al. 2020).

Copepod carotenoid quantification has significant implications for estimates of the transfer of antioxidants throughout food webs, from primary production to human consumers, and to evaluate the quality of fish stocks. Indeed, fish larvae exhibit a better coloration when they eat copepods fed with a diet enriched with carotenoids (Hynes et al. 2009, Azani and Rasdi 2021), and the benefits of astaxanthin in fish for antioxidant and anti-inflammatory properties, egg quality, growth performance, immune system, lipid metabolism, or muscle pigmentation are unequivocal (Nakano and Wiegertjes 2020). For example, in Inuit communities relying on a traditional diet for their food security, salmonid fish (*Arctic char*) are chosen for their color traditionally known to reflect their quality (Bolduc 2021). Carotenoid-rich (fish) diets have indeed been proven beneficial for human health with therapeutic potential for Alzheimer, Parkinson, cardiovascular diseases and cancer (Donoso et al. 2021), to the point that some companies began to harvest copepods to produce carotenoids-rich dietary supplements for humans (Pedersen et al. 2014, Eysteinsson et al. 2018, Daďová et al. 2020). Accumulation of carotenoid pigments functioning as powerful antioxidants through the food chain thus represents an ecosystem service (Sandifer and Sutton-Grier 2014), and performing routine measurements of copepods' color could provide new information for a better monitoring of aquatic ecosystem health, also useful for human populations depending on them (Table 2.3).

Table 2.3. Suggestions for potential research fields associated with astaxanthin pigmentation in copepods.

Scale	Study suggestion	Existing literature
Molecular	Molecular cloning of enzymes-coding genes or mutant analysis, to identify astaxanthin biosynthesis enzymes potentially linked to mitochondrial functioning	Mojib et al. 2014 Powers et Hill 2021 Powers et al. 2022
	Performing transcriptomics approaches to characterize fine-tuned controls on pigment synthesis in response to light or predators induced stress	Hykander 2009a Gorokhova et al. 2013
	Investigating the molecular link between lipid and astaxanthin synthesis	Schneider et al. 2016 Grosbois & Rautio 2018
	Exploring microbiota composition in relation with pigmentation	Chae et al. 2021
	Understanding molecular controls of blue to red color change according to time or between body structures (*i.e.* eggs)	Herring 1965 Mojib et al. 2014 Vestheim et al. 2005
	Investigating the temperature dependance of astaxanthin stability (in its various forms, including caroteno-proteins)	Pedersen et al. 2014 Schneider et al. 2016 Rahlff et al. 2018

Individual/ Population	Determining concentrations and proportions of astaxanthin forms (free, esters, caroteno-protein) with ontogenic development	Lotocka et al. 2004 Schneider et al. 2016 Cui et al. 2021
	Assessing eggs hatching success and nauplii survival according to astaxanthin content	Hylander 2009a Powers et al. 2021
	Investigating pigmentation variations according to living depth and/or to vertical migration	Hays et al. 1994 Vestheim et al. 2005
	Testing sexual selection by blue pigmentation for neustonic copepods	Cohen and Forward 2002
	Developing routine measures of pigmentation as one fitness index (e.g. using individual images or remote sensing)	Brusin et al. 2016 Lindeque et al. 2022 Basedow et al. 2019
Ecosystem	Investigating copepods' astaxanthin content according to latitude at global scale	Hansson et al. 2007 Hylander et al. 2009a
	Testing red color as a camouflage strategy at depth	Johnsen 2001, 2005 Vestheim & Kaartvedt 2006
	Exploring the impact of anthropogenic pressures (pollutants, eutrophication) on astaxanthin production and copepod fitness	Medina et al. 2008 Caramujo et al. 2012 Holeton et al. 2009
	Exploring the link between copepod pigmentation and fish population success	Hynes et al. 2009 Azani and Rasdi 2021

2.8. References

Albini, D., M. S. Fowler, C. Llewellyn, and K. W. Tang. 2019. Reversible colony formation and the associated costs in *Scenedesmus obliquus*. Journal of Plankton Research 41:419–429.

Allaire, J., Y. Xie, J. McPherson, J. Luraschi, K. Ushey, A. Atkins, H. Wickham, J. Cheng, W. Chang, and R. Iannone. 2021. Rmarkdown: Dynamic Documents for R.

Amoatey, P., and M. S. Baawain. 2019. Effects of pollution on freshwater aquatic organisms. Water Environment Research 91:1272–1287.

Andersson, M., L. Van Nieuwerburgh, and P. Snoeijs. 2003. Pigment transfer from phytoplankton to zooplankton with emphasis on astaxanthin production in the Baltic Sea food web. Marine Ecology Progress Series 254:213–224.

Asker, D. 2017. Isolation and Characterization of a Novel, Highly Selective Astaxanthin-Producing Marine Bacterium. Journal of Agricultural and Food Chemistry 65:9101–9109.

Azani, N., and N. W. Rasdi. 2021. Effect of enriched copepods on the growth, survival, and colouration of angelfish (Pterophyllum scalare). Universiti Malaysia Terengganu Journal of Undergraduate Research 3:25–36.

Babin, A., C. Biard, and Y. Moret. 2010. Dietary Supplementation with Carotenoids Improves Immunity without Increasing Its Cost in a Crustacean. The American Naturalist 176:234–241.

Bandaranayake, W. M., and P. Gentien. 1982. Carotenoids of temora turbinata, centropages furcatus, undinula vulgaris and euchaeta russelli. Comparative Biochemistry and Physiology Part B: Comparative Biochemistry 72:409–414.

Basedow, S. L., D. McKee, I. Lefering, A. Gislason, M. Daase, E. Trudnowska, E. S. Egeland, M. Choquet, and S. Falk-Petersen. 2019. Remote sensing of zooplankton swarms. Scientific Reports 9:686.

Balaban, R. S., S. Nemoto, and T. Finkel. 2005. Mitochondria, Oxidants, and Aging. Cell 120:483–495.

Båtnes, A. S., C. Miljeteig, J. Berge, M. Greenacre, and G. Johnsen. 2015. Quantifying the light sensitivity of Calanus spp. during the polar night: potential for orchestrated migrations conducted by ambient light from the sun, moon, or aurora borealis? Polar Biology 38:51–65.

Beaugrand, G. 2002. Reorganization of North Atlantic Marine Copepod Biodiversity and Climate. Science 296:1692–1694.

Benedetti, F., S. Gasparini, and S.-D. Ayata. 2016. Identifying copepod functional groups from species functional traits. Journal of Plankton Research 38:159–166.

Benedetti, F., J. Wydler, and M. Vogt. 2022. Copepod functional traits and groups show divergent biogeographies in the global ocean. Journal of Biogeography:jbi.14512.

Berge, J., T. M. Gabrielsen, M. Moline, and P. E. Renaud. 2012. Evolution of the Arctic Calanus complex: an Arctic marine avocado? Journal of Plankton Research 34:191–195.

Blanchard, R. 1890. Sur une matière colorante des Diaptomus, analogues à la carotine des végétaux. Compt. Rend, de l'Acad. des Sci., Paris 110:292–294.

Bolduc, S. 2021. Indicateurs de la qualité de la chair de l'omble chevalier anadrome et ses liens avec les préférences alimentaires des Inuit du Nunavik, Master thesis, Département de Biologie, Université Laval, Québec, Canada.

Brehm, V. V. 1938. DIE ROTFÄRBUNG VON HOCHGEBIRGSSEE-ORGANISMEN. Biological Reviews 13:307–318.

Browman, H., C. Rodriguez, F. Béland, J. Cullen, R. Davis, J. Kouwenberg, P. Kuhn, B. McArthur, J. Runge, J. St-Pierre, and R. Vetter. 2000. Impact of ultraviolet radiation on marine crustacean zooplankton and ichthyoplankton: a synthesis of results from the estuary and Gulf of St. Lawrence, Canada. Marine Ecology Progress Series 199:293–311.

Brun, P., M. R. Payne, and T. Kiørboe. 2016. Trait biogeography of marine copepods - an analysis across scales. Ecology Letters 19:1403–1413.

Brüsin, M., P. A. Svensson, and S. Hylander. 2016. Individual changes in zooplankton pigmentation in relation to ultraviolet radiation and predator cues: Individual Changes in Zooplankton Pigmentation. Limnology and Oceanography 61:1337–1344.

Byron, E. R. 1981. Metabolic stimulation by light in a pigmented freshwater invertebrate. Proceedings of the National Academy of Sciences 78:1765–1767.

Byron, E. R. 1982. The Adaptive Significance of Calanoid Copepod Pigmentation: A Comparative and Experimental Analysis. Ecology 63:1871.

Caramujo, M.-J., C. C. C. R. de Carvalho, S. J. Silva, and K. R. Carman. 2012. Dietary Carotenoids Regulate Astaxanthin Content of Copepods and Modulate Their Susceptibility to UV Light and Copper Toxicity. Marine Drugs 10:998–1018.

de Carvalho, C. C. C. R., and M. J. Caramujo. 2017. Carotenoids in Aquatic Ecosystems and Aquaculture: A Colorful Business with Implications for Human Health. Frontiers in Marine Science 4.

Cavallo, A., and L. S. Peck. 2020. Lipid storage patterns in marine copepods: environmental, ecological, and intrinsic drivers. ICES Journal of Marine Science 77:1589–1601.

Chae, J., and S. Nishida. 1995. Vertical distribution and diel migration in the iridescent copepods of the family Sapphirinidae:a unique example of reverse migration? Marine Ecology Progress Series 119:111–124.

Chae, Y.-J., H.-J. Oh, K.-H. Chang, I.-S. Kwak, and H. Jo. 2021. Application of Next-Generation Sequencing for the Determination of the Bacterial Community in the Gut Contents of Brackish Copepod Species (*Acartia hudsonica, Sinocalanus tenellus, and Pseudodiaptomus inopinus*). Animals 11:542.

Cheesman, D. F., W. L. Lee, and P. F. Zagalsky. 1967. Carotenoproteins in invertebrates. Biological Reviews 42:131–160.

Chew, B. P., and J. S. Park. 2004. Carotenoid Action on the Immune Response. The Journal of Nutrition 134:257–261.

Choquet, M., K. Kosobokova, S. Kwaśniewski, M. Hatlebakk, A. K. S. Dhanasiri, W. Melle, M. Daase, C. Svensen, J. E. Søreide, and G. Hoarau. 2018. Can morphology reliably distinguish between the copepods *Calanus finmarchicus* and *C. glacialis*, or is DNA the only way?: Morphological misidentification in *Calanus*. Limnology and Oceanography: Methods 16:237–252.

Cohen, J. H., and R. B. Forward. 2002. Spectral Sensitivity of Vertically Migrating Marine Copepods. The Biological Bulletin 203:307–314.

Cui, S., Y. Li, L. Liu, Q. Wang, and F. Chen. 2021. Changes in astaxanthin and fatty acid concentrations during the developmental process in the calanoid *Arctodiaptomus walterianus* in an alpine lake at low latitudes. Journal of Plankton Research 43:314–324.

Culverhouse, P. F., R. Williams, M. Benfield, P. R. Flood, A. F. Sell, M. G. Mazzocchi, I. Buttino, and M. Sieracki. 2006. Automatic image analysis of plankton: future perspectives. Marine Ecology Progress Series 312:297–309.

Czeczuga, B. 1975. Carotenoids in *Eudiaptomus amblyodon marenz* (crustacea) during ontogenetic development. Comparative Biochemistry and Physiology Part A: Physiology 50:665–668.

Czeczuga, B., and R. Czerpak. 1966. Carotenoids in certain diaptomidae (crustacea). Comparative Biochemistry and Physiology 17:523–534.

Czeczuga, B., M. Kozłowska, and E. Czeczuga-Semeniuk. 2000. Adaptative role of carotenoids and carotenoproteins in *Cyclops kolensis* Lilljeborg (Crustacea: Copepoda) specimens to extremely eutrophical conditions. Folia Biologica 48:77–84.

Daase, M., J. Berge, J. E. Søreide, and S. Falk-Petersen. 2021. Ecology of Arctic Pelagic Communities. Pages 219–259 *in* D. N. Thomas, editor. Arctic Ecology. First edition. Wiley.

Daďová, K., M. Petr, M. Šteffl, L. Sontáková, M. Chlumský, M. Matouš, V. Štich, M. Štěpán, and M. Šiklová. 2020. Effect of *Calanus* Oil Supplementation and 16 Week Exercise Program on Selected Fitness Parameters in Older Women. Nutrients 12:481.

Davenport, J., A. Aine Healy, N. Casey, and J. Heffron. 2004. Diet-dependent UVAR and UVBR resistance in the high shore harpacticoid copepod *Tigriopus brevicornis*. Marine Ecology Progress Series 276:299–303.

Donoso, A., J. González-Durán, A. A. Muñoz, P. A. González, and C. Agurto-Muñoz. 2021. Therapeutic uses of natural astaxanthin: An evidence-based review focused on human clinical trials. Pharmacological Research 166:105479.

Eysteinsson, S. T., M. Gudjónsdóttir, S. H. Jónasdóttir, and S. Arason. 2018. Review of the composition and current utilization of *Calanus finmarchicus* – Possibilities for human consumption. Trends in Food Science & Technology 79:10–18.

Falk-Petersen, S., P. Mayzaud, G. Kattner, and J. R. Sargent. 2009. Lipids and life strategy of Arctic *Calanus*. Marine Biology Research 5:18–39.

Finkel, T., and N. J. Holbrook. 2000. Oxidants, oxidative stress and the biology of ageing. Nature 408:239–247.

Fisher, L. R., S. K. Kon, and S. Y. Thompson. 1964. Vitamin A and Carotenoids in Certain Invertebrates VII. Crustacea: Copepoda. Journal of the Marine Biological Association of the United Kingdom 44:685–692.

Flemming, C. A., and J. T. Trevors. 1989. Copper toxicity and chemistry in the environment: a review. Water, Air, and Soil Pollution 44:143–158.

Fortune, S., S. Ferguson, A. Trites, B. LeBlanc, V. LeMay, J. Hudson, and M. Baumgartner. 2020. Seasonal diving and foraging behaviour of Eastern Canada-West Greenland bowhead whales. Marine Ecology Progress Series 643:197–217.

Foss, P., B. Renstrøm, and S. Liaaen-Jensen. 1987. Natural occurrence of enantiomeric and Meso astaxanthin 7∗-crustaceans including zooplankton. Comparative Biochemistry and Physiology Part B: Comparative Biochemistry 86:313–314.

Garcia, P. E., A. P. Perez, M. d. C. Dieguez, M. A. Ferraro, and H. E. Zagarese. 2008. Dual control of the levels of photoprotective compounds by ultraviolet radiation and temperature in the freshwater copepod *Boeckella antiqua*. Journal of Plankton Research 30:817–827.

Gasmi, A., P. K. Mujawdiya, M. Shanaida, A. Ongenae, R. Lysiuk, M. D. Doşa, O. Tsal, S. Piscopo, S. Chirumbolo, and G. Bjørklund. 2020. *Calanus* oil in the treatment of obesity-related low-grade inflammation, insulin resistance, and atherosclerosis. Applied Microbiology and Biotechnology 104:967–979.

Girotti, A. W. 1985. Mechanisms of lipid peroxidation. Journal of Free Radicals in Biology & Medicine 1:87–95.

Gorokhova, E., M. Lehtiniemi, and N. H. Motwani. 2013. Trade-Offs between Predation Risk and Growth Benefits in the Copepod *Eurytemora affinis* with Contrasting Pigmentation. PLoS ONE 8:e71385.

Grosbois, G., and M. Rautio. 2018. Active and colorful life under lake ice. Ecology 99:752–754.

Guerin, M., M. E. Huntley, and M. Olaizola. 2003. *Haematococcus* astaxanthin: applications for human health and nutrition. Trends in Biotechnology 21:210–216.

Hairston, N. C. 1976. Photoprotection by carotenoid pigments in the copepod *Diaptomus nevadensis*. Proceedings of the National Academy of Sciences 73:971–974.

Hairston, N. G. 1979. The adaptive significance of color polymorphism in two species of *Diaptomus* (Copepoda)1: Diaptomid pigmentation. Limnology and Oceanography 24:15–37.

Hairston, N. G. 1981. The interaction of salinity, predators, light and copepod color. Hydrobiologia 81:151–158.

Hansson, L. 2000. Induced pigmentation in zooplankton: a trade–off between threats from predation and ultraviolet radiation. Proceedings of the Royal Society of London. Series B: Biological Sciences 267:2327–2331.

Hansson, L.-A. 2004. Plasticity in pigmentation induced by conflicting threats from predation and UV radiation. Ecology 85:1005–1016.

Hansson, L.-A., S. Hylander, and R. Sommaruga. 2007. Escape from UV threats in zooplankton: a cocktail of behavior and protective pigmentation. Ecology 88:1932–1939.

Hays, G. C., C. A. Proctor, A. W. G. John, and A. J. Warner. 1994. Interspecific differences in the diel vertical migration of marine copepods: The implications of size, color, and morphology. Limnology and Oceanography 39:1621–1629.

Herring, P. J. 1965. Blue Pigment of a Surface-living Oceanic Copepod. Nature 205:103–104.

Herring, P. J. 1972. Depth Distribution of the Carotenoid Pigments and Lipids of Some Oceanic Animals 1. Mixed Zooplankton, Copepods and Euphausiids. Journal of the Marine Biological Association of the United Kingdom 52:179–189.

Holeton, C., K. Lindell, T. Holmborn, H. Hogfors, and E. Gorokhova. 2009. Decreased astaxanthin at high feeding rates in the calanoid copepod *Acartia bifilosa*. Journal of Plankton Research 31:661–668.

Horne, C. R., A. G. Hirst, D. Atkinson, A. Neves, and T. Kiørboe. 2016. A global synthesis of seasonal temperature-size responses in copepods: Seasonal temperature-size responses in copepods. Global Ecology and Biogeography 25:988–999.

Huang, Y., L. Zhang, G. Wang, and S. Huang. 2022. De novo assembly transcriptome analysis reveals the genes associated with body color formation in the freshwater ornamental shrimps *Neocaridina denticulate sinensis*. Gene 806:145929.

Humes, A. G. 1994. How many copepods? Pages 1–7 *in* F. D. Ferrari and B. P. Bradley, editors. Ecology and Morphology of Copepods. Springer Netherlands, Dordrecht.

Hylander, S., W. J. Boeing, W. Granéli, J. Karlsson, J. von Einem, K. Gutseit, and L.-A. Hanssona. 2009. Complementary UV protective compounds in zooplankton. Limnology and Oceanography 54:1883–1893.

Hylander, S., J. C. Grenvald, and T. Kiørboe. 2014. Fitness costs and benefits of ultraviolet radiation exposure in marine pelagic copepods. Functional Ecology 28:149–158.

Hylander, S., T. Kiørboe, P. Snoeijs, R. Sommaruga, and T. G. Nielsen. 2015. Concentrations of sunscreens and antioxidant pigments in Arctic *Calanus* spp. in relation to ice cover, ultraviolet radiation, and the phytoplankton spring bloom: MAAs and astaxanthin in copepods. Limnology and Oceanography 60:2197–2206.

Hylander, S., M. S. Souza, E. Balseiro, B. Modenutti, and L.-A. Hansson. 2012. Fish-mediated trait compensation in zooplankton: Pigmentation and oxidative stress. Functional Ecology 26:608–615.

Hynes, N., E. S. Egeland, W. Koppe, G. Baardsen, and V. Kiron. 2009. *Calanus* oil as a natural source for flesh pigmentation in Atlantic salmon (*Salmo salar* L.). Aquaculture Nutrition 15:202–208.

Jin, Y., S. Li, Y. Yu, C. Zhang, X. Zhang, and F. Li. 2021. Transcriptome Analysis Provides Insights into the Mechanism of Astaxanthin Enrichment in a Mutant of the Ridgetail White Prawn *Exopalaemon carinicauda*. Genes 12:618.

Johnsen, S. 2001. Hidden in Plain Sight: The Ecology and Physiology of Organismal Transparency. The Biological Bulletin 201:301–318.

Johnsen, S. 2002. Cryptic and conspicuous coloration in the pelagic environment. Proceedings of the Royal Society of London. Series B: Biological Sciences 269:243–256.

Johnsen, S. 2005. The Red and the Black: Bioluminescence and the Color of Animals in the Deep Sea. Integrative and Comparative Biology 45:234–246.

Johnsen, S. 2014. Hide and Seek in the Open Sea: Pelagic Camouflage and Visual Countermeasures. Annual Review of Marine Science 6:369–392.

Jónasdóttir, S. H., A. W. Visser, K. Richardson, and M. R. Heath. 2015. Seasonal copepod lipid pump promotes carbon sequestration in the deep North Atlantic. Proceedings of the National Academy of Sciences 112:12122–12126.

Juhl, A. R., M. D. Ohman, and R. Goericke. 1996. Astaxanthin in *Calanus pacificus* : Assessment of pigment-based measures of omnivory. Limnology and Oceanography 41:1198–1207.

Kiko, R., P. Brandt, S. Christiansen, J. Faustmann, I. Kriest, E. Rodrigues, F. Schütte, and H. Hauss. 2020. Zooplankton-Mediated Fluxes in the Eastern Tropical North Atlantic. Frontiers in Marine Science 7:358.

Kimura, T., M. Takasaki, R. Hatai, Y. Nagai, K. Uematsu, Y. Oaki, M. Osada, H. Tsuda, T. Ishigure, T. Toyofuku, S. Shimode, and H. Imai. 2020. Guanine crystals regulated by chitin-based honeycomb frameworks for tunable structural colors of sapphirinid copepod, *Sapphirina nigromaculata*. Scientific Reports 10:2266.

Kinnard, C., C. M. Zdanowicz, D. A. Fisher, E. Isaksson, A. de Vernal, and L. G. Thompson. 2011. Reconstructed changes in Arctic sea ice over the past 1,450 years. Nature 479:509.

Kiørboe, T., S. Ceballos, and U. H. Thygesen. 2015. Interrelations between senescence, life-history traits, and behavior in planktonic copepods. Ecology 96:2225–2235.

Kleppel, G. S., L. Willbanks, and R. E. Pieper. 1985. Diel variation in body carotenoid content and feeding activity in marine zooplankton assemblages. Journal of Plankton Research 7:569–580.

Krumova, K., and G. Cosa. 2016. Chapter 1. Overview of Reactive Oxygen Species. Pages 1–21 in S. Nonell and C. Flors, editors. Comprehensive Series in Photochemical & Photobiological Sciences. Royal Society of Chemistry, Cambridge.

Kvile, K. Ø., C. Ashjian, and R. Ji. 2019. Pan-Arctic Depth Distribution of Diapausing *Calanus* Copepods. The Biological Bulletin 237:76–89.

Land, M. F. 1988. The optics of animal eyes. Contemporary Physics 29:435–455.

Lee, M., H. Zhang, Y. Sha, A. Hegg, G. E. Ugge, J. Vinterstare, M. Škerlep, V. Pärssinen, S. D. Herzog, C. Björnerås, R. Gollnisch, E. Johansson, N. Hu, P. A. Nilsson, K. Hulthén, K. Rengefors, R. B. Langerhans, C. Brönmark, and L.-A. Hansson. 2019. Low-latitude zooplankton pigmentation plasticity in response to multiple threats. Royal Society Open Science 6:190321.

Lee, R. F., J. C. Nevenzel, and A. G. Lewis. 1974. Lipid changes during life cycle of marine copepod *Euchaeta japonica marukawa*. Lipids 9:891–898.

Lemoine, Y., and B. Schoefs. 2010. Secondary ketocarotenoid astaxanthin biosynthesis in algae: a multifunctional response to stress. Photosynthesis Research 106:155–177.

Lerner, A., and H. I. Browman. 2016. The copepod *Calanus* spp. (Calanidae) is repelled by polarized light. Scientific Reports 6:35891.

Lindeque, P. K., I. Hann, H. E. Parry, K. B. Cook, A. J. W. Lindley, and D. J. Mayor. 2022. Red Pigmentation Can Be Used to Reliably Distinguish Between Live *Calanus finmarchicus* and *Calanus glacialis* Females in the Fram Strait. Frontiers in Marine Science 9:906465.

Lopes, R. J., J. D. Johnson, M. B. Toomey, M. S. Ferreira, P. M. Araujo, J. Melo-Ferreira, L. Andersson, G. E. Hill, J. C. Corbo, and M. Carneiro. 2016. Genetic Basis for Red Coloration in Birds. Current Biology 26:1427–1434.

Lotocka, M. 2004. Changes in carotenoid composition in different developmental stages of copepods: *Pseudocalanus acuspes* Giesbrecht and *Acartia* spp. Journal of Plankton Research 26:159–166.

Luecke, C., and W. J. O'Brien. 1981. Phototoxicity and fish predation: Selective factors in color morphs in *Heterocope*: Coloration of Heterocope. Limnology and Oceanography 26:454–460.

Manor, S., O. Polak, W. M. Saidel, T. L. Goulet, and N. Shashar. 2009. Light intensity mediated polarotaxis in *Pontella karachiensis* (Pontellidae, Copepoda). Vision Research 49:2371–2378.

Martin, G. G., C. Speekmann, and S. Beidler. 2005. Photobehavior of the harpacticoid copepod *Tigriopus californicus* and the fine structure of its nauplius eye. Invertebrate Biology 119:110–124.

Martini, S., F. Larras, A. Boyé, E. Faure, N. Aberle, P. Archambault, L. Bacouillard, B. E. Beisner, L. Bittner, E. Castella, M. Danger, O. Gauthier, L. Karp-Boss, F. Lombard, F. Maps, L. Stemmann, E. Thiébaut, P. Usseglio-Polatera, M. Vogt, M. Laviale, and S. Ayata. 2021. Functional trait-based approaches as a common framework for aquatic ecologists. Limnology and Oceanography 66:965–994.

Matsuno, T. 2001. Aquatic animal carotenoids. Fisheries Science 67:771–783.

McGraw, K. J. 2005. The antioxidant function of many animal pigments: are there consistent health benefits of sexually selected colourants? Animal Behaviour 69:757–764.

McNulty, H. P., J. Byun, S. F. Lockwood, R. F. Jacob, and R. P. Mason. 2007. Differential effects of carotenoids on lipid peroxidation due to membrane interactions: X-ray diffraction analysis. Biochimica et Biophysica Acta (BBA) - Biomembranes 1768:167–174.

Medellín-Mora, J., R. Escribano, A. Corredor-Acosta, P. Hidalgo, and W. Schneider. 2021. Uncovering the Composition and Diversity of Pelagic Copepods in the Oligotrophic Blue Water of the South Pacific Subtropical Gyre. Frontiers in Marine Science 8:625842.

Medina, M. H., B. Morandi, and J. A. Correa. 2008. Copper effects in the copepod *Tigriopus angulatus* Lang, 1933: natural broad tolerance allows maintenance of food webs in copper-enriched coastal areas. Marine and Freshwater Research 59:1061.

de Melo Júnior, M., L. K. Miyashita, and R. M. Lopes. 2021. A 3-year study of the seasonal variability of abundance, biomass and reproductive traits of *Oncaea venusta* (Copepoda, Oncaeidae) in a subtropical coastal area. Journal of Plankton Research 43:751–761.

Miki, W. 1991. Biological functions and activities of animal carotenoids. Pure and Applied Chemistry 63:141–146.

Miller, C. B. 1988. *Neocalanus flemingeri*, a new species of Calanidae (Copepoda: Calanoida) from the subarctic Pacific Ocean, with a comparative redescription of *Neocalanus plumchrus* (Marukawa) 1921. Progress in Oceanography 20:223–273.

Moeller, R. E., S. Gilroy, C. E. Williamson, G. Grad, and R. Sommaruga. 2005. Dietary acquisition of photoprotective compounds (mycosporine-like amino acids, carotenoids) and acclimation to ultraviolet radiation in a freshwater copepod. Limnology and Oceanography 50:427–439.

Mojib, N., M. Amad, M. Thimma, N. Aldanondo, M. Kumaran, and X. Irigoien. 2014. Carotenoid metabolic profiling and transcriptome-genome mining reveal functional equivalence among blue-pigmented copepods and appendicularia. Molecular Ecology 23:2740–2756.

Monaghan, P., N. B. Metcalfe, and R. Torres. 2009. Oxidative stress as a mediator of life history trade-offs: mechanisms, measurements and interpretation. Ecology Letters 12:75–92.

Mundy, N. I., J. Stapley, C. Bennison, R. Tucker, H. Twyman, K.-W. Kim, T. Burke, T. R. Birkhead, S. Andersson, and J. Slate. 2016. Red Carotenoid Coloration in the Zebra Finch Is Controlled by a Cytochrome P450 Gene Cluster. Current Biology 26:1435–1440.

Naguib, Y. M. A. 2000. Antioxidant Activities of Astaxanthin and Related Carotenoids. Journal of Agricultural and Food Chemistry 48:1150–1154.

Nakajima, R., T. Yoshida, B. H. R. Othman, and T. Toda. 2013. First record of a blue-pigmented Acartiid copepod in the tropical coral reef waters of Malaysia. Galaxea, Journal of Coral Reef Studies 15:27–28.

Nakano, T., and G. Wiegertjes. 2020. Properties of Carotenoids in Fish Fitness: A Review. Marine Drugs 18:568.

Negro, J. J., G. R. Bortolotti, J. L. Tella, K. J. Fernie, and D. M. Bird. 1998. Regulation of integumentary colour and plasma carotenoids in American Kestrels consistent with sexual selection theory. Functional Ecology 12:307–312.

Nielsen, T. G., S. Kjellerup, I. Smolina, G. Hoarau, and P. Lindeque. 2014. Live discrimination of *Calanus glacialis* and *C. finmarchicus* females: can we trust phenological differences? Marine Biology 161:1299–1306.

Ohtsuka, S., and R. Huys. 2001. Sexual dimorphism in calanoid copepods: morphology and function. Hydrobiologia 453/454:441–466.

Orenstein, E. C., S. Ayata, F. Maps, É. C. Becker, F. Benedetti, T. Biard, T. de Garidel-Thoron, J. S. Ellen, F. Ferrario, S. L. C. Giering, T. Guy-Haim, L. Hoebeke, M. H. Iversen, T. Kiørboe, J. Lalonde, A. Lana, M. Laviale, F. Lombard, T. Lorimer, S. Martini, A. Meyer, K. O. Möller, B. Niehoff, M. D. Ohman, C. Pradalier, J. Romagnan, S. Schröder, V. Sonnet, H. M. Sosik, L. S. Stemmann, M. Stock, T. Terbiyik-Kurt, N. Valcárcel-Pérez, L. Vilgrain, G. Wacquet, A. M. Waite, and J. Irisson. 2022. Machine learning techniques to characterize functional traits of plankton from image data. Limnology and Oceanography 67:1647–1669.

Ory, N. C., P. Sobral, J. L. Ferreira, and M. Thiel. 2017. Amberstripe scad Decapterus muroadsi (Carangidae) fish ingest blue microplastics resembling their copepod prey along the coast of Rapa Nui (Easter Island) in the South Pacific subtropical gyre. Science of The Total Environment 586:430–437.

Pedersen, A. M., B. Vang, and R. L. Olsen. 2014. Oil from *Calanus finmarchicus* —Composition and Possible Use: A Review. Journal of Aquatic Food Product Technology 23:633–646.

Persaud, A. D., R. E. Moeller, C. E. Williamson, and C. W. Burns. 2007. Photoprotective compounds in weakly and strongly pigmented copepods and co-occurring cladocerans. Freshwater Biology 52:2121–2133.

Pettersson, A., and Å. Lignell. 1999. Astaxanthin Deficiency in Eggs and Fry of Baltic Salmon (*Salmo salar*) with the M74 Syndrome. Ambio 28:43–47.

Pickova, J., A. Kiessling, A. Pettersson, and P. C. Dutta. 1998. Comparison of fatty acid composition and astaxanthin content in healthy and by M74 affected salmon eggs from three Swedish river stocks. Comparative Biochemistry and Physiology Part B: Biochemistry and Molecular Biology 120:265–271.

Porter, M. L., M. Steck, V. Roncalli, and P. H. Lenz. 2017. Molecular Characterization of Copepod Photoreception. The Biological Bulletin 233:96–110.

Powers, M. J., and G. E. Hill. 2021. A Review and Assessment of the Shared-Pathway Hypothesis for the Maintenance of Signal Honesty in Red Ketocarotenoid-Based Coloration. Integrative and Comparative Biology 61:1811–1826.

Powers, M. J., G. E. Hill, and R. J. Weaver. 2019. An experimental test of mate choice for red carotenoid coloration in the marine copepod *Tigriopus californicus*. Ethology 126:344–352.

Powers, M. J., J. A. Baty, A. M. Dinga, J. H. Mao, and G. E. Hill. 2022. Chemical manipulation of mitochondrial function affects metabolism of red carotenoids in a marine copepod (*Tigriopus californicus*). Journal of Experimental Biology 225(12):jeb244230.

Purcell, J. E. 1983. Digestion rates and assimilation efficiencies of siphonophores fed zooplankton prey. Marine Biology 73:257–261.

R Core Team. 2021. R: A language and environment for statistical computing. R Foundation for Statistical Computing, Vienna, Austria.

Rahlff, J., M. Ribas-Ribas, S. M. Brown, N. I. H. Mustaffa, J. Renz, M. A. Peck, K. Bird, M. Cunliffe, K. Melkonian, and C. J. Zappa. 2018. Blue pigmentation of neustonic copepods benefits exploitation of a prey-rich niche at the air-sea boundary. Scientific Reports 8:11510.

Rautio, M., S. Bonilla, and W. Vincent. 2009. UV photoprotectants in arctic zooplankton. Aquatic Biology 7:93–105.

Record, N. R., R. Ji, F. Maps, Ø. Varpe, J. A. Runge, C. M. Petrik, and D. Johns. 2018. Copepod diapause and the biogeography of the marine lipidscape. Journal of Biogeography 45:2238–2251.

Rhodes, A. C. E. 2007. Dietary effects on carotenoid composition in the marine harpacticoid copepod *Nitokra lacustris*. Journal of Plankton Research 29:i73–i83.

Ringelberg, J., and G. M. Hallegraeff. 1976. Evidence for a diurnal variation in the carotenoid content of *Acanthodiaptomus denticornis* (Crustacea, copepoda) in Lac Pavin (Auvergne, France). Hydrobiologia 51:113–118.

Sandifer, P. A., and A. E. Sutton-Grier. 2014. Connecting stressors, ocean ecosystem services, and human health: Connecting stressors, ocean ecosystem services, and human health. Natural Resources Forum 38:157–167.

Schmid, M. S., F. Maps, and L. Fortier. 2018. Lipid load triggers migration to diapause in Arctic *Calanus* copepods—insights from underwater imaging. Journal of Plankton Research 40:311–325.

Schneider, T., G. Grosbois, W. F. Vincent, and M. Rautio. 2016. Carotenoid accumulation in copepods is related to lipid metabolism and reproduction rather than to UV-protection: Copepod carotenoids and lipids. Limnology and Oceanography 61:1201–1213.

Schneider, T., G. Grosbois, W. F. Vincent, and M. Rautio. 2017. Saving for the future: Pre-winter uptake of algal lipids supports copepod egg production in spring. Freshwater Biology 62:1063–1072.

Schneider, T., A. Herzig, K. A. Koinig, and R. Sommaruga. 2012. Copepods in Turbid Shallow Soda Lakes Accumulate Unexpected High Levels of Carotenoids. PLoS ONE 7:e43063.

Seehausen, O. 1997. Cichlid Fish Diversity Threatened by Eutrophication That Curbs Sexual Selection. Science 277:1808–1811.

Siefken, M., and K. B. Armitage. 1968. Seasonal variation in metabolism and organic nutrients in three *Diaptomus* (Crustacea: Copepoda). Comparative Biochemistry and Physiology 24:591–609.

Smith, L. V. 1941. *Labidocera glauca* sp. nov., a blue copepod of Puerto Galera bay, Mindoro. Philippine Journal of Science 75:307–322.

Snoeijs, P., and N. Häubner. 2014. Astaxanthin dynamics in Baltic Sea mesozooplankton communities. Journal of Sea Research 85:131–143.

Soloperto, S., D. Altin, A. Hallmann, E. Skottene, B. H. Hansen, B. M. Jenssen, and T. M. Ciesielski. 2022. Oil-mediated oxidative-stress responses in a keystone zooplanktonic species, *Calanus finmarchicus*. Science of The Total Environment 806:151365.

Sommaruga, R. 2010. Preferential accumulation of carotenoids rather than of mycosporine-like amino acids in copepods from high altitude Himalayan lakes. Hydrobiologia 648:143–156.

Sommer, F., C. Agurto, P. Henriksen, and T. Kiørboe. 2006. Astaxanthin in the calanoid copepod *Calanus helgolandicus*: dynamics of esterification and vertical distribution in the German Bight, North Sea. Marine Ecology Progress Series 319:167–173.

Takahashi, K., T. Ichikawa, and K. Tadokoro. 2015. Diel colour changes in male *Sapphirina nigromaculata* (Cyclopoida, Copepoda). Journal of Plankton Research:fbv088.

Tartarotti, B. 1999. Survivorship of *Cyclops abyssorum tatricus* (Cyclopoida, Copepoda) and *Boeckella gracilipes* (Calanoida, Copepoda) under ambient levels of solar UVB radiation in two high-mountain lakes. Journal of Plankton Research 21:549–560.

Tartarotti, B., A. Alfreider, M. Egg, N. Saul, T. Schneider, R. Sommaruga, A. Tischler, and J. Vetter. 2018. Seasonal plasticity in photoprotection modulates UV-induced *hsp* gene expression in copepods from a clear lake. Limnology and Oceanography 63:1579–1592.

Tedetti, M., and R. Sempéré. 2006. Penetration of Ultraviolet Radiation in the Marine Environment. A Review. Photochemistry and Photobiology 82:389.

Terao, J. 1989. Antioxidant activity of β-carotene-related carotenoids in solution. Lipids 24:659–661.

Tester, P., J. Cohen, and G. Cervetto. 2004. Reverse vertical migration and hydrographic distribution of *Anomalocera ornata* (Copepoda: Pontellidae) in the US South Atlantic Bight. Marine Ecology Progress Series 268:195–204.

Torres, R., and A. Velando. 2005. Male preference for female foot colour in the socially monogamous blue-footed booby, *Sula nebouxii*. Animal Behaviour 69:59–65.

Trudnowska, E., K. Balazy, J. Stoń-Egiert, I. Smolina, T. Brown, and M. Gluchowska. 2020. In a comfort zone and beyond—Ecological plasticity of key marine mediators. Ecology and Evolution:ece3.6997.

Trudnowska, E., K. Dragańska-Deja, S. Sagan, and K. Błachowiak-Samołyk. 2022. Cells of matter and life – towards understanding the structuring of particles and plankton patchiness in the Arctic fjords. Frontiers in Marine Science 9:909457.

Tsuboko-Ishii, S., and R. S. Burton. 2018. Individual Culturing of *Tigriopus* Copepods and Quantitative Analysis of Their Mate-guarding Behavior. Journal of Visualized Experiments:58378.

Turner, J. T. 2015. Zooplankton fecal pellets, marine snow, phytodetritus and the ocean's biological pump. Progress in Oceanography 130:205–248.

Twyman, H., N. Valenzuela, R. Literman, S. Andersson, and N. I. Mundy. 2016. Seeing red to being red: conserved genetic mechanism for red cone oil droplets and co-option for red coloration in birds and turtles. Proceedings of the Royal Society B: Biological Sciences 283:20161208.

Van Nieuwerburgh, L., I. Wänstrand, J. Liu, and P. Snoeijs. 2005. Astaxanthin production in marine pelagic copepods grazing on two different phytoplankton diets. Journal of Sea Research 53:147–160.

Veen, I. T. 2005. Costly carotenoids: a trade-off between predation and infection risk? Journal of Evolutionary Biology 18:992–999.

Venkataramana, V., S. C. Tripathy, and N. P. Anilkumar. 2017. The occurrence of blue-pigmented Pontella valida Dana, 1852 (Copepoda: Calanoida: Pontellidae) in the equatorial Indian Ocean. Journal of Crustacean Biology 37:512–515.

Vestheim, H., S. Kaartvedt, and B. Edvardsen. 2005. State-dependent vertical distribution of the carnivore copepod *Pareuchaeta norvegica*. Journal of Plankton Research 27:19–26.

Vestheim, H., and S. Kaartvedt. 2006. Plasticity in coloration as an antipredator strategy among zooplankton. Limnology and Oceanography 51:1931–1934.

Vilgrain, L., F. Maps, M. Picheral, M. Babin, C. Aubry, J. Irisson, and S. Ayata. 2021. Trait-based approach using in situ copepod images reveals contrasting ecological patterns across an Arctic ice melt zone. Limnology and Oceanography:lno.11672.

Vilgrain, L. 2023, February 23. laurvi/copepods-true-colors: Copepods' true colors - Data and code for Ecosphere publication. Zenodo DOI: https://doi.org/10.5281/zenodo.7671742

Violle, C., M.-L. Navas, D. Vile, E. Kazakou, C. Fortunel, I. Hummel, and E. Garnier. 2007. Let the concept of trait be functional! Oikos 116:882–892.

Weaver, R. J., P. A. Cobine, and G. E. Hill. 2018a. On the bioconversion of dietary carotenoids to astaxanthin in the marine copepod, *Tigriopus californicus*. Journal of Plankton Research 40:142–150.

Weaver, R. J., B. K. Gonzalez, S. R. Santos, and J. C. Havird. 2020. Red Coloration in an Anchialine Shrimp: Carotenoids, Genetic Variation, and Candidate Genes. The Biological Bulletin 238:119–130.

Weaver, R. J., G. E. Hill, P.-L. Kuan, and Y.-C. Tseng. 2016. Copper exposure reduces production of red carotenoids in a marine copepod. Ecological Indicators 70:393–400.

Weaver, R. J., P. Wang, G. E. Hill, and P. A. Cobine. 2018b. An *in vivo* test of the biologically relevant roles of carotenoids as antioxidants in animals. The Journal of Experimental Biology 221:jeb183665.

Wilson, C. B. 1950. Copepods gathered by the United States Fisheries steamer Albatross from 1887 to 1909, chiefly in the Pacific Ocean: contributions to the biology of the Philippine Archipelago and adjacent regions. United States National Museum Bulletin 100.

Woodall, A. A., G. Britton, and M. J. Jackson. 1997. Carotenoids and protection of phospholipids in solution or in liposomes against oxidation by peroxyl radicals: Relationship between carotenoid structure and protective ability. Biochimica et Biophysica Acta (BBA) - General Subjects 1336:575–586.

Wybouw, N., A. H. Kurlovs, R. Greenhalgh, A. Bryon, O. Kosterlitz, Y. Manabe, M. Osakabe, J. Vontas, R. M. Clark, and T. Van Leeuwen. 2019. Convergent evolution of cytochrome P450s underlies independent origins of keto-carotenoid pigmentation in animals. Proceedings of the Royal Society B: Biological Sciences 286:20191039.

Ye, L., X. Zhu, T. Wu, W. Wang, D. Zhao, C. Bi, and X. Zhang. 2018. Optimizing the localization of astaxanthin enzymes for improved productivity. Biotechnology for Biofuels 11:278.

Zalasiewicz, J., C. N. Waters, E. C. Ellis, M. J. Head, D. Vidas, W. Steffen, J. A. Thomas, E. Horn, C. P. Summerhayes, R. Leinfelder, J. R. McNeill, A. Gałuszka, M. Williams, A. D. Barnosky, D. de B. Richter, P. L. Gibbard, J. Syvitski, C. Jeandel, A. Cearreta, A. B. Cundy, I. J. Fairchild, N. L. Rose, J. A. Ivar do Sul, W. Shotyk, S. Turner, M. Wagreich, and J. Zinke. 2021. The Anthropocene: Comparing Its Meaning in Geology (Chronostratigraphy) with Conceptual Approaches Arising in Other Disciplines. Earth's Future 9.

Zhang, C., X. Chen, and H.-P. Too. 2020. Microbial astaxanthin biosynthesis: recent achievements, challenges, and commercialization outlook. Applied Microbiology and Biotechnology 104:5725–5737

3. Automatic quantification of red astaxanthin pigmentation on stereo-microscope images of Arctic copepods (*Calanus* spp.)

3.1. Résumé

Dans les régions arctiques, les copépodes du genre *Calanus* dominent la biomasse du zooplancton. Ces crustacés sont les proies préférentielles de nombreux poissons, oiseaux et mammifères marins, qui profitent des réserves d'acides gras accumulés par les copépodes pour survivre à la longue période hivernale. Pour comprendre leur importance dans les écosystèmes, deux traits fonctionnels clés sont principalement étudiés par les scientifiques : leur taille et leur quantité de lipides. Depuis une dizaine d'années, ces traits sont quantifiés à partir de photographies prises lors d'observations au stéréomicroscope, après un échantillonnage par traits de filets à plancton. Les *Calanus* possèdent par ailleurs une intense coloration rouge, souvent visible sur les images. Cette coloration est induite par l'astaxanthine, un pigment caroténoïde qui améliore le succès écologique des copépodes par ses fortes propriétés antioxydantes. Ce trait est pourtant peu étudié, notamment à cause de la difficulté de quantifier chimiquement les pigments. Pour pallier à cette limite, nous développons ici une méthode de quantification automatique de la rougeur sur des images en couleur (RGB) de copépodes. Nous utilisons 699 images d'individus échantillonnés dans la région arctique du Svalbard, associées à des mesures chimiques de la concentration en astaxanthine. Dans une première étape d'intercalibration, les moyennes des canaux de couleur des pixels sont normalisées entre les images (« *gray world algorithm* »), afin de rendre les teintes des images comparables malgré des conditions d'éclairement variables au moment de la prise de vue. Dans une seconde étape, une méthode de déconvolution de la couleur est utilisée pour quantifier entre 0 et 1 l'intensité de la rougeur induite par l'astaxanthine pour chaque pixel. Cette valeur est multipliée par l'aire d'un pixel afin de produire un indice de couleur rouge spécifique à chaque image. Pour les 699 images analysées, les indices de rougeur varient entre 10.53 to 442.70 et ont été comparés aux quantités d'astaxanthine obtenues par chromatographie liquide allant de 0.034 à 4.798 ng.copepod^{-1} (valeurs moyennes pour un échantillon de dix copépodes). Les variations de l'indice de rougeur expliquent 60% des variations d'astaxanthine quantifiée chimiquement (données log-transformées). D'après l'inspection visuelle de la segmentation des pixels rouges, la méthode est satisfaisante. Nous discutons des sources d'erreurs pouvant induire la part de variabilité non expliquée. Cette analyse d'images pourrait être généralisée à d'autres jeux de données historiques comme futurs, afin de comparer la coloration des copépodes en utilisant des paramètres de calcul fixes (moyenne des canaux de couleur pour la calibration, seuil de segmentation des pixels, etc.). L'utilisation d'un tel indice permettra de mieux comprendre le rôle

écologique des pigments caroténoïdes chez les copépodes *Calanus* (protection contre le stress lumineux, préservation des réserves lipidiques, transfert dans les œufs, camouflage), et d'étudier le transfert de ces antioxydants dans les réseaux alimentaires de l'Arctique.

3.2. Abstract

In Arctic regions, *Calanus* copepods dominate zooplankton biomass. These crustaceans are the preferred prey of many fish, birds and marine mammals, which benefit from their rich fatty acid reserves accumulated to survive the long polar winter. To understand their importance in ecosystems, scientists are focusing on two key functional traits: size and lipid content. For the past ten years, these traits have been quantified from photographs taken during observations under the stereo-microscope after sampling via plankton nets. Strikingly, *Calanus* individuals often show an intense red coloration, visible in these images. This color is induced by astaxanthin, a carotenoid pigment that enhances the ecological success of copepods through its strong antioxidant properties. Yet, this trait has been little studied, most likely because of the difficulty to chemically quantify these pigments. In this study, we develop a method to automatically quantify redness in color (RGB) images of copepods. We use 699 images of individuals sampled in the Svalbard arctic region, associated with chemical measurements of astaxanthin concentration. In a first intercalibration step, averages of pixel color channels are normalized between images (following the "*gray world algorithm*"), to make image hues comparable despite variable illumination conditions at the time of image capture. In a second step, a color deconvolution method is used to quantify between 0 and 1 the intensity of the astaxanthin-induced red color for each pixel. This value is multiplied by the area of a pixel to produce a red color index specific to each image. For the 699 images analyzed here, redness indices ranged from 10.53 to 442.70 and were compared with astaxanthin quantities obtained by liquid chromatography, ranging from 0.034 to 4.798 ng.copepod^{-1} (average values for samples of ten copepods). Variations in redness indices explained about 60% of variations in chemically quantified astaxanthin. Visual inspection of the red pixel segmentation produces good results and we discuss the sources of error that may induce the unexplained variability. The image analysis could be generalized to other historical or future datasets, and copepod redness could be compared using fixed calculation parameters (e.g. average of color channels for calibration, pixel segmentation threshold, etc.). The use of such an index will help to better understand the ecological role of carotenoid pigments in *Calanus* copepods (protection against light stress, preservation of lipid reserves, transfer to eggs, camouflage), and to study the transfer of these antioxidants in Arctic food webs.

3.3. Introduction

Copepods belong to a taxonomic group of more than 12,000 small crustacean species found in high abundances in lakes, rivers, estuaries, continental shelves, open ocean and deep seas (Humes 1994, Kooistra et al. 2007, Bron et al. 2011). Beyond the taxonomic diversity, studying their ecology using trait-based approaches helps to understand the links between community structure, ecosystem functioning and ecosystem service provision in aquatic ecosystems (Martini et al. 2021). Functional traits are properties measurable at the individual level and impacting survival, growth and reproduction (*fitness*, Violle et al. 2007). For copepods, the main functional traits studied are size, reproduction mode, feeding modes, myelination and dormancy strategies (Kiørboe et al. 2015, Benedetti et al. 2022). In arctic and subarctic environments, three *Calanus* species dominate mesozooplankton biomass (Aarflot et al. 2018, Carstensen et al. 2019) and share several functional traits such as a large size, herbivory/omnivory, current-filter feeding, accumulation of lipid reserves and overwintering at depth during the non-productive season strategy (*i.e.* diapause) (Daase et al. 2021, Benedetti et al. 2022). They also bear a strong red pigmentation, intense to the point that *Calanus finmarchicus* have been nicknamed "red feed" in aquaculture studies (Pedersen et al. 2014) This color is also a functional trait, but remains surprisingly overlooked in ecological studies (Vilgrain et al. 2023).

As in many other crustaceans, *Calanus'* red pigmentation is caused by astaxanthin molecules, one type of carotenoid synthesized from algal precursors (Matsuno 2001, Andersson et al. 2003). Astaxanthin provides strong antioxidant properties and induces a red coloration that can influence behavior of visual predators according to their light environment (Miki 1991, Naguib 2000, Johnsen 2005). Astaxanthin-based pigmentation was identified in at least 170 species and is influenced by factors such as diet quality and quantity, temperature, ultraviolet radiation stress, predation pressure, lipid metabolism, and reproduction. Owing to its strong antioxidant power and its finely tuned metabolism, astaxanthin pigmentation can be considered a plastic defense trait for copepod fitness (Hansson 2004, Powers and Hill 2021, Vilgrain et al. 2023). Beyond the advantages provided to copepods, antioxidants carotenoid availability is important when passing through food chains for the success of fish larvae (Nakano and Wiegertjes 2020, Azani and Rasdi 2021) and might be transferred to higher trophic levels, including humans (Hatlen et al. 1998, Hynes et al. 2009, Bolduc 2021).

Astaxanthin redness was identified in *Calanus finmarchicus* in 1964 and 1987 (Fisher et al. 1964, Foss et al. 1987) and was then mostly studied for purposes unrelated to its potential ecological roles. Pigmentation was used to distinguish individuals from congeneric species of *C. finmarchicus* and *C. glacialis* (Nielsen et al. 2014, Choquet et al. 2018, Lindeque et al. 2022), and then to detect

red swarms on satellite images, a promising opportunity to quantify their biomass and understand their mesoscale distribution (Basedow et al. 2019). The hypothesis that astaxanthin pigments are used against oxidative stress induced by ultraviolet radiation was proposed twice (Hylander et al. 2015, Vilgrain et al. 2021), but more efforts are definitely needed to tackle this question. Another study showed that *C. finmarchicus* and *C. glacialis* exhibited a pronounced red color when inhabiting their preferred water mass, suggesting that pigment metabolism occurs in optimal environmental conditions ("comfort zone" hypothesis) (Trudnowska et al. 2020). Also, it is very likely that pigments are used as a protection of lipid reserves and eggs for species inhabiting highly seasonal environments (Schneider et al. 2016). Finally, as specific structures are pigmented in *Calanus* spp. (antennas, extremity of the lipid sac/digestive tract and genital segment), we suggest a potential role of pigmentation to hide parts of their body by crypticity (red appears dark when blue light is absorbed by water molecules) (Johnsen 2005).

The difficulty in tackling those questions may be linked to the difficulty in measuring astaxanthin pigmentation. Indeed, most past studies used High Performance Liquid Chromatography (HPLC) methods to quantify pigment contents. This requires copepods to be frozen right after collection to preserve their color, with no thawing before laboratory work takes place. Furthermore, because of the detection limits of the instruments, HPLC quantification must be performed on pooled samples (on the order of ten individuals) leading to a loss of individual-level information. One option to avoid cumbersome HPLC measurements is the analysis of copepod images observed under the stereomicroscope. Color images can be taken right after sampling without the need to freeze samples, and pigmentation could be measured concurrently with other morphological traits such as prosome length and lipid sac volume (Maps et al. 2010, Nielsen et al. 2014, Trudnowska et al. 2020).

Vogedes et al. (2010) have shown that the size of the lipid sac outlined on a photo is proportional to the amount of lipid quantified by chemical methods. Since then, a lot of studies have used this approach in order to answer ecological questions (e.g. (Jónasdóttir et al. 2015, Daase et al. 2018, Schultz et al. 2020, Tarling et al. 2022). The lipid sac segmentation has been done through manual image analysis until now (Schmid et al. 2018), but machine learning segmentation algorithms are being developed to automate the process (see Orenstein et al. 2022). It is possible to create the same type of quantitative and automatic approach for astaxanthin redness, and to revisit information from thousands of images accumulated by researchers working on arctic and subarctic pelagic ecology. Examples of known datasets include: ~1,500 images from Norwegian waters, >10,000 images from the Svalbard Archipelago, and >7,000 images from the Gulf of St. Lawrence (Basedow et al. 2019, Trudnowska et al. 2020, Blais 2021).

Some studies have already used image analysis methods to quantify redness on images, using a thresholding tool in the ImageJ software (Nielsen et al. 2014) or a L*a*b* color space from the Photoshop Lab color (Brüsin et al. 2016, Lee et al. 2019). Those techniques have offered interesting insights to help with copepod species identification and to tackle trade-offs between UV and predation effects on individual pigmentation. Still, they present limitations such including the need for standardized lighting conditions, making each experiment unique (it is difficult to imagine the same condition created in various laboratories or ships), and the manual segmentation of some copepod parts before the automatic color quantification. These steps are time-consuming and may reduce the number of images possibly analyzed and thus the scales of potential ecological studies in time and space.

We propose a new methodology to analyze *Calanus* spp. pigmentation on color images taken from stereomicroscopy. Our goal is to obtain a redness index that is (*i*) fast and efficient to compute, (*ii*) independent of the light conditions within which the image was taken, (*iii*) specific to astaxanthin and (*vi*) quantitative at the pixel level. To do so, we worked on a dataset of 699 color high resolution images of *Calanus* individuals sampled in Svalbard waters (77°N, 16°E), photographed right after sampling. Images show large pigmentation variability and are associated with corresponding astaxanthin concentrations assessed via HPLC (Trudnowska et al. 2020). The research questions addressed for this analysis are: 1) How to make color information of stereomicroscope images of *Calanus* spp. comparable (intercalibration)? 2) How to quantify astaxanthin redness at the pixel level? 3) Is this astaxanthin-based redness index coherent with astaxanthin concentrations measured by HPLC? Obtaining such an index will allow us to improve our understanding of pigmentation variability in copepods in response to environmental conditions (Vilgrain et al., 2023). Because astaxanthin has been proven to be beneficial for copepod success (survival, growth, reproduction), this index could be implemented to an automatic trait-based approach in complement to current image-based ecological analyses.

3.4. Material and methods

3. 4. 1 Dataset of images associated to chemical quantification of astaxanthin

The dataset is composed of 699 images of *Calanus* copepods (*C. finmarchicus, C. glacialis*) sampled in the polar region of the Svalbard Archipelago (77°N, 16°E) in summer 2018 and 2019 aboard the R/V *Oceania* (Institute of Oceanology Polish Academy of Sciences, IO PAN). In 2018, zooplankton was sampled at four stations: in Atlantic open waters, in Arctic open waters, in the main basin of the

Hornsund fjord and in its glacial bay (Trudnowska et al. 2020). In 2019, zooplankton was sampled in four fjords: Isfjorden, Kongsfjorden, Hornsund, Bellsund. At each station, groups of 10 *Calanus* copepods (CV life stages, and some females) with visually homogeneous size and pigmentation were pooled together for further chemical analyses. A total of 70 samples were available for both years (69 samples of 10 individuals, 1 sample of 9 individuals) (Fig. 3.1A). Each individual copepod was photographed using Olympus SZX16 stereomicroscope equipped with a digital camera (Olympus SC50 CMOS Color Camera) at a constant magnification and known scale. Images are of a very good quality and the large majority represents a single copepod on an homogeneous background. Some of our images have confounding elements, such as a part of another copepod or the borders of the Petri dish within which the picture was taken. According to size measurements done afterwards with the ImageJ software, pixel pitch (equivalent to pixel side length) was 2.19 µm in 2018 and 2.72 µm in 2019. Then, each group of 10 copepods was frozen in order to quantify astaxanthin content by High Performance Liquid Chromatography (HPLC) in the Institute of Oceanology Polish Academy of Sciences (Sopot, Poland). According to Stoń-Egiert and Kosakowska (2005), astaxanthin was isolated from previously lyophilized and weighed *Calanus* individuals by mechanical grinding in 90% acetone and sonication (2 min, 20 kHz, Cole Parmer, 4710 Series) for 2 hours in darkness. After clarification, the extract was subjected to chromatographic analysis. The HP1200 system (Agilent, Perlan Technologies) was equipped with a C18 LichroCART™LiChrospher™ 100 RP18e (Merck) analytical column (dimensions 250 × 4 mm, particle size 5 µm, and pore size 100 Å). Pigments were separated in a gradient mixture of methanol, 1 ammonium acetate, and acetone. Calibration was conducted with commercially available standards (The International Agency for ^{14}C Determination DHI Institute for Water and Environment in Denmark), which allowed for the qualitative assessment of astaxanthin (based on retention time and similarity with the absorbance spectrum of the standards) and quantitative assessment (based on response factor values obtained during the calibration procedure).

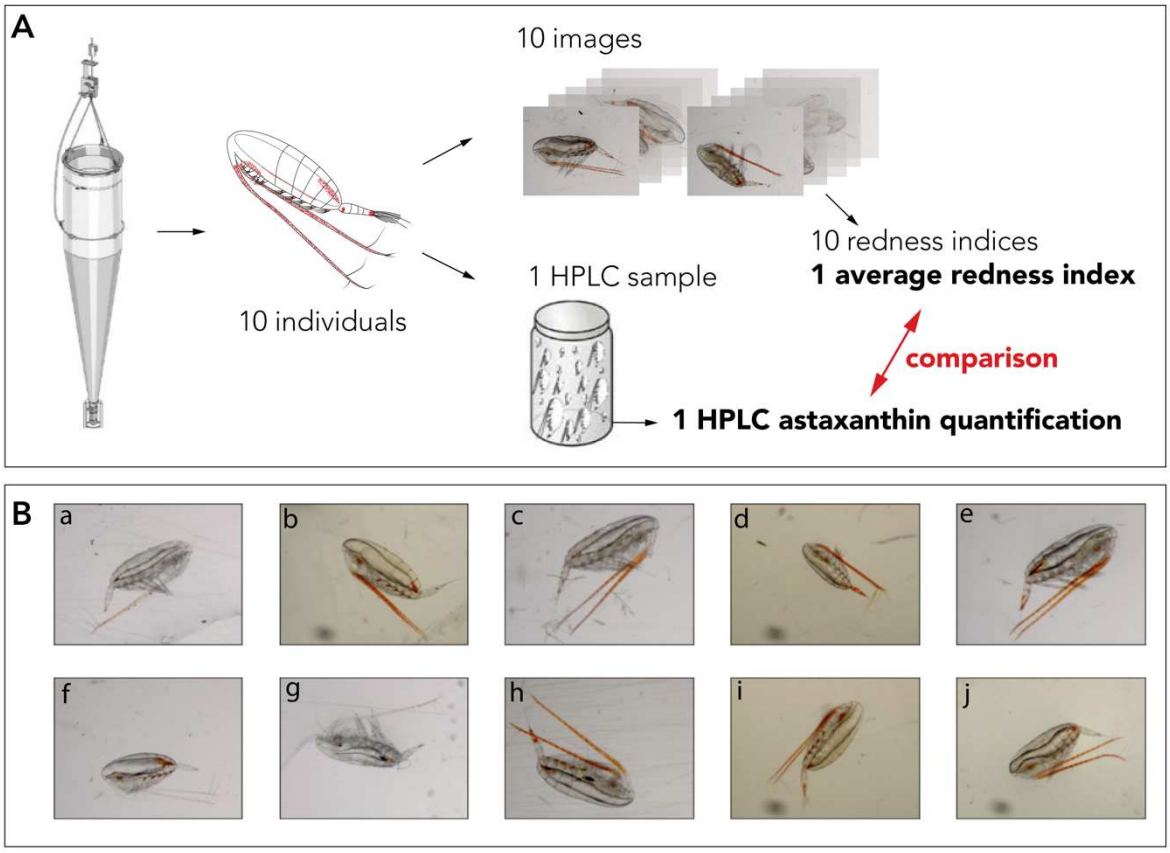

Figure 3.1. Images and High Performance Liquid Chromatography (HPLC) samples to analyze *Calanus* pigmentation. (A) Creation of one sample combining images and HPLC information (70 samples are analyzed in this study). Ten individuals are sampled by net, individually photographed and grouped into one sample to perform an HPLC quantification of astaxanthin pigments. The 10 images at the top right belong to one sample. **(B)** Variability of lighting conditions and copepod redness illustrated by 10 images coming from different samples. We can see that variations of redness (e.g. a, c and e) and of lightning conditions (e.g. h, i and j) can be important between images.

3. 4. 2 Intercalibration of color channels across images

One of our main objectives is to compare images taken in various light conditions (Fig. 3.1B). To this end, we applied a color constancy principle, defined as the ability of a system to recognize the true colors in objects independently of the illuminant present in a scene (Finlayson et al. 1999, Cepeda-Negrete and Sanchez-Yanez 2015). We used a gray-world algorithm method, based on the assumption that a scene with various colors should produce a neutral gray on average in an image. Thus, if the image is not neutral gray on average, the average reflected color is caused by the light source. Therefore, the gray-world algorithm produces an estimate of illumination by computing the

average of each channel in an image, and uses this estimate to correct each pixel and create a neutral gray scene (Buchsbaum 1980, Gasparini and Schettini 2004). The gray world method is particularly adapted for images with a predominant color (Gasparini and Schettini 2004), which is the case when copepods are imaged in front of a homogeneous background with a single light source directed towards them.

To convert an image into a gray world, the Red, Green and Blue (RGB) values of each pixel are transformed to have equalized averages in R, G and B channels. Concretely, for each pixels of one image, 1) a color channel value (*e.g.* the R value) is divided by the average of the channel in the image (*e.g.* average R values for all pixels), and 2) the result is multiplied by the average value of all channels (average RGB value for all pixels). Step 1 normalizes each color channel and step 2 normalizes color channels among them.

We adapted this method to the specificity of our images. Because all images need to be intercomparable, our goal is to apply the gray world algorithm across all images. Thus, we modified step (2) by using the RGB pixel values of *all* the 699 images (not only the pixels in a single image). Furthermore, we decided to calibrate images according to the background only, to remove the influence of the object of interest (the copepod) or of other extreme values like the edges of the Petri box within which the picture is taken. To this end, we used medians instead of averages in the computation. Indeed, median RGB values provide information from the pixels situated in the background (because a large majority of pixels are in the background), rather than from the pixels in the copepod (extreme values in RGB). Hence, for each pixel, R, G and B pixels values were modified according to this formula:

$$R^*_{pix} = \frac{R_{pix}}{R_{med}} \times \sum_{i=0}^{n} \frac{RGB_{med}}{n} \qquad (1)$$

with R^*_{pix} the final corrected value of the red channel by the gray-world algorithm for one pixel, R_{pix} the initial value of the red channel of the pixel, R_{med} the median of the red channel within one image, RGB_{med} the median of R, G and B channels in the image, and n the total number of images (here, n = 699). The same was performed for green and blue channels:

$$G^*_{pix} = \frac{G_{pix}}{G_{med}} \times \sum_{i=0}^{n} \frac{RGB_{med}}{n} \qquad (2)$$

$$B^*_{pix} = \frac{B_{pix}}{B_{med}} \times \sum_{i=0}^{n} \frac{RGB_{med}}{n} \qquad (3)$$

To validate the calibration, we computed the standard variation of R, G and B channel averages before and after the calibration and we proceeded to a visual inspection of a representative sample of images.

3. 4. 3 Segmentation of astaxanthin red pixels using RGB color deconvolution

After obtaining background color-calibrated images, a color deconvolution method is used to identify astaxanthin red pixels and obtain a quantitative measure of redness per pixel. Our analysis is based on the method of Ruifrok & Johnston (2001), initially developed to separate specific staining of cell components for immunology and histology studies. The method is meant to deconvolve the color information of microscope observations imaged with RGB cameras, which is easily applicable to our case.

The principle of the method is to do a product between the image and a matrix containing RGB values associated with pigmented substances, resulting in a quantification by pixel of pigmentation levels for each pigmented substance. The initial 3x3 matrix is called the Optical Density matrix (OD matrix) and contains RGB values calculated from pigment absorbance spectra (Ruifrok & Johnston, 2001):

$$\text{OD matrix : } \begin{bmatrix} R_1 & G_1 & B_1 \\ R_2 & G_2 & B_2 \\ R_3 & G_3 & B_3 \end{bmatrix} \begin{matrix} \text{Pigment 1} \\ \text{Pigment 2} \\ \text{Pigment 3} \end{matrix}$$

Ruifrok & Johnston (2001) used RGB values from three biological stains to highlight cell components on stained tissues (nucleus, cytoplasm, antigens). For the analysis of copepod redness, we are only interested in the RGB value for a single pigment, the astaxanthin. Thus, only the first line was completed with R, G and B value associated to astaxanthin pigment (R_a, G_a, B_a). The second line was filled with R, G and B value for the white color (R_w, G_w, B_w), and the third is a placeholder with artificial R, G and B values (a, b, c) chosen to make the matrix invertible. Thus, the OD matrix for our analysis is in the form of:

$$\text{OD matrix : } \begin{bmatrix} R_a & G_a & B_a \\ R_w & G_w & B_w \\ a & b & c \end{bmatrix} \begin{matrix} \text{Astaxanthin} \\ \text{White} \\ \text{Placeholder} \end{matrix}$$

To find specific R_a, G_a and B_a values, the astaxanthin absorbance spectrum was extracted from Ronsholdt & McLean (2001). The python library *colour* was used to convert this spectrum into an RGB-tuple using a color and an illumination model (see section 3.4.6 for code details). The responsivity of one specific camera sensor channel (R, G, or B) can be described by a curve depending on the wavelength (λ), noted $r(\lambda)$, similar to the absorption spectrum with light intensity $i(\lambda)$. The response of one channel (R, G, or B) is calculated by the integral of the spectrum over all wavelengths:

$$\int_{-inf}^{inf} r(\lambda) * i(\lambda)\, d\lambda \qquad (4)$$

Three color channel values XYZ are obtained and then translated to R_a,G_a, B_a. The R_w, G_w, B_w values of the white color are equal to 1, and the placeholder of the last line is computed by doing the cross product of the two first ones, making the OD matrix orthogonal and invertible. Indeed, it is necessary to first invert the OD matrix to obtain the color Deconvolution matrix (D matrix) that will finally be used to correct the image.
The OD matrix is:

OD matrix :

1	0.70	0.65
1	1	1
0.05	0.35	0.30

Astaxanthin
White
Placeholder

After inversion of the OD matrix, a Deconvolution matrix (D) is obtained:

D matrix :

3.00	-2.01	0.22
-1.16	1.24	-1.61
-1.84	1.77	1.39

The deconvolution color matrix (D) is used in the matrix product with the image [y] in order to obtain a matrix of Corrected optical density values (C):

$$C = D\,[y] \qquad (5)$$

For each image, a C matrix is created that corresponds to an "orthogonal representation of the stains forming the image" (Ruifrok & Johnston, 2001). C matrices contain continuous values (here varying between -0.43 and 0.22) which are called "corrected optical density values" in Ruifrok & Johnston (2001). We can name them "astaxanthin redness values" as they quantify how red a pixel is, because of the astaxanthin pigment. In this first raw output, 0.22 indicates no astaxanthin redness, and the more negative the value is, the redder the pixel is.

Our objective is to obtain an astaxanthin redness value by pixel varying between 0 and 1 across all images. To this end, we took the negative of the raw astaxanthin redness to have high values reflecting a high redness. Then, all values were normalized between 0 and 1 using the minimum and maximum optical density across the 699 images.

Each pixel is finally characterized by a continuous value between 0 (= no redness) and 1 (= maximal redness). To segment red pixels, we then used a threshold of 0.5 according to the distribution of astaxanthin optical density values (Appendix C1) and a visual assessment of resulting images. A threshold of 0.45 was automatically defined from the histogram using the Otsu method (Otsu 1979), but was not specific enough when looking at images so we kept the 0.5 value. At the end of the color deconvolution method, each copepod image has a total number of red pixels, themselves characterized by a continuous value of astaxanthin redness between 0.5 and 1.

3. 4. 4 Integrating pixel size to obtain a redness index for each individual image

To obtain a redness index for each copepod image, we need to integrate an information of size. Indeed, two images can have the same quantity of redness, but the real content of pigments depends on the size of the organism. Pixel size information is generally available for *Calanus* image datasets because images are usually taken to measure prosome length or lipid sac surface (Vogedes et al. 2010, Jónasdóttir et al. 2015, Daase et al. 2018, Schultz et al. 2020, Tarling et al. 2022). As mentioned in section 3.2.1, pixel pitch (equivalent to pixel side length) was 2.19 µm in 2018 and 2.72 µm in 2019 in our dataset, and we used pixel area as a multiplication factor of the cumulative sum of redness from segmented pixels:

$$RI_{cop} = \frac{1}{1000} \left(\sum_{i=0}^{n_{pix}} OD_{>0.5} * (pixel\ pitch)^2 \right) \qquad (6)$$

with RI_{cop} the Redness Index by individual copepod ($x10^{-3}$ µm^2), $OD_{>0.5}$ the astaxanthin optical density by pixel if superior to 0.5 and n_{pix} the total number of pixels with more than 0.5 in OD. The initial sum of OD values by image were between 600 and more than 1 million, which reflects the high number of pixels by image (each image contained 4 million pixels including 64,802 red segmented

pixels on average with our method). We thus arbitrarily divided redness indices by 1,000 to obtain numbers in a range easier to represent and to handle. This copepod redness index is then comparable to real pigment content estimated through HPLC methods. This step of integration for the pixel size is specific to each dataset, but mandatory to obtain the final redness index.

3. 4. 5 Validating the method with HPLC measurements

To compare redness indices with HPLC quantification of astaxanthin, the average of the 10 image redness indices by HPLC sample is computed:

$$\overline{RI} = \frac{1}{n_{sample}} \sum_{i}^{n_{sample}} RI_{cop} \qquad (7)$$

with $\overline{RI}$ the average redness index for one copepod sample, RI_{cop} the redness index by individual copepod image and n_{sample} the number of individuals by sample, equals to 10 for all samples but one containing only 9 individuals (Fig. 3.1).

We then tested how this index ($\overline{RI}$) makes it possible to predict the average astaxanthin content by individual ($\overline{AC}$), calculated as the total astaxanthin content of a sample divided by the number of copepods in a sample, n_{sample}. We used a log-log transformation of data to represent this allometric relationship, that can be expressed by the following power law relation:

$$Y = aX^b \Leftrightarrow ln(a) + b.ln(X) \qquad (8a)$$

Indeed, we are comparing the redness index defined on image pixels (x10^3 µm^2) with a pigment quantity extracted from a copepod volume (ng of astaxanthin), which is comparable with the relation between lipid sac area and total lipid content from Vogedes et al. (2010). We chose to express the average astaxanthin content by sample ($\overline{AC}$) as a function of the redness index by sample ($\overline{RI}$), to see if the redness index could be used as a good predictor of the astaxanthin content:

$$(\overline{AC}) = a.\overline{RI}^b \Leftrightarrow ln(a) + b.ln(\overline{RI}) \qquad (8b)$$

A linear correlation was tested on log-transformed data, normality of residuals and diagnosis graphics of the linear model were verified.

3. 4. 6 Computational tools

All image analyses were done using the python environment and code is available on a GitHub repository (https://github.com/laurvi/copepods-redness-indices.git). The open source *colour* library was used to convert astaxanthin spectrum into RGB (https://github.com/colour-science/colour). The color deconvolution method is coded in the open source library *scikit-image* described here: https://github.com/scikit-image/scikit-image/blob/main/skimage/color/colorconv.py#L1552-L1625. The regression between redness indices et HPLC quantification was done in the programming environment R 4.1.2 (R Core Team 2021).

3.5. Results

3. 5. 1 Intercalibration of RGB color channels

The gray world algorithm was applied to correct RGB channels of images. The aim is to obtain similar R, G, and B average values within an image, and across all images. Results for a selection of three typical images are presented on Fig. 3.2. We can see that original images appeared with variable hues, as a consequence of the lighting conditions when the picture was taken. The average RGB value of 172.3 ± 17.6 across all original images was changed to 171.9 ± 3.43 on calibrated images. All color channels were effectively centralized around a common value, which can be visualized on the histograms of R, G and B channels next to each image. For example, R, G and B averages were 186, 179 and 160 respectively in the original image *i*, and were corrected to 173, 171 and 170, which is much more homogeneous, and make the color comparable to other images. A residual variability remains but could be considered as acceptable (examples for 10 images in Figure C.2).

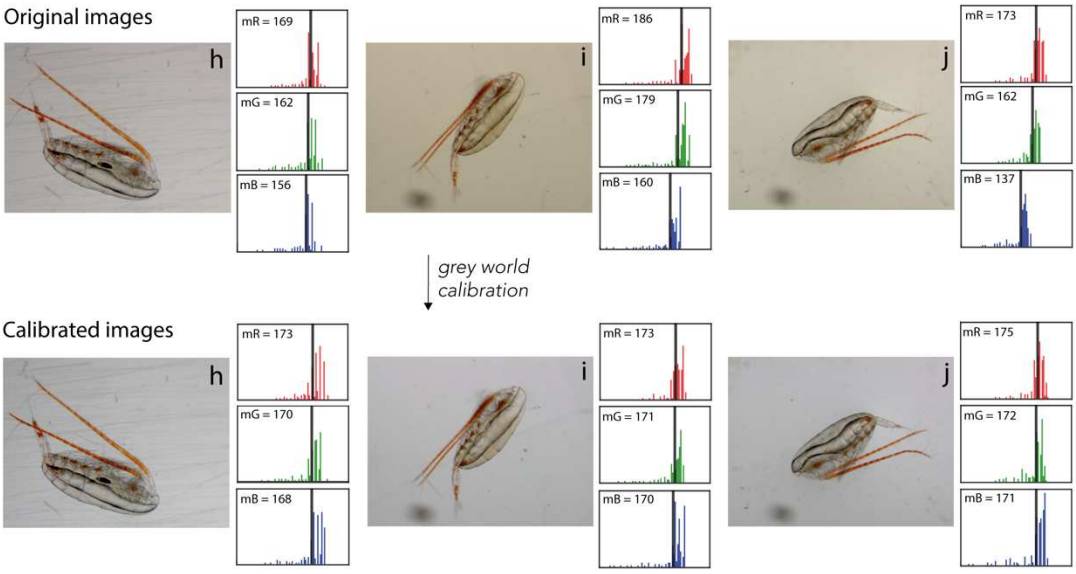

Figure 3.2. Three images coming from different samples, before and after gray-world calibration. Images were taken in various light conditions. Distribution of R, G, and B color channels are presented next to each image, with the average of each channel indicated. We can see the centralization of R, G and B pixel values with the calibration process.

3. 5. 2 Redness index computation

The results of redness index computation are summarized in Fig. 3.3 for three images illustrating variability in redness. First, the color deconvolution step allows to obtain raw optical density (OD) values of astaxanthin for red pixels. Raw values vary between -0.22 and 0.43 but are specific to each image. The second step of normalization extends the range between 0 (= no redness) and 1 (= maximal redness) for each pixel across images. At the third step, a threshold of 0.5 is applied on the normalized OD values to segment red pixels (Fig. C.1), which are highlighted on the calibrated image or visualized as a mask (Fig 3.3). The redness index is finally computed as the sum of all normalized OD values within the segmented red pixels, multiplied by the pixel area. For the 10 images presented in Fig. 3.1, the results of methodological steps from calibration to redness segmentation for the 10 images are visible in Fig. C.2.

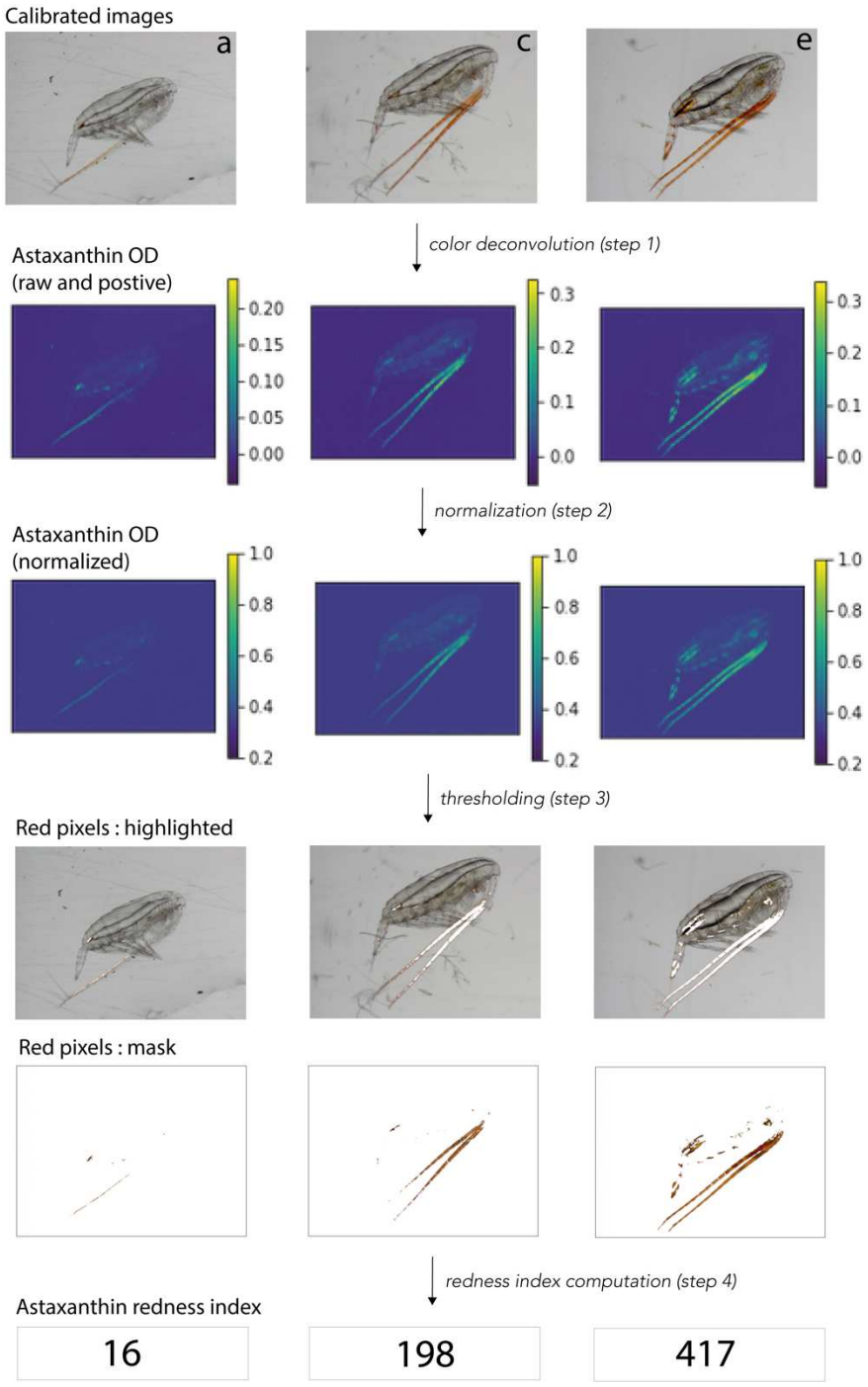

Figure 3.3 Automatic quantification of astaxanthin redness indices on images of *Calanus* observed by stereomicroscopy. Three images are chosen to illustrate the range of color variability observed. Step 1: the color deconvolution is applied on the calibrated image to obtain astaxanthin optical density values by pixel, quantifying how red a pixel is. Step 2: the raw values, which have an arbitrary range, are normalized between 0 and 1 to be comparable among images. Step 3: a threshold is applied on normalized OD values to segment red pixels. Step 4: the redness index is computed by summing all OD value values of segmented pixels and multiplying the result by the pixel area (see section 3.2.4 for details).

The method may have led to a slight underestimation of the number of red pixels, since pale red pixels are sometimes missed, such as in the extremities of antennas visible on Fig. 3.3, image *c*. However, this bias is constant and variations of redness among images are coherent (Fig. 3.3). According to a visual assessment of each image individually, pixel segmentation appears efficient: redness indices follow pigmentation patterns visible on images. Also, segmentation is specific because only astaxanthin redness is tackled: no other colors or incoherent parts of the copepod or of the background of the images were identified. However, validation was only done visually (by looking at images with highlighted pixels), and more objective validation methods should be developed in the near future.

3. 5. 3 Validation of the method with pigment HPLC quantification

Since we were developing an approach to quantifying red pigmentation in individual copepods images, we explored whether the average astaxanthin content of a copepod ($\overline{AC}$, average in a sample of 9 or 10 individuals) could be predicted by the average redness indices from copepods forming the associated sample ($\overline{RI}$). Copepods' average redness indices range from 10.53 to 442.70 µm^2, and were compared to the average astaxanthin content varying between 0.034 and 4.798 ng.copepod^{-1} (large green points on Fig. 3.4). In addition, we represented the individual redness indices for each of the 699 images, to illustrate the variability within a sample (small gray points on Fig. 3.4). At this individual level, redness indices have a higher variability and range from 0.61 to 1046.63 µm^2.

The linear regression between log-transformed data is positive and highly significant (p-value < 0.001, n = 70, Adjusted R^2 = 0.6) (Fig. 3.4), and can be expressed as $ln(a) + b * ln(\overline{RI})$ with $ln(a)$ = -4.12 and b = 0.83 :

$$\ln(\overline{AC}) = -4.12 + 0.83 * \ln(\overline{RI})$$

$$\Leftrightarrow$$

$$\overline{AC} = 0.016 * \overline{RI}^{0.83}$$

For this linear model, the residuals are normally distributed (shapiro test: *p-value = 0.3,* not possible to reject the null hypothesis: the distribution is not significantly different from a normal distribution) and observation of the diagnostic graphs confirmed that none of the points could be considered as statistically extreme (cook distance < 0.5, valid homoscedasticity in residuals).

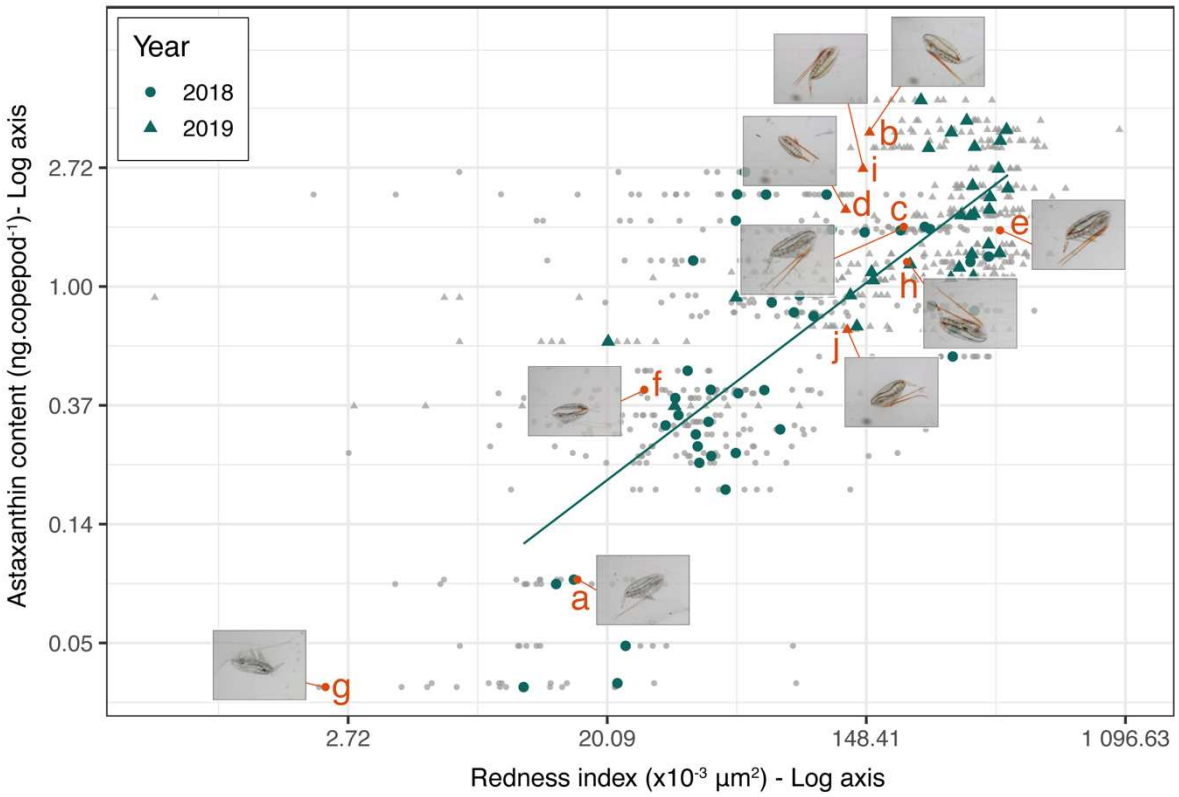

Figure 3.4. Astaxanthin content (ng.copepod^{-1}) obtained by HPLC expressed as a function of redness indices from images (x10^{-3} µm^2), using log-transformed values. We compared the average astaxanthin content of a pooled sample of 10 copepods ($\overline{AC}$) with the average redness index for the 10 associated images ($\overline{RI}$) (large green points). All images are represented by small gray points (699 images) in order to show the variability of redness indices within a sample. The shape of points represents the year of sampling (circles = 2018, triangles = 2019). The 10 images presented in Fig 3.1 are shown. A linear model fitted for this log-log relationship is significant (p-value < 0.001, n = 70, adjusted R-squared = 0.599) and can be expressed as $\ln(\overline{AC}) = -4.12 + 0.83*\ln(\overline{RI}) \Leftrightarrow \overline{AC} = 0.016*\overline{RI}^{0.83}$.

$\overline{AC}$ and $\overline{RI}$ are not normally distributed, and we can observe three main groups of points ($\overline{AC} < 0.1$; $0.1 < \overline{AC} < 0.7$; $\overline{AC} > 0.7$) instead of an homogenous distribution. This might be caused by the grouping of copepods according to their apparent coloration to create homogeneous samples for HPLC. The grouping may have created spurious ranges of redness variations, but could also reflect "real" steps in pigmentation levels. Also, we can note that year of sampling is an important source of variability. Indeed, in 2018 (circles on Fig. 3.3), redness was generally less important, with copepods with low-medium redness; while most copepods have a higher redness in 2019 (triangles), probably because more *C. glacialis* than *C. finmarchicus* (generally pale in Svalbard fjords) were sampled.

3.6. Discussion

3. 6. 1 General assessment of the methodology

The computation of an astaxanthin redness index from copepod images produces coherent and reliable results, which provides a valuable and useful methodology for ecological studies based on pigmentation traits. First, the calibration of the image successfully produces a neutral gray image with reduced variability in the RGB color channels. The color deconvolution is operational, as the segmentation of red pixels on images seems specific and precise (only astaxanthin redness is identified, but no other parts of the image such as algal pigments from the copepods' gut for example). The log-log regression between the average astaxanthin content ($\overline{AC}$) and redness indices ($\overline{RI}$) is very significant, which is promising for the future use of the redness index as a proxy of astaxanthin content. The variation of average redness indices across images explains 60% of the variations in astaxanthin content, a large proportion, but which also indicates non-negligible sources of variability that are discussed hereafter. In any case, the major advantage of this method is that it is much easier to perform than HPLC quantifications since there is no need for sample preservation, including maintenance of frozen samples, and meticulous laboratory analyses. Furthermore, the method can analyze a large number of images (quantitative analysis) at low cost, while allowing the characterization of individual variability at the same time. The process is quite fast despite that code is not optimized for the moment: 28 minutes are necessary to analyze 699 images from the raw file to the final redness index, which correspond to 2.4 seconds of analysis by image. Finally, it is a nondestructive method (contrary to HPLC measurements), so it is possible to go back to specific images if needed, offering new possibilities for experiments and analysis (see Conclusion).

3. 6. 2 Sources of variability in astaxanthin quantification and limits of the method

Despite the good explanation power of the regression between astaxanthin content and average redness indices, some variance (40%) remains to be explained. This variability can be explained by potential errors in astaxanthin quantification, whether by HPLC quantification or image analyses. Astaxanthin quantification by HPLC has inherent errors and limitations, and cannot be considered as an exact measure of astaxanthin content. To quantify the pigments after sampling, organisms have to be kept at -80°C for transportation and storage, pigments are extracted in a specific solvent and analyzed by a machine. Final astaxanthin quantity is deducted from a calibration curve

obtained with a given product of reference and these steps are often done by different persons. Thus, there is no reason to think that errors induced during this process should be smaller overall than errors linked to copepod image analysis. Also, in the HPLC analysis performed here, only the peak associated with free astaxanthin was used, so only free forms (no mono- and di-esters) are quantified, which can be a limitation as an important proportion of astaxanthin is esterified in *Calanus* copepods (Chapter 2; Vilgrain et al. 2023).

A source of variability specific to image analysis lies in the potential errors in redness segmentation. We can distinguish two types of points quite distant from the main cloud of points, even if not considered as statistical outliers (see section 3.5.3). First, some images have high redness indices even though their $\overline{AC}$ is medium, while the average redness index of the associate sample stays coherent (Fig. C.3, purple ellipse). To explain such overestimation of redness indices in these images, our main hypothesis was the presence of red parts belonging to other copepods in the frame of an image (*e.g.* parts of antennae), leading to an artificial increase in total redness in the image. Looking in detail at this image dataset, we found only 15 images matching this hypothesis (2.15% of the dataset). The redness indices from those images are obviously overestimated, but they were not the most extreme indices in the dataset. The highest redness index (RI_{cop} = 1046) was for a single copepod whose body was almost completely red and was not an artefact. At the image level, high redness indices did not seem to be caused by neither the algorithm nor some problems with the image, but rather reflected interindividual variability in pigmentation.

Second, some images of entire samples (10 individuals) have redness indices consistently low in comparison with HPLC astaxanthin content (6 points are lower than the fitted curve, Fig. C.3, green ellipse). Our two main underestimation hypotheses are that some red pixels were missed if antennae (often bright red in *Calanus*) are cut off by the frame of the image, or if two antennae are superimposed in the image (fewer red pixels identified). Looking at these images in detail, we found 29 images with antennas cut by the frame of the image, a proportion (4.1%) of images that should not be a cause of major underestimation overall. Still, this problem may be easily avoided while taking the photos. Then, in the rare cases where both antennae were superimposed, the pixels had a higher redness index. The color underestimation was limited.

In fact, the main underestimation of redness indices in comparison with HPLC astaxanthin content was for 6 samples, all coming from Atlantic waters in 2018 (AT_p105, AT_p117, AT_p117, AT_p118, AT_p119, AT_p120, Fig. C.3 green ellipse). We checked these images and found that all copepods had very gray prosomes with a lipid sac apparently broken in small droplets. In each image, redness pigmentation is present, but quite low and spread out in tiny dots at the surface of the exoskeleton. This type of redness with small points on the exoskeleton is also visible in other images,

and is remarkably different from the more common redness localized in antennae, bases of periods, genital segments or extremity of the lipid sac. The redness index is low because the computation identified those small dots on the animal, and it is questionable whether the chemical analysis detects such high abundances of astaxanthin. In fact, all images were taken of dying individuals, which led to this gray appearance; and four out of six samples were composed of females (and not CV copepods). Thus, the underestimation may be caused by: *(i)* the dominance astaxanthin in the free form in females that don't need to accumulate lipids at the end of their life cycle, with free forms better estimated by the HPLC than other esterified forms present in CV copepod images, *(ii)* the lack of transparency diminishing the ability of the computational to capture red pixels of the other side of these dying copepods. In the future, we will remove the females and dead animals from the dataset to have homogeneous images of CV copepods stages.

3. 6. 3 Comparison with other methods of redness quantification from images

Other computational methods quantifying red pigmentation from image analysis have already been proposed to address the limitations of HPLC analyses. To distinguish *C. finmarchicus* and *C. glacialis*, Nielsen et al (2014) and Lindeque et al. (2022) used the "Threshold Color " plug-in of the ImageJ software. Pixels of a cropped part from a copepod image were segmented and quantified using a Hue-Saturation-Brightness (HSB) color model (with H: 0–23, S: 75–255, B:1–255). Other studies have used the Photoshop® software to convert a copepod image into a L*a*b* color space based on the CIE (Commission International de l'Éclairage) (Brüsin et al. 2016, Lee et al. 2019). In this color space, the a* and b* channels are used as proxies for carotenoid-based coloration (Svensson et al. 2005, Martin et al. 2014), with a* correlating with red carotenoids such as astaxanthin, and b* with yellow carotenoids such as lutein. This method was also used to quantify color Arctic char fillet (Hatlen et al. 1998) and wheat (Humphries et al. 2004), explaining 50–90% of the variation in carotenoid concentration.

Such methods have produced interesting results, helping the taxonomic identification, and testing the hypothesis of the photoprotection role of pigments in copepods. However, the methodology we developed tries to overcome some of their limitations. First, the calibration part allows us to analyze images taken in different light conditions, contrary to previous studies in which authors mentioned light standardization (i.e., dark room, a unique light source, a consistent angle for the light beam, etc.) (Brüsin et al. 2016, Lee et al. 2019). The calibration step is critical to compare color information among historical (and future) image datasets, especially because copepods are generally photographed right after sampling, and the same conditions cannot be created in various laboratories or research vessels. A second aspect is that values of HSB or a* and b* used are not

specific to the astaxanthin color. With our method, we used the absorbance spectrum of the astaxanthin molecule in order to derive the RGB values contained in the color deconvolution matrix. As this pigment is predominant in copepods (dominant in 96% of carotenoids measurements in copepods, see Chapter 2; Vilgrain et al. 2023), it is interesting to identify red pixels specifically associated with the astaxanthin color. One other benefit of our redness index is to integrate continuous OD values instead of the binary number of red pixels only. Redness indices explain the variations in astaxanthin content a little better (2% more) than the number of red pixels, showing that the intensity of pigmentation is interesting to take into account. Finally, a limitation of the previous methods was that parts of the copepod had to be selected manually in order to compare and apply a quantification method. In Brüsin et al. (2016) and Lee et al. (2019), the cephalosome was selected by a photoshop tool, to then quantify average a* and b* values while avoiding potential other colors in the image. In Nielsen et al. (2014) this image cropping was also done by hand to answer an ecological question: is pigmentation of some parts associated with the species? In an ideal case, our method might be used with a complementary automatic segmentation to tackle such questions. In general, avoiding time-consuming image manipulation by hand using interactive software is likely to minimize errors and biases, produce results independent from human accuracy and increase dramatically the number of images analyzed and thus the scales of ecological studies in time and space.

3. 6. 4 Generalization and improvement of the methodology

The main objective for the development of this redness index is to be able to quantify the color information on images and to revisit past image datasets. The performance and the reproducibility of the method lies in the choice of some determining parameters, summarized in Table 3.1. First, the reproducibility could depend on the RGB value on which the color channels are calibrated (Table 3.1A). We used medians and averages of RGB values from our images to calibrate them, so calibration is dependent on the initial dataset: the larger the color variability, the larger the standard deviation will be in R, G and B values. Since the range of the standard deviation will always be impacted by this variability, we should choose a value on which all RGB channels should be centered on to make other datasets comparable (we could take the reference of 171.9 of our calibrated dataset, see section 3.3.1). Second, the RGB value chosen in the color deconvolution matrix, and the threshold used to segment red pixels certainly influence the quality of the segmentation (Table 3.1.B, C). In this study, we took astaxanthin RGB values of [1, 0.7, 0.65] extracted from astaxanthin spectrum found in a fish (Rønsholdt and McLean 2001). It could be relevant to test other spectrums, especially ones from copepods' astaxanthin. For the threshold, we used the semi-arbitrary value of 0.5 to segment astaxanthin, based on a frequency distribution (Fig. C.1) and the quality of

segmentation observed on images. As described in the Methods section, we tried another thresholding method (Otsu, 1979) which was not conclusive, but others could be tested. Third, OD values should be normalized in the same way if we want to have comparable redness indices (Table 3.1.D). In our dataset raw OD values varied between -0.22 and 0.43, and we used these minimal and maximal values to normalize OD values between 0 and 1, before applying the segmentation threshold of 0.5. The normalization should always be done using the same minimal and maximal OD values. If copepods of another dataset are redder, normalized OD values will be superior to 1 which is not a problem in the computation of the redness index. Finally, past and future images can have various resolutions (number and size of pixels), which will impact the number of red pixels segmented. As pixel area is considered in the computation of the redness index, this effect should be mitigated but is still interesting to quantify.

Table 3.1. Values of parameters chosen for the reproducibility of gray world calibration, color deconvolution and red pixels segmentation methods made on other datasets.

Parameters	**Values used in this study**	**Other values suggested**
A - Final RGB average in gray world calibration	$\overline{R} = \overline{G} = \overline{B} = 171.9$	Keep this value or find one representative of a more diverse dataset
B - R_a,G_a,B_a values in the deconvolution matrix	R_a,G_a,B_a: [1, 0.7, 0.65] (Rønsholdt and McLean 2001)	R_a,G_a,B_a values from copepod's astaxanthin absorbance spectrum
C - Segmentation threshold	thr = 0.5	*Otsu* thresholding method produced a threshold of 0.45, not selective enough, other objective thresholding methods could be used
D - Minimum and maximum raw OD values for normalization	min = -0.22 max = 0.43	Keep those values or find new ones that represent a more diverse dataset

In the future, we wish to develop a ground truth dataset using a subsample of our images, with red pixels annotated by hand. To assess the quality of the values described in Table 3.1 and improve the method, sensitivity tests will be performed with the ground truth dataset used to quantify

the method's performance. It must be kept in mind that optimal results will be obtained with a good quality of dataset: ideally, copepods should be photographed with only one individual per image and antennae within the frame of the photo. A last way to improve the method is to optimize the code, which would minimize the time and energy needed for the process.

3.7. Conclusion

The redness index developed in this study is easy to obtain at the individual level, specific to astaxanthin pigmentation and non-destructive. Using this redness index could probably be useful to better understand ecological causes and physiological mechanisms leading to copepod pigmentation. Because astaxanthin molecules provide a strong antioxidant power and induce an intense red (or blue) coloration, copepod pigmentation has historically been associated with a photoprotection role hypothesis (Chapter 2; Vilgrain et al. 2023). However, because astaxanthin seems useful in many ecosystem conditions and controlled by a finely tuned metabolism, it could be considered as a "swiss army knife" against oxidative stress induced by external stressors (like ultraviolet radiations) but also by internal factors such as high metabolism and rapid growth (Lotocka 2004, Hansson 2004, Chapter 2; Vilgrain et al. 2023). In addition, the red pigmentation of pelagic animals living at depth was suggested as a camouflage strategy, so individuals appear black in the potential searchlights of visual predators (Johnsen 2005, 2014). All those hypotheses could be studied using the image redness index developed for *Calanus* spp., and generalizable to other copepods species. Historical image datasets could be analyzed, or new datasets could be acquired to study, for example, pigmentation variations according to depth, to daily or seasonal temporal series. In laboratory experiments this nondestructive method can allow people to take photos of individuals while maintaining them alive under any experimental condition.

3.8. References

Aarflot, J. M., H. R. Skjoldal, P. Dalpadado, and M. Skern-Mauritzen. 2018. Contribution of Calanus species to the mesozooplankton biomass in the Barents Sea. ICES Journal of Marine Science 75:2342–2354.

Andersson, M., L. Van Nieuwerburgh, and P. Snoeijs. 2003. Pigment transfer from phytoplankton to zooplankton with emphasis on astaxanthin production in the Baltic Sea food web. Marine Ecology Progress Series 254:213–224.

Azani, N., and N. W. Rasdi. 2021. Effect of enriched copepods on the growth, survival, and colouration of angelfish (Pterophyllum scalare). Universiti Malaysia Terengganu Journal of Undergraduate Research 3:25–36.

Basedow, S. L., D. McKee, I. Lefering, A. Gislason, M. Daase, E. Trudnowska, E. S. Egeland, M. Choquet, and S. Falk-Petersen. 2019. Remote sensing of zooplankton swarms. Scientific Reports 9:686.

Benedetti, F., J. Wydler, and M. Vogt. 2022. Copepod functional traits and groups show divergent biogeographies in the global ocean. Journal of Biogeography:jbi.14512.

Blais, M. 2021. Les conditions océanographiques chimiques et biologiques dans l'estuaire et le golfe du Saint-Laurent en 2020. Secrétariat canadien de consultation scientifique (SCCS), Ottawa (Ontario).

Bolduc, S. 2021. Indicateurs de la qualité de la chair de l'omble chevalier anadrome et ses liens avec les préférences alimentaires des Inuit du Nunavik, Master thesis, Département de Biologie, Université Laval, Québec, Canada.

Bron, J. E., D. Frisch, E. Goetze, S. C. Johnson, C. Lee, and G. A. Wyngaard. 2011. Observing copepods through a genomic lens. Frontiers in Zoology 8:22.

Brüsin, M., P. A. Svensson, and S. Hylander. 2016. Individual changes in zooplankton pigmentation in relation to ultraviolet radiation and predator cues: Individual Changes in Zooplankton Pigmentation. Limnology and Oceanography 61:1337–1344.

Buchsbaum, G. 1980. A spatial processor model for object colour perception. Journal of the Franklin Institute 310:1–26.

Carstensen, J., A. Olszewska, and S. Kwasniewski. 2019. Summer Mesozooplankton Biomass Distribution in the West Spitsbergen Current (2001–2014). Frontiers in Marine Science 6:202.

Cepeda-Negrete, J., and R. E. Sanchez-Yanez. 2015. Automatic selection of color constancy algorithms for dark image enhancement by fuzzy rule-based reasoning. Applied Soft Computing 28:1–10.

Choquet, M., K. Kosobokova, S. Kwaśniewski, M. Hatlebakk, A. K. S. Dhanasiri, W. Melle, M. Daase, C. Svensen, J. E. Søreide, and G. Hoarau. 2018. Can morphology reliably distinguish between the copepods *Calanus finmarchicus* and *C. glacialis*, or is DNA the only way?: Morphological misidentification in Calanus. Limnology and Oceanography: Methods 16:237–252.

Daase, M., J. Berge, J. E. Søreide, and S. Falk-Petersen. 2021. Ecology of Arctic Pelagic Communities. Pages 219–259 *in* D. N. Thomas, editor. Arctic Ecology. First edition. Wiley.

Daase, M., K. Kosobokova, K. Last, J. Cohen, M. Choquet, M. Hatlebakk, and J. Søreide. 2018. New insights into the biology of Calanus spp. (Copepoda) males in the Arctic. Marine Ecology Progress Series 607:53–69.

Finlayson, G. D., S. D. Hordley, and P. M. Hubel. 1999. Colour by correlation: a simple, unifying approach to colour constancy. Pages 835–842 volume2 Proceedings of the Seventh IEEE International Conference on Computer Vision. IEEE, Kerkyra, Greece.

Fisher, L. R., S. K. Kon, and S. Y. Thompson. 1964. Vitamin A and Carotenoids in Certain Invertebrates VII. Crustacea: Copepoda. Journal of the Marine Biological Association of the United Kingdom 44:685–692.

Foss, P., B. Renstrøm, and S. Liaaen-Jensen. 1987. Natural occurrence of enantiomeric and Meso astaxanthin 7∗-crustaceans including zooplankton. Comparative Biochemistry and Physiology Part B: Comparative Biochemistry 86:313–314.

Gasparini, F., and R. Schettini. 2004. Color balancing of digital photos using simple image statistics. Pattern Recognition 37:1201–1217.

Hansson, L.-A. 2004. Plasticity in pigmentation induced by conflicting threats from predation and UV radiation. Ecology 85:1005–1016.

Hatlen, B., M. Jobling, and B. Bjerkeng. 1998. Relationships between carotenoid concentration and colour of fillets of Arctic chair, *Salvelinus alpinus* (L.), fed astaxanthin. Aquaculture Research 29:191–202.

Humes, A. G. 1994. How many copepods? Pages 1–7 *in* F. D. Ferrari and B. P. Bradley, editors. Ecology and Morphology of Copepods. Springer Netherlands, Dordrecht.

Humphries, J. M., R. D. Graham, and D. J. Mares. 2004. Application of reflectance color measurement to the estimation of carotene and lutein content in wheat and triticale. Journal of Cereal Science 40:151–159.

Hylander, S., T. Kiørboe, P. Snoeijs, R. Sommaruga, and T. G. Nielsen. 2015. Concentrations of sunscreens and antioxidant pigments in Arctic *Calanus* spp. in relation to ice cover, ultraviolet radiation, and the phytoplankton spring bloom: MAAs and astaxanthin in copepods. Limnology and Oceanography 60:2197–2206.

Hynes, N., E. S. Egeland, W. Koppe, G. Baardsen, and V. Kiron. 2009. *Calanus* oil as a natural source for flesh pigmentation in Atlantic salmon (*Salmo salar* L.). Aquaculture Nutrition 15:202–208.

Johnsen, S. 2005. The Red and the Black: Bioluminescence and the Color of Animals in the Deep Sea. Integrative and Comparative Biology 45:234–246.

Johnsen, S. 2014. Hide and Seek in the Open Sea: Pelagic Camouflage and Visual Countermeasures.

Annual Review of Marine Science 6:369–392.

Jónasdóttir, S. H., A. W. Visser, K. Richardson, and M. R. Heath. 2015. Seasonal copepod lipid pump promotes carbon sequestration in the deep North Atlantic. Proceedings of the National Academy of Sciences 112:12122–12126.

Kiørboe, T., S. Ceballos, and U. H. Thygesen. 2015. Interrelations between senescence, life-history traits, and behavior in planktonic copepods. Ecology 96:2225–2235.

Kooistra, W. H. C. F., R. Gersonde, L. K. Medlin, and D. G. Mann. 2007. The Origin and Evolution of the Diatoms: Their Adaptation to a Planktonic Existence. Pages 207–249 Evolution of Primary Producers in the Sea. Elsevier.

Lee, M., H. Zhang, Y. Sha, A. Hegg, G. E. Ugge, J. Vinterstare, M. Škerlep, V. Pärssinen, S. D. Herzog, C. Björnerås, R. Gollnisch, E. Johansson, N. Hu, P. A. Nilsson, K. Hulthén, K. Rengefors, R. B. Langerhans, C. Brönmark, and L.-A. Hansson. 2019. Low-latitude zooplankton pigmentation plasticity in response to multiple threats. Royal Society Open Science 6:190321.

Lindeque, P. K., I. Hann, H. E. Parry, K. B. Cook, A. J. W. Lindley, and D. J. Mayor. 2022. Red Pigmentation Can Be Used to Reliably Distinguish Between Live *Calanus finmarchicus* and *Calanus glacialis* Females in the Fram Strait. Frontiers in Marine Science 9:906465.

Lotocka, M. 2004. Changes in carotenoid composition in different developmental stages of copepods: *Pseudocalanus acuspes* Giesbrecht and *Acartia* spp. Journal of Plankton Research 26:159–166.

Maps, F., S. Plourde, and B. Zakardjian. 2010. Control of dormancy by lipid metabolism in *Calanus finmarchicus*: a population model test. Marine Ecology Progress Series 403:165–180.

Martin, R. A., R. Riesch, J. L. Heinen-Kay, and R. B. Langerhans. 2014. Evolution of male coloration during a post-pleistocene radiation of Bahamas mosquitofish (*Gambusia hubbsi*): evolution of male coloration. Evolution 68:397–411.

Martini, S., F. Larras, A. Boyé, E. Faure, N. Aberle, P. Archambault, L. Bacouillard, B. E. Beisner, L. Bittner, E. Castella, M. Danger, O. Gauthier, L. Karp-Boss, F. Lombard, F. Maps, L. Stemmann, E. Thiébaut, P. Usseglio-Polatera, M. Vogt, M. Laviale, and S. Ayata. 2021. Functional trait-based approaches as a common framework for aquatic ecologists. Limnology and Oceanography 66:965–994.

Matsuno, T. 2001. Aquatic animal carotenoids. Fisheries Science 67:771–783.

Miki, W. 1991. Biological functions and activities of animal carotenoids. Pure and Applied Chemistry 63:141–146.

Naguib, Y. M. A. 2000. Antioxidant Activities of Astaxanthin and Related Carotenoids. Journal of

Agricultural and Food Chemistry 48:1150–1154.

Nakano, T., and G. Wiegertjes. 2020. Properties of Carotenoids in Fish Fitness: A Review. Marine Drugs 18:568.

Nielsen, T. G., S. Kjellerup, I. Smolina, G. Hoarau, and P. Lindeque. 2014. Live discrimination of *Calanus glacialis* and *C. finmarchicus* females: can we trust phenological differences? Marine Biology 161:1299–1306.

Orenstein, E. C., S. Ayata, F. Maps, É. C. Becker, F. Benedetti, T. Biard, T. de Garidel-Thoron, J. S. Ellen, F. Ferrario, S. L. C. Giering, T. Guy-Haim, L. Hoebeke, M. H. Iversen, T. Kiørboe, J. Lalonde, A. Lana, M. Laviale, F. Lombard, T. Lorimer, S. Martini, A. Meyer, K. O. Möller, B. Niehoff, M. D. Ohman, C. Pradalier, J. Romagnan, S. Schröder, V. Sonnet, H. M. Sosik, L. S. Stemmann, M. Stock, T. Terbiyik-Kurt, N. Valcárcel-Pérez, L. Vilgrain, G. Wacquet, A. M. Waite, and J. Irisson. 2022. Machine learning techniques to characterize functional traits of plankton from image data. Limnology and Oceanography 67:1647–1669.

Otsu, N. 1979. A Threshold Selection Method from Gray-Level Histograms. IEEE Transactions on Systems, Man, and Cybernetics 9:62–66.

Pedersen, A. M., B. Vang, and R. L. Olsen. 2014. Oil from *Calanus finmarchicus* —Composition and Possible Use: A Review. Journal of Aquatic Food Product Technology 23:633–646.

Powers, M. J., and G. E. Hill. 2021. A Review and Assessment of the Shared-Pathway Hypothesis for the Maintenance of Signal Honesty in Red Ketocarotenoid-Based Coloration. Integrative and Comparative Biology 61:1811–1826.

Rønsholdt, B., and E. McLean. 2001. Determination of Total Carotenoid Content in Rainbow Trout Muscle by Multivariate Calibration of VIS Reflectance Spectra. Journal of Food Composition and Analysis 14:345–357.

Ruifrok, A. C., and D. A. Johnston. 2001. Quantification of histochemical staining by color deconvolution. Analytical and quantitative cytology and histology 23:291–299.

Schmid, M. S., F. Maps, and L. Fortier. 2018. Lipid load triggers migration to diapause in Arctic *Calanus* copepods—insights from underwater imaging. Journal of Plankton Research 40:311–325.

Schneider, T., G. Grosbois, W. F. Vincent, and M. Rautio. 2016. Carotenoid accumulation in copepods is related to lipid metabolism and reproduction rather than to UV-protection: Copepod carotenoids and lipids. Limnology and Oceanography 61:1201–1213.

Schultz, M., T. G. Nielsen, and E. F. Møller. 2020. The importance of temperature and lipid accumulation for initiation and duration of Calanus hyperboreus spawning. Journal of Plankton Research 42:159–171.

Stoń-Egiert, J., and A. Kosakowska. 2005. RP-HPLC determination of phytoplankton pigments—comparison of calibration results for two columns. Marine Biology 147:251–260.

Svensson, P. A., E. Forsgren, T. Amundsen, and H. N. Sköld. 2005. Chromatic interaction between egg pigmentation and skin chromatophores in the nuptial coloration of female two-spotted gobies. Journal of Experimental Biology 208:4391–4397.

Tarling, G. A., A. Belcher, M. Blackwell, C. Castellani, K. B. Cook, F. R. Cottier, V. Dewar-Fowler, J. J. Freer, L. Gerrish, M. L. Johnson, K. S. Last, P. K. Lindeque, D. J. Mayor, H. E. Parry, G. Stowasser, and M. Wootton. 2022. Carbon and Lipid Contents of the Copepod Calanus finmarchicus Entering Diapause in the Fram Strait and Their Contribution to the Boreal and Arctic Lipid Pump. Frontiers in Marine Science 9:926462.

Trudnowska, E., K. Balazy, J. Stoń-Egiert, I. Smolina, T. Brown, and M. Gluchowska. 2020. In a comfort zone and beyond—Ecological plasticity of key marine mediators. Ecology and Evolution:ece3.6997.

Vilgrain, L., F. Maps, M. Picheral, M. Babin, C. Aubry, J. Irisson, and S. Ayata. 2021. Trait-based approach using in situ copepod images reveals contrasting ecological patterns across an Arctic ice melt zone. Limnology and Oceanography:lno.11672.

Violle, C., M.-L. Navas, D. Vile, E. Kazakou, C. Fortunel, I. Hummel, and E. Garnier. 2007. Let the concept of trait be functional! Oikos 116:882–892.

Vogedes, D., Ø. Varpe, J. E. Søreide, M. Graeve, J. Berge, and S. Falk-Petersen. 2010. Lipid sac area as a proxy for individual lipid content of arctic calanoid copepods. Journal of Plankton Research 32:1471–1477.

Conclusion

Les chapitres de cette thèse ont démontré que l'étude de la morphologie d'organismes à partir d'images individuelles apporte un nouveau point de vue sur l'écologie des communautés de copépodes planctoniques des hautes latitudes. En réponse aux problématiques définies dans l'introduction, je discuterai du lien entre les dynamiques environnementales de ces écosystèmes et les traits morphologiques des copépodes, ainsi que des relations entre la variation de ces traits et le fonctionnement des réseaux trophiques. En réponse à la question méthodologique principale, je discuterai des avantages de l'analyse d'un grand nombre d'images pour obtenir des tendances sur les traits d'une communauté d'espèces, sans perdre la variabilité interindividuelle. Enfin, je soulignerai les perspectives que ces approches morphologiques ont apportées pour d'autres études, et je terminerai en ouvrant une réflexion sur l'optimisation de la collecte et de l'analyse des grands jeux de données planctoniques dans un contexte de changement climatique.

Dynamiques environnementales et traits morphologiques des copépodes de hautes latitudes, avec une emphase sur la pigmentation caroténoïde

Comme défini dans l'introduction de ce manuscrit, cette thèse a tout d'abord abordé les variations des traits morphologiques des copépodes du genre *Calanus* selon les conditions environnementales des régions arctiques et subarctiques (fortes saisonnalités, dynamiques de glace, etc). Le Chapitre 1 a permis d'étudier le cas concret de la variation de traits morphologiques dérivés d'images *in situ* en fonction des dynamiques printanières de la banquise et de l'efflorescence des microalgues. La projection dans un espace statistique dataset de plus de 28 000 images de copépodes prises par l'Underwater Vision Profiler (UVP) a permis d'observer les informations morphologiques qui expliquaient le plus de variations entre les individus. A partir des axes de cet espace statistique, des traits morphologiques synthétiques ont été définis : taille, variations d'opacité (révélant la présence des structures colorées) et posture des individus (révélant probablement un taux d'activité). En associant ces traits à des caractéristiques environnementales, nous avons pu montrer qu'ils étaient significativement reliés aux dynamiques de la glace et aux conditions environnementales associées. Des communautés d'individus plus grands (les analyses par filet ont confirmé que les populations étaient plus âgées) vivaient dans les eaux où la banquise était encore formée. Des individus très opaques ont été observés dans les zones marginales nouvellement stratifiées par la fonte récente de la glace, lorsque l'efflorescence algale se trouve proche de la surface. Enfin, les zones d'eau libre où le maximum de chlorophylle est plus profond (l'évolution du bloom l'efflorescence étant plus

avancée) étaient marquées par la naissance de jeunes individus, plus petits, et possédant une activité alimentaire plus importante qu'ailleurs.

Une des conclusions principales du premier chapitre était la part importante de l'opacité pour expliquer les variations morphologiques visibles chez les copépodes photographiés par l'UVP (25.9%). Nous avons relié ces variations à la présence de structures colorées des individus (gonades, contenu digestif, pigmentation rouge). Puisque l'UVP utilise une lumière rouge pour produire les images, nous pensons que les différences d'opacité sont majoritairement liées à des différences de couleur rouge, qui apparait très contrastée sur les images en noir et blanc. Les questions de recherche sur cette pigmentation ont été approfondies dans les deux chapitres suivants. La pigmentation rouge des copépodes est liée à l'astaxanthine, un pigment caroténoïde largement dominant chez les crustacés, et synthétisé à partir d'autres caroténoïdes présentes dans les microalgues. Le Chapitre 2 a permis d'étudier en détail les conditions environnementales qui influencent l'accumulation de l'astaxanthine pour différents écosystèmes aquatiques à l'échelle globale. Cette revue de la littérature nous donne des pistes pour comprendre les variations de la concentration de pigments des *Calanus* arctiques et subarctiques. L'hypothèse du rôle photoprotecteur des pigments est la plus défendue et testée sur le terrain, et en laboratoire. A titre d'exemple, les copépodes connus les plus colorés de la planète sont soumis à de grandes quantités de radiations lumineuses puisqu'ils vivent dans des lacs d'altitude peu profonds ou dans des bassins de littoraux rocheux (Hansson 2000, Davenport et al. 2004, Hylander et al. 2009, Sommaruga 2010, Cui et al. 2021). Cependant, il existe des exemples contradictoires : des individus vivants dans l'obscurité totale pendant l'hiver sous un couvert de glace, dans certaines eaux turbides, ou en profondeur, peuvent aussi avoir une coloration rouge importante (Johnsen 2005, Schneider et al. 2016, Grosbois & Rautio 2018, Trudnowska et al. 2020). Plus généralement, le Chapitre 2 a montré que les conditions environnementales principales associées au trait de pigmentation sont les fortes intensités lumineuses et/ou les faibles températures. Il a été suggéré que les espèces dépendant de réserves lipidiques à long terme pour survivre dans les écosystèmes froids pourraient accumuler des esters d'astaxanthine associés aux acides gras afin de les protéger à long terme contre l'oxydation (Foss et al. 1987, Juhl et al. 1996, Sommer et al. 2006, Schneider et al. 2016). Pour plusieurs espèces, un transfert des pigments des réserves lipidiques vers les œufs a été observé (Holeton et al. 2009, Schneider et al. 2017, Weaver et al. 2018).

Il est intéressant de mettre ces hypothèses en relation avec l'écologie des copépodes des écosystèmes arctiques et subarctiques. Dans le Chapitre 1, nous avons conclu que l'augmentation de l'opacité des copépodes sur les images UVP en association à des conditions de lisière de glace (forte stratification, maximum de chlorophylle en sub-surface peu profond, forte densité de diatomées)

pourrait être liée à un rôle photoprotecteur. L'accumulation de pigments d'astaxanthine pourraient être stimulée lorsque les individus sont soumis au rayonnement lumineux (Tedetti & Sempéré 2006) et qu'ils se nourrissent de l'efflorescence printanière d'algues sympagiques (qui se développent dans la couche inférieure de la glace de mer) et planctoniques dans les zones stratifiées de surface. Hylander et al. (2015) avaient effectivement démontré une augmentation des concentrations d'astaxanthine chez les *Calanus* entre mars et mai en Arctique (Disko Bay, Groenland), mais sans synchronisation significative avec la fonte de la banquise et l'efflorescence phytoplanctonique. D'autres études sont nécessaires pour délier les effets du stress lumineux et de l'alimentation sur l'accumulation de pigments caroténoïdes au cours du printemps. Un autre point important est la grande plasticité de la pigmentation chez les *Calanus*, comme pour d'autres espèces : « les individus peuvent passer du rouge au pâle en l'espace d'une heure (par exemple, lorsqu'ils se trouvent dans un seau au réfrigérateur sans lumière) mais ils peuvent devenir rouges presque immédiatement lorsqu'ils sont exposés à une source de lumière » (Trudnowska et al. 2020). Cette plasticité implique un contrôle finement ajusté du métabolisme de l'astaxanthine (Powers & Hill 2021 ; Chapitre 2), qui nécessite d'être démontré à l'échelle moléculaire.

Les trois espèces de copépodes *Calanus* arctiques vivent dans des écosystèmes froids et possèdent un long cycle de vie (de 1 à 4 ans), pendant lequel ils accumulent de grandes réserves lipidiques au printemps et passent la saison hivernale en profondeur (diapause) (Record et al. 2018). Comme démontré chez leurs congénères des lacs subpolaires vivant au rythme du couvert de glace (Schneider et al. 2016, Grosbois et al. 2018), peut-être qu'un lien existe entre le métabolisme lipidique, la pigmentation astaxanthine et le succès évolutif/écologique des *Calanus*. Un suivi très complet des teneurs en astaxanthine réalisé sur une série temporelle de 18 mois a démontré le lien entre le métabolisme des lipides et la reproduction chez des copépodes *Leptodiaptomus* d'un lac du Québec (Schneider et al. 2016). Les molécules d'astaxanthine étaient majoritairement sous forme estérifiées avec les acides gras (62 à 93 %) et présentaient une accumulation nette à la fin de l'automne avec un maximum au milieu de l'hiver. Les deux périodes de perte nette de la pigmentation coïncidaient avec les pics de production d'œufs au printemps et en été, conduisant à une teneur minimale en astaxanthine en automne (Figure 13). L'hypothèse d'une relation entre pigmentation caroténoïde utilisée, métabolisme lipidique et transfert des pigments aux œufs est très plausible pour les *Calanus* polaires et subpolaires. Pour l'instant, seulement quelques études ont essayé de tester le lien entre le contenu lipidique et la pigmentation n'ont pas montré de résultats significatifs (Trudnowska et al. 2020). Une série temporelle saisonnière permettrait de démontrer un tel lien chez les *Calanus* : des études à faibles résolutions temporelles ne sont pas suffisante puisque le taux de

changements de la pigmentation serait plus probablement corrélé au contenu lipidique que le contenu lipidique lui-même (comme présenté par Schneider et al., 2016).

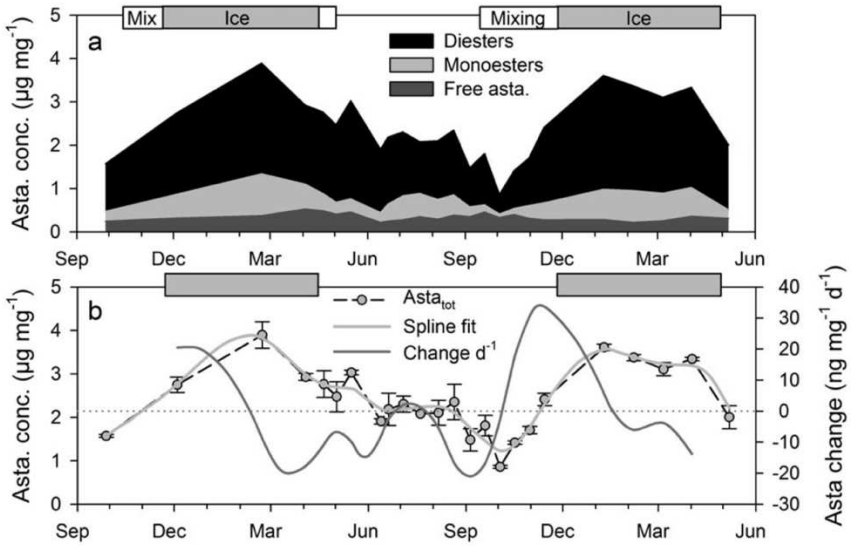

Figure 13. Variations saisonnières de la concentration en caroténoïdes de copépodes lacustres *Leptodiaptomus minutus* (Québec, Canada). (a) Fractions d'astaxanthine. (b) Astaxanthine totale (6 SE), ajustement spline et taux de variation. Les périodes de couverture glaciaire et de mélange de la colonne d'eau sont indiquées par des barres grises et blanches, respectivement. Figure et légende issues de Schneider et al. (2016).

Les chapitres 1 et 2 ont donc permis de mettre en relation certains traits morphologiques et les conditions environnementales de glace, de stratification et de température, et de préciser les hypothèses relatives aux variations de pigmentation rouge des copépodes. Selon ces résultats, l'hypothèse la plus probable concerne l'utilisation de la pigmentation caroténoïde comme protection des réserves lipidiques, en lien avec la forte saisonnalité des écosystèmes boréaux et arctiques. En associant des approches de transcriptomique et de protéomique et une analyse du trait de pigmentation basée sur la méthodologie développée dans le chapitre 3, il serait ainsi possible de tester les ajustements de pigmentation réalisés en réponse à différents stress environnementaux (lumière, température, etc.). Cette approche combinée permettrait en particulier d'identifier les voies métaboliques impliquées dans ces ajustements et de mieux comprendre les mécanismes de régulation sous-jacents.

De l'image individuelle au fonctionnement des réseaux trophiques arctiques et subarctiques

Dans les deux premiers chapitres j'ai cherché à comprendre comment la distribution des traits des copépodes pouvait être utilisée pour étudier le fonctionnement des écosystèmes. Une des motivations principales de l'utilisation de l'approche par trait est de pouvoir révéler le fonctionnement de l'écosystème à travers la distribution spatio-temporelle des caractéristiques morphologiques et physiologiques individuelles, sans passer par l'intermédiaire de l'estimation du rôle supposé de chaque taxon (Mcgill et al. 2006, Kiørboe et al. 2018). Certains traits des copépodes, comme la taille ou le contenu lipidique, ont été utilisés pour aborder l'export de carbone (Stamieszkin et al. 2015, Brun et al. 2019) ou l'énergie disponible pour les réseaux trophiques (Renaud et al. 2018). Ces fonctionnalités peuvent participer à la compréhension des services écosystémiques de régulation et d'approvisionnement (Fig. 4 dans l'introduction). Néanmoins, l'utilisation de cette approche en écologie planctonique reste récente et exploratoire (Litchman et al. 2013, Martini et al. 2021), en particulier pour les traits étudiés dans le cadre de cette thèse.

Parmi l'ensemble des copépodes pélagiques, les espèces du genre *Calanus* possèdent une place clé dans les réseaux trophiques arctiques et subarctiques. Comme présenté sur la Figure 14, à droite, ce sont les premiers consommateurs du phytoplancton et d'algues de glace, et ils sont prédatés de façon préférentielle par les poissons pélagiques (morue arctique, capelan), les oiseaux de mer, et certaines espèces de baleines (comme la baleine boréale en arctique, ou la baleine franche de l'Atlantique Nord dans les zones subarctiques) (Mayo & Marx 1990, Darnis & Fortier 2014, Pedro et al. 2023). En partant de ce constat, nous discutons ici en détail de deux traits nouvellement abordés par cette thèse et importants pour le fonctionnement des réseaux trophiques : l'activité alimentaire et la pigmentation caroténoïde.

Activité alimentaire

L'activité alimentaire a été quantifiée par la moyenne des coordonnées sur l'axe 4 de l'espace morphologique pour tous les copépodes imagés dans une couche de surface (PC4, Fig. 1.3). A l'échelle de la communauté de copépodes, une valeur élevée signifie qu'un plus grand nombre d'individus ont été imagés par l'UVP dans une position dite "active". Cette position est supposée active car les individus possèdent un périmètre complexe, avec les antennes et péréiopodes déployées, ce qui serait typique de la position des copépodes créant un courant d'eau pour intercepter les particules alimentaires (filter-feeders, Kiørboe 2011), en opposition à la position de diapause dans

laquelle tous les appendices sont repliés le long de leur corps (Lenz & Roncalli 2019). Cet indice repose sur plusieurs hypothèses qui peuvent être remises en question (voir paragraphe suivant). Néanmoins, je l'ai utilisé dans une étude complémentaire réalisée en collaboration avec des collègues de l'Université Laval et d'Aix-Marseille Université, dans le but de savoir si le broutage des copépodes herbivores a pu influencer la préservation du matériel algal sympagique libéré dans la colonne d'eau (Rontani et al. 2022). La valeur moyenne de l'activité alimentaire (PC4) a été utilisée en association à la concentration totale de copépodes à chaque station, pour donner une idée de la pression de broutage.

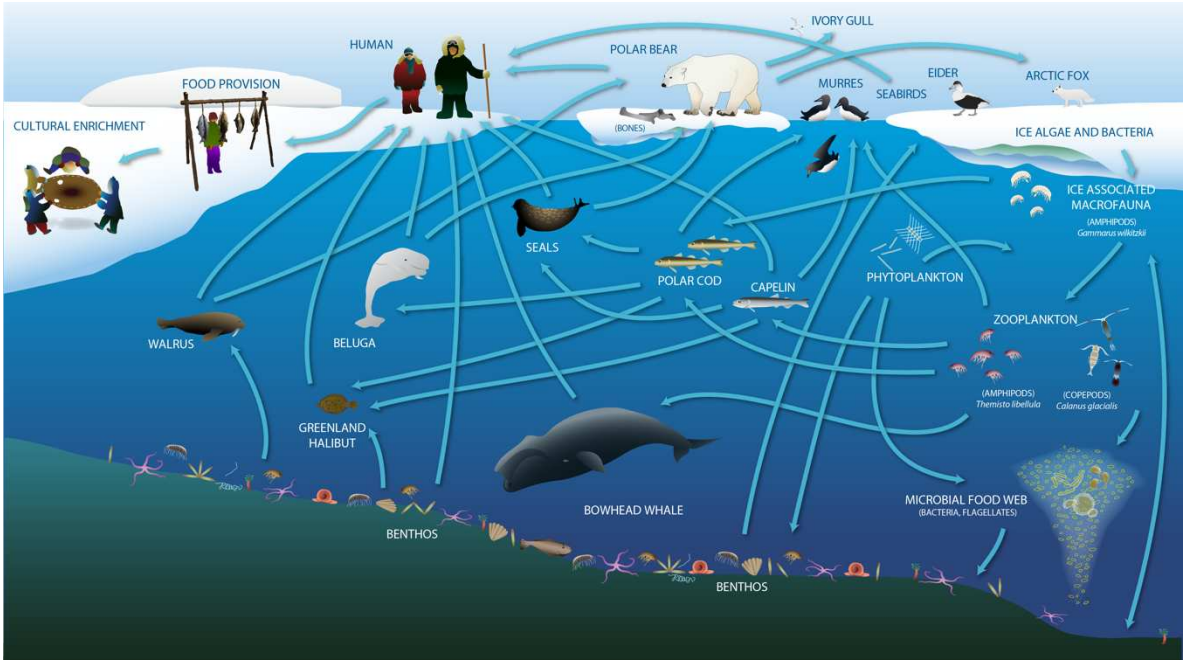

Figure 14. Le réseau trophique de l'arctique canadien, avec une transition des écosystèmes côtiers à océaniques (de gauche à droite). © Conservation of Arctic Flora and Fauna (CAFF) - Tom Barry, adapté de Darnis et al. (2012) et de l'Inuit Circumpolar Council-Alaska (2015).

L'analyse de ces données ont montré que les copépodes n'étaient pas particulièrement plus abondants ou plus actifs aux stations où le matériel algal était le plus dégradé (stations 405, 609, 707 sur la Fig. D1), et donc que d'autres mécanismes de dégradation étaient impliqués (Rontani et al. 2022). Cet exemple n'est pas concluant à lui seul quant à la qualité de l'indice d'activité alimentaire, mais nous donne une idée de la façon dont ce trait morphologique pourrait être utilisé pour comprendre une composante clé des écosystèmes pélagiques : la pression de broutage sur la production primaire.

Pigmentation caroténoide

La majeure partie de ce doctorat s'est intéressée à la pigmentation caroténoïde des copépodes. Ce trait reste peu étudié dans son contexte écologique chez les *Calanus*, malgré les implications possibles pour les niveaux trophiques supérieurs, incluant les humains. La pigmentation induite par les molécules d'astaxanthine a une influence directe sur le succès écologique des copépodes (survie, reproduction, croissance) (Chapitre 2) et peut donc, dans une certaine mesure, influencer la capacité de ces populations à maintenir les très fortes biomasses dont dépendent une grande partie du réseau trophiques (Pedro et al. 2023 : Fig. 15, sur cette figure l'aire des nœuds représente la biomasse). Sur cette figure, nous pouvons observer que les *Calanus* sont les proies préférentielles des crustacés planctoniques carnivores (amphipodes, krill) et de la morue arctique. Ces deux nœuds sont ensuite utilisés par l'omble chevalier, le flétan, les phoques, les baleines et narvals, importants pour la subsistance et les traditions des populations humaines. La bonne santé (et la forte biomasse) des populations de copépodes *Calanus* est donc déterminante pour une large partie des réseaux trophiques arctiques et subarctiques.

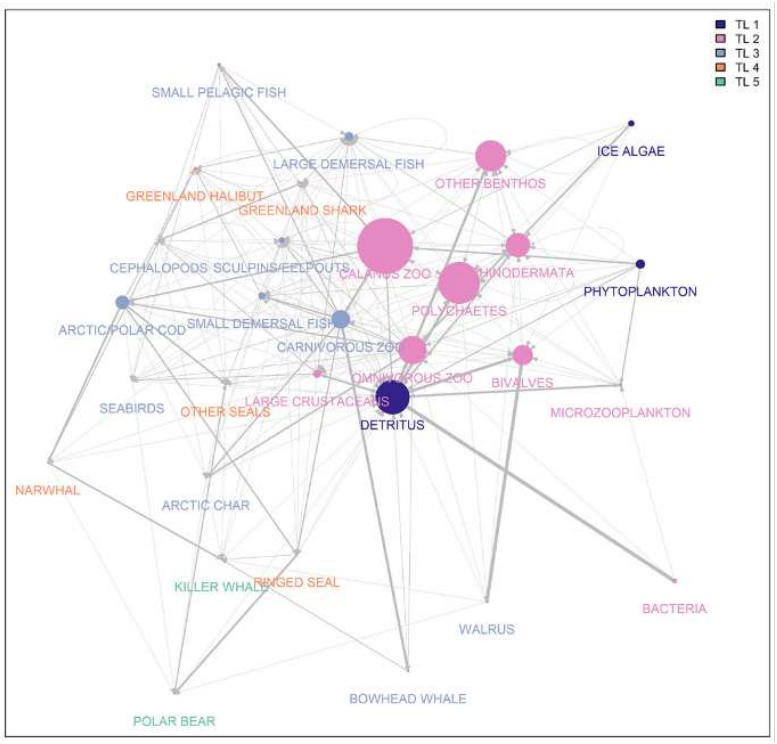

Figure 15. Représentation des interactions dans les réseaux trophiques du plateau occidental de la baie de Baffin. L'aire des nœuds représente la biomasse relative, tandis que les différentes couleurs indiquent le niveau trophique. L'épaisseur des liens représente la contribution en pourcentage au régime alimentaire des prédateurs, indiquée par les flèches. Figure de Pedro et al. (2023).

Les *Calanus* sont le maillon des réseaux trophiques qui transforme les pigments caroténoïdes des algues (β-carotène, lutéine et zéaxanthine) en astaxanthine via des réactions d'oxydoréduction (Weaver et al. 2018). Ainsi, au-delà des bénéfices apportés pour le propre succès écologique et évolutif de ces copépodes, les molécules d'astaxanthine et leurs propriétés antioxydants vont être transférées aux niveaux trophiques supérieurs. Par exemple, l'omble chevalier est un poisson faisant partie de la nourriture traditionnelle (parfois quotidienne) des populations vivant sur les côtes de la baie de Baffin et de la baie d'Hudson (Rapinski et al. 2018, Sansoulet et al. 2020). Ces poissons se nourrissent de copépodes et surtout d'amphipodes, d'euphausiacées et de *Mysis*, prédateurs des *Calanus* (Ulrich & Tallman 2021) et tous très pigmentés. Les ombles chevaliers sont choisis par les populations humaines notamment selon la couleur de leur chair, aussi causée par l'astaxanthine (Hatlen et al. 1998, Bjerkeng et al. 2000). Comme chez les autres espèces de Salmonidés, la couleur rouge est considérée comme un marqueur visuel de la qualité alimentaire du poisson (Bolduc 2021). Par ailleurs, il est démontré que les grandes propriétés antioxydants de l'astaxanthine (10 fois plus que les autres caroténoïdes, Miki 1991) est utile pour prévenir les maladies de ces poissons (Nakano & Wiegertjes 2020), notamment en aquaculture (Hynes et al. 2009). Relier la pigmentation de ces poissons à celle des *Calanus* et au potentiel succès écologique de leurs populations respectives est une piste de recherche.

Au-delà des propriétés antioxydants, les pigments rouges peuvent influencer les relations avec les autres espèces de l'écosystème dans le cas où la couleur est perçue par des systèmes visuels. Une grande majorité des organismes planctoniques vivant en profondeur sont de couleur rouge, contrairement aux organismes vivant en surface, majoritairement bleus (Johnsen 2014). La raison écologique proposée pour expliquer cette pigmentation est une stratégie de camouflage : comme les molécules d'eau absorbent très rapidement des longueurs d'ondes élevées, les individus rouges apparaissent cryptiques (noirs) aux prédateurs visuels, et particulièrement à ceux utilisant la bioluminescence pour révéler leurs proies (Johnsen 2005). Cette hypothèse est tout à fait valable pour les copépodes *Calanus* qui résident en profondeur une grande partie de l'année et dont les prédateurs (voir paragraphe précédent) possèdent des systèmes visuels. Peut-être que cette hypothèse pourrait expliquer pourquoi leur pigmentation est souvent spécifique à certaines structures corporelles non transparentes, qui doivent être cachées pendant la plus grande partie de leurs cycles de vie (extrémité du sac lipidique / tube digestif et segment génital), surtout si elles sont très mobiles (antennes). Le lien entre la migration verticale (journalière ou ontogénique), la présence de prédateurs et les stratégies de camouflage pourrait être testée en quantifiant automatiquement la rougeur sur des images prises après échantillonnage par filets stratifiés.

Analyser un grand nombre d'images : un cas idéal pour passer de l'échelle individuelle à celle de la communauté

La dernière question soulevée dans l'introduction était : "Comment identifier automatiquement et objectivement des traits fonctionnels sur des images de copépode" ? Dans les Chapitres 1 et 3 nous avons proposé des méthodes pour quantifier des traits fonctionnels qui ont une signature morphologique, en s'appuyant sur les qualités de deux types d'images : l'acquisition automatique d'images de copépodes *in situ* avec l'UVP et la haute résolution des images en couleur prises lors d'observations au stéréo-microscope (la description détaillée des deux types d'images est dans la Table 1 de l'introduction).

Dans les deux cas, les travaux d'analyse reposent sur un premier avantage méthodologique : un grand nombre d'images permet de révéler des tendances statistiques, même avec des signaux faibles, et d'accéder à des échelles spatiales inédites, qu'elles soient petites ou grandes. Par exemple, dans le cas du Chapitre 1, des gradients continus de traits ont été révélés sur une grande partie de la Baie de Baffin à partir de plusieurs milliers d'images. Cette résolution est rendue possible par l'automatisation de l'acquisition et du traitement des images. D'ailleurs, l'échantillonnage par filet a été réalisé avec une moins bonne couverture spatiale pendant la campagne GreenEdge simplement en raison des contraintes logistiques d'échantillonnage inhérentes à cette approche historique. Le second avantage, qui renforce l'intérêt de l'imagerie pour les changements d'échelles, est la possibilité de retourner a posteriori aux images individuelles pour comprendre plus précisément les grandes tendances observées. Par exemple, à partir de la distribution des traits au sein de la baie (Fig. 1.4), nous avons pu sélectionner des images des morphologies extrêmes (en prenant les 10% des images avec les plus hautes valeurs sur les axes de l'espace morphologique) pour observer plus finement les traits.

Le Chapitre 3 propose l'analyse de jeux de données qui seront nécessairement moins grands (pas d'automatisation dans l'acquisition des images), mais l'indice de couleur rouge a été développé dans la même optique : pouvoir analyser beaucoup d'images et retourner à la variabilité individuelle si nécessaire. Pour l'instant, 699 images ont été utilisées pour développer cet indice de rougeur et le valider avec des concentrations pigmentaires obtenues par dosage HPLC. Au cours de cette analyse, des points "extrêmes" ont pu être identifiés et permettent de vérifier si certaines caractéristiques de l'image ne viennent pas fausser l'analyse, et donc de valider la méthode. Les outils d'analyse d'images développés dans les Chapitre 1 et 3 offrent des avantages pour l'interprétation des mécanismes écologiques de l'échelle individuelle à celle de la communauté, ce qui est beaucoup plus difficile avec

les méthodes conventionnelles destructives ou invasives (taxonomie à partir d'échantillons fixés, HPLC ou séquençage).

L'approche par trait à partir d'images sera toujours contrainte par les limitations intrinsèques à l'imagerie et notamment la résolution assez faible des appareils actuels tels que l'UVP ou le fait que l'animal soit projeté en deux dimensions, entraînant des pertes d'information. Néanmoins, ces deux chapitres ont permis de démontrer qu'il était possible, malgré ces limites, d'exploiter le maximum d'informations contenues dans ces images, qui selon Giering et al. (2022), vont continuer à être utilisées de manière complémentaire en écologie planctonique.

Développement de méthodologies pour l'analyse d'images : de nouvelles pistes

Le développement de ces techniques d'analyse d'image offre de nouvelles perspectives. Tout d'abord, nous pouvons discuter des pistes ouvertes par la création de l'espace morphologique. Au-delà de la définition de traits par les coordonnées des axes d'une analyse statistique multivariée, il est possible d'utiliser cet espace afin de caractériser une diversité fonctionnelle morphologique. Des regroupements (clusters) peuvent être produits sur les coordonnées des axes, pour définir des morphotypes et calculer la richesse et la régularité de la diversité morphologique à partir de ces groupes, en s'inspirant d'indices de diversité fonctionnelle (Villéger et al. 2008). L'influence des variations environnementales sur cette diversité morphologique peut être intéressante à étudier. Par exemple, une comparaison pourrait être effectuée entre la diversité morphologique saisonnière à partir des images UVP prises lors de la campagne DarkEdge en 2021 au moment de la formation hivernale de la banquise, et celles issue de la communauté printanière de la mission GreenEdge en 2016. Dans un contexte de changement global, l'analyse de la diversité fonctionnelle et/ou morphologique du plancton montre une augmentation de la richesse en morphotypes avec celle de l'oligotrophie en Méditerranée (Beck et al. *soumis*). La structure de l'espace morphologique a également été mis en relation directe l'export de carbone (Perhirin et al. *soumis*, Trudnowska et al. 2021).

Il est important de noter que l'espace morphologique est formé par une analyse en composantes principales, dont le but premier est de synthétiser et représenter les variations de nombreuses variables. Généralement, ce type d'analyse statistique multivariée est utilisé comme une analyse exploratoire et je pense que c'est dans cette optique que l'espace morphologique doit être utilisé. L'interprétation des axes comme des axes morphologiques est informative mais ne peut pas

suffire à définir un trait morphologique précisément. C'est en utilisant cette approche exploratoire que nous avons observé l'importance des variations d'opacité, mais nous avons ensuite développé une méthode pour quantifier précisément ce trait. Il serait pertinent d'adopter la même approche pour l'activité alimentaire et de développer un indice plus précis que la complexité du contour des individus. Orenstein et al. (2022) ont proposé que la posture des copépodes pourrait être déterminée par des algorithmes d'apprentissage machine par la pose de points clés sur certaines zones des individus ("keypoint pose"). Un tel indice pourrait permettre de répondre avec davantage de confiance à la question de l'intensité de la pression de broutage dans les écosystèmes pélagiques, discutée ci-dessus. Par ailleurs, dans une étude complémentaire à mon doctorat, j'ai également participé au déploiement d'un UVP6 dans le lac Champlain (Université du Vermont, États-Unis, collaboration avec Jason Stockwell) dans le but d'obtenir pour la première fois des images *in situ* de *Mysis* de milieux d'eau douce. L'analyse plus précise de la morphologie des *Mysis*, facilitée par leur grande taille, permettra de mieux évaluer leur activité.

Récemment, l'espace morphologique a également été utilisé pour des photos de plancton en couleur prises par le PlanktoScope (Pollina et al. 2022), un imageur à bas coût du microplancton. Les variations de couleur sur les images étaient représentées sur le second axe de l'espace morphologique, surpassant l'importance des variations d'opacité (Mériguet et al. 2022). L'acquisition automatique d'images couleur du plancton pourrait offrir de nouvelles opportunités pour combiner les méthodes développées dans les Chapitres 1 et 3.

Enfin, pour produire des études en écologie fonctionnelle plus informatives, différents outils pourraient être combinés afin de quantifier des traits fonctionnels en synergie. Par exemple, avec des données d'imagerie, l'indice de rougeur pour les copépodes *Calanus* pourrait être analysé dans le même temps que d'autres traits dérivés d'images, tels que la taille, le contenu en lipides (Vogedes et al. 2010), la maturation des gonades (Hirche & Niehoff 1996) ou le contenu digestif. D'ailleurs, puisque la méthode de déconvolution se base sur des valeurs RGB issues d'un spectre d'absorbance, on pourrait inclure les valeurs associées à la chlorophylle a pour identifier les pixels verts du tube digestif. La pigmentation rouge pourrait être corrélée avec des traits connus au niveau de l'espèce ou de la communauté, tels que les taux de production d'œufs, la durée de vie ou la motilité (Martini et al. 2021), ou utilisée en combinaison avec d'autres outils comme des données acoustiques. La combinaison des résulats de l'accoustique et de l'imagerie permettrait de mieux associer les échelles de l'individu à la communauté et fera l'objet de mes études en post-doctorat à l'Université Memorial de Terre-Neuve et Labrador (Canada) avec Maxime Geoffroy. Il sera intéressant, par exemple, de relier certains traits fonctionnels issus des images avec les dynamiques migration nycthémérale et

ontogénique du zooplancton, et les effets associés de la lumière et de la prédation par les poissons mésopélagiques.

Optimisation et sobriété dans la collecte et l'analyse de grands jeux de données

Les missions océanographiques permettant la collecte de données scientifiques, dont font partie les images du plancton, sont particulièrement exigeantes en ressources énergétiques et logistiques (notamment en Arctique). L'ensemble des données obtenues pendant ces missions permet d'obtenir des informations écologiques importantes pour comprendre le fonctionnement des écosystèmes, et prévoir leur évolution dans un contexte de changements climatiques. De plus, l'expérience de terrain permet de mieux réaliser les conditions des écosystèmes, et donc de mieux communiquer ces sujets par la transmission d'expérience. Néanmoins, les conclusions scientifiques reposent déjà avec une confiance très haute sur de nombreuses études, et sont sans appel quant à la nécessité d'une baisse radicale des émissions de gaz à effet de serre d'ici 2050 (Intergovernmental Panel on Climate Change, IPCC, 2022). Aujourd'hui, nous devons nous questionner sur la valeur finale de ces informations, en comparaison aux moyens déployés pour les obtenir, et à leur bilan carbone. Binley et al. (2023) insistent le fait que la surveillance des écosystèmes peut aussi retarder des actions concrètes et absorber des ressources précieuses et limitées. Ils montrent que dans de nombreux cas, les données nécessaires pour répondre à des questions urgentes existent déjà, et doivent simplement être rendues plus accessibles. Selon eux, le fait de chercher à utiliser le plus de données historiques n'aidera pas seulement à minimiser la perte de données, mais aboutira à des résultats plus précis et à de meilleures décisions de conservation (Binley et al. 2023).

Afin d'éviter une dynamique d'acquisition toujours plus grande et énergivore de données, il apparaît donc nécessaire 1) d'extraire un maximum d'informations lorsqu'un jeu de données est créé, 2) d'exploiter les données historiques avant d'en reprendre de nouvelles, et 3) de développer des moyens efficaces de mise en commun et d'accès ouvert des données. Les types de données et d'analyses exploitées dans cette thèse essaient de répondre à ces trois points. Premièrement, nous avons proposé d'exploiter le maximum de chaque image (UVP et stéréo-microscope), en dépassant la classification taxonomique, afin d'obtenir des informations complémentaires sur les traits fonctionnels morphologiques des organismes. Comme des dizaines de millions d'images de l'UVP sont actuellement disponibles (Irisson et al. 2022), cette méthode peut permettre l'analyse de données

existantes, à grande échelle. Deuxièmement, l'indice de rougeur développé au chapitre 3 est fait pour pouvoir être appliqué à n'importe quel jeu de données, notamment grâce à l'étape de calibration permettant la comparaison d'images prises par des appareils différents et dans des conditions variées. Ces articles et les codes qui y sont associés ont été publiés de façon ouverte. Enfin, si le stockage, la classification et le partage des images UVP peuvent se faire très facilement à travers la plateforme web Ecotaxa, il reste beaucoup d'efforts à faire pour mettre en commun les jeux de données d'images de plancton prises par d'autres systèmes d'imagerie (comme les images couleurs du Chapitre 3).

Plus généralement, dans le contexte d'une diminution nécessaire des impacts anthropiques sur les systèmes naturels, les scientifiques doivent, plus que n'importe qui, réfléchir collectivement aux enjeux énergétiques associés à la collecte et à l'analyse des données. Nous pouvons notamment nous demander si nos objectifs, même s'ils sont légitimes d'un point de vue scientifique, méritent d'être résolus avec l'impact environnemental qui leur est associé. Comme proposé dans le guide de Holste et al. (2022) intitulé « Reducing CO2 Emissions in Arctic Science", nous pouvons également questionner la fréquence, la durée et le types de transports déployés pour répondre à ces objectifs.

Résumé et perspectives

En résumé, les conclusions principales de mon travail de thèse sont :

1. Les traits morphologiques des copépodes arctiques peuvent être explorés et synthétisés en projetant les images prises *in situ* par l'Underwater Vision Profiler dans un espace morphologique.
2. Dans cet espace, les axes sont stables et définissent des variations de taille, d'opacité (reflétant les variations de structures pigmentées), et de complexité du contour (indiquant probablement un taux d'activité). Les variations de ces traits sont étroitement liées aux dynamiques de la banquise dans la Baie de Baffin au printemps.
3. Les variations d'opacité montraient des dynamiques surprenantes : l'opacité des copépodes était maximale à la lisière de glace, dans des zones fortement stratifiées par la fonte récente de la banquise, et où le maximum de chlorophylle était peu profond.
4. Une revue de la littérature a permis de démontrer les conditions écologiques les plus propices au trait de pigmentation caroténoïdes chez les copépodes : de fortes intensités lumineuses, une faible profondeur des milieux aquatiques, de faibles températures associées à des besoin de stockage de l'énergie sous forme de lipides et une faible pression de prédation visuelle (dans des eaux claires).
5. La pigmentation rouge des copépodes, induite par les molécules d'astaxanthine qui possédent de grandes propriétés antioxydantes, offre un meilleur succès écologique des individus (croissance, survie, reproduction = *fitness*). Comme la pigmentation apparaît avantageuse au sein d'une grande variété d'écosystèmes et qu'elle est ajustable rapidement selon les conditions écologiques, elle peut être considérée comme un de "couteau-suisse" de protection métabolique.
6. Un indice de rougeur a pu être quantifié automatiquement par la déconvolution de la couleur sur des images individuelles de copépodes *Calanus* observés au stéréomicroscope. Cet indice est *(i)* rapide et efficace à calculer, *(ii)* indépendant des conditions de luminosité dans lesquelles la photo a été prise, *(iii)* spécifique à l'astaxanthine (car calculé à partir de son spectre d'absorbance) *(vi)* et quantitatif au niveau du pixel.
7. L'analyse de grands jeux de données d'images en utilisant une approche par traits fonctionnels permet de dégager des tendances à fine résolution, sans perdre l'accès à la variabilité interindividuelle.

Ces conclusions permettent d'envisager les perspectives de recherche suivantes :

1. La structure de l'espace morphologique peut être reliée aux fonctionnalités des écosystèmes, comme leur résilience ou leur capacité à exporter le carbone, notamment en quantifiant la richesse et la régularité de la diversité morphologique.
2. La construction de l'espace morphologique par une analyse en composante principale doit probablement être considérée comme une analyse exploratoire. Chaque trait peut ensuite être quantifié plus précisément par des analyses de vision par ordinateur ou d'apprentissage machine (comme la pigmentation ou l'activité alimentaire, par exemple).
3. L'indice de rougeur des copépodes *Calanus* pourrait être utilisé comme un indice de *fitness* de leurs populations arctiques et subarctique. L'évolution saisonnière de cet indice pourrait être mise en relation avec le succès de leurs prédateurs (notamment, des amphipodes *Themisto* sp., de la morue arctique et de l'omble chevalier).
4. La quantification de plusieurs traits pourrait être réalisée en synergie et avec différents outils. Sur une même image, les traits morphologiques comme la taille, le contenu lipidique et la couleur des *Calanus* peuvent être comparés. En utilisant les données acoustiques, ces traits morphologiques peuvent être reliés à l'intensité des migrations verticales et à la pression de prédation.
5. Il est important d'effectuer toutes les analyses futures en s'assurant de la mise en commun des données et des techniques d'analyses. Dans un contexte de changement climatique, il est nécessaire de valoriser toutes les données récupérées à l'aide d'importantes ressources énergétiques et logistiques, et d'exploiter l'ensemble des données historiques avant d'en reprendre de nouvelles.

Bibliographie

Aarflot, J. M., H. R. Skjoldal, P. Dalpadado, and M. Skern-Mauritzen. 2018. Contribution of Calanus species to the mesozooplankton biomass in the Barents Sea. ICES Journal of Marine Science 75:2342–2354.

Ardyna, M., and K. R. Arrigo. 2020. Phytoplankton dynamics in a changing Arctic Ocean. Nature Climate Change 10:892–903.

Barth-Jensen, C., M. Daase, M. R. Ormańczyk, Ø. Varpe, S. Kwaśniewski, and C. Svensen. 2022. High abundances of small copepods early developmental stages and nauplii strengthen the perception of a non-dormant Arctic winter. Polar Biology 45:675–690.

Basedow, S. L., D. McKee, I. Lefering, A. Gislason, M. Daase, E. Trudnowska, E. S. Egeland, M. Choquet, and S. Falk-Petersen. 2019. Remote sensing of zooplankton swarms. Scientific Reports 9:686.

Beaugrand, G. 2002. Reorganization of North Atlantic Marine Copepod Biodiversity and Climate. Science 296:1692–1694.

Behrenfeld, M. J., K. H. Halsey, E. Boss, L. Karp-Boss, A. J. Milligan, and G. Peers. 2021. Thoughts on the evolution and ecological niche of diatoms. Ecological Monographs 91.

Benedetti, F., J. Wydler, and M. Vogt. 2022. Copepod functional traits and groups show divergent biogeographies in the global ocean. Journal of Biogeography:jbi.14512.

Binley, A. D., B. P. M. Edwards, G. Dansereau, E. C. Knight, and I. Momeni-Dehaghi. 2023. Minimizing Data Waste: Conservation in the Big Data Era. The Bulletin of the Ecological Society of America 104:e02056.

Berge, J., T. M. Gabrielsen, M. Moline, and P. E. Renaud. 2012. Evolution of the Arctic Calanus complex: an Arctic marine avocado? Journal of Plankton Research 34:191–195.

Berge, J., P. E. Renaud, G. Darnis, F. Cottier, K. Last, T. M. Gabrielsen, G. Johnsen, L. Seuthe, J. M. Weslawski, E. Leu, M. Moline, J. Nahrgang, J. E. Søreide, Ø. Varpe, O. J. Lønne, M. Daase, and S. Falk-Petersen. 2015. In the dark: A review of ecosystem processes during the Arctic polar night. Progress in Oceanography 139:258–271.

Biard, T., L. Stemmann, M. Picheral, N. Mayot, P. Vandromme, H. Hauss, G. Gorsky, L. Guidi, R. Kiko, and F. Not. 2016. In situ imaging reveals the biomass of giant protists in the global ocean. Nature 532:504–507.

Bjerkeng, B., B. Hatlen, and M. Jobling. 2000. Astaxanthin and its metabolites idoxanthin and crustaxanthin in flesh, skin, and gonads of sexually immature and maturing Arctic charr (Salvelinus alpinus (L.)). Comparative Biochemistry and Physiology Part B: Biochemistry and Molecular Biology 125:395–404.

Blais, M. 2021. Les conditions océanographiques chimiques et biologiques dans l'estuaire et le golfe du Saint-Laurent en 2020. Secrétariat canadien de consultation scientifique (SCCS), Ottawa (Ontario).

Bolduc, S. 2021. Indicateurs de la qualité de la chair de l'omble chevalier anadrome et ses liens avec les préférences alimentaires des Inuit du Nunavik, Master thesis, Département de Biologie, Université Laval, Québec, Canada.

Bouchard, C., and L. Fortier. 2020. The importance of Calanus glacialis for the feeding success of young polar cod: a circumpolar synthesis. Polar Biology 43:1095–1107.

Bradford-Grieve, J. M. 2002. Colonization of the pelagic realm by calanoid copepods. Hydrobiologia 485:223–244.

Brun, P., K. Stamieszkin, A. W. Visser, P. Licandro, M. R. Payne, and T. Kiørboe. 2019. Climate change has altered zooplankton-fuelled carbon export in the North Atlantic. Nature Ecology & Evolution 3:416–423.

Carstensen, J., A. Olszewska, and S. Kwasniewski. 2019. Summer Mesozooplankton Biomass Distribution in the West Spitsbergen Current (2001–2014). Frontiers in Marine Science 6:202.

Choquet, M., K. Kosobokova, S. Kwaśniewski, M. Hatlebakk, A. K. S. Dhanasiri, W. Melle, M. Daase, C. Svensen, J. E. Søreide, and G. Hoarau. 2018. Can morphology reliably distinguish between the copepods *Calanus finmarchicus* and *C. glacialis*, or is DNA the only way?: Morphological misidentification in Calanus. Limnology and Oceanography: Methods 16:237–252.

Corsini, A., M. Pezzoni, and F. Visentin. 2022. What makes a productive Ph.D. student? Research Policy 51:104561.

Costanza, R., R. d'Arge, R. de Groot, S. Farber, M. Grasso, B. Hannon, K. Limburg, S. Naeem, R. V. O'Neill, J. Paruelo, R. G. Raskin, P. Sutton, and M. van den Belt. 1997. The value of the world's ecosystem services and natural capital. Nature 387:253–260.

Cowen, R. K., and C. M. Guigand. 2008. In situ ichthyoplankton imaging system (*I* SIIS): system design and preliminary results: In situ ichthyoplankton imaging system. Limnology and Oceanography: Methods 6:126–132.

Cui, S., Y. Li, L. Liu, Q. Wang, and F. Chen. 2021. Changes in astaxanthin and fatty acid concentrations during the developmental process in the calanoid *Arctodiaptomus walterianus* in an alpine lake at low latitudes. Journal of Plankton Research 43:314–324.

Daase, M., J. Berge, J. E. Søreide, and S. Falk-Petersen. 2021. Ecology of Arctic Pelagic Communities. Pages 219–259 *in* D. N. Thomas, editor. Arctic Ecology. First edition. Wiley.

Darnis, G., D. G. Barber, and L. Fortier. 2008. Sea ice and the onshore–offshore gradient in pre-winter zooplankton assemblages in southeastern Beaufort Sea. Journal of Marine Systems 74:994–1011.

Darnis, G., and L. Fortier. 2014. Temperature, food and the seasonal vertical migration of key arctic copepods in the thermally stratified Amundsen Gulf (Beaufort Sea, Arctic Ocean). Journal of Plankton Research 36:1092–1108.

Davenport, J., A. Aine Healy, N. Casey, and J. Heffron. 2004. Diet-dependent UVAR and UVBR resistance in the high shore harpacticoid copepod *Tigriopus brevicornis*. Marine Ecology Progress Series 276:299–303.

Dolan, J. R. 2021. Pioneers of plankton research: Victor Hensen (1835–1924). Journal of Plankton Research 43:507–510.

Dolan, J. R. 2023. Beauty of the plankton: from the first issue of Haeckel's *Art Forms of Nature*. Journal of Plankton Research:fbac076.

Ershova, E. A., K. N. Kosobokova, N. S. Banas, I. Ellingsen, B. Niehoff, N. Hildebrandt, and H. Hirche. 2021. Sea ice decline drives biogeographical shifts of key *Calanus* species in the central Arctic Ocean. Global Change Biology 27:2128–2143.

Falk-Petersen, S., P. Mayzaud, G. Kattner, and J. R. Sargent. 2009. Lipids and life strategy of Arctic *Calanus*. Marine Biology Research 5:18–39.

Forest, A., L. Stemmann, M. Picheral, L. Burdorf, D. Robert, L. Fortier, and M. Babin. 2012. Size distribution of particles and zooplankton across the shelf-basin system in southeast Beaufort Sea: combined results from an Underwater Vision Profiler and vertical net tows. Biogeosciences 9:1301–1320.

Fortune, S., S. Ferguson, A. Trites, B. LeBlanc, V. LeMay, J. Hudson, and M. Baumgartner. 2020. Seasonal diving and foraging behaviour of Eastern Canada-West Greenland bowhead whales. Marine Ecology Progress Series 643:197–217.

Foss, P., B. Renstrøm, and S. Liaaen-Jensen. 1987. Natural occurrence of enantiomeric and Meso astaxanthin 7∗-crustaceans including zooplankton. Comparative Biochemistry and Physiology Part B: Comparative Biochemistry 86:313–314.

Freer, J. J., M. Daase, and G. A. Tarling. 2022. Modelling the biogeographic boundary shift of *Calanus finmarchicus* reveals drivers of Arctic Atlantification by subarctic zooplankton. Global Change Biology 28:429–440.

Giering, S. L. C., P. F. Culverhouse, D. G. Johns, A. McQuatters-Gollop, and S. G. Pitois. 2022. Are plankton nets a thing of the past? An assessment of in situ imaging of zooplankton for large-scale ecosystem assessment and policy decision-making. Frontiers in Marine Science

9:986206.

Gorsky, G., M. D. Ohman, M. Picheral, S. Gasparini, L. Stemmann, J.-B. Romagnan, A. Cawood, S. Pesant, C. Garcia-Comas, and F. Prejger. 2010. Digital zooplankton image analysis using the ZooScan integrated system. Journal of Plankton Research 32:285–303.

Greer, A. T., M. S. Schmid, P. I. Duffy, K. L. Robinson, M. A. Genung, J. Y. Luo, T. Panaïotis, C. Briseño-Avena, M. E. Frischer, S. Sponaugle, and R. K. Cowen. 2023. In situ imaging across ecosystems to resolve the fine-scale oceanographic drivers of a globally significant planktonic grazer. Limnology and Oceanography 68:192–207.

Grime, J. P. 1974. Vegetation classification by reference to strategies. Nature 250:26–31.

Grosbois, G., and M. Rautio. 2018. Active and colorful life under lake ice. Ecology 99:752–754.

Guidi, L., A. Fernàndez-Guerra, C. Canchaya, E. Curry, F. Foglini, J.-O. Irisson, K. Malde, C. T. Marshall, M. Obst, and R. P. Ribeiro. 2020. Big data in marine science. Page Marine Board Future Science Brief.

Hairston, N. C. 1976. Photoprotection by carotenoid pigments in the copepod *Diaptomus nevadensis*. Proceedings of the National Academy of Sciences 73:971–974.

Hairston, N. G. 1979. The adaptive significance of color polymorphism in two species of *Diaptomus* (Copepoda)1: Diaptomid pigmentation. Limnology and Oceanography 24:15–37.

Hansson, L. 2000. Induced pigmentation in zooplankton: a trade–off between threats from predation and ultraviolet radiation. Proceedings of the Royal Society of London. Series B: Biological Sciences 267:2327–2331.

Hansson, L.-A. 2004. Plasticity in pigmentation induced by conflicting threats from predation and UV radiation. Ecology 85:1005–1016.

Hatlen, B., M. Jobling, and B. Bjerkeng. 1998. Relationships between carotenoid concentration and colour of fillets of Arctic chair, *Salvelinus alpinus* (L.), fed astaxanthin. Aquaculture Research 29:191–202.

Hildebrandt, N., B. Niehoff, and F. J. Sartoris. 2014. Long-term effects of elevated CO2 and temperature on the Arctic calanoid copepods Calanus glacialis and C. hyperboreus. Marine Pollution Bulletin 80:59–70.

Hirche, H.-J., and B. Niehoff. 1996. Reproduction of the Arctic copepod *Calanus hyperboreus* in the Greenland Sea - field and laboratory observations. Polar Biology 16:209–219.

Holeton, C., K. Lindell, T. Holmborn, H. Hogfors, and E. Gorokhova. 2009. Decreased astaxanthin at high feeding rates in the calanoid copepod *Acartia bifilosa*. Journal of Plankton Research 31:661–668.

Holste, Svenja, Rasch, Morten, and Topp-Jørgensen, Elmer. 2022. INTERACT Reducing CO2

Emissions of Arctic Science.

Hopcroft, R. R., C. Clarke, R. J. Nelson, and K. A. Raskoff. 2005. Zooplankton communities of the Arctic Canada Basin: the contribution by smaller taxa. Polar Biology 28:198–206.

Hylander, S., W. J. Boeing, W. Granéli, J. Karlsson, J. von Einem, K. Gutseit, and L.-A. Hanssona. 2009. Complementary UV protective compounds in zooplankton. Limnology and Oceanography 54:1883–1893.

Hylander, S., T. Kiørboe, P. Snoeijs, R. Sommaruga, and T. G. Nielsen. 2015. Concentrations of sunscreens and antioxidant pigments in Arctic *Calanus* spp. in relation to ice cover, ultraviolet radiation, and the phytoplankton spring bloom: MAAs and astaxanthin in copepods. Limnology and Oceanography 60:2197–2206.

Hynes, N., E. S. Egeland, W. Koppe, G. Baardsen, and V. Kiron. 2009. *Calanus* oil as a natural source for flesh pigmentation in Atlantic salmon (*Salmo salar* L.). Aquaculture Nutrition 15:202–208.

Intergovernmental Panel on Climate Change (IPCC). 2022. The Ocean and Cryosphere in a Changing Climate: Special Report of the Intergovernmental Panel on Climate Change. First edition. Cambridge University Press.

Irigoien, X., R. P. Harris, H. M. Verheye, P. Joly, J. Runge, M. Starr, D. Pond, R. Campbell, R. Shreeve, P. Ward, A. N. Smith, H. G. Dam, W. Peterson, V. Tirelli, M. Koski, T. Smith, D. Harbour, and R. Davidson. 2002. Copepod hatching success in marine ecosystems with high diatom concentrations. Nature 419:387–389.

Irisson, J.-O., S.-D. Ayata, D. J. Lindsay, L. Karp-Boss, and L. Stemmann. 2022. Machine Learning for the Study of Plankton and Marine Snow from Images. Annual Review of Marine Science 14:null.

Jakobsen, H., and J. Carstensen. 2011. FlowCAM: Sizing cells and understanding the impact of size distributions on biovolume of -planktonic community structure. Aquatic Microbial Ecology 65:75–87.

Johnsen, S. 2005. The Red and the Black: Bioluminescence and the Color of Animals in the Deep Sea. Integrative and Comparative Biology 45:234–246.

Johnsen, S. 2014. Hide and Seek in the Open Sea: Pelagic Camouflage and Visual Countermeasures. Annual Review of Marine Science 6:369–392.

Jónasdóttir, S. H., A. W. Visser, K. Richardson, and M. R. Heath. 2015. Seasonal copepod lipid pump promotes carbon sequestration in the deep North Atlantic. Proceedings of the National Academy of Sciences 112:12122–12126.

Juhl, A. R., M. D. Ohman, and R. Goericke. 1996. Astaxanthin in *Calanus pacificus* : Assessment of

pigment-based measures of omnivory. Limnology and Oceanography 41:1198–1207.

Karnovsky, N., S. Kwasniewski, J. Weslawski, W. Walkusz, and A. Beszczynska-Möller. 2003. Foraging behavior of little auks in a heterogeneous environment. Marine Ecology Progress Series 253:289–303.

Kiko, R., M. Picheral, D. Antoine, M. Babin, L. Berline, T. Biard, E. Boss, P. Brandt, F. Carlotti, S. Christiansen, L. Coppola, L. de la Cruz, E. Diamond-Riquier, X. Durrieu de Madron, A. Elineau, G. Gorsky, L. Guidi, H. Hauss, J.-O. Irisson, L. Karp-Boss, J. Karstensen, D. Kim, R. M. Lekanoff, F. Lombard, R. M. Lopes, C. Marec, A. M. P. McDonnell, D. Niemeyer, M. Noyon, S. H. O'Daly, M. D. Ohman, J. L. Pretty, A. Rogge, S. Searson, M. Shibata, Y. Tanaka, T. Tanhua, J. Taucher, E. Trudnowska, J. S. Turner, A. Waite, and L. Stemmann. 2022. A global marine particle size distribution dataset obtained with the Underwater Vision Profiler 5. Earth System Science Data 14:4315–4337.

Kiørboe, T. 2011. How zooplankton feed: mechanisms, traits and trade-offs. Biological Reviews 86:311–339.

Kiørboe, T., A. Visser, and K. H. Andersen. 2018. A trait-based approach to ocean ecology. ICES Journal of Marine Science 75:1849–1863.

Kooistra, W. H. C. F., R. Gersonde, L. K. Medlin, and D. G. Mann. 2007. The Origin and Evolution of the Diatoms: Their Adaptation to a Planktonic Existence. Pages 207–249 Evolution of Primary Producers in the Sea. Elsevier.

Kortsch, S., R. Primicerio, M. Fossheim, A. V. Dolgov, and M. Aschan. 2015. Climate change alters the structure of arctic marine food webs due to poleward shifts of boreal generalists. Proceedings of the Royal Society B: Biological Sciences 282:20151546.

Lafond, A., K. Leblanc, B. Quéguiner, B. Moriceau, A. Leynaert, V. Cornet, J. Legras, J. Ras, M. Parenteau, N. Garcia, M. Babin, and J.-E. Tremblay. 2019. Late spring bloom development of pelagic diatoms in Baffin Bay. Elem Sci Anth 7:44.

Lauritano, C., Y. Carotenuto, A. Miralto, G. Procaccini, and A. Ianora. 2012. Copepod Population-Specific Response to a Toxic Diatom Diet. PLoS ONE 7:e47262.

Lenz, P. H., and V. Roncalli. 2019. Diapause within the Context of Life-History Strategies in Calanid Copepods (Calanoida: Crustacea). The Biological Bulletin 237:170–179.

Lindeque, P. K., I. Hann, H. E. Parry, K. B. Cook, A. J. W. Lindley, and D. J. Mayor. 2022. Red Pigmentation Can Be Used to Reliably Distinguish Between Live Calanus finmarchicus and Calanus glacialis Females in the Fram Strait. Frontiers in Marine Science 9:906465.

Litchman, E., M. D. Ohman, and T. Kiørboe. 2013. Trait-based approaches to zooplankton communities. Journal of Plankton Research 35:473–484.

Lombard, F., E. Boss, A. M. Waite, M. Vogt, J. Uitz, L. Stemmann, H. M. Sosik, J. Schulz, J.-B. Romagnan, M. Picheral, J. Pearlman, M. D. Ohman, B. Niehoff, K. O. Möller, P. Miloslavich, A. Lara-Lpez, R. Kudela, R. M. Lopes, R. Kiko, L. Karp-Boss, J. S. Jaffe, M. H. Iversen, J.-O. Irisson, K. Fennel, H. Hauss, L. Guidi, G. Gorsky, S. L. C. Giering, P. Gaube, S. Gallager, G. Dubelaar, R. K. Cowen, F. Carlotti, C. Briseño-Avena, L. Berline, K. Benoit-Bird, N. Bax, S. Batten, S. D. Ayata, L. F. Artigas, and W. Appeltans. 2019. Globally Consistent Quantitative Observations of Planktonic Ecosystems. Frontiers in Marine Science 6:196.

Lovejoy, C., L. Legendre, M.-J. Martineau, J. Bâcle, and C. H. von Quillfeldt. 2002. Distribution of phytoplankton and other protists in the North Water. Deep Sea Research Part II: Topical Studies in Oceanography 49:5027–5047.

Maps, F., S. Plourde, and B. Zakardjian. 2010. Control of dormancy by lipid metabolism in Calanus finmarchicus: a population model test. Marine Ecology Progress Series 403:165–180.

Martini, S., F. Larras, A. Boyé, E. Faure, N. Aberle, P. Archambault, L. Bacouillard, B. E. Beisner, L. Bittner, E. Castella, M. Danger, O. Gauthier, L. Karp-Boss, F. Lombard, F. Maps, L. Stemmann, E. Thiébaut, P. Usseglio-Polatera, M. Vogt, M. Laviale, and S. Ayata. 2021. Functional trait-based approaches as a common framework for aquatic ecologists. Limnology and Oceanography 66:965–994.

Matsuno, T. 2001. Aquatic animal carotenoids. Fisheries Science 67:771–783.

Mayo, C. A., and M. K. Marx. 1990. Surface foraging behaviour of the North Atlantic right whale, *Eubalaena glacialis* , and associated zooplankton characteristics. Canadian Journal of Zoology 68:2214–2220.

Mcgill, B., B. Enquist, E. Weiher, and M. Westoby. 2006. Rebuilding community ecology from functional traits. Trends in Ecology & Evolution 21:178–185.

Méral, P. 2012. Le concept de service écosystémique en économie : origine et tendances récentes. Natures Sciences Sociétés 20:3–15.

Meredith, M., M. Sommerkorn, S. Cassotta, C. Derksen, A. Ekaykin, A. Hollowed, G. Kofinas, A. Mackintosh, J. Melbourne-Thomas, and M. M. C. Muelbert. 2019. Polar Regions. Chapter 3, IPCC Special Report on the Ocean and Cryosphere in a Changing Climate.

Mériguet, Z., A. Oddone, D. Le Guen, T. Pollina, R. Bazile, C. Moulin, R. Troublé, M. Prakash, C. de Vargas, and F. Lombard. 2022. Basin-Scale Underway Quantitative Survey of Surface Microplankton Using Affordable Collection and Imaging Tools Deployed From Tara. Frontiers in Marine Science 9:916025.

Michels, J., and S. N. Gorb. 2015. Mandibular Gnathobases of Marine Planktonic Copepods—Structural and Mechanical Challenges for Diatom Frustules. Pages 59–73 *in* C. Hamm,

editor. Evolution of Lightweight Structures. Springer Netherlands, Dordrecht.

Miesner, A. K., N. Lundholm, B. Krock, and T. G. Nielsen. 2016. The effect of *Pseudo-nitzschia seriata* on grazing and fecundity of *Calanus finmarchicus* and *Calanus glacialis*. Journal of Plankton Research 38:564–574.

Miki, W. 1991. Biological functions and activities of animal carotenoids. Pure and Applied Chemistry 63:141–146.

Møller, E. F., M. Maar, S. H. Jónasdóttir, T. G. Nielsen, and K. Tönnesson. 2012. The effect of changes in temperature and food on the development of *Calanus finmarchicus* and *Calanus helgolandicus* populations. Limnology and Oceanography 57:211–220.

Nakano, T., and G. Wiegertjes. 2020. Properties of Carotenoids in Fish Fitness: A Review. Marine Drugs 18:568.

Nielsen, T. G., S. Kjellerup, I. Smolina, G. Hoarau, and P. Lindeque. 2014. Live discrimination of *Calanus glacialis* and *C. finmarchicus* females: can we trust phenological differences? Marine Biology 161:1299–1306.

Ohman, M. D. 2019. A sea of tentacles: optically discernible traits resolved from planktonic organisms in situ. ICES Journal of Marine Science 76:1959–1972.

Ohman, M. D., R. E. Davis, J. T. Sherman, K. R. Grindley, B. M. Whitmore, C. F. Nickels, and J. S. Ellen. 2019. *Zooglider:* An autonomous vehicle for optical and acoustic sensing of zooplankton. Limnology and Oceanography: Methods 17:69–86.

Orenstein, E. C., S. Ayata, F. Maps, É. C. Becker, F. Benedetti, T. Biard, T. de Garidel-Thoron, J. S. Ellen, F. Ferrario, S. L. C. Giering, T. Guy-Haim, L. Hoebeke, M. H. Iversen, T. Kiørboe, J. Lalonde, A. Lana, M. Laviale, F. Lombard, T. Lorimer, S. Martini, A. Meyer, K. O. Möller, B. Niehoff, M. D. Ohman, C. Pradalier, J. Romagnan, S. Schröder, V. Sonnet, H. M. Sosik, L. S. Stemmann, M. Stock, T. Terbiyik-Kurt, N. Valcárcel-Pérez, L. Vilgrain, G. Wacquet, A. M. Waite, and J. Irisson. 2022. Machine learning techniques to characterize functional traits of plankton from image data. Limnology and Oceanography 67:1647–1669.

Pančić, M., R. R. Torres, R. Almeda, and T. Kiørboe. 2019. Silicified cell walls as a defensive trait in diatoms. Proceedings of the Royal Society B: Biological Sciences 286:20190184.

Pedro, S., M. Lemire, C. Hoover, B. Saint-Béat, M. Y. Janjua, J. Herbig, M. Geoffroy, G. Yunda-Guarin, M.-A. Moisan, J. Boissinot, J.-É. Tremblay, M. Little, L. Chan, M. Babin, T.-A. Kenny, and F. Maps. 2023. Structure and function of the western Baffin Bay coastal and shelf ecosystem. Elementa: Science of the Anthropocene 11:00015.

Petrucciani, A., P. Chaerle, and A. Norici. 2022. Diatoms Versus Copepods: Could Frustule Traits Have a Role in Avoiding Predation? Frontiers in Marine Science 8:804960.

Picheral, M., C. Catalano, D. Brousseau, H. Claustre, L. Coppola, E. Leymarie, J. Coindat, F. Dias, S. Fevre, L. Guidi, J. O. Irisson, L. Legendre, F. Lombard, L. Mortier, C. Penkerch, A. Rogge, C. Schmechtig, S. Thibault, T. Tixier, A. Waite, and L. Stemmann. 2022. The Underwater Vision Profiler 6: an imaging sensor of particle size spectra and plankton, for autonomous and cabled platforms. Limnology and Oceanography: Methods 20:115–129.

Picheral, M., S. Colin, and J.-O. Irisson. 2017. EcoTaxa, a tool for the taxonomic classification of images. http://ecotaxa.obs-vlfr.fr.

Picheral, M., L. Guidi, L. Stemmann, D. M. Karl, G. Iddaoud, and G. Gorsky. 2010. The Underwater Vision Profiler 5: An advanced instrument for high spatial resolution studies of particle size spectra and zooplankton: Underwater vision profiler. Limnology and Oceanography: Methods 8:462–473.

Pierson, J. J., H. Batchelder, W. Saumweber, A. Leising, and J. Runge. 2013. The impact of increasing temperatures on dormancy duration in Calanus finmarchicus. Journal of Plankton Research 35:504–512.

Pollina, T., A. G. Larson, F. Lombard, H. Li, D. Le Guen, S. Colin, C. de Vargas, and M. Prakash. 2022. PlanktoScope: Affordable Modular Quantitative Imaging Platform for Citizen Oceanography. Frontiers in Marine Science 9:949428.

Powers, M. J., and G. E. Hill. 2021. A Review and Assessment of the Shared-Pathway Hypothesis for the Maintenance of Signal Honesty in Red Ketocarotenoid-Based Coloration. Integrative and Comparative Biology 61:1811–1826.

Rapinski, M., A. Cuerrier, C. Harris, E. of Ivujivik, E. of Kangiqsujuaq, and M. Lemire. 2018. Inuit Perception of Marine Organisms: From Folk Classification to Food Harvest. Journal of Ethnobiology 38:333.

Record, N. R., R. Ji, F. Maps, Ø. Varpe, J. A. Runge, C. M. Petrik, and D. Johns. 2018. Copepod diapause and the biogeography of the marine lipidscape. Journal of Biogeography 45:2238–2251.

Record, N., J. Runge, D. Pendleton, W. Balch, K. Davies, A. Pershing, C. Johnson, K. Stamieszkin, R. Ji, Z. Feng, S. Kraus, R. Kenney, C. Hudak, C. Mayo, C. Chen, J. Salisbury, and C. Thompson. 2019. Rapid Climate-Driven Circulation Changes Threaten Conservation of Endangered North Atlantic Right Whales. Oceanography 32.

Renaud, P. E., M. Daase, N. S. Banas, T. M. Gabrielsen, J. E. Søreide, Ø. Varpe, F. Cottier, S. Falk-Petersen, C. Halsband, D. Vogedes, K. Heggland, and J. Berge. 2018. Pelagic food-webs in a changing Arctic: a trait-based perspective suggests a mode of resilience. ICES Journal of Marine Science 75:1871–1881.

Riisgaard, K., R. Swalethorp, S. Kjellerup, T. Juul-Pedersen, and T. Nielsen. 2014. Trophic role and top-down control of a subarctic protozooplankton community. Marine Ecology Progress Series 500:67–82.

Rombouts, I., G. Beaugrand, F. Ibaňez, S. Gasparini, S. Chiba, and L. Legendre. 2009. Global latitudinal variations in marine copepod diversity and environmental factors. Proceedings of the Royal Society B: Biological Sciences 276:3053–3062.

Saiz, E., A. Calbet, S. Isari, M. Antó, E. M. Velasco, R. Almeda, J. Movilla, and M. Alcaraz. 2013. Zooplankton distribution and feeding in the Arctic Ocean during a Phaeocystis pouchetii bloom. Deep Sea Research Part I: Oceanographic Research Papers 72:17–33.

Sameoto, D., P. Wiebe, J. Runge, L. Postel, J. Dunn, C. Miller, and S. Coombs. 2000. Collecting zooplankton. Pages 55–81 ICES Zooplankton Methodology Manual. Elsevier.

Sansoulet, J., M. Therrien, J. Delgove, G. Pouxviel, J. Desriac, N. Sardet, and J.-P. Vanderlinden. 2020. An update on Inuit perceptions of their changing environment, Qikiqtaaluk (Baffin Island, Nunavut). Elementa: Science of the Anthropocene 8:025.

Sardet, C., R. D. Rosengarten, T. Rosengarten, D. Sardet, and M. Ohman. 2015. Plankton: Wonders of the Drifting World. University of Chicago Press.

Schmid, M. S., F. Maps, and L. Fortier. 2018. Lipid load triggers migration to diapause in Arctic *Calanus* copepods—insights from underwater imaging. Journal of Plankton Research 40:311–325.

Schneider, T., G. Grosbois, W. F. Vincent, and M. Rautio. 2016. Carotenoid accumulation in copepods is related to lipid metabolism and reproduction rather than to UV-protection: Copepod carotenoids and lipids. Limnology and Oceanography 61:1201–1213.

Schneider, T., G. Grosbois, W. F. Vincent, and M. Rautio. 2017. Saving for the future: Pre-winter uptake of algal lipids supports copepod egg production in spring. Freshwater Biology 62:1063–1072.

Schröder, S.-M., R. Kiko, and R. Koch. 2020. MorphoCluster: Efficient Annotation of Plankton Images by Clustering. Sensors 20:3060.

Scott, C., S. Kwasniewski, S. Falk-Petersen, and J. Sargent. 2002. Species differences, origins and functions of fatty alcohols and fatty acids in the wax esters and phospholipids of *Calanus hyperboreus*, *C. glacialis* and *C. finmarchicus* from Arctic waters. Marine Ecology Progress Series 235:127–134.

Shoval, O., H. Sheftel, G. Shinar, Y. Hart, O. Ramote, A. Mayo, E. Dekel, K. Kavanagh, and U. Alon. 2012. Evolutionary Trade-Offs, Pareto Optimality, and the Geometry of Phenotype Space. Science 336:1157–1160.

Sommaruga, R. 2010. Preferential accumulation of carotenoids rather than of mycosporine-like amino acids in copepods from high altitude Himalayan lakes. Hydrobiologia 648:143–156.

Sommer, F., C. Agurto, P. Henriksen, and T. Kiørboe. 2006. Astaxanthin in the calanoid copepod *Calanus helgolandicus*: dynamics of esterification and vertical distribution in the German Bight, North Sea. Marine Ecology Progress Series 319:167–173.

Søreide, J. E., E. Leu, J. Berge, M. Graeve, and S. Falk-Petersen. 2010. Timing of blooms, algal food quality and *Calanus glacialis* reproduction and growth in a changing Arctic. Global Change Biology 16:3154–3163.

Sosik, H. M., and R. J. Olson. 2007. Automated taxonomic classification of phytoplankton sampled with imaging-in-flow cytometry: Phytoplankton image classification. Limnology and Oceanography: Methods 5:204–216.

Stamieszkin, K., A. J. Pershing, N. R. Record, C. H. Pilskaln, H. G. Dam, and L. R. Feinberg. 2015. Size as the master trait in modeled copepod fecal pellet carbon flux: Copepod size structure and carbon flux. Limnology and Oceanography 60:2090–2107.

Steinberg, D. K., and M. R. Landry. 2017. Zooplankton and the Ocean Carbon Cycle. Annual Review of Marine Science 9:413–444.

Stoecker, D. K., and P. J. Lavrentyev. 2018. Mixotrophic Plankton in the Polar Seas: A Pan-Arctic Review. Frontiers in Marine Science 5:292.

Stoń-Egiert, J., and A. Kosakowska. 2005. RP-HPLC determination of phytoplankton pigments—comparison of calibration results for two columns. Marine Biology 147:251–260.

Tarling, G. A., A. Belcher, M. Blackwell, C. Castellani, K. B. Cook, F. R. Cottier, V. Dewar-Fowler, J. J. Freer, L. Gerrish, M. L. Johnson, K. S. Last, P. K. Lindeque, D. J. Mayor, H. E. Parry, G. Stowasser, and M. Wootton. 2022. Carbon and Lipid Contents of the Copepod Calanus finmarchicus Entering Diapause in the Fram Strait and Their Contribution to the Boreal and Arctic Lipid Pump. Frontiers in Marine Science 9:926462.

Tedetti, M., and R. Sempéré. 2006. Penetration of Ultraviolet Radiation in the Marine Environment. A Review. Photochemistry and Photobiology 82:389.

Townsend, M., K. Davies, N. Hanley, J. E. Hewitt, C. J. Lundquist, and A. M. Lohrer. 2018. The Challenge of Implementing the Marine Ecosystem Service Concept. Frontiers in Marine Science 5:359.

Trudnowska, E., K. Balazy, J. Stoń-Egiert, I. Smolina, T. Brown, and M. Gluchowska. 2020. In a comfort zone and beyond—Ecological plasticity of key marine mediators. Ecology and Evolution:ece3.6997.

Trudnowska, E., K. Dragańska-Deja, S. Sagan, and K. Błachowiak-Samołyk. 2022. Cells of matter

and life – towards understanding the structuring of particles and plankton patchiness in the Arctic fjords. Frontiers in Marine Science 9:909457.

Trudnowska, E., L. Lacour, M. Ardyna, A. Rogge, J. O. Irisson, A. M. Waite, M. Babin, and L. Stemmann. 2021. Marine snow morphology illuminates the evolution of phytoplankton blooms and determines their subsequent vertical export. Nature Communications 12:2816.

Turner, J. T. 2004. The importance of small planktonic copepods and their roles in pelagic marine food webs. Zoological Studies 43:255–266.

Turner, J. T. 2015. Zooplankton fecal pellets, marine snow, phytodetritus and the ocean's biological pump. Progress in Oceanography 130:205–248.

Ulrich, K. L., and R. F. Tallman. 2021. The Capelin invasion: evidence for a trophic shift in Arctic Char populations from the Cumberland Sound region, Nunavut, Canada. Arctic Science 7:413–435.

Usseglio-Polatera, P., M. Bournaud, P. Richoux, and H. Tachet. 2000. Biological and ecological traits of benthic freshwater macroinvertebrates: relationships and definition of groups with similar traits. Freshwater Biology 43:175–205.

Vacht, P., T. Koff, B. Plüschke-Altof, and A. Müüripeal. 2018. Les services écosystémiques de la ville de Tallinn : les réussites et les défis. Dynamiques environnementales:122–145.

Villéger, S., N. W. H. Mason, and D. Mouillot. 2008. New multidimensional functional diversity indices for a multifaceted framework in functional ecology. Ecology 89:2290–2301.

Vincent, F., and C. Bowler. 2022. An Integrated View of Diatom Interactions. Pages 59–86 *in* A. Falciatore and T. Mock, editors. The Molecular Life of Diatoms. Springer International Publishing, Cham.

Violle, C., M.-L. Navas, D. Vile, E. Kazakou, C. Fortunel, I. Hummel, and E. Garnier. 2007. Let the concept of trait be functional! Oikos 116:882–892.

Vogedes, D., Ø. Varpe, J. E. Søreide, M. Graeve, J. Berge, and S. Falk-Petersen. 2010. Lipid sac area as a proxy for individual lipid content of arctic calanoid copepods. Journal of Plankton Research 32:1471–1477.

Wassman, P., and M. Reigstad. 2011. Future Arctic Ocean Seasonal Ice Zones and Implications for Pelagic-Benthic Coupling. Oceanography 24:220–231.

Weaver, R. J., P. A. Cobine, and G. E. Hill. 2018. On the bioconversion of dietary carotenoids to astaxanthin in the marine copepod, *Tigriopus californicus*. Journal of Plankton Research 40:142–150.

Wilson, R. J., N. S. Banas, M. R. Heath, and D. C. Speirs. 2016. Projected impacts of 21st century climate change on diapause in *Calanus finmarchicus*. Global Change Biology 22:3332–3340.

Annexe A - Chapitre 1

Table A.1. Taxonomic categories of living organisms imaged by the UVP. The scale bar is 2mm.

Crustacea	
Copepoda	
like<Copepoda	
Copepoda_with_eggs	
Eumalacostraca	
Ostracoda	

	
Amphipoda_tot	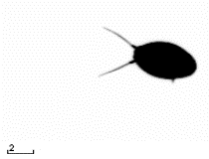
Larvae	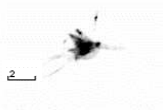
Limacinidae	
Gymnosomata	
Veliger	
Appendicularia_living	

Salpida	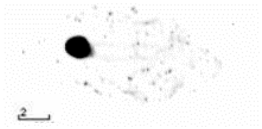
Annelida	
Chaetognatha	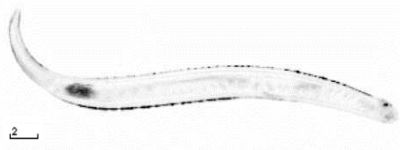
Ctenophora	 
Beroe	
Cnidaria	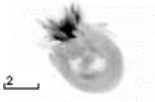

Siphonophorae

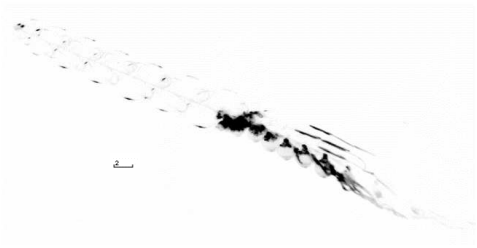

Hydrozoa

Aglantha digitale

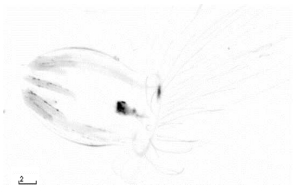

Halicreatidae

Narcomedusae

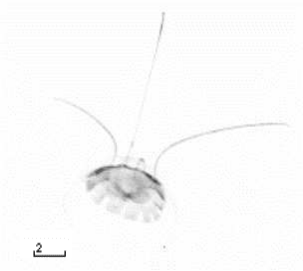

Solmundella bitentaculata	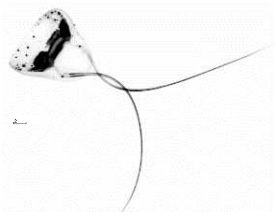
Sarsia	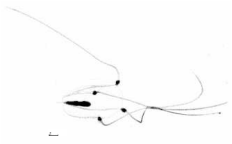
Rhizaria	
Acantharea	
Collodaria	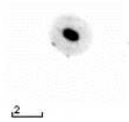
Phaeodaria	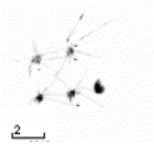

Aulacantha	
Aulosphaeridae	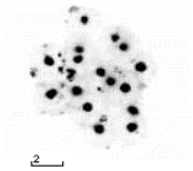 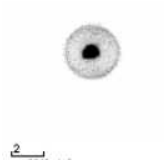
Cannosphaeridae	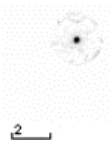
Coelographis_tot	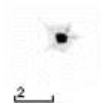
Gnathostomata	
t004 (unknown)	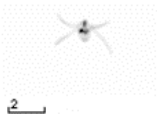
t002 (unknown)	

Table A.2. Morphological descriptors computed by Zooprocess (Gorsky et al. 2010) and used to construct the morphological space (Figure 1.3).

Size	**Major** = primary axis of an ellipse fitted on the object
	Minor = secondary axis of an ellipse fitted on the object
	Area = object area (i.e. number of pixels belonging to the object)
	Feret = distance between the 2 further points along object's perimeter
	Perim. = perimeter length of the object
Shape	**Circ.** = circularity measure = (4*π*area)/perim., 1 = circle, 0 = line.
	Elongation = major/minor, 1 = circular >1 = elongated
	Thickr = Thickness ratio, relation between the maximum thickness of an object and the average thickness of the object excluding the maximum (Romagnan et al. 2016)
	Ver.Sym. = bilateral symmetry index
	Ver.Sym.2 = bilateral symmetry index taking into account only 75% of the darker pixels)
Transparency	**Mean.gray** = average gray value within the object ; sum of the gray values of all pixels in the object divided by the number of pixels (low = dark objects, high = clear objects) **Med.gray** = median gray value within the object **Hist.gray 75%** = gray level value at 75% of the normalized cumulative histogram of gray levels **Sdev.gray** = standard deviation of the gray value used to generate the mean gray value **Skew.gray** = skewness of the histogram of gray level values
Complexity	**Perim./Major** = Refers to both complexity (high values if the perimeter is particularly complex for an object of a given size) and circularity (round objects have a high perimeter/diameter ratio). **Perim./Feret** = same interpretation **Fractal** = fractal dimension of perimeter (Bérubé and Jébrak 1999)

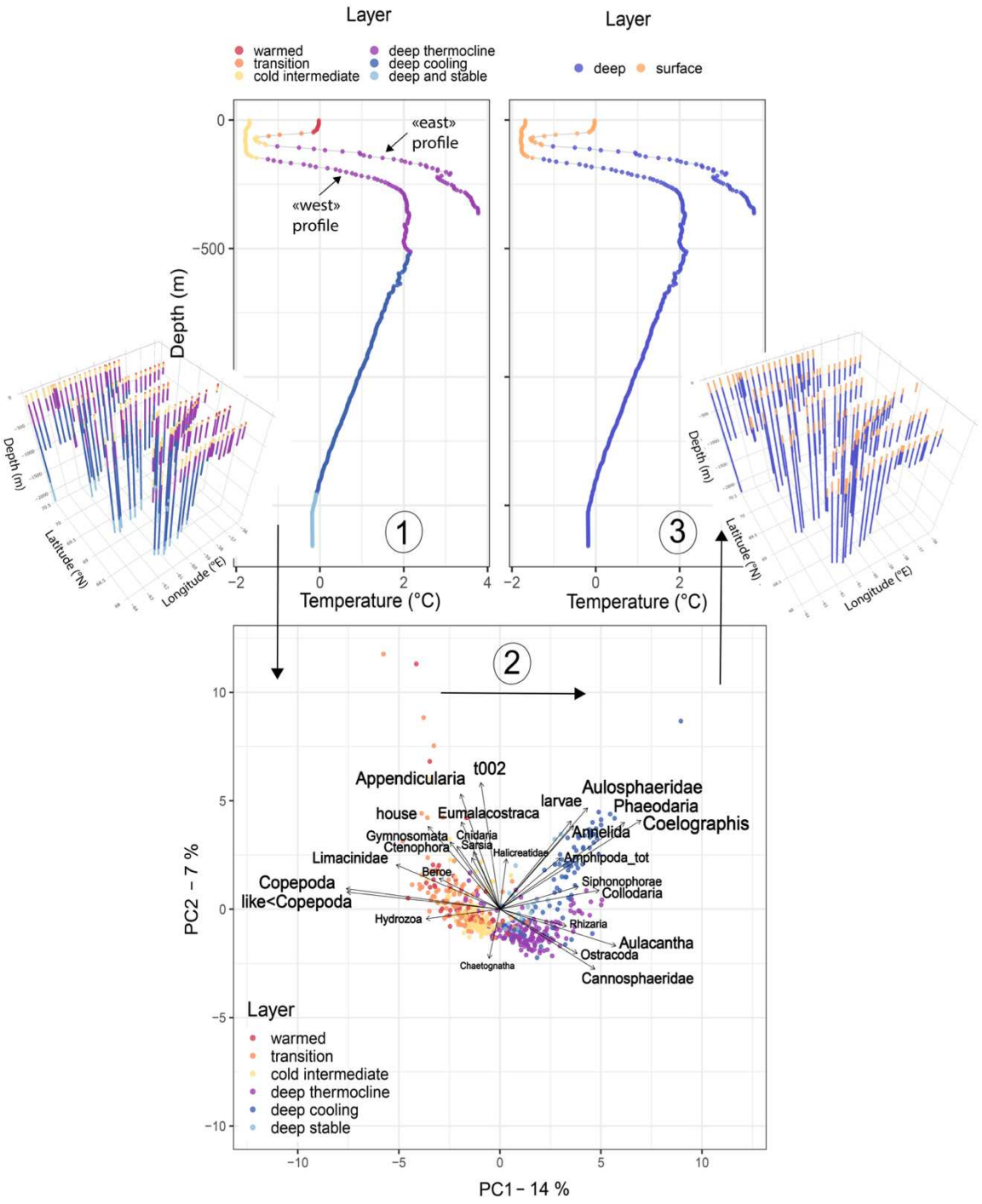

Figure A.1. Example of a water column zonation according to physical and biological criteria. We defined a surface layer consistent in terms of physical conditions and zooplanktonic community composition. Temperature profiles presented strong gradients that captured changes in other variables (density, salinity, fluorescence). They were used to vertically segment the water column into six layers ①: warm surface layer, transition layer, cold intermediate layer, deep thermocline layer, deep cooling layer and deep stable layer. Practically, we first looked for the intermediate minimum of temperature, part of the Winter Atlantic Water

masses and typical of this Arctic system (Tang et al. 2004; Randelhoff et al. 2019). The cold intermediate layer (yellow) was defined by the isotherms corresponding to the minimum of temperature + 0.3°C. The seasonal warm surface layer (red) had temperatures above the minimum +1°C. Between these two layers, there was a transition layer (orange). Then, a deep temperature maximum (a physical signature of Atlantic Waters, Randelhoff et al. 2019) was identified. Above this maximum, we delimited a deep thermocline layer (in purple, where temperature sharply increase), while under this maximum laid a deep cooling layer (in marine blue, temperature slowly decreasing) above a deep stable layer (pale blue, temperature is stable, less than 0.1°C of variation from the deepest temperature). A Principal Component Analysis (PCA) was performed on the planktonic concentrations within these layers (obtained from the UVP images), to characterize plankton distribution across depth ②. The analysis separated the first three layers from the deeper ones, revealing different zooplankton communities according to depth. Warm, transition and cold intermediate layers were merged into one surface layer characterized by a homogenous community dominated by copepods ③.

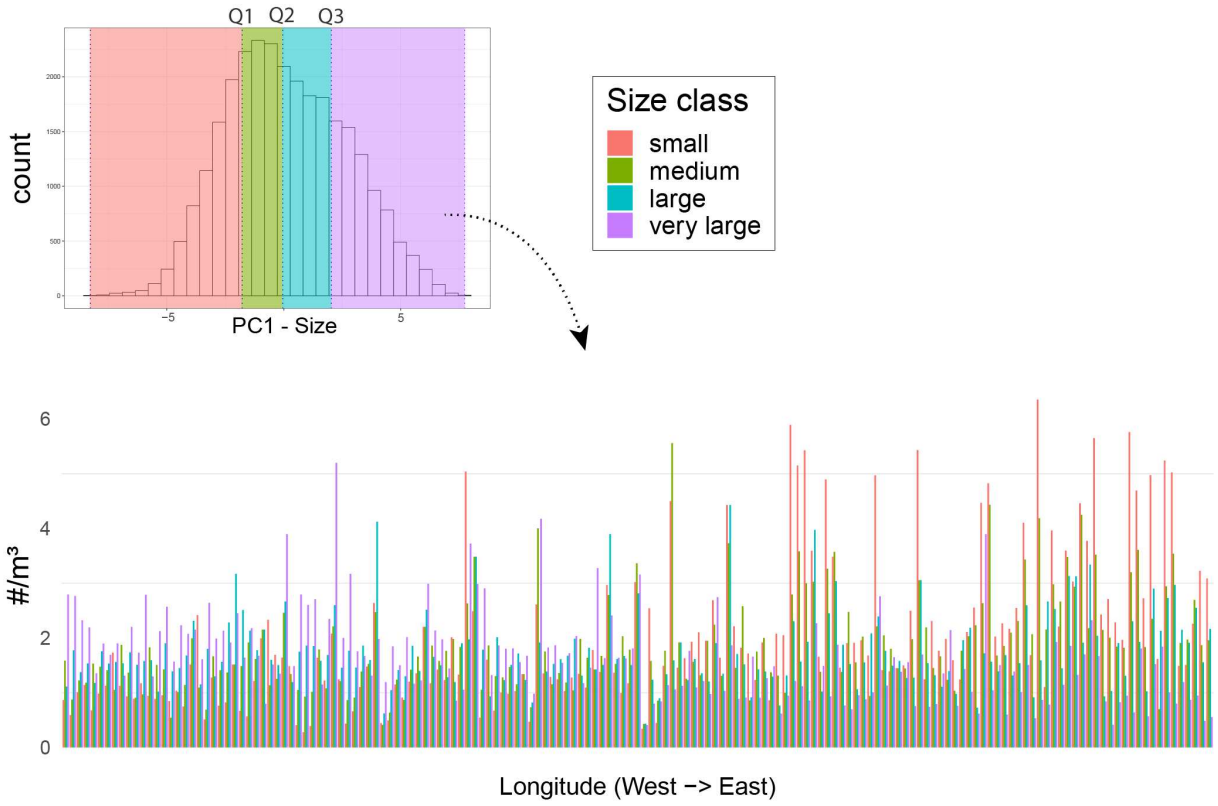

Figure A.2. Distribution of copepod abundances according to longitude and size class. For the ~28,000 individual copepod images, size classes were defined according to PC1 quartiles (small: PC1 value ⩽ Q1, medium: Q1 < PC1 value ⩽ Q2, large: Q2 < PC1 value ⩽ Q3, very large: PC1 value > Q3). Then, abundances of each size class are represented according to station longitude.

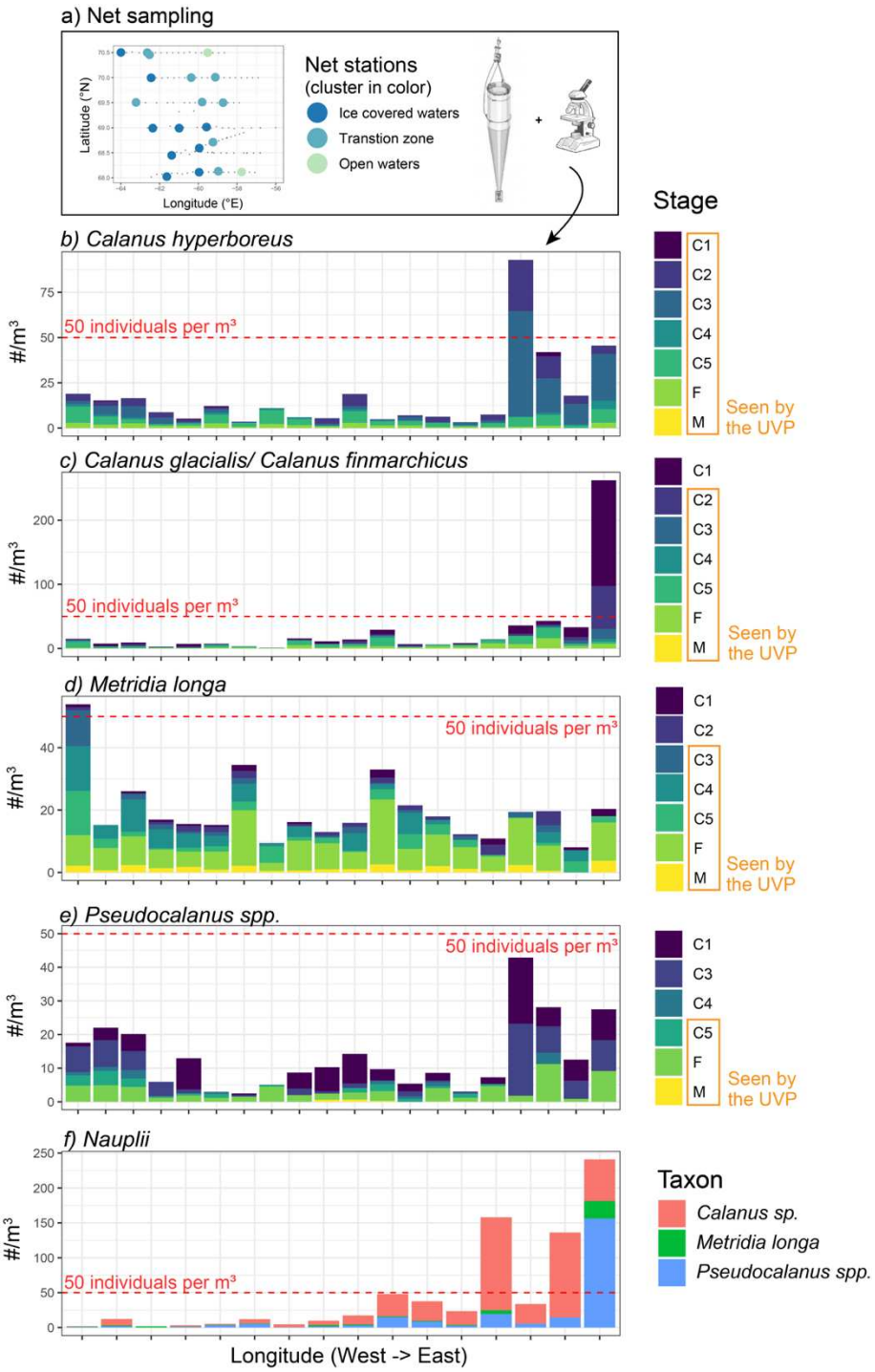

Figure A.3. Copepod species and development stage abundances from net sampling. Vertical tows were performed with a 200 µm mesh net at 20 stations during the GreenEdge cruise (a). Net tows were carried out between 270 and 700m depth to the surface and captures were integrated over than range. For copepods specifically, these depth-integrated tows are interesting to compare to the surface layer UVP data we studied here, because copepods were mostly present in that surface layer. Indeed, in the UVP data, 76% of all copepod images were within the surface layer. Note that tows were mainly performed in ice-covered waters and transition

zones, stations in open waters are not well represented. After subsampling for large and small size fractions, zooplankton were sorted taxonomically under the microscope. Abundances m^{-3} were estimated using volume estimated by a flowmeter. They are reported here according to the longitude of sampled stations, for *Calanus hyperboreus* (b), *C. glacialis* and *C. finmarchicus* (c), *Metridia longa* (d), *Pseudocalanus spp.* (e) and for the nauplii of these main species (f). Since y-axes scales are different between the subplots, the horizontal red dashed line indicates the threshold of 50 individuals m^{-3}. The fraction represented by the various development stages (copepodites C1 to C5, females F and males M) are shown in colors for panels (b) to (e). Only stages framed by an orange rectangle were large enough to be imaged by the UVP during the GreenEdge cruise (ESD > 0.85 mm; Forest et al. 2012).

Annexe B - Chapitre 2

Table B.1. Conversions of carotenoid concentrations in copepods. On a total of 286 values, that includes 11 NAs from studies that quantified carotenoids proportions but did not give a total carotenoid content, 202 quantifications of carotenoids were expressed as µg per mg of dry weight. We have tried to convert values from other units (73 values), insofar as they were quantified for monospecific samples of late copepodites (CV) or adults' copepods. We did not convert measures performed for mixed species or mixed development stages samples because it is not possible to find specific conversion factors and relationships (16 values); we did not convert measures in optical density (OD) or absorbance (A) per mg of dry weight (28 values) because too many parameters would have been estimated (extinction coefficients, solvent, maximum of absorption chosen, length of the optical path); we did not convert measures from image analyses because methods were not reproducible and intercomparable (16 values). Thus, we tried to convert the 13 measures left, as detailed in the table below. If available in the literature, species-specific conversions factors were used; if not, we used factors for copepods of the same taxonomical order and range size. As 4 conversions were uncoherent, 9 converted values were included in Data1 and identified with by a *yes* in the column *unit_conversion*. Finally, 211 values in µg.mgDM^{-1} will be used for quantitative analyses in the article.

Study	**Species**	**Initial concentration**	**Relationships from various studies**	**Conversionvalue used (average value)**	**Final concen-tration (µg.mgDM^{-1})**	**Comments**
Buffan-Dubau et al. 1996	*Canuella perplexa*	0.00835 ng.ind^{-1}	Body length (BL): 1.4 mm (Scott 1893) -- Estimation of DM for harpacticoid copepods (Goodman 1979): DM = 14.01*BL(mm) - 5.69 DM = 14.01*1.4 -5.69 = **13,7 µg.ind^{-1}**	14 µg.ind^{-1}	0.0006	Authors mentioned an underestimation because of a loss of color
Goodwin & Srisukh 1949	*Tigriopus fulvus* (adults)	5542.5 ng.ind^{-1}	**10 µg.ind^{-1}** (*Tigriopus californicus*, Weaver et al. 2018) **2.1 µg.ind^{-1}** (Various *Tigriopus spp.,* Finney 1979) **5 µg.ind^{-1}** (*T. brevicornis*; Mc Allen and Taylor 2001)	6 µg.ind^{-1}	923	**Uncoherent result:** all copepod biomass would be pigments
Hairston 1980	*Diaptomus sanguineus*	38 ng.ind^{-1}	Body length (BL): 1.2-2.5 mm: *Diaptomus sanguineus* has the same size as *D. minutus* (Duerden et al. 1973)	8 µg.ind^{-1}	4.75	

			1.3mm (Holden 1995) 1.591-1.730mm (Humes and Wilson 1951) -- Estimation of DM from body length (for adults *D.minus* (Lawrence et al. 1987, Table 4) : Ln(DM)= ln(a) +b*ln(BL) = 1.0332 + 2.6060*ln(BL) -- With BL from 1.2 to 2.5mm: 1.5 < Ln(DM) < 2.461604 Exp(1.5)<DM<exp(2. 461604) **4.48 µg.ind^{-1} < DM < 11.72 µg.ind^{-1}**			
Hairston 1980	*Diaptomus sanguineus*	31 ng.ind^{-1}	Same as previous	8 µg.ind^{-1}	3.88	
Hairston 1980	*Diaptomus sanguineus*	78 ng.ind^{-1}	Same as previous	8 µg.ind^{-1}	9.75	
Hairston 1980	*Diaptomus sanguineus*	32 ng.ind^{-1}	Same as previous	8 µg.ind^{-1}	4.00	
Juhl et al. 1996	*Calanus pacificus (adults females)*	53.9 ng.ind^{-1}	**228 µg.ind^{-1}** (Harris 1982) **90 µg.ind^{-1}** (Håkanson 1987) **70 - 300 µg.ind^{-1}** (Vidal 1980)	172 µg.ind^{-1}	0.31	
Juhl et al. 1996	*Calanus pacificus* (adults females)	70.6 ng.ind^{-1}	Same as previous	172 µg.ind^{-1}	0.41	
Ohman et al. 1989	*Neocalanus tonsus (*late copepodits)	93 ng.ind^{-1}	**470 µg.ind^{-1}** (from Ohman et al. 1989, Fig. 2, first panel for CV stages, (sampling of copepods for pigment analysis in november)	470 µg.ind^{-1}	0.2	
Ohman et al. 1989	*Neocalanus tonsus* (late copepodits)	164 ng.ind^{-1}	Same as previous	470 µg.ind^{-1}	0.35	
Czeczuga 1975	*Eudiaptomus amblyodon* (adults)	0.012 µg.mg LM^{-1}	We suppose that live weight = wet weight -- Using log(DM)= -0.67+0.96*log(LW)	0.21mgDM. mgLW^{-1}	0.06	**Uncoherent result:** too small, outsider

			(Kiørboe 2013, Table II, for copepods) >1mgLW = 0.21mgDM			
Czeczuga1975	*Eudiaptomus amblyodon* (adults)	0.00342 µg.mg LM^{-1}	Same as previous	0.21mgDM. $mgLW^{-1}$	0.016	**Uncoherent result:** too small, outsider
Czeczuga1975	*Eudiaptomus amblyodon* (adults)	0.00613 µg.mg LM^{-1}	Same as previous	0.21mgDM. $mgLM^{-1}$	0.029	**Uncoherent result:** too small, outsider

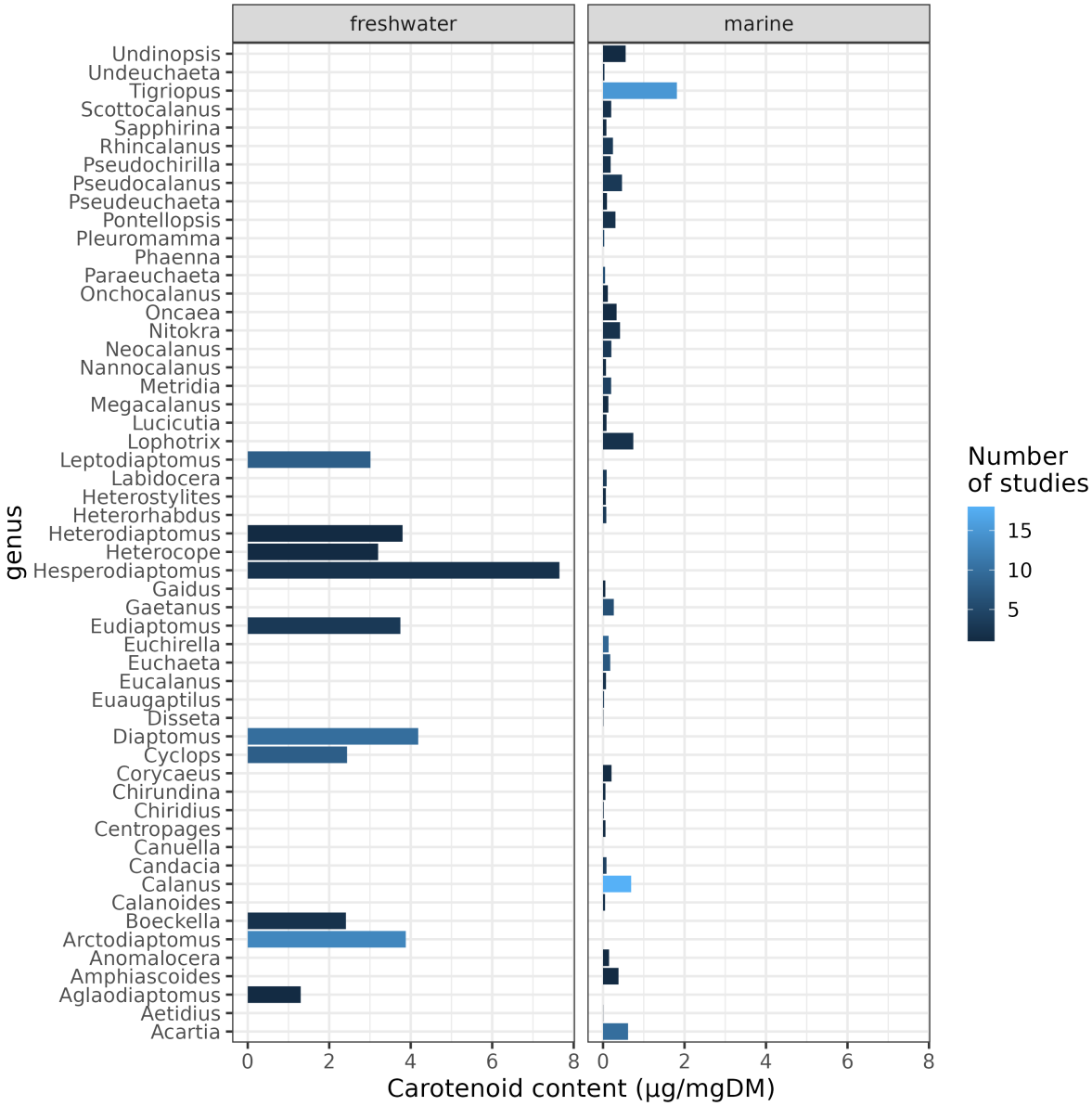

Figure B.1. Average carotenoid concentration (µg.mgDM^{-1}) in different freshwater and marine copepod genus. Color corresponds to the number of studies which were used to compute the average carotenoid content.

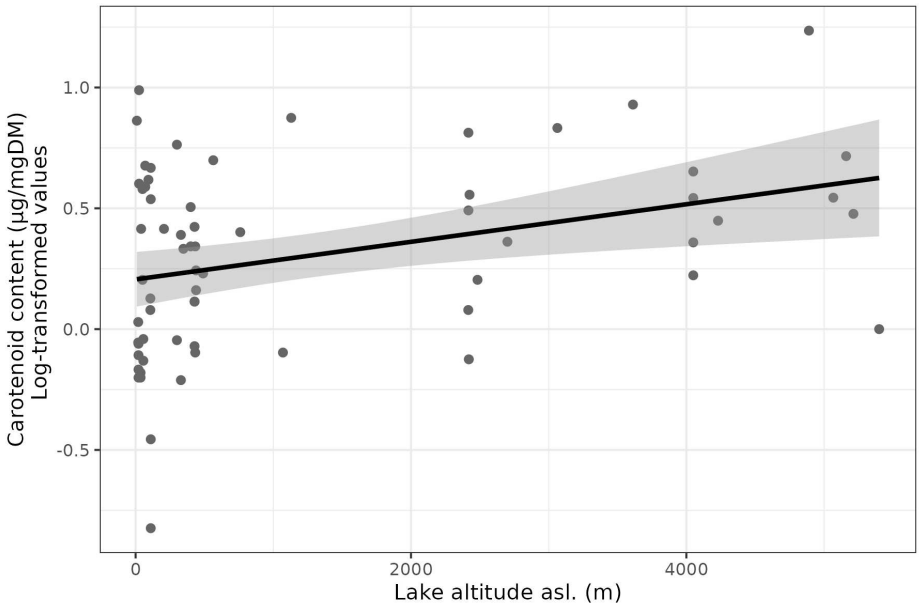

Figure B.2. Carotenoid concentrations (µg.mgDM^{-1}, log-transformed values) in freshwater copepods according to lake altitude above sea level (m). A linear model fitted and significant *(p-value < 0.001, Adjusted R-squared = 0.1021*).

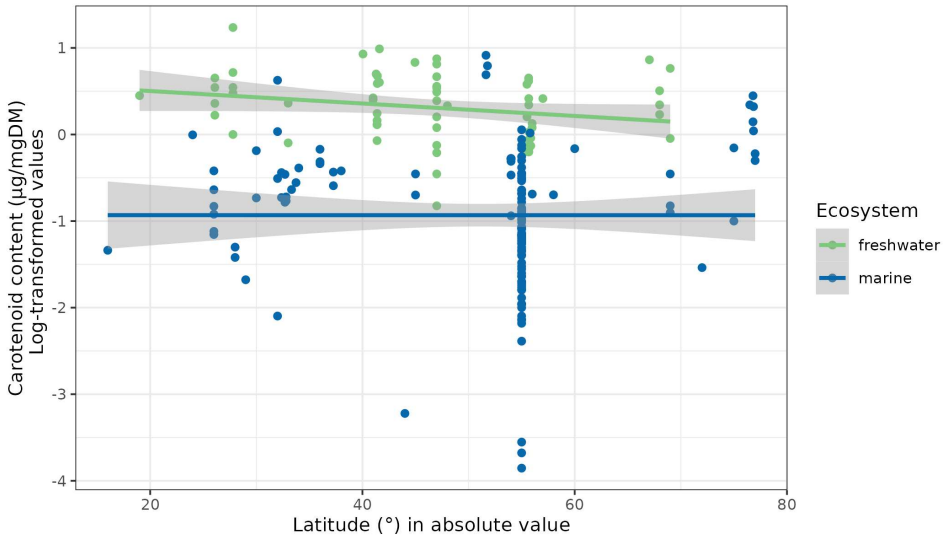

Figure B.3. Carotenoid concentrations (µg/mgDM, log-transformed values) from freshwater and marine copepods according to latitude (°) in absolute value. Linear models are fitted but are *not significant* (*marine: p-value = 0.99836, freshwater: p-value =0.07085*).

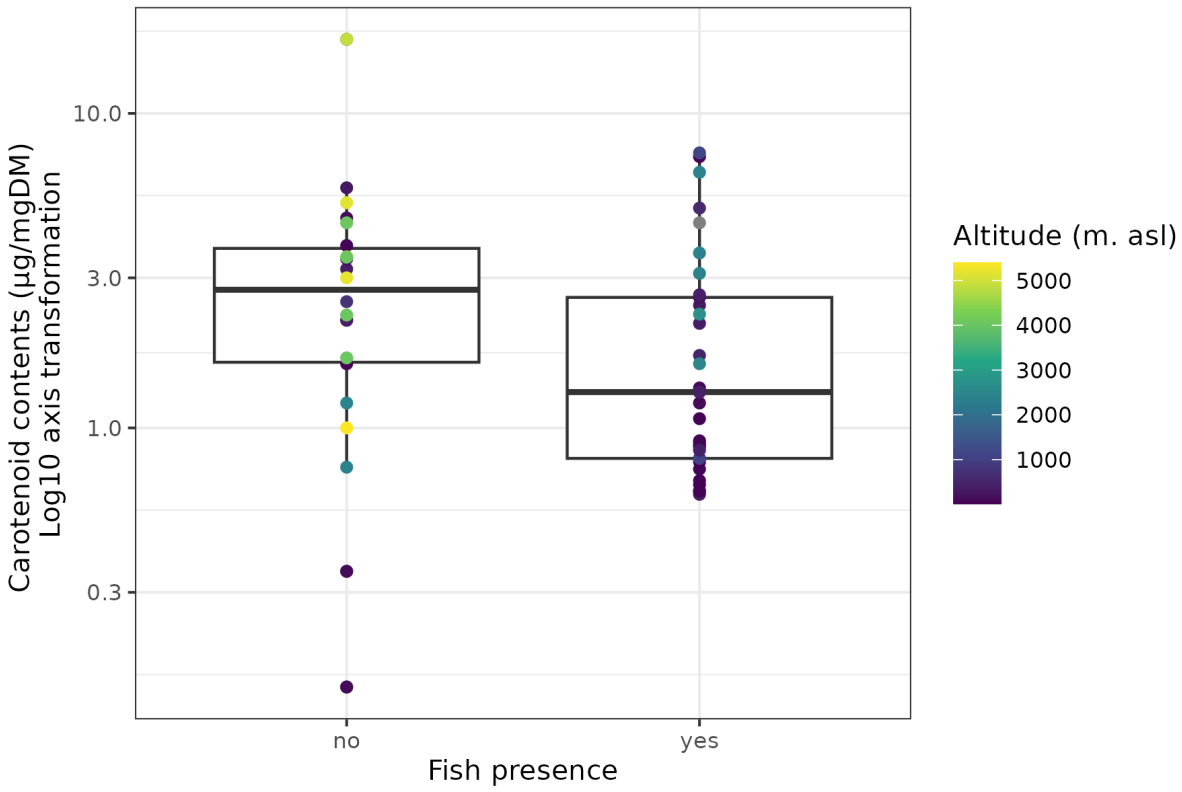

Figure B.4. Distribution of carotenoids concentrations (µg.mgDM^{-1}, log transformation of y-axis) from lakes where fish predators are present (« yes ») or not (« no »). Differences in carotenoid concentrations according to predator presence is significant (*Wilcoxon test, p-value* = 0.03597). Points are also colored according to lake altitude above sea level, which may also influence pigmentation (see body of the article).

Annexe C - Chapitre 3

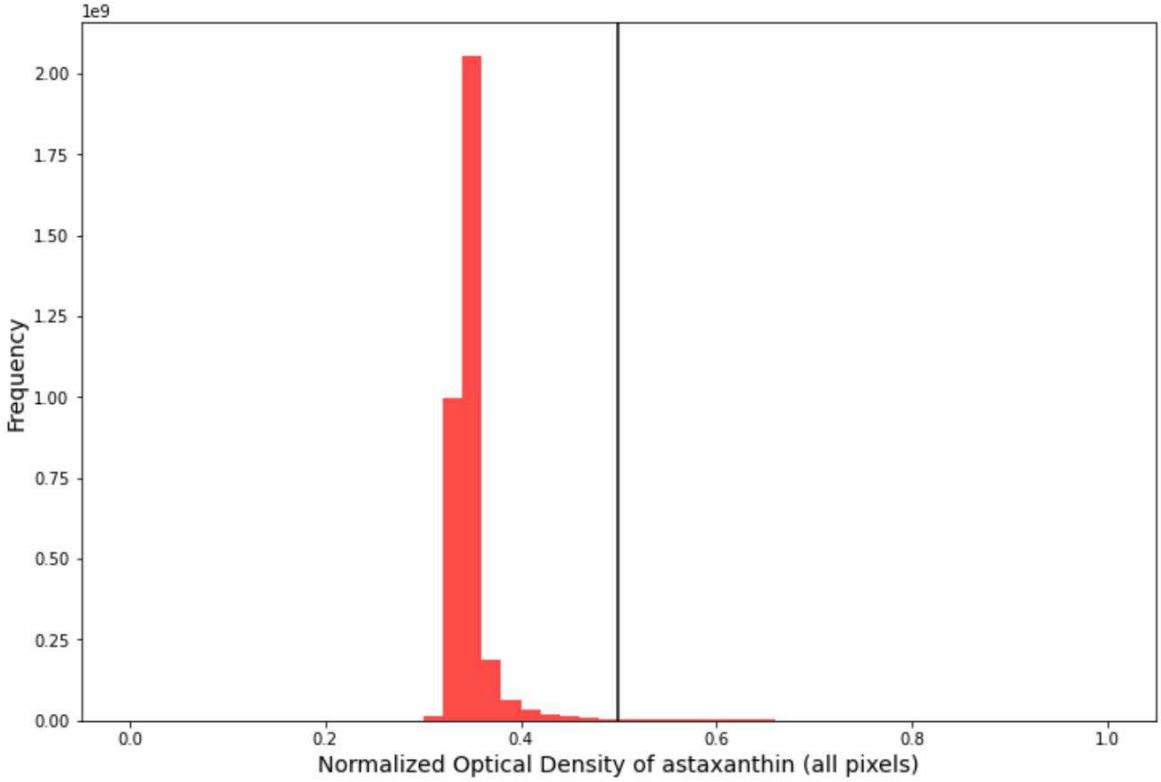

Figure C.1. Histogram of normalized astaxanthin optical density (OD) values resulting from the color deconvolution for 100 randomly selected images. The chosen threshold of 0.5 is visualized by the vertical line, and separates astaxanthin red pixels from others

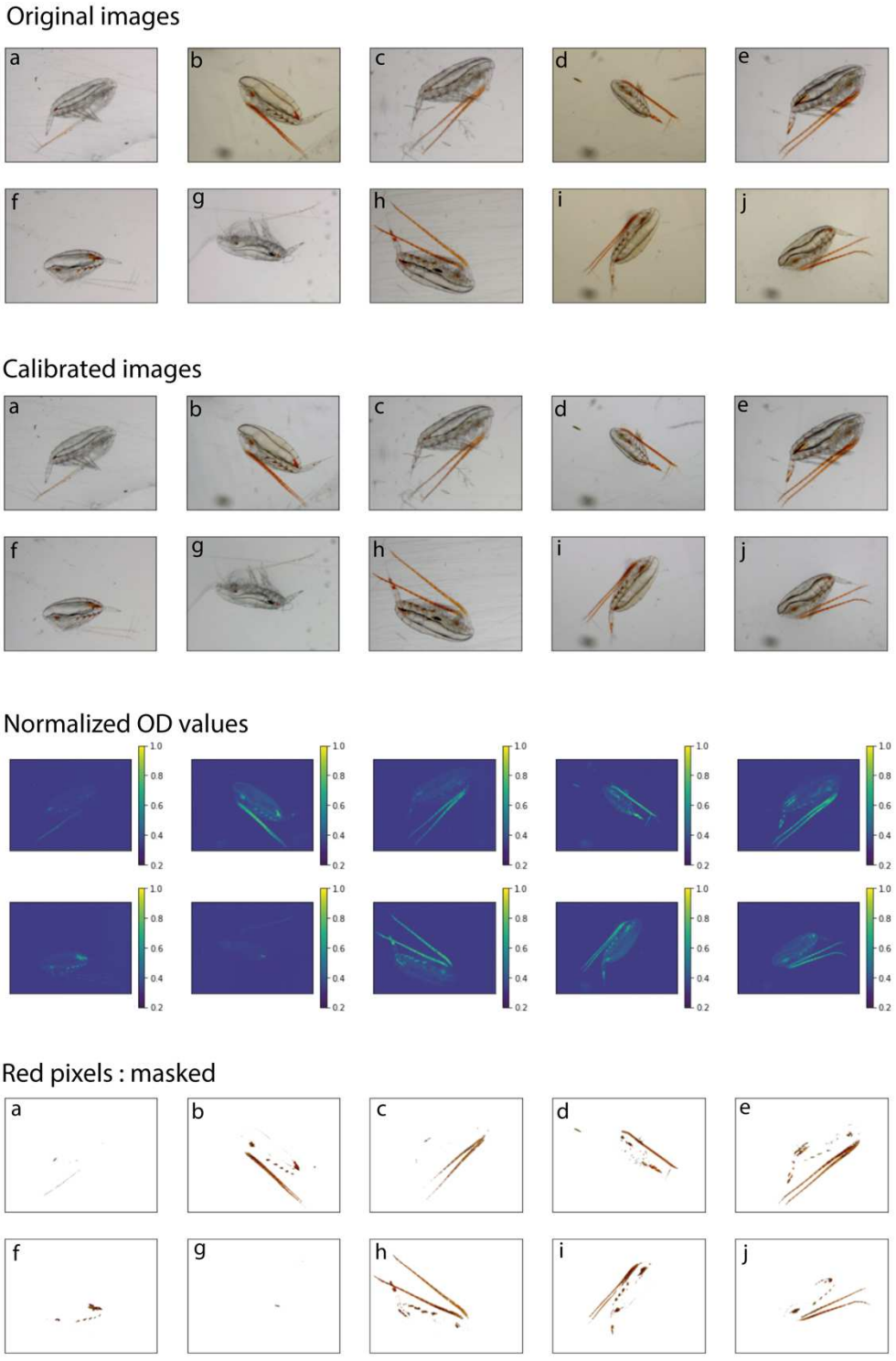

Figure C.2. Details of results from RGB calibration, astaxanthin color deconvolution and red pixels segmentation, for the 10 images presented in Fig. 3.1 and Fig. 3.3.

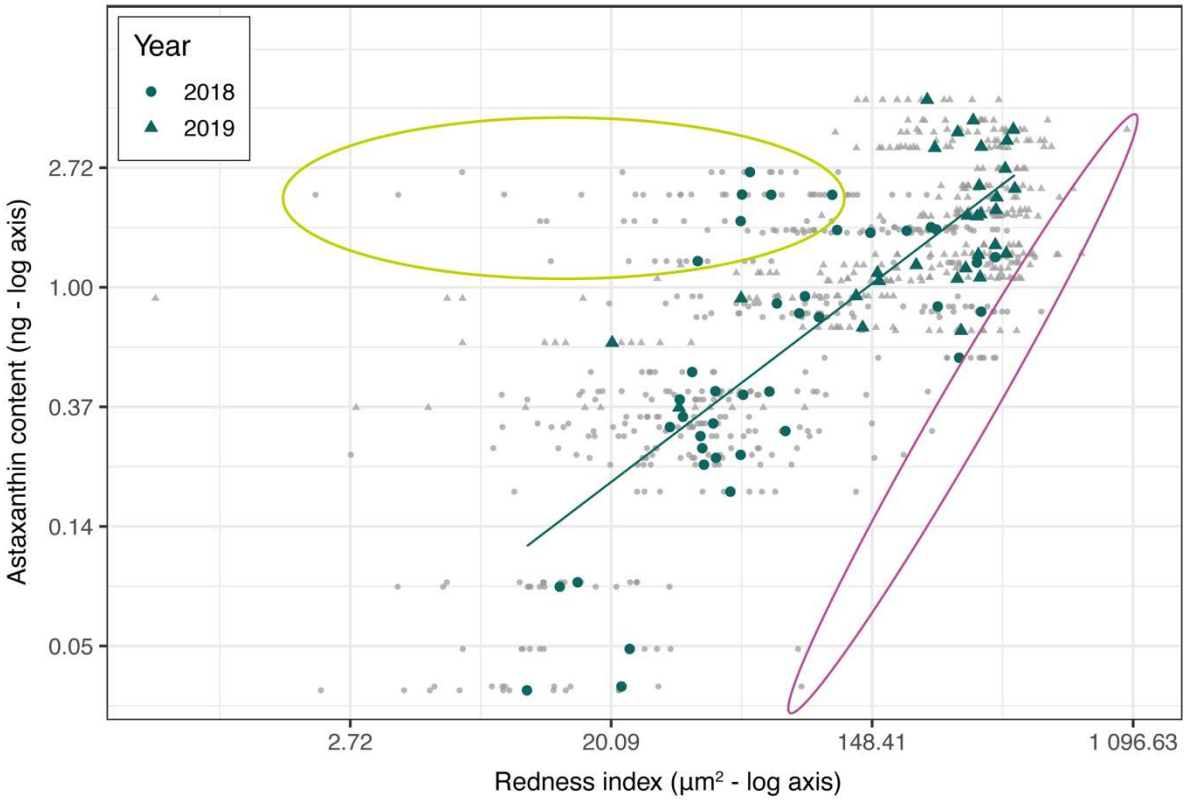

Figure C.3. Images with supposed incoherent redness indices highlighted on the regression between astaxanthin content and redness indices (Fig. 3.3). The purple ellipse highlights individual images with large redness indices within their sample (note that the log scale diminishes this variability on the graphic). The green eclipse highlights six samples with redness indices consistently low in comparison with the predicted regression.

Annexe D - Conclusion

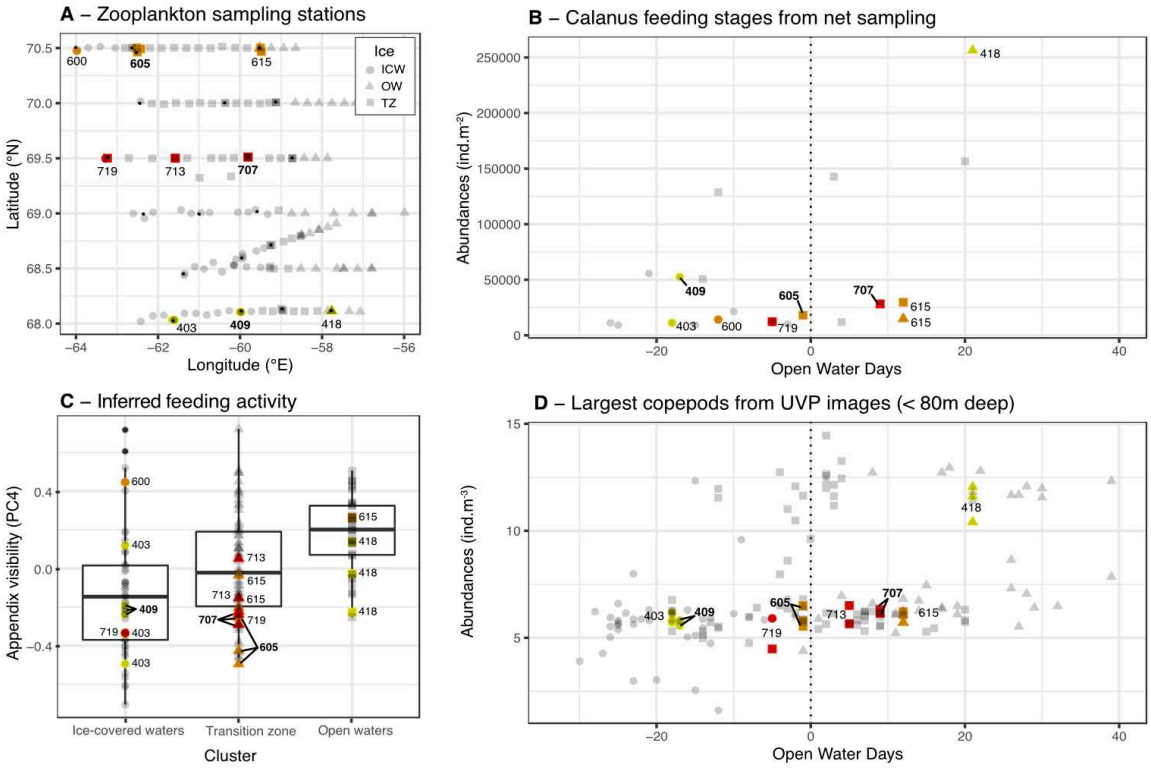

Figure D.1. Copepod concentrations and feeding activities from net sampling and in situ quantitative imagery. The nine stations analyzed for sympagic material are colored in yellow, orange and red according to the transects. The three stations with well-preserved sympagic material in sediments are labeled in bold (409, 605, 707). (A) Zooplankton sampling stations: each gray point is a sampling station where the Underwater Vision Profiler 5 (UVP5) was deployed, net sampling of zooplankton was also performed in stations marked with a black dot. Point shapes representing ice conditions: ICW = ice-covered waters, TZ = transition zone, OW = open waters (defined in Vilgrain et al., 2021). (B) Calanus feeding stages from net sampling: integrated concentrations of third stage nauplii to adult Calanus, estimated by microscope counts after net sampling, according to Open Water Days. (C) Inferred feeding activity estimated from copepod position on images in the three ice conditions. (D) Integrated concentrations of copepods in a surface layer (<80 m) calculated from UVP images according to Open Water Days.